Fully Integrated Rechargeable PEDOT:PSS Energy Storage Device for Smart Textiles Applications

Volledig geïntegreerd oplaadbaar PEDOT:PSS-energie-opslagapparaat voor smart-textiletoepassingen

Ida Nuramdhani

Promotor: prof. dr. ir. L. Van Langenhove
Proefschrift ingediend tot het behalen van de graad van
Doctor in de ingenieurswetenschappen: materiaalkunde

UNIVERSITEIT
GENT

Vakgroep Materialen, Textiel en Chemische Proceskunde
Voorzitter: prof. dr. P. Kiekens
Faculteit Ingenieurswetenschappen en Architectuur
Academiejaar 2018 - 2019

ISBN 978-94-6355-249-3
NUR 971, 959
Wettelijk depot: D/2019/10.500/57

Examination committee:

prof. dr. ir. Luc Taerwe (chairman)	Ghent University
dr. Benny Malengier (secretary)	Ghent University
prof. dr. ir. Lieva Van Langenhove (promotor)	Ghent University
prof. dr. ir. Gilbert De Mey	Ghent University
prof. dr. ir. Katrien Strubbe	Ghent University
prof. dr. ir. Wim Deferme	Hasselt University
prof. dr. ir. Anne Schwarz-Pfeiffer	HS-Niederrhein, Germany
prof. dr. ir. Vladan Koncar	ENSAIT, France
dr. Mohamad Widodo	Politeknik STTT Bandung, Indonesia

Fully Integrated Rechargeable PEDOT:PSS Energy Storage Device for Smart Textiles Applications

Dutch translation of the title:

Volledig geïntegreerd oplaadbaar PEDOT:PSS-energie-opslagapparaat voor smart-textiletoepassingen

FACULTY OF ENGINEERING AND ARCHITECTURE

Politeknik STTT Bandung
"Polytechnic of Textile Technology"

The research was mainly performed in the Department of Materials, Textiles, and Chemical Engineering (Ghent University, Zwijnaarde, Belgium) and in the Department of Textile Chemistry, Polytechnic of STT Tekstil Bandung (Bandung, Indonesia)

UNIVERSITEIT GENT

The research was funded by the Ghent University Council under the Special Research Fund for Developing Countries – BOF (Bijzonder Onderzoekfond)

Acknowledgement

The research reported in this dissertation would have been next to impossible without continual assistances and commitments of many individuals. I would like to take this opportunity to express my sincere gratitude to them who helped me with and/or contributed to this project.

First and foremost, my thanks go to my promotor, Prof. Lieva Van Langenhove, for her friendliness since my very first time to meet her, which was continued with her positive encouragement to do the PhD in UGent and apply for the BOF scholarship, for her warm welcome to be a part of her research group that provided me valuable experiences of learning and research in Smart Textiles. She also has perfectly taken care of me with my academic welfare and a bit of complication in administration matters. Thank you to my supervisors, Prof. Gilbert De Mey and Dr. Benny Malengier, and former supervisor, Dr. Carla Hertleer for their inputs, patience in discussions, and scientific supports during the time of study, especially with the area of applied physics and electrical matters that I had no background at all. Many thanks also go to Dr. Mohamad Widodo who has been my supervisor-like and nice partner for the enlightening discussions about the research, especially during my period of stay in Politeknik STTT Bandung, Indonesia, and Dr. Sheilla Atieno Odhiambo who helped me to start the work smoothly in the department of Textiles, UGent. Many thanks also to Dr. rer.nat. Rino Mukti from Bandung Institute of Technology (ITB, Bandung, Indonesia) for his willingness to become my supervisor for the BOF application, although the constructive collaboration has not been really continued due to some technical constraints.

I am also thankful to Prof. Luc Taerwe, Dr. Mohamad Widodo, Prof. Anne Schwarz-Pfeiffer, Prof. Vladan Koncar, Prof. Wim Deferme, Prof. Katrien Strubbe, Prof. Gilbert De Mey, and Dr. Benny Malengier for their willingness to become the member of the examination committee, as well as for their constructive inputs and suggestions prior to and during the internal defense.

Thank you to the Research Council of Ghent University for the opportunity to do this sandwich scheme doctoral study with the funding from BOF (Bijzonder Onderzoekfond-Special Research Fund), by which I have had splendid experiences of studying, attending

international conferences, meeting with many people from the same field of study and interests as well as living here in the very nice city, Gent, Belgium.

I would specially like to thank Dr. Argun Gokceoren from the Department of Chemistry, Istanbul Technical University, Turkey, for teaching and helping me with the CV and EIS analysis, Prof. Wim Deferme and Manoj Jose, and some of their colleagues in UHasselt, who gave me opportunity to experience working in their nice laboratory with polymer coating, NMR and ICP-OES analysis, Dr. Valentinus Galih Vidia Putra and Gunawan, M.Sc. from Politeknik STTT for their helps on physics matters, and operation in knitting and weaving machines respectively.

My many thanks go to Atiyyah Musa, my best office-mate, study-mate, and live-mate during the PhD study in the department, Jerry Ochola, the former member of the group and the first friend of mine here in Gent, who nicely introduced me with the department and the city, and also the other members of the Smart Textiles group, Iza, Hardianto, Abdul, Jason, Granch, Yetana, who have made my study life an enjoyable experience.

I am greatly appreciative of academic, technical, and administration staff of the Department of Materials, Textiles and Chemical Engineering at the Ghent University, Johanna, Katrien, Judith, Thomas, Sabine, Martine, Sigrid, etc, for being so helpful and friendly in taking care of my academic welfare. Very special thanks go to Katrien Hooreman, who has been so committed to help me with almost all administration matters.

Thanks also go to all members of the Indonesian student fellows and extended the other Indonesian community in Gent (especially Ann Djudzman and Francis, Koh Jul and Cik Lanny, Kak Tiar and Kak Lely), who have become very best family of mine here in Gent, and also all of my international friends here in Belgium, as well as all from OBSG who gave me opportunity to experience the big family-like life in Gent. Being an international student became much easier with their open mind and friendly relationships. Moreover, I would like to send my very sincere gratitude to my very best-mates, fellow Indonesian PhD student in UGent, Kang Asep W Permana, and Dimas who have been my special companies inthe very difficult times during my last few months of finishing this PhD. Nothing canreplace all sincere kindness and “love” you have given to me, guys.

I would like to send my deepest gratitude to my mum (Darsih Muyani) and dad (Dayat Hidayat) for their endless loves, supports, and prayers, as well as my father and mother

in law (Sjamsuddin Gunawan and Tuti Kurniati). Finally, my heartfelt appreciation goes to my husband, Tisna Kusumah, for his countless loves, patience, support, and understanding, as well as my lovely daughter, Yashilla, and son, Alfarras, who always colour and fill my days with joys and happiness, especially during the challenging times, when I was physically absent in some of their important moments. I believe, the times of trouble make your heart stronger, and so verily, in the difficulties, there is a relief.

“The energy of mind is the essence of life”
(Aristotle)

“So verily, in the difficulties, there is a relief”
(The Quran, 94:5)

Contents

List of Figures

List of Tables

List of Abbreviations

AC	Alternate current
AFM	Atomic force microscopy
Ag	Argentum (silver)
C	Capacitors
CPE	Constant phase elements
CV	Cyclic voltammetry
DC	Direct current
EDLC	Electrical double layer capacitor
EDS	Electron dispersive spectroscopy
EIS	Electrochemical impedance spectroscopy
ES	Electrochemical supercapacitor
ESR	Equivalent series resistance
E-Textiles	Electronic textiles
FBS	Fiber/yarn-based supercapacitor
FSC/S	Fiber/yarn-shaped capacitor/supercapacitor
FSE	Fiber-shaped electrode
GCD	Galvanostatic charge-discharge
HAADF	High angle annular dark field (in STEM)
ICP	Intrinsically conducting polymer
ICP-OES	Inductively coupled plasma-optical emission spectroscopy
MWCNT	Multi-walled carbon nanotube
NI	National Instrument
NMR	Nuclear magnetic resonance
OLED	Organic light-emitting diode
PANI	Polyaniline
PBO	Polybenzoxazole
PEDOT	Polyethylenedioxythiophene
PPy	Polypyrrole
PSS	Polystyrenesulfonate
PTh	Polythiophene

R	Resistors
SEM	Scanning electron microscopy
SS	Stainless-steel
STEM	Scanning transmission electron microscopy
STM	Scanning tunneling microscope
SWCNT	Single-walled carbon nanotube
TESD	Textile energy storage device
TGA	Thermogravimetric analysis
TPU	Thermoplastic polyurethane
WR	Water repellent

Summary

"If you want to find the secrets of the universe, think in terms of energy, frequency and vibration"

– Nikola Tesla -

Smart textiles have built-in functions, such as sensing, data processing, actuation, energy supply and communications and yet still feel and function like fabrics. Energy supply/storage device, in particular, is an important component of the smart textile system as it provides the required energy to power the system. So far, the successful commercialization of smart garments is hindered by the lack of fully integrated energy storage facilities. A simple but promising lightweight, flexible, and low-cost PEDOT:PSS-based textile energy storage device (TESD) had been successfully developed for the first time in Prof. Lieva Van Langenhove's research group of smart textiles. The present work was a continuation of the previous study and was mainly aimed at improving the device performance and appearance through the improvement of the fabrication techniques and researching the working principle and mechanism of the device. Further on the research background, objectives and outline are presented in detail in Chapter 1 of this thesis.

In Chapter 2, recent progress on the development of PEDOT:PSS-based textile energy storage device is comprehensively reviewed. A brief introduction about energy storage and textile-based energy storage devices including those using electroconductive materials other than PEDOT:PSS is presented in the first part of the review. The properties of PEDOT:PSS which include chemical and physical, electrical and electronic, morphology as well as transport properties are elaborated. A solid understanding of the working principles of the device and the mechanisms of energy storage is crucial for the improvement of device performance. In light of this argument different mechanisms of charge transport and its correlation with the storage of energy and performances is discussed to

address the subject matter. Additionally, the review also highlights the fabrication techniques and structural design of the device. The review ends with a discussion on different models and constructions of TESD particularly with respect to the possibility of designing a seamlessly integrated textile that incorporates all the current collecting, electrodes, separator and electrolyte materials in one piece of fabric or clothing and wearables.

As detailed in Chapter 3, to improve the device performance and appearance, the device developed in the recent study has transformed from its earliest design into its latest form through four different and improved fabrication methods. The device named TESD 3.3 has 3 layers of fabric and 3 threads of electrode yarn, whereas TESD 3.2 has 3 layers of fabric and 2 threads of electrode yarn. In order to understand the role of the middle electrode, comparison was made between TESD 3.3 and TESD 3.2 hoping that performance would be improved in TESD 3.2. The next logical step was to see how coating might affect the storage of charge and improve the performance. So, TESD 3.3 THL (THL stands for thick layer) with modified drop-coating method was fabricated and tested. This modification was mainly motivated by the inadvertent observation of the noise phenomenon in some of the experiments. The results and data that were collected and analyzed from TESD 3.3, TESD 3.3 THL, and TESD 3.2, led to the fabrication of TESD 1.2 THL and improvement of cell design and performance. It is the best form of our textile energy storage device up to this point. It is made of only one layer of fabric, which means that it is much thinner compared to the original design and thus more flexible as well as feasible for clothing. It consists of only two threads of electrode which gave a better charge storage capability. It also has a more defined PEDOT:PSS polymer in the cell area of the device because of two factors: (1) the application of water repellent agent which was very helpful to avoid diffusion of the dilute PEDOT:PSS dispersion during the drop-coating process; (2) modification of the drop-coating process as applied in the making process of the TESD 3.3 THL.

Chapter 4 presents some results from the study of the mechanism that have

been carried out through several approaches in the current research. Cyclic voltammetry and electrochemical impedance analysis were used as one of the approaches to investigate ionic and electronic activities in the bulk of PEDOT:PSS and at its interfaces with stainless steel yarn. From this technique, the complex behavior of ionic and electronic origins was also observed in the interfacial region between the conductive polymer and the electrodes. By presenting the cyclic voltammograms of PEDOT:PSS in the form of electrochemical solution and in its solid state on the glass and the fabric surfaces, ionic behavior of the electroactive polymer PEDOT:PSS has been confirmed through the redox reaction. The migration and diffusion of the ions involved were confirmed by the presence of the Warburg element with a phase shift of 45° (n = 0.5). Two different equivalent circuit models were found by simulating the model with the experimental results: (QR)(QR)(QR) for uncharged and (QR)(QR)(Q(RW)) for charged samples. The analyses also showed that the further the distance between the electrodes, the lower the capacitance of the cell. The distribution of polymer on the cell surface also were found to play an important role to change the capacitance of the device. Furthermore, study on the effect of the PEDOT to PSS ratio and the configuration of the electrode yarns are another approach taken to study the principle mechanism of the device. For this study, three commercial PEDOT:PSS yarns, Clevios P-VP-AI-4083, Ossila AI 4083, and Orgacon ICP 1050, as well as stainless steel and silver-coated polybenzoxazole (Ag/PBO) yarns, in various combinations, were used as solid electrolytes and electrodes, respectively. Analyses with NMR, ICP-OES, TGA, and resistivity measurement were employed to characterize the PEDOT:PSS. The device charge-discharge performance was measured by the Arduino microcontroller. Clevios and Ossila were found to have identical characteristics with a similar ratio, that is, 1:5.26, hence a higher resistivity of 1000 Ω.cm, while Orgacon had a lower PEDOT to PSS ratio, that is, 1:4.65, with a lower resistivity of 0.25–1 Ω.cm. The thermal stability of PEDOT:PSS up to 250 °C was proven. Devices with PEDOT:PSS having lower conductivity, such as Clevios P-VP-AI-4083 or Ossila AI 4083, showed capacitive behavior. For a better charge-discharge profile, it is also suggested that the PEDOT to electrode

resistance should be low. These results led to a conclusion that a larger ratio of PEDOT to PSS, having higher resistivity, is more desirable, but further research is needed.

Fastness to washing is one of the basic important quality requirements for wearable textiles and clothing. Concerning the daily used conditions, mechanical stresses provoked by the washing process is the other major aspect to consider. The PEDOT:PSS used in our device is known to have good water solubility, which will make it prone to being washed away in regular and repeated washing during the use of the product. Chapter 5 presents our initial study on washability of the devices. Two approaches aiming at creating a water-resistant surface are presented: (1) by covering the cell surface with a layer of thermoplastic polyurethane (TPU); and (2) by applying a fluorocarbon-based water-repellent chemical on the cell surface. The effect of both treatments to the charge-discharge profile was observed. The washing tests were then carried out step by step from the very mild and soft condition up to the standardized real daily washing condition to see the effect of each washing method. Possible changes on the cell morphology were also characterized by using scanning electron microscopy (SEM). The results showed that the TPU-covered device exhibited the best performance, where the capacitive behavior was still retained after two times of washing 3 (based on the SNI-ISO C06: 2010). Also, there was no significant change in the morphology of the TPU-covered device after the sequence of washings. The results are promising for further study as well as for further development of a more applicable textile energy storage device.

Finally, Chapter 6 elaborates our conceptual design for the integration of our TESD in clothing and reports the preliminary work that has been done toward its realization. It also serves as point of departure for our planned further research in the development of electronic-based smart garment. In this chapter, approaches and procedure for the integration, which started with the simplest form of insertion technique in knitting and weaving, is explained and discussed with an intention to obtain an understanding about the challenges and prospect for

improvement. This is still an early stage but we have obtained promising results that confirms our approach and direction. Integration of PEDOT:PSS TESD into textile structure with bottom-up approach by insertion *via* knitting and weaving has been performed and was successful. Generally, except for one device with shorter distance in the knitted fabric, the integrated devices performed well and did not show any significant changes that can be attributed to the process of integration. The strategy and direction for further work is confirmed. Although it is still preliminary, it is noteworthy that, at the same distance between electrodes, the device in knitted structure showed higher discharge profiles than the device in woven structure. More systematic tests and characterizations are still needed to these types of device configurations.

Additionally, statistical analysis to test the reliability and reproducibility of the device fabrication as well as measurements have been carried out. As presented in the Appendix, the reliability tests confirmed that all repeated measurements to a device showed valid, reliable, and consistent results. The t-test which was performed to examine the reproducibility of the fabrication method also confirmed that the two identical devices compared in this test are significantly identical by showing p-value > 0.05, i.e. 0.161 and 0.178.

Samenvatting

"Als je de geheimen van het universum wilt vinden, denk dan in termen van energie, frequentie en vibratie"

– Nikola Tesla -

Slim textiel heeft ingebouwde functies, zoals detectie, gegevensverwerking, activering, energievoorziening en communicatie en voelt en functioneert toch als textielstof. Met name de energievoorziening / het opslagapparaat is een belangrijk onderdeel van een slim textielsysteem omdat het de vereiste energie levert om het systeem van stroom te voorzien. Tot dusverre wordt de succesvolle commercialisering van slimme kleding gehinderd door het gebrek aan volledig geïntegreerde energieopslagfaciliteiten. Een eenvoudig maar veelbelovend, lichtgewicht, flexibel en goedkoop PEDOT: PSS-gebaseerd textielopslagapparaat voor textiel werd voor het eerst met succes ontwikkeld in de onderzoeksgroep van Smart Textiles van Prof. Lieva Van Langenhove. Het huidige werk was een voortzetting van de vorige studie, die vooral gericht was op het verbeteren van de prestaties en het uiterlijk van het apparaat door de verbetering van de fabricagetechnieken en het onderzoeken van het werkingsprincipe en mechanisme van het apparaat. Verderop in Hoofdstuk 1 worden de onderzoeksachtergrond, de doelstellingen en het schema van dit proefschrift gedetailleerd beschreven.

In Hoofdstuk 2 wordt de recente vooruitgang in de ontwikkeling van het PEDOT:PSS-gebaseerd textielopslagapparaat (TESD) voor textiel uitgebreid besproken. Een korte inleiding over energieopslag en op textiel gebaseerde energieopslagapparaten, inclusief apparaten die andere elektrogeleidende materialen dan PEDOT: PSS gebruiken, wordt gepresenteerd in het eerste deel van de review. De eigenschappen van PEDOT:PSS die chemische en fysische, elektrische en elektronische, morfologische alsmede transporteigenschappen omvatten, zijn uitgewerkt. Een goed begrip van de werkingsprincipes van het

apparaat en de mechanismen van energieopslag is cruciaal voor het verbeteren van de prestaties van het apparaat. In het licht van dit argument worden verschillende mechanismen van ladingstransport en de correlatie ervan met de opslag van energie en prestaties besproken om het onderwerp aan te pakken. Bovendien worden in de review ook de fabricagetechnieken en het structurele ontwerp van het apparaat benadrukt. De bespreking eindigt met een bespreking van verschillende modellen en constructies van TESD, met name met betrekking tot de mogelijkheid om een naadloos geïntegreerd textiel te ontwerpen dat alle huidige verzamel-, elektroden-, separator- en elektrolytmaterialen in één stuk weefsel of kleding en wearables bevat.

Zoals beschreven in Hoofdstuk 3, is het apparaat dat in de recente studie is ontwikkeld, van de vroegste naar de nieuwste vorm getransformeerd door vier verschillende en verbeterde fabricagemethoden om de prestaties en het uiterlijk van het apparaat te verbeteren. Het apparaat met de naam TESD 3.3 heeft 3 lagen stof en 3 draden elektrodengaren, terwijl TESD 3.2 3 lagen stof en 2 draden elektrodengaren heeft. Om de rol van de middelste elektrode te begrijpen, werd een vergelijking gemaakt tussen TESD 3.3 en TESD 3.2 in de hoop dat de prestaties zouden worden verbeterd in TESD 3.2. De volgende logische stap was om te zien hoe coating de opslag van lading kan beïnvloeden en de prestaties kan verbeteren. Dus, TESD 3.3 THL (THL staat voor dikke laag, *thick layer*) werd met gemodificeerde druppelbekledingsmethode gefabriceerd en getest. Deze wijziging werd voornamelijk ingegeven door de onopzettelijke observatie van het ruisfenomeen in sommige van de experimenten. De resultaten en gegevens die werden verzameld en geanalyseerd vanuit TESD 3.3, TESD 3.3 THL en TESD 3.2, leidden tot de fabricage van TESD 1.2 THL en verbetering van het ontwerp en de prestaties van de cellen. Het is de beste vorm van ons textiel-energieopslagapparaat tot op dit punt. Het is gemaakt van slechts één laag stof, wat betekent dat het veel dunner is in vergelijking met het oorspronkelijke ontwerp en dus flexibeler en ook haalbaarder voor kleding. Het bestaat uit slechts twee draden van de elektrode die een betere ladingopslagcapaciteit gaven. Het heeft ook een meer gedefinieerd PEDOT:PSS-polymeer in het celgebied van het

apparaat vanwege twee factoren: (1) de toepassing van een waterafstotend middel dat zeer nuttig was om diffusie van de verdunde PEDOT:PSS-dispersie tijdens de druppelbekleding te voorkomen; (2) modificatie van het druppelbekledingsproces zoals toegepast bij het maken van de TESD 3.3 THL.

Hoofdstuk 4 presenteert enkele resultaten van het onderzoek naar mechanismen die zijn uitgevoerd via verschillende benaderingen in het huidige onderzoek. Cyclische voltammetrie en elektrochemische impedantie-analyse werden gebruikt als een van de benaderingen voor het onderzoeken van ionische en elektronische activiteiten in het grootste deel van PEDOT:PSS en op zijn grensvlakken met roestvrijstalen garen. Via deze techniek werd ook het complexe gedrag van ionische en elektronische oorsprong waargenomen in het grensvlakgebied tussen het geleidende polymeer en de elektroden. Door het presenteren van de cyclische voltammogrammen van PEDOT:PSS in de vorm van een elektrochemische oplossing en in vaste vorm op glas en de oppervlakken van het weefsel, is het ionengedrag van het elektroactieve polymeer PEDOT:PSS bevestigd door de redoxreactie. De migratie en diffusie van de betrokken ionen werden bevestigd door de aanwezigheid van het Warburg-element met een faseverschuiving van 45 ° (n = 0,5). Twee verschillende equivalente circuitmodellen werden gevonden door het model te simuleren gebruik makende van de experimentele resultaten: (QR) (QR) (QR) voor ongeladen en (QR) (QR) (Q (RW)) voor geladen monsters. De analyses toonden ook aan dat hoe verder de afstand tussen de elektroden, hoe lager de capaciteit van de cel. De verdeling van polymeer op het celoppervlak bleek ook een belangrijke rol te spelen bij het veranderen van de capaciteit van de TESD Onderzoek naar het effect van de PEDOT naar PSS-verhouding en de configuratie van de elektrodegarens zijn een andere benadering om het hoofdmechanisme van het apparaat te bestuderen. Voor dit onderzoek werden drie commerciële PEDOT: PSS-garens, Clevios P-VP-AI-4083, Ossila AI 4083 en Orgacon ICP 1050, evenals garens van roestvrij staal en zilver gecoat polybenzoxazool (Ag / PBO), in verschillende combinaties, gebruikt als respectievelijk vaste elektrolyten en elektroden. Analyses met NMR, ICP-OES, TGA en resistiviteitsmeting werden gebruikt om de PEDOT:PSS te karakteriseren.

De lading/ontlading van het apparaat werd gemeten met een Arduino microcontroller. Clevios en Ossila bleken identieke kenmerken te hebben met een vergelijkbare verhouding, dat wil zeggen 1:5.26, vandaar een hogere soortelijke weerstand van 1000 Ω.cm, terwijl Orgacon een lagere PEDOT tot PSS-verhouding had, dat wil zeggen 1:4.65, met een lagere soortelijke weerstand van 0.25-1 Ω.cm. De thermische stabiliteit van PEDOT: PSS tot 250°C werd bewezen. Apparaten met PEDOT: PSS met lagere geleidbaarheid, zoals Clevios P-VP-AI-4083 of Ossila AI 4083, vertoonden capacitief gedrag. Voor een beter laad-ontlaadprofiel wordt ook gesuggereerd dat de PEDOT naar elektrode-weerstand laag zou moeten zijn. Deze resultaten leidden tot de conclusie dat een grotere verhouding tussen PEDOT en PSS, met hogere resistiviteit, wenselijker is, maar verder onderzoek is nodig.

Behoud van eigenschappen na wassen is een van de fundamentele belangrijke kwaliteitseisen voor draagbaar textiel en kleding. Met betrekking tot de dagelijks gebruikte omstandigheden, is mechanische stress veroorzaakt door het wasproces het andere belangrijke aspect om te overwegen. Van de PEDOT:PSS die in ons apparaat wordt gebruikt, is bekend dat deze een goede wateroplosbaarheid heeft, waardoor het bij regelmatig en herhaald wassen tijdens het gebruik van het product kan worden weggespoeld. Hoofdstuk 5 presenteert ons eerste onderzoek naar de wasbaarheid van de apparaten. Twee benaderingen die zijn gericht op het creëren van een waterbestendig oppervlak worden gepresenteerd: (1) door het celoppervlak te bedekken met een laag thermoplastisch polyurethaan (TPU); en (2) door op het celoppervlak een waterafstotende chemische stof op basis van fluorocarbon toe te passen. Het effect van beide behandelingen op het lading-ontlaadprofiel werd waargenomen. De wastesten werden vervolgens stapsgewijs uitgevoerd van de zeer milde en zachte toestand tot de gestandaardiseerde dagelijkse wasvoorwaarde om het effect van elke wasmethode te onderzoeken. Mogelijke veranderingen in de celmorfologie werden ook gekarakteriseerd door scanning electronenmicroscopie (SEM) te gebruiken. De resultaten toonden aan dat het TPU-bedekte apparaat de beste prestaties vertoonde, waarbij het capacitieve gedrag nog steeds werd behouden

na twee keer wassen met methode 3 (op basis van de SNI-ISO C06: 2010). Ook waren er geen significante veranderingen in de morfologie van het TPU-bedekte apparaat na de reeks wasbeurten. De resultaten zijn veelbelovend voor verder onderzoek en voor de verdere ontwikkeling van een meer toepasbaar textielapparaat voor energieopslag.

Ten slotte wordt in Hoofdstuk 6 ons conceptontwerp uitgewerkt voor de integratie van ons TESD in kleding en worden de voorbereidende werkzaamheden voor de realisatie ervan vermeld. Het dient ook als vertrekpunt voor ons geplande verdere onderzoek naar de ontwikkeling van een op elektronica gebaseerd slim kledingstuk. In dit hoofdstuk worden de benaderingen en procedures voor de integratie, die begonnen met de eenvoudigste vorm van invoegtechniek namelijk breien en weven, uitgelegd en besproken met de bedoeling om inzicht te krijgen in de uitdagingen en het vooruitzicht op verbetering. Dit is nog in een vroeg stadium maar we hebben veelbelovende resultaten behaald die onze aanpak en richting bevestigen. Integratie van PEDOT:PSS TESD in textielstructuur met bottom-up benadering door inbrengen via breien en weven is uitgevoerd en was succesvol. Over het algemeen presteerden de geïntegreerde apparaten, met uitzondering van apparaten met kortere afstand in de gebreide stof, goed en vertoonden geen significante wijzigingen die aan het integratieproces kunnen worden toegeschreven. De strategie en richting voor verder werk wordt bevestigd. Hoewel het nog steeds voorlopig is, is het opmerkelijk dat, op dezelfde afstand tussen elektroden, TESDs in gebreide structuur hogere ontladingsprofielen vertoonden dan apparaten in geweven structuur. Meer systematische tests en karakteriseringen zijn evenwel nog nodig voor elk type apparaatconfiguratie.

Daarnaast is statistische analyse uitgevoerd om de betrouwbaarheid en reproduceerbaarheid van de fabricage van het apparaat te testen, evenals metingen. Zoals gepresenteerd in de Appendix, bevestigden de betrouwbaarheidstests dat alle herhaalde metingen van een apparaat geldige, betrouwbare en consistente resultaten opleverden. De t-test die werd uitgevoerd

om de reproduceerbaarheid van de fabricagemethode te onderzoeken bevestigde ook dat de twee identieke apparaten die in deze test werden vergeleken, significant identiek zijn (p-waarde> 0.05, d.w.z. 0.161 en 0.178).

1

Introduction

"Energy and persistence conquer all things"

– Benjamin Franklin -

This chapter conveys a general introduction of the research, consisting of three sections: background, objectives, and research outline. The background describes the research motivation and significance, previous related work with its potential and problem, as well as problem statement of the present study. The general and specific objectives of each part of the study are presented in the second Section. The Chapter ends with the presentation of the research roadmap, presenting a complete picture of works that have been done in the study and their position relative to the previous works, and the direction for further developments.

1.1 Research Background

An easy-to-use wearable technology between devices and humans has long been envisaged as the next generation technology, which actually has been around for some time now. Prototypes and products targeting applications in healthcare and sports as well as active lifestyles, for examples, have been around on the market for more than a decade (**Figure 1.1**). Apple, Fitbit, Garmin, Xiaomi, Samsung, and Huawei are some of the brands who are competing to capture the growing market. According to the recent market report released by International Data Corporation, the worldwide wearables market continued its upward trajectory in both the fourth quarter (4Q17) and full year 2017 with total shipment volumes reaching new records of 115.4 million units, up 10.3% from the 104.6 million units shipped in 2016 [1]. Being motivated by the same market drive, fashion brands partnering with some of the above technology companies enter the market with their new or existing lines of products. Brands such as Hermes, Tag Heuer, Fossil, Michael Korrs have stepped into the wearable spaces [2].

Figure 1.1. Prototypes and products of wearable technology in healthcare [3]

The concept of giving people personalized healthcare, support, and information in one platform and in close proximity with the target of the service, can be realized through multifunctional fabrics, commonly referred to as electronic textiles (e-textiles) or smart textiles [4], [5]. Caution must be exerted in using the two terminologies. In e-textiles, electronic components are incorporated into the structure of textile material. However, only having electronics by itself does not necessarily make the material smart. It requires elements of smart (sensing ability, responsiveness, and adaptability) that are embedded or ideally integrated in the system to make e-textiles become smart textiles/clothing. Such concept has been envisaged as both inventive and high knowledge-content garments [5], capable of making daily life healthier, safer, and more comfortable.

Figure 1.2 shows the evolutionary development of electronic-based smart textiles/clothing from the standpoint of electronic devices. From that point of view, textiles have not been looked upon as an integral part of the system and instead have been conceived only as a platform. Alternatively, from the standpoint of textiles and clothing as a product of technology and fashion, the so-called fashionable technology [6], such textiles and clothing are the devices themselves.

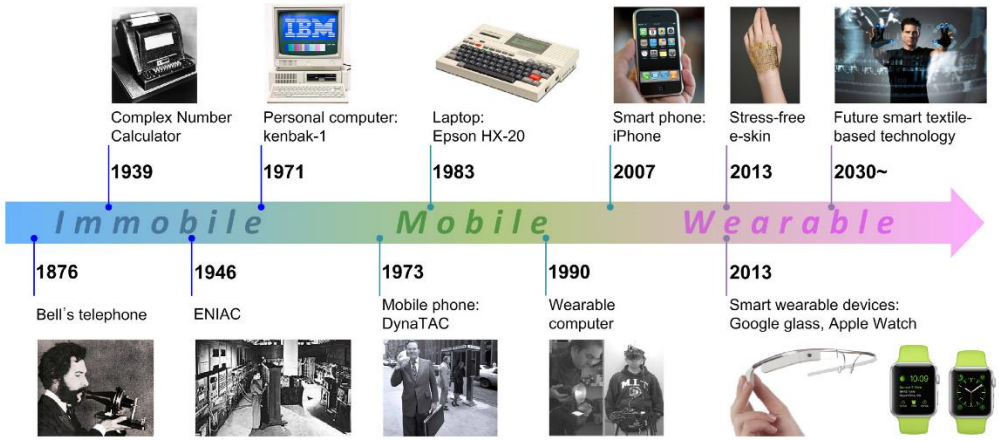

Figure 1.2. The evolutionary development of electronics from immobile to mobile, and finally to wearable textile-based electronics [7].

As shown in **Figure 1.3**, some examples of the e-textiles include digital music player system which are integrated in the proposed textile design [8], application of piezoelectric material in textiles for shape sensing, sound detection and sound emission in the form of a glove [9], as well as integration of textile sensors to detect the human breathing in form of a belt fastened around the patient's chest [10].

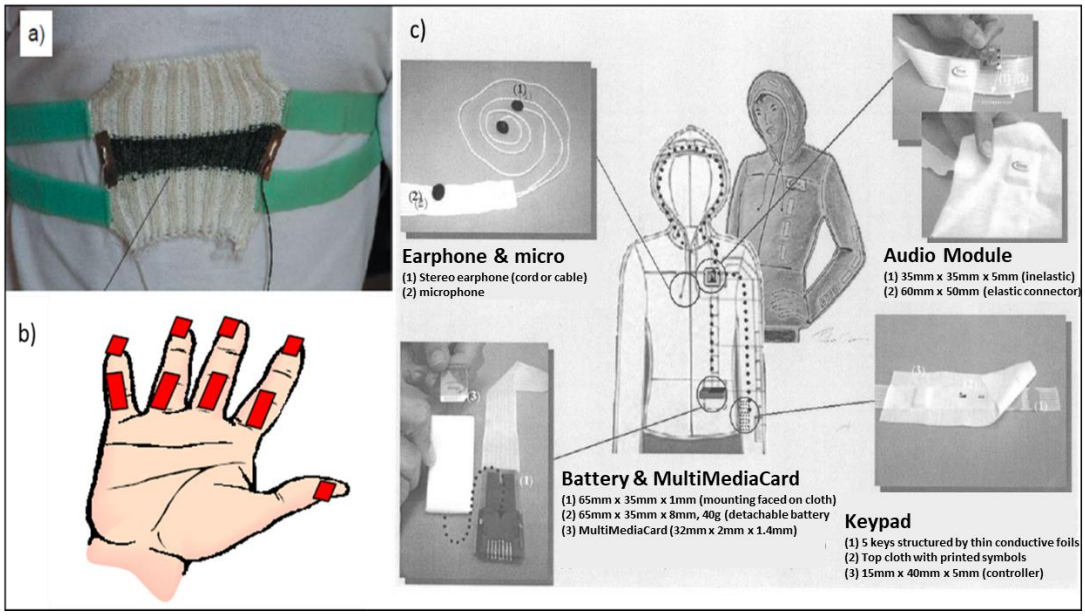

Figure 1.3. Examples of e-textiles: (a) textile sensors belt to detect human breathing [10]; (b) sensor arrangement for applying piezoelectric materials in glove [9]; (c) digital music player in proposed textile design [8]

Recently, Google launched Jacquard™ (**Figure 1.4**) that allows clothes to behave just like the touchscreen in smartphones and as points of connection with many functionalities within the garment or beyond [11]. The technology was based on the ability to insert and weave multi-fiber conductive yarn seamlessly to become an integral part of the textile structure. In later development, Google Jacquard™ was used to empower Levi's® Commuter™ Trucker jacket with interesting customizable abilities, which include communication, navigation, and music [12].

Figure 1.4. Google Jacquard™ (above) [11] and Levi's® Commuter™ Trucker jacket (bottom) [12].

As previously mentioned, smart textiles have built-in functions, such as sensing, data processing, actuation, energy supply (storage or scavenging) and communications and yet still feel and function like fabrics [13]. Examples of potential applications of this technology include military garment devices, firefighter garments, and personal electronics [14]. The energy supply/storage device, in particular, is an important component of a smart textile system; it provides the required energy to power the system. So far, the successful commercialization of smart garments is hindered by the lack of fully integrated energy storage facilities. Development of an energy generation and storage system to power many functions in different areas of application of smart textiles such as in health, military, protection, and even in fashion is therefore of an important significance. Ideally, the device should integrate seamlessly and becomes by itself an integral part of the textile structure without compromising the comfort and other

desirable aspects of clothing. **Figure 1.5** shows one concept of energy storage integration in smart technical garment [15].

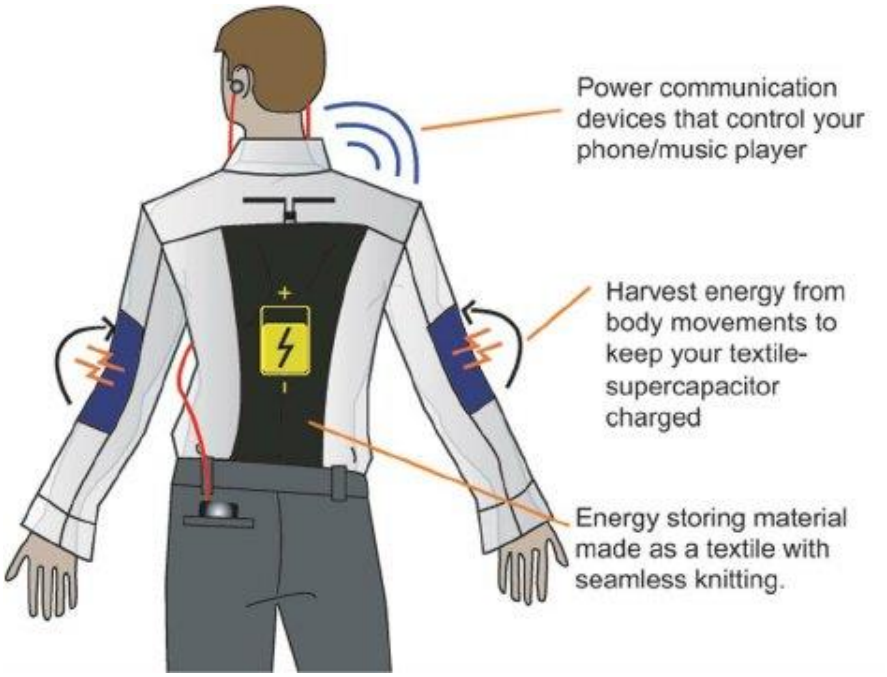

Figure 1.5. One possible application of an integrated energy storage material to power communication devices in a smart garment [15]

The development of smart textiles focusing on integrated solution has been one of the focuses in Prof. Lieva Van Langenhove' s research group of smart textiles at Ghent University. A simple but promising lightweight, flexible, and low-cost textile energy storage device was successfully developed for the first time in the group by the work of dr. Sheilla A. Odhiambo during the course of her PhD study [16]. The work constituted the investigation of fabrication of a textile-based energy storage device made with PEDOT:PSS (poly(3,4-ethylenedioxythiophene) : poly(styrenesulfonate)) and stainless steel conductive yarns. The device was developed based on the work of Bhattacharya *et al*. [17] that used a coating of PEDOT:PSS as solid electrolyte between three plies of silver-coated polyamide yarns. Through a simple fabrication, a rechargeable polymeric textile battery was produced. In the work of Odhiambo et al. [18], [19], a functional cell was assembled

on a three layered porous laminate of textile fabric made of polyester/cotton with three conductive yarn electrodes and PEDOT:PSS which was functioned as the electrolyte. PEDOT:PSS, an electro-active polymer used in the mentioned previous studies, is known to be capable of being an electrode and electrolyte material [20], [21] with high thermal properties, flexibility in terms of its chemical and physical properties as well as decent electrochemical stability, charge capacity, and ionic conductivity [20], [21].

As an electrode, electro-conductive stainless-steel filament yarns showed an encouraging performance. When compared with silver and copper coated PBO (polybenzoxazole), higher capability to store charge with higher voltage value in a longer time was shown by the less expensive stainless-steel yarn electrode [19]. Additionally, the stainless-steel filament yarns are also flexible, and can be comfortably incorporated into textile fabrics. They showed good electrical and thermal conductivity with high melting point that give further advantages of using this electro-conductive yarn as a bipolar electrode fabricated in a textile-based energy storage device [18].

The previous work in the group has established solid grounds for further development of the device, which include the initial method of fabrication, the selection of components used in the device system, as well as basic performance of the developed devices based on various parameters like the effects of charging time and diameter of the electrodes. The rechargeability of the devices was also established and it was found that such device could be recharged and maintain its performance up to 15 times before its capability to store charges degraded. As for the study on the principle behind the device, it was initially predicted that the mechanism involved in the charge storage was mainly through separation of charges within the electrolyte and following the charge storage principles of electrical double layer on the electrode surfaces. However, it was still an early

assumption made based on presumption from the measurement results that the accumulated charge in the devices during discharge was not proportional to the charging time. On the other hand, Bhattachraya *et al*. [17] had indicated that their developed device worked according to the principle of a battery in which chemical interaction occurred at the Ag/PEDOT:PSS interface. As the stainless steel electrode yarn used in the work of our group is chemically inert and covered by a very thin layer of chrome oxide (Cr_2O_3) [14], it is plausible that similar chemical interaction also occurred at the interface of the polymer and electrode. Thus, the potential for further study to understand the cell behavior as well as ultimately its mechanism is still widely open. In fact, the search for the underlying mechanism of the device has become one of the important parts in the present study.

Apart from the study on the mechanism, attempts to realize an integrated system of energy storage device with adequate performance is another significant goal. The keywords for the desired device are an integrated system, high electrical performance, mechanical integrity, and ease of production with reasonable degree of flexibility. Therefore, improvements of fabrication method have also become imperative. When it comes to the idea of applying the technology into wearable products, issue on washability is another critical concern.

1.2 Research Objectives

Departing from the results of the previous works [9], it is believed that at the end, results of this project must lead to improvement and a robust design of the PEDOT:PSS-based textile energy storage device (TESD). For aesthetic and technical reasons, it is also highly desirable that the developed cell should be incorporated in such a way that it becomes an integral part of the garments without compromising the comfort and other desirable aspects of the clothing. To move closer to the expected end results of this study, the present work was aimed at obtaining also a further understanding on the underlying mechanism of the device. The obtained

knowledge on the mechanism has led to the improvement of the fabrication techniques. Partial objectives of each interwoven area of study in the present research then are:

1. To investigate the working principle and mechanism of the developed PEDOT:PSS-based textile energy storage device (TESD). Here, the study includes confirming the physical mechanism of charge storage in PEDOT:PSS (the electrochemical cell was a battery, a capacitor, or hybrid), studying the ratio of PEDOT:PSS and introducing the effect of conductivity or resistivity to the charge-discharge performance of the developed device, as well as studying the effect of various parameters like charging voltage, time, the presence of middle electrode, and selection of types and configuration of the electrode yarns.
2. To improve the technical and aesthetical aspects of the device. This includes the improvement of performance and appearance of the device, which are mutually interconnected. Here, the study includes the attempt to reduce the diffusion of the PEDOT:PSS polymer in the textile substrate which can decrease its possibility to interact with the electrode yarns by introducing the application of water repellent agent on the textile fabric used as the cell basis.
3. To investigate and test the mechanical integrity and washability of the cell against the conditions of everyday use and care, including an investigation on the use of a protective layer that shields the cell without having to create any obstruction to the desirable properties of textiles to which the cell will be incorporated.
4. To create an integrated TESD by different techniques of textile knitting and weaving.

1.3 Research Outline

Since the present research is a continuation from the previous works, it is noteworthy to outline what has been done in the present study compared and related with the previous works, which then become a significant basis for its continuation. **Figure 1.6** presents the graphical illustration of the research, showing the previous and present work and results as well as potentials and outlooks for future work. As can be seen in the graph, the present work has covered more than 80% of the total required work leaving 20% of the work for further research, which mainly related with integration of cell and improvement in performance. Except for sub-areas that were saved for further work in the near future, the five areas of study in this research have been fully covered as planned. With the five classifications of the area of study in the present work, the results presented in this thesis are structured as depicted in the thesis outline shown in **Figure 1.7**.

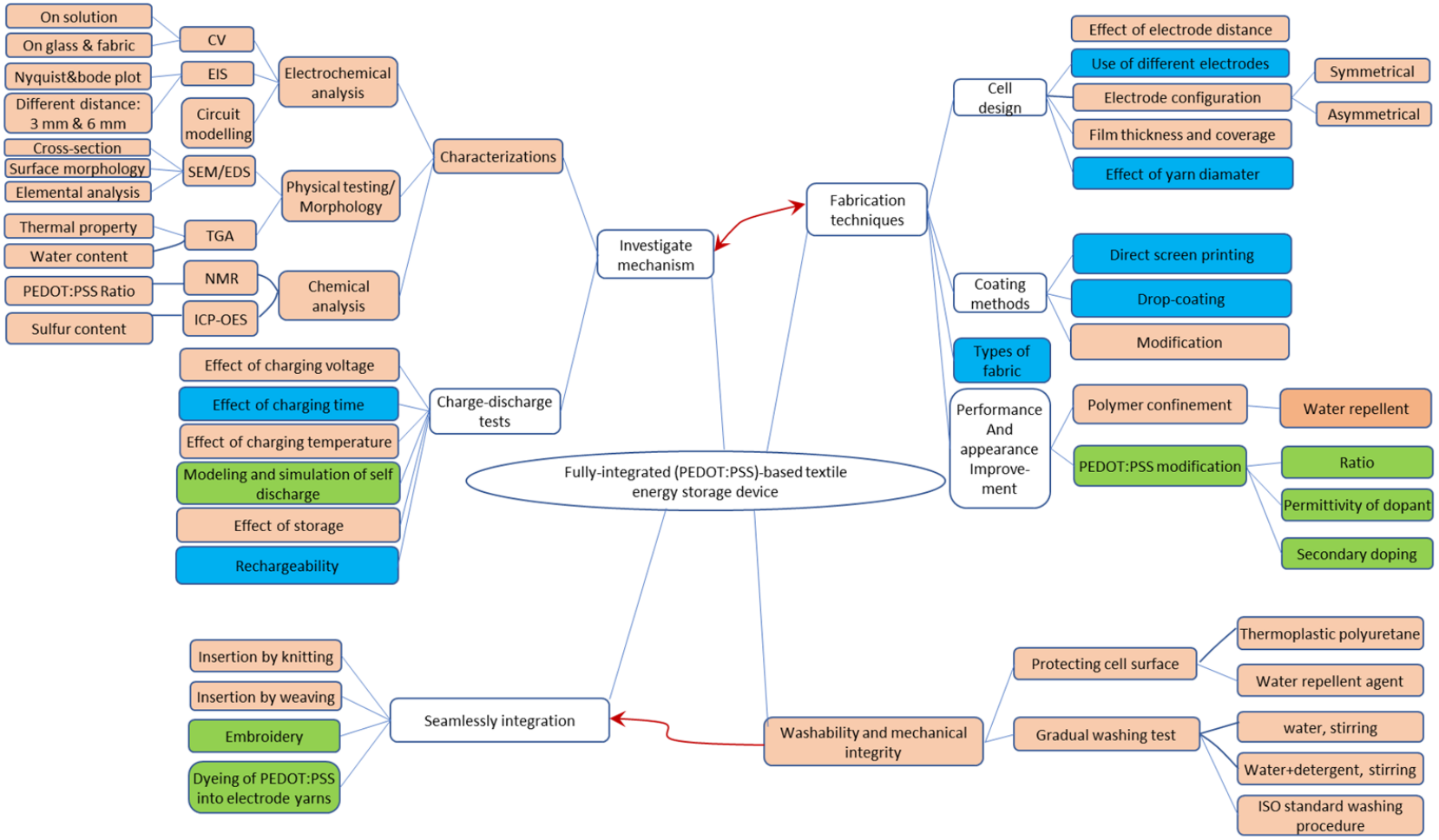

Note: : Past works; : Present works; : Potential future works

Figure 1.6. Research Outline

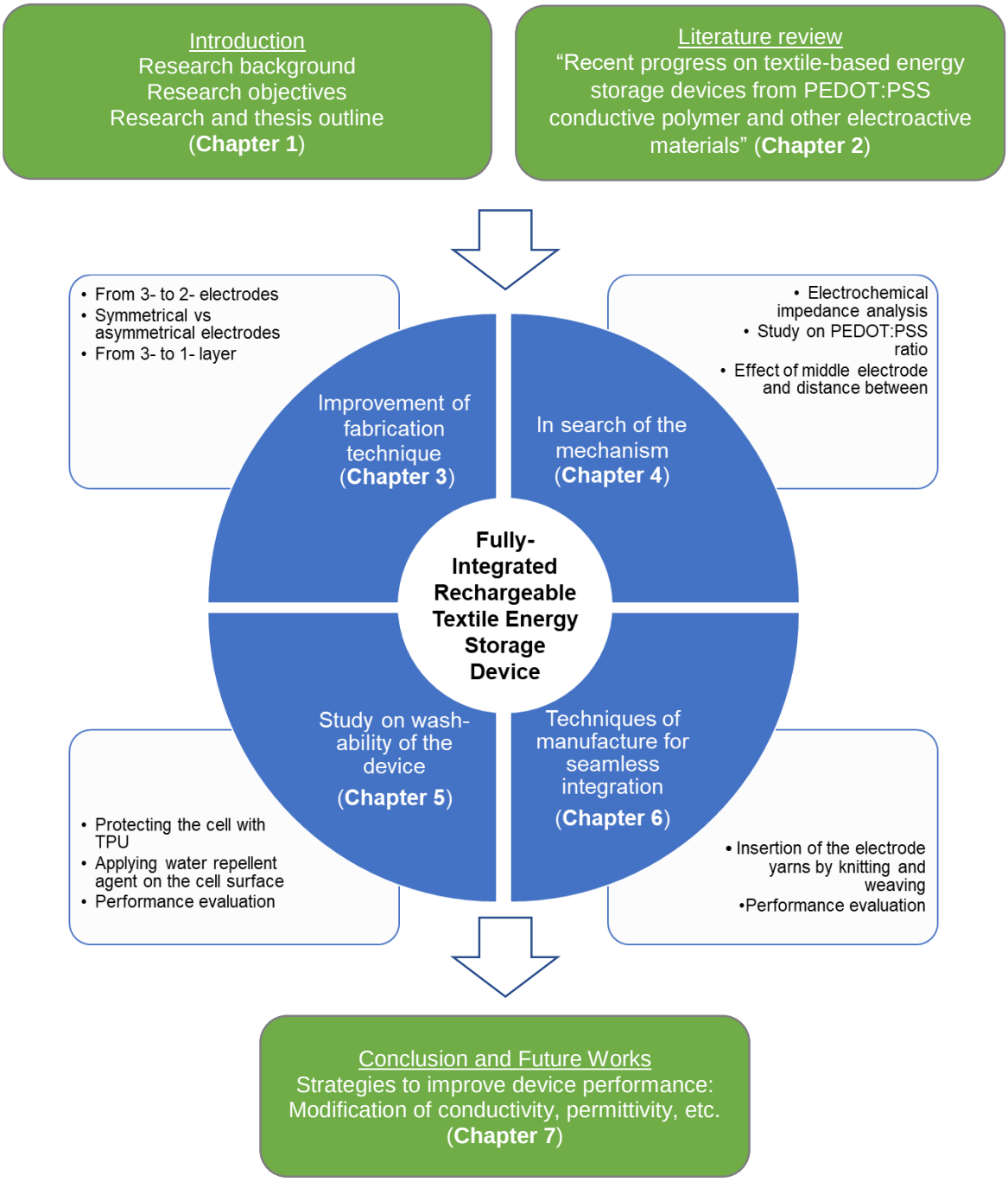

Figure 1.7. Thesis outline

Bibliography

[1] https://www.idc.com/getdoc.jsp?containerId= prUS43598218, accessed on the 10th of February 2019.

[2] https://www.lifewire.com/wearables-and-accessories-from-your-favorite-fashion-brands-4079785, accessed on the 10th of February 2019.

[3] https://techno-soft.com/wearable-technology-in-healthcare.html, accessed on the 10th of February 2019.

[4] A. Schwarz, L. Van Langenhove, P. Guermonprez, and D. Deguillemont, "A Roadmap on Smart Textiles," *Textile Prog.*, vol. 42, no. 2, pp. 99–180, Jun. 2010.

[5] F. Carpi and D. De Rossi, "Electroactive Polymer-Based Devices for e-Textiles in Biomedicine," *IEEE Trans. Inf. Technol. Biomed.*, vol. 9, no. 3, pp. 295–318, 2005.

[6] S. Seymour, "Fashionable Technology: The Intersection of Design, Fashion, Science, and Technology, Springer-Verlag/Wien, New York: 2008, ISBN: 978-3-211-74498-7.

[7] Kaushik *et al.*, "Textile-Based Electronic Components for Energy Applications: Principles, Problems, and Perspective," *Nanomaterials*, vol. 5, no. 3, pp. 1493-1531, 2015, doi:10.3390/nano5031493.

[8] D. Marculescu *et al.*, "Electronic Textiles: A Platform for Pervasive Computing," *Proc. IEEE*, vol. 91, no. 12, pp. 1995–2018, 2003.

[9] J. Edmison, M. Jones, Z. Nakad, and T. Martin, "Using Piezoelectric Materials for Wearable Electronic Textiles," *Proc. 6th Int. Symp. Wearable Comput. ISWC'02*, 2002.

[10] J. Zieba and M. Frydrysiak, "Textronics – Electrical and Electronic Textiles. Sensors for Breathing Frequency Measurement," *FIBRES Text. East. Eur.*, vol. 15, no. 5(59), pp. 43–48, 2006.

[11] https://atap.google.com/jacquard/, accessed on the 12th of February 2019.

[12] http://www.wearables.com/google-smart-clothing-levis/, accessed on the 12th of February 2019.

[13] K. Jost, G. Dion, and Y. Gogotsi, "Textile energy storage in perspective," *J Mater Chem A*, vol. 2, no. 28, p. 10776, 2014.

[14] D. Meoli and T. May-Plumleee, "Interactive Electronic Textile Development: A Review of Technologies," *J. Text. Appar. Technol. Manag.*, vol. 2, no. 2, 2002.

[15] K. Jost *et al.*, "Knitted and screen printed carbon-fiber supercapacitors for applications in wearable electronics," *Energy Environ. Sci.*, 2013.

[16] S. Odhiambo, "PEDOT:PSS CHarge Storage Devices Integrated into Textiles for Smart Textile Application," Ghent University, Belgium, 2015.

[17] R. Bhattacharya, M. M. de Kok, and J. Zhou, "Rechargeable electronic textile battery," *Appl. Phys. Lett.*, vol. 95, no. 22, p. 314, 2009.

[18] S. Odhiambo, G. De Mey, C. Hertleer, A. Schwarz, and L. Van Langenhove, "Discharge characteristics of poly(3,4-ethylene dioxythiophehe):poly(styrene-sulfonate) (PEDOT:PSS) textile batteries; comparison of silver coated yarn electrode devices and pure stainless steel filament yarn electrode devices," *Text. Res. J.*, vol. 84, no. 4, pp. 347–354, 2014.

[19] S. Odhiambo, G. De Mey, C. Hertleer, and L. Van Langenhove, "Reliability Testing of PEDOT:PSS Capacitors Integrated Into Textile Fabrics," *Eksploat. Niezawodn. - Maint. Reliab.*, vol. 16, no. 3, pp. 447–451, 2014.

[20] A. Elschner, S. Kirchmeyer, W. Lovenich, U. Merker, and K. Reuter, *PEDOT: Principles and Application of an Intrinsically Conductive Polymer*. USA: CRC Press, 2011.

[21] X. Crispin *et al.*, "The origin of the high conductivity of poly(3,4-ethylenedioxythiophene)-poly(styrenesulfonate) (PEDOT-PSS) plastic electrodes," *J Mater Chem A*, vol. 18, no. 18, pp. 4354–4360, 2006.

2

Recent Progress on Textile-Based Energy Storage Devices from PEDOT:PSS and Other Electroactive Materials: A Critical Review

Advanced Energy Materials, Volume: 6, Issue: 22, First published: 27 July 2016, DOI: (10.1002/aenm.201600783)

2.1 Introduction

E-textiles (electronic textiles) or smart textiles have emerged as a new generation of technology which is driven mostly by the recent developments in electronics. Depending on the perspective, it can be viewed as an electronic device in the form of textile or it can be looked upon as textiles with electronics and electrical functionality. Either way, in their most advanced form, e-textiles or smart textiles are products of hybridization of electronics and textiles which seamlessly integrate to each other in one platform. Basically, such textiles consist of fabric – woven, knitted as well as nonwoven, that provides advanced functions in the form of electronic features or interconnection with the ability to automatically sense and respond to their environmental stimuli in a useful and predictable manner as well as to use the information to adjust the systems' configuration and functionality, which shows the form of an advanced dynamic adaptability. One of a few examples for the latter is the so-called "bionic bra" developed by Gordon Wallace and his team of researchers at the University of Wollongong (Australia). It is a sports bra that responds to the breast movement in an adaptive manner. With the new sensing and actuator technologies the bra is capable of instantly tightening and loosening its straps or stiffening cups when it detects excessive movement [1], [2].

According to the way they perceive and respond to their environment, smart textiles can be divided into passive smart, active smart and very smart materials. Passive smart materials can only sense the environmental conditions or stimuli; active smart materials will sense and react to the conditions or stimuli; very smart materials can sense, react and adapt themselves accordingly [3], [4]. An even higher level of intelligence can be achieved from those intelligent materials and structures capable of responding or activated to perform a function in a manual or pre-programmed manner [3].

The words "E-textiles" and "smart textiles" have been used interchangeably

in literature. However, it must be noted that the two terminologies are not by themselves interchangeable and can only be used one for another under the assumption that the system exhibits the elements of intelligence described above. Otherwise, it would be just textiles with electronic functions and interconnectivity and this is not necessarily smart. On the other hand, it is also noteworthy that smart textiles are not always based on electronics because they can also be built on, made of or effected by smart materials, e.g. stimuli responsive polymers.

Compared with other flexible materials such as paper, plastic and even metal sheets or wires, textiles are particularly interesting for the most part because of their versatility and unique mechanical properties such as lightweight, flexibility and most importantly wearable [5]. Textiles have not only become the ideal supporting substrate but also the promising components for smart wearable electronics themselves. They outweighed the other flexible substrates because they also offer the most in terms of their versatility of processing in the fabrication of devices, feasibility for integration into various areas such as clothing, household and even medical and building areas, and integration into existing wearable products with minimum disruption [5].

Depending on how the interconnectivities are formed on textile substrate, E-textiles or smart textiles can be categorized into two types: (1) classical, where the electronic components are embedded into garments and (2) integrated, where the electronic components are directly integrated into textile substrates [6], [7]. **Figure 2.1** shows an example of classical smart textiles and gives an idea about the current development stage of smart textiles in general, i.e. an organic LED [8] was embedded in a knitted T-shirt. In integrated smart textiles, the electronic components become part of the textile which among others may take the form of conductive yarns being woven or knitted into fabric structure or printed design on fabric surface that provide connectivity, film coating of solid electrolyte for energy

device, or even embroideries that act as sensors.

Figure 2.1. Organic LED threads embedded into knitted structure [8].

Fashion world and sportswear brands have been quick to adopt this technology [1], [9], [10]. CuteCircuit[1], for example, is a London-based luxury fashion brand founded by Francesca Rosella and Ryan Genz in 2004 with a vision of bringing electronics textiles and wearable technology into the world of high fashion. According to the co-founder, Francesca Rosella, as quoted by Forbes[2], it is the first wearable technology fashion brand. They have produced a series of innovative products such as HugShirt™, which was quoted to be the first haptic telecommunication garment and awarded one of the Best Inventions of the Year by

[1] http://cutecircuit.com/. Accessed March 9, 2019.
[2] https://www.forbes.com/sites/kittyknowles/2018/03/29/cutecircuits-fantastic-fashion-tech-world-firsts/#50d408ec1ee6. Accessed March 9, 2019.

Time Magazine in 2006, Galaxy Dress and Soundshirt to name a few examples. The latter has been evolved from HugShirt™ and became the first haptic garment that allows a deaf person to feel and interact with music and experience a live symphony orchestra by senses on their skin. The Soundshirt features 16 micro-actuators embedded in the fabric of the garment that receive wirelessly and in real-time the music, transformed in data and captured on stage, while the orchestra is playing. It represents partially integrated smart textiles because there are no wires and all of the conductive pathways within the garment are composed of woven conductive textiles that are seamlessly integrated into the fabric of the garment. Both HugShirt and Soundshirt were quoted to be rechargeable and washable. **Figure 2.2 a-c** show HugShirt™ and Soundshirt respectively.

In sportswear, big brands such as Adidas, Nike, Under Armour to name just a few examples have been focusing attention on smart fibres and fabrics for performance athlete sportswear. For example, in 2008, Adidas bought Textronics®, a team of experts in the fields of textiles and electronics to design sportswear using the latest fabric technologies [1]. Their designs have utilized conductive fibers and piezoelectric/piezoresistive polymer coating, that exhibits changes in electrical conductivity as the material is stretched, as soft textile sensors that capture the electrical activity or the mechanical movements of the body. These polymers, with variable resistance properties, can behave as strain gauges, switches and sensors to track and capture a materiality of movement. The current focus of sportswear brands has shifted from functional textiles such as comfort and protection to fabric technologies that extend the fabric capacity for computation and data collection for better performance of an athlete or health monitoring. The idea behind it is to make sportswear a data space with the body as data-generating device. The captured data can then be used to evaluate and improve the performance of an athlete. However, at present, smart shirts often still need some data storage capacity as the fabric itself does not have computing power. Pieces of hardware are still necessary, but they

are now available in miniaturized and flexible forms [1], which can be detached from the garments when washed although it may make the product less attractive due to the troubles of detaching and re-attaching the components.

(a)

(b)

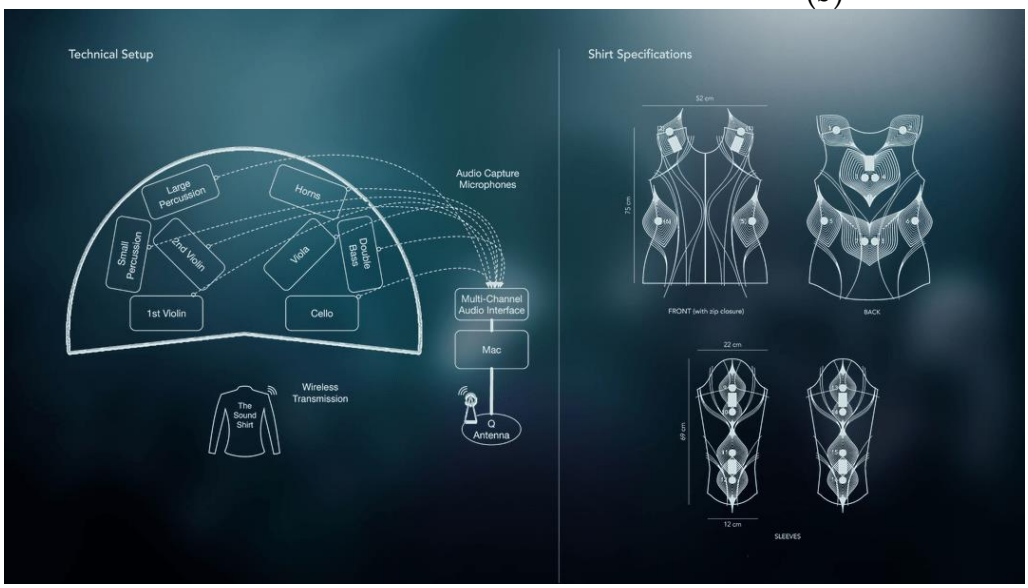

(c)

Figure 2.2. HugShirt© (a) and Soundshirt© garment (b) and (c) its schematic technical design.

Key areas that need innovative improvements include: (1) materials that are more flexible in order to align with the dynamic shapes of the body; and (2)

contextually-driven and adaptive interfaces which will become more intuitive with the actions of the body and eventually begin to disappear [1]. In a fully seamlessly integrated smart textiles, not only all the components are integrated but the boundaries between the electronics and textile become nonexistent. The fibers and the fabric are not only the platform but are the device themselves. **Figure 2.3** shows the visualization of the technology concept where some of the smart functions are indicated, i.e. electrochemical energy storage, external communication, internal data transfer via conductive path created by conductive yarns or conductive coating, and sensors. Other main functions of smart textiles that are not shown in **Figure 2.3** are data processing units and actuators which can be seen in **Figure 2.4**.

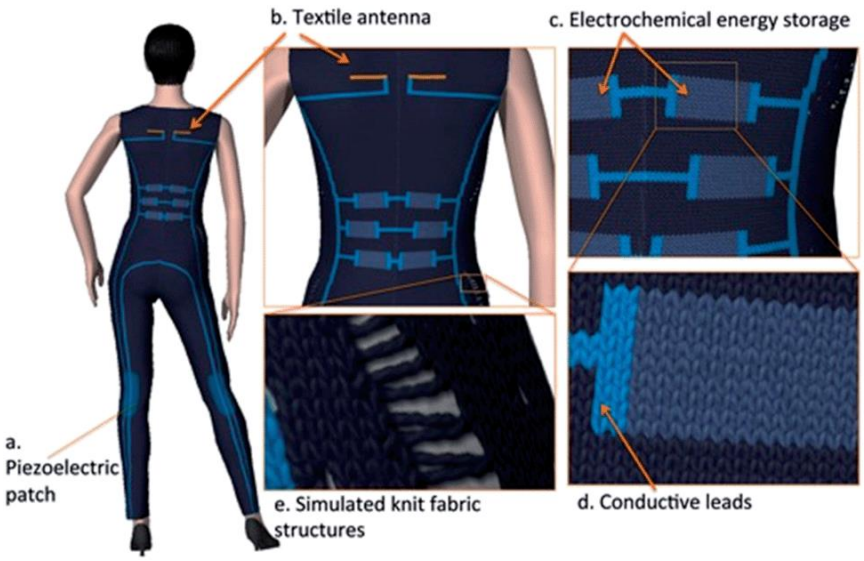

Figure 2.3. Seamless integration of electronics in textile structure by knitting and coating. [6]

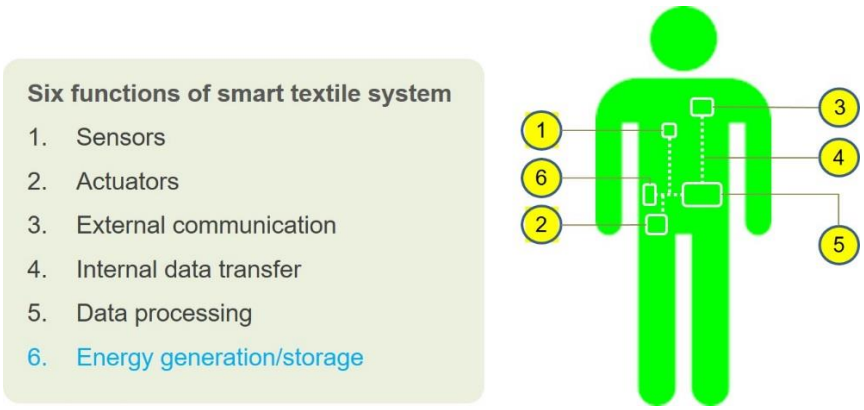

Figure 2.4. Main functions of smart textiles.

In order to ensure that all the main functions and their extended functionalities perform whenever we need, energy harvesting and storage devices with the merits of lightweight, flexibility, and high energy/power performance are highly required [5], [7]. Recent comprehensive surveys and reviews have appeared in the literature covering the last ten years of development of textile-based electrochemical energy devices with in-depth discussion on material characteristics, electrode fabrication, device performance, criteria metrics, and scalability [5], [7], [11]–[16]. Kaushik et al. [7] discussed in their review the development of various key components that are required for E-textiles, which include the materials and fabrication of conductive textiles and a survey on textile-based energy devices focusing on energy harvesting system based on human motion, solar cells on textiles, and fabric supercapacitors. Earlier on, Zeng et al. [12] have also contributed a critical review of the state-of-art of fiber-based wearable electronic products with respect to materials, fabrication techniques, and structural design of devices as well as their applications. They also elaborated the performance requirements of the fiber-based wearable electronic products, especially regarding the correlation among materials, fiber/textile structures and electronic as well as mechanical functionalities of fiber-based electronic devices. Additionally, limitations of current materials, fabrication techniques, manufacturability and performance as well as scientific understanding that must

be improved prior to their wide adoption were also elucidated.

A review by Wang et al. [15] appeared in literature and specifically focused on fiber electrodes and flexible fiber energy storage devices containing solid-state supercapacitors (SCs) and lithium-ion batteries (LIBs) with particular emphasis on electrode fabrication, structure design and flexibility. In addition, they also specifically highlighted the emerging wire-shaped integrated energy systems, combined energy storage and solar cells, as well as other electronic devices to realize self-charging and self-powered integrated systems. Some groups of authors [5], [11], [16] reported the development of numerous fiber and planar-shaped electrochemical energy storage devices with promising electrochemical and mechanical performances on a large variety of different flexible substrates such as metal sheets, papers, wires, plastic thin films, fibers and other forms of textile materials. One of the most recent surveys on the subject was given by Liu et al. [14] who also focused on supercapacitors, lithium ion batteries (LIBs) and some other representative battery systems. Challenges and perspectives for future development were also critically discussed.

An extensive list of selected works by [11] that were discussed in the above cited reviews is reproduced in **Table 2.1** to show the breadth of the topics and scope that have been covered and discussed pertaining to the materials used, designs and configurations, and how the electrical energy is stored in the device. The table is preserved in its original form as in [11] including the citation number of the references to make it easy for the readers to follow. Altogether, these reviews have provided a comprehensive embodiment of the state-of-art and the development of textile-based energy storage which provided the basis as well as a framework for a more focused review dedicated specifically to the recent progress of TESD from PEDOT:PSS conductive polymer that forms this chapter.

Tabel 2.1. Summary of textile supercapacitors using existing textiles [11].

Current collector	Textile substrate	Electrode material	Deposition method	Electrolyte	Capacitive performance	Ref.
Textiles coated with conductive carbon nanomaterials as current collectors						
SWCNT coated textile (1 Ω/sq)	Cotton and polyester	SWCNT (8 mg/cm^2) or SWCNT (0.24 mg/cm^2)/MnO_2 (1.6 mg/cm^2)	Dip/dry, electrodeposition	1 M $LiPF_6$	480 mF/cm^2 @ 200 μA/cm^2	[14]
				2 M Li_2SO_4	410 mF/cm^2 @ 20 μA/cm^2	
SWCNT coated textile	Cotton	SWCNT (0.47 mg/cm^2)	Dip/dry	2 M Li_2SO4	33.6 mF/cm^2 @ 10 μA/cm^2	[15]
SWCNT coated textile (10 Ω/sq)	Polyester	SWCNT (0.2 mg/cm^2)/MnO_2 8.3 mg/cm^2	Dip/dry, electrodeposition	0.5 M Na_2SO_4	2800 mF/cm^2 @ 0.05 mV/s	[16]
SWCNT coated textile (30 Ω/sq)	Paper/polyester	SWCNT/MnO_2/SWCNT	Dip/dry, electrodeposition	1 M Na_2SO_4	327 F/g @ 10 mV/s	[17]
SWCNT coated textile (30% elongation)	Polyester and cotton	SWCNTs (0.065/cm^2)/MnO_2	Dip/dry, electrodeposition	1 M Na_2SO_4	85.7 F/g or 142 F/g @ 200 mA/g	[18]
SWCNT coated textile (850 Ω/sq)	Cotton	SWCNT (0.065 mg/cm^2), MnO_2, PPy* (70 nm)	Dip/dry, electrodeposition	PEO gel	461 F/g @ 0.2 A/g	[19]
MWCNT coated textile	Cotton	MWCNT (0.25 mg/cm^2)/MnO_2 (3.5 mg/cm^2)	Dip/dry, electrodeposition	1 M Na_2SO_4	247 F/g @ 1 A/g	[20]
MWCNT coated textile	Cotton	MWCNT/$Co(OH)_2$	Dip/dry, hydrothermal synthesis	3 M KOH	11220 mF/cm^2 @ 15 mA/cm^2	[21]
Graphene coated textile (700 Ω/sq)	Polyester	Graphene, MnO_2 (0.25 mg/cm^2)	Dip/dry, electrodeposition	0.5 M Na_2SO_4	315 F/g @ 2 mV/s	[22]
rGO coated textile (0.5 Ω cm)	Electrospun polyamide-66 nanofiber textile	rGO sheets (250–450 nm) 3.36 mg/cm^2)	Dip, hydrazine reduction	1 M H_2SO_4	931 mF/cm^2 and 213 mF/cm^2 @ 0.5 A/g	[23]
rGO coated textile (560 Ω/sq)	Cotton	GO (9.3 wt%)	Dip/dry, $NaBH_4$ reduction	1 M Na_2SO_4	40 F/g at 5 mV/s	[24]
Textiles coated with conductive polymers as current collectors						
PPy coated textile (149 Ω/sq)	Nylon lycra	PPy (6.36 wt%)	*In situ* polymerization	1.0 M NaCl	123.3 F/g @ 10 mV/s	[25]

Current collector	Textile substrate	Electrode material	Deposition method	Electrolyte	Capacitive performance	Ref.
Lignosulfonate doped PPy coated textile (3.03 S/cm)	Cotton	PPy and lignosulfonate (26.6 wt%)	*In situ* polymerization	2.0 M NaCl	304 F/g @ 0.1 A/g	[26]
Ppy/CuO coated textile (10 S/cm)	Cotton	CuO (0.5 g/0.4 g fabrics) PPy (53 wt%)	*In situ* polymerization	2.0 M NaCl	225 F/g at 0.6 mA/cm^2	[27]
rGO and PPy coated textile (1.2 S/cm)	Cotton	GO, PPy (1.5 mg/cm^2)	Dip/dry, 250 °C, *in situ* polymerization	2.0 M NaCl	336 F/g at 0.6 mA/cm^2	[28]
Carbon fiber textiles as current collectors						
Carbon fiber textile	Carbon fiber	Ni–Co layered double hydroxide/ZnO nanowires (0.98 mg/cm^2)	Hydrothermal synthesis	6 M KOH	1927 F/g @ 2 A/g	[29]
Carbon fiber textile	Carbon fiber	$NiCo_2O_4$ nanowires	Hydrothermal synthesis	6 M KOH	1010 F/g @ 20 A/g	[30]
Carbon fiber textile	Carbon fiber	$CuCo_2O_4$@MnO_2 (1.8 mg/cm^2)	Hydrothermal synthesis	PVA/KOH	714 mF/cm^2 @ 1 mA/cm^2	[31]
Carbon fiber textile	Carbon fiber	MnO_2 (2.86 nmol) WO_3 (0.94 nmol)	Electrodeposition	0.5 M Na_2SO_4 gel	334.7 F/g @ 1 A/g, 283.9 F/g at 0.2 A/g	[32]
Carbon fiber textile (60 Ω/cm^2)	Carbon fiber	MWCNT (28.7 wt%), graphene (2.1 wt%)	Impregnation and freeze-drying in liquid N_2	6 M KOH	3350 mF/cm^2	[33]
Carbon fiber textile	Carbon fiber	Carbon nanoparticles/MnO_2 (0.562 mg/cm^2)	Flame synthesis, electrodeposition	PVA/H_3PO_4 gel	6.1 mF/cm^2 @ 5 mV/s 109 mF/cm^2	[34]
Carbon fiber textile	Carbon fiber	WO_{3-x}@Au@MnO_2 core–shell nanowires	Physical evaporation deposition, sputtering, electrodeposition	3 M KOH / PVA–H_3PO_4 gel	588 F/g at 10 mV/s	[35]
Carbonized cotton textiles as current collectors						
Carbonized cotton textile (10–20 Ω/sq)	Cotton	MnO_2	Carbonization (1000 °C), electrodeposition	1 M Na_2SO_4	70.2 F/g @ 2 mV/s for carbon / 269.5 F/g @ 2 mV/s for carbon/MnO_2	[36]
Carbonized cotton textile (<5 Ω/sq)	Cotton	Carbonized cotton (0.5 mm)	Carbonization (1000 °C), electrodeposition	1 M Na_2SO_4	0.7 mF/cm^2 @ 11.2 μA/cm^2	[37]
Carbonized cotton textile (10–20 Ω/sq)	Cotton	$NiCo_2O_4$ (2.63 mg/cm^2)	Carbonization (1000 °C), hydrothermal synthesis, in situ chemical deposition	PVA/KOH gel	1929 F/g @ 1 mA/cm^2	[38]

Current collector	Textile substrate	Electrode material	Deposition method	Electrolyte	Capacitive performance	Ref.
Textiles coated metals as current collectors						
Cu/Au coated textile	PET	MWCNT/Cu (0.2 μm)	Electroplating, dip/dry	PVA/H_3PO_4	4.312 mF/cm^2	[39]
		MWCNT/Au (0.2 μm)			3.683 mF/cm^2	
		MWCNT/Au/PANI			103 mF/cm^2 @ 1 mA/cm^2	
Cu coated textile	PET	β-$Co(OH)_2$ (45–55 nm)	Electrochemical deposition	1 M KOH	108.7 F/g @ 1 A/g	[40]
Ni/Cu/Ni/Au coated textile	Polyester	V_2O_5 anchored MWCNTs and graphene (3 nm)	Electroplating layer by layer assembly	2 M KCl	2590 F/g @ 1 mV/s	[41]
Ni/Cu/Ni/Au coated textile	Polyester	$Ni(OH)_2$ (2 nm)/ZnO nanowires	Hydrothermal synthesis	1 M LiOH	3150 F/g @ 5 mV/s	[42]
Au coated textile	Textile	Ni–Co double hydrides coated on ZnO nanoflakes (0.9 mg/cm^2)	Hydrothermal synthesis	1 M LiOH	1624 F/g @ 10 A/g	[43]
Au coated PET textile	PET	PAAMPSA	Drop casting	2 M H_2SO4 1 M Na_2SO_4	190 mF/cm^2 and 210 mF/cm^2 @ 20 mV/s	[44]
Metals as current collectors						
Stainless steel sheets	Woven cotton and polyester	Activated carbon (4 mg/cm^2) or carbon onions	Screen printing	1 M Na_2SO_4 2 M Li_2SO_4	430 mF/cm^2 @ 1 mV/s	[45]
Ni foam	Cotton	GO (1.08 mg/cm^2, 225 Ω/cm)	Brush/dry, 300 °C in Ar	6 M KOH	81.7 F/g	[46]
Ni foam	Flax	MnO_2+carbon (5.04 mg/cm2)	Carbonization (1000 °C), *in situ* chemical deposition	0.1 M Na_2SO_4	683.7 F/g @ 2 A/g	[47]
rGO coated textile in strips connected to copper foil	Cotton	rGO (2.15 mg/cm^2)	Dip and dry, 300 °C in Ar	6 M KOH	87.53 mF/cm^2 @ 2 mV/s	[48]

A brief introduction about energy storage and textile-based energy storage devices is presented in the first part of the review. Then it continues with an elaboration on the properties of PEDOT:PSS which includes chemical and physical properties, electrical and electronic properties, morphology and transport properties and forms the basis for scientific understanding of the roles the conductive polymer is playing in the storage of energy and for the search of the mechanisms behind it. A solid understanding of the working principles of the device and the mechanisms of energy storage is crucial for the improvement of device performance. In light of this argument, different mechanisms of charge transport and its correlation with the storage of energy and performances are discussed to address the subject matter. Additionally, the review will also highlight the fabrication techniques and structural design of the device. The review will end with a discussion on different models and constructions of TESD particularly with respect to the possibility of designing a seamlessly integrated textile that incorporates all the current collecting, electrodes, separator and electrolyte materials in one piece of fabric or clothing.

2.2 Textile-Based Energy Storage Devices

2.2.1 Energy Storage Systems: The Basics

Basically, there are two fundamental ways in which electrical energy can be stored [17]. First, it is stored indirectly in batteries as potentially available chemical energy in the active materials of the electrodes. It requires Faradaic oxidation and reduction of the electrochemically active reagents to release charges that can perform electrical work when they flow between two electrodes having different electrode potentials at the opposite poles of battery cells, which is why it is called Faradaic electrical energy storage. Secondly, electrical energy can be stored directly in an electrostatic way, as negative and positive charges on the plates of a capacitor, and thus a non-Faradaic electrical energy storage.

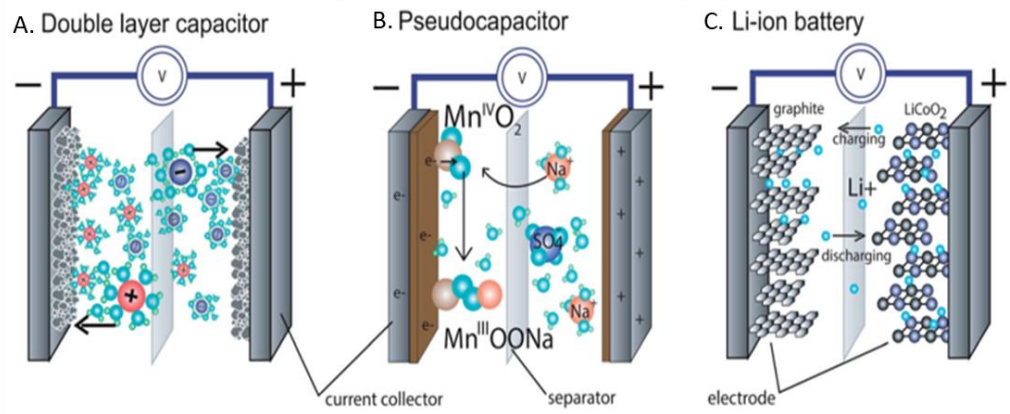

Figure 2.5. Energy storage devices: (A) EDLC, (B) pseudocapacitor), (C) lithium ion batteries (LIBs) (Reproduced from Ref [6]).

Generally, a battery provides a high energy density, but a low power density, and a limited cycle life. Conventional capacitors, which include both electrostatic and electrolytic capacitors, on the other hand, offer a high-power density, but a very low energy density. Supercapacitors or electrochemical capacitors bridge the gap between conventional capacitors and batteries, providing a high-power density and a reasonable energy density. Shown in **Figure 2.5** is a series of basic energy storage systems that comprises of batteries, conventional capacitors, and supercapacitors or electrochemical capacitors (which include electric double layer capacitors or EDLCs and pseudocapacitors). **Table 2.2** and **Table 2.3** below compares the basic characteristics of the three forms of energy devices [18] and summarizes the energy storage systems and their mechanisms in storing the charge [17] respectively.

Table 2.2. Main characteristics of electrolytic capacitors, supercapacitors (EDLCs), and batteries. [18]

	Nature of energy storage	Charge time	Discharge time	Energy density (Wh/kg)	Power density (kW/kg)	Charge/Discharge efficiency (%)	Cycle life
Batteries	chemical	1-5 h	0.3-3 h	20-100	0.5-1	50-90	500-2000
Supercapacitors (EDLCs)	physical	1-30 s	1-30 s	1-10	5-10	75-95	> 500,000
Electrolytic capacitors	physical	10^{-6}-10^{-1} s	10^{-6}-10^{-1} s	< 0.1	≈ 10	≈ 100	infinite

Table 2.3. Types of capacitors and battery and their modes of energy storage. [17]

Type		Basis of charge or energy storage	Examples
Capacitors	**Vacuum**	Electrostatic	-
	Dielectric	Electrostatic	Mica, Mylar, paper
	Oxide electrolytic (thin film)	Electrostatic	Ta_2O_5, Al_2O_3
	Double layer	Electrostatic (charge separation at double-layer at electrode interface)	C preparations, powders, fibers
	Colloidal electrolyte	Electrostatic (special double-layer system)	Undeveloped
	Redox oxide film	Faradaic charge transfer (pseudocapacitance)	RuO_x, IrO_x, Co_3O_4
	Redox polymer film	Faradaic charge transfer (pseudocapacitance)	Polyaniline, polythiophenes
	Soluble redox system	Faradaic charge transfer (pseudocapacitance)	$Fe(CN)_6^{4-}$, $-F(CN)_6^{3-}$, $V^{2+}/V^{3+}/VO^{2+}$
Batteries	**Primary**	-	Leclanche, zinc-MnO_2
		Faradaic	Alkaline, zinc-MnO_2 Mg-$AgCl_2$ Mg-$PbCl_2$ Li-$SOCl_2$ and other cathodes Li-CF_x Al-air (catalyzed) Zn-air (catalyzed)
	Secondary	Faradaic	Lead acid, $PbPbO_2$ Nickel-cadmium, Ni.O.OH-Cd Nickel-hydrogen, Ni.O.OH-metal hydride Nickel-zinc, Ni.O.OH-Zn Mercuric oxide-zinc, AgO-Zn Zinc-air (catalyzed)
		Faradaic (exhibiting intercalative pseudocapacitance)	Li-TiS_2 Li-MoS_2 Li-MnO_2 Li-CoO_2 Li-C-CoO_2 and other cathodes Li-iron sulfides Na-S

2.2.2 Components of Energy Devices

From **Figure 2.5**, it can be seen that there are at least three components that typically compose both supercapacitors and batteries: (1) two electrodes, (2) an electrolyte and (3) a separator. Electrodes can be either active materials attaching to current collectors or freestanding active materials, whose properties greatly affect and determine their energy storage capability. To date, various active materials, including carbon-based materials, transition metal oxides, conducting polymers, and their hybrids, have been used with different textile substrates and exhibited remarkable

electrochemical performances [5], [11]–[12], [16], [19].

For both supercapacitors and batteries, the electrolyte provides ionic conductivity allowing the movement of ions during charge and discharge events and thus facilitates charge compensation on each electrode in the cell. The electrolyte within a supercapacitor not only plays a fundamental role in the EDL formation (in EDLCs) and the reversible redox process for the charge storage (in pseudocapacitors) but also determines the supercapacitor performance. Compared to the number of reviews and research papers on electrodes, there were only few that discussed electrolytes for electrochemical supercapacitors.

2.2.2.1 Electrode Materials

In general, the electrode materials of electrochemical supercapacitors (ES) can be categorized into three types [19], [20]: (1) carbon materials with high specific surface area, (2) faradaic materials or conducting polymers, and (3) metal oxides, such as RuO_2, IrO_2, MnO_2, NiO, Co_2O_3, SnO_2, V_2O_5, and MoO. The advantages of carbon materials include abundance, lower cost, easy processing, non-toxicity, higher specific surface area, good electronic conductivity, high chemical stability, and wide operating temperature range making them prospective electrode materials for industrialization [19]. As shown in **Figure 2.6.a**, cyclic voltammetry (CV) curves of carbon materials have good rectangular shapes, suggesting appropriate materials with strong capacitive performance for ES. **Figure 2.6.b** shows their galvanostatic charge–discharge (GCD) profile, with its triangular symmetrical distribution, also indicative of good capacitive properties for ES [21]. The capacitive performance and some physical properties of various carbon and carbon-based electrode materials are summarized in **Table 2.4**, which is based on a literature survey done by L. L. Zhang and Zhao [22].

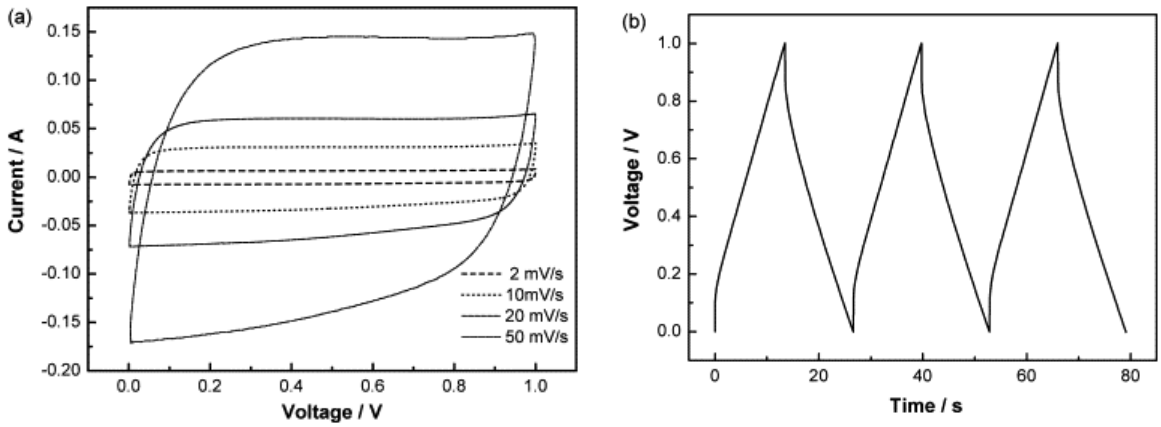

Figure 2.6. (a) Cyclic voltammetry of activated carbon fiber cloth electrode at different scan rate; (b) Charge–discharge curve of activated carbon fiber cloth electrode recorded at 180 mA (~5000 mA g^{-1}). [21]

Table 2.4. Properties and characteristics of various carbon and carbon-based materials as supercapacitors electrode materials [22].

Materials	Specific surface area/m^2 g^{-1}	Density/g cm^{-3}	Aqueous electrolyte /F g^{-1}	Aqueous electrolyte /F cm^{-3}	Organic electrolyte /F g^{-1}	Organic electrolyte /F cm^{-3}
Carbon materials						
Commercial activated carbons (ACs)	1000–3500	0.4–0.7	< 200	< 80	< 100	< 50
Particulate carbon from SiC/TiC	1000–2000	0.5–0.7	170–220	< 120	100–120	< 70
Functionalized porous carbons	300–2200	0.5–0.9	150–300	< 180	100–150	< 90
Carbon nanotube (CNT)	120–500	0.6	50–100	< 60	< 60	< 30
Templated porous carbons (TC)	500–3000	0.5–1	120–350	< 200	60–140	< 100
Activated carbon fibers (ACF)	1000–3000	0.3–0.8	120–370	< 150	80–200	< 120
Carbon cloth	2500	0.4	100–200	40–80	60–100	24–40
Carbon aerogels	400–1000	0.5–0.7	100–125	< 80	< 80	< 40
Carbon-based composite materials						
TC–RuO_2 composite	600	1	630	630	—	—
CNT–MnO_2 composite	234	1.5	199	300	—	—
AC–polyaniline composite	1000	—	300	—	—	—

Since carbon materials store charges mainly in an electrochemical double-layer formed at the interface between the electrode and the electrolyte, the capacitance predominantly depends on the surface area accessible to the electrolyte ions. Therefore, important factors influencing their electrochemical performance are specific surface area, pore size distribution, pore shape and structure, electrical conductivity, and surface functionality [19]. As suggested by Conway [17], the carbon for double-layer type supercapacitors must have three properties: (1) high specific areas, in the order of 1000 m^2 g^{-1}, (2) good intra- and interparticle conductivity in

porous matrices, and (3) good electrolyte accessibility to the intrapore space of carbon materials. In order to optimize overall capacitance and conductivity without compromising stability, it is believed that the development of carbon electrodes must be directed for higher specific surface area, rational pore distribution, and moderate surface modification [19], [22]. **Figure 2.7** shows the SEM images of carbon coated cotton and polyester fabric for electrochemical supercapacitors and their corresponding cyclic voltammograms.

Supercapacitors made of redox-active materials bearing pseudocapacitance generally have specific capacitance 10-50 times greater than EDLCs. This kind of material is generally classified into two types: (1) conducting polymers and (2) electroactive metal oxides. Conducting polymers are suitable materials for ES because they have high voltage window, high conductivity in a doped state, high storage capacity and porosity as well as reversibility and adjustable redox activity through chemical modification [19], [24]. Additionally, they are low cost and have low environmental impact. Their higher capacitance is a result of redox reaction throughout the bulk of material, not just on the surface, that leads to greater amount of stored charge and reduced self-discharge [19], [24]. One significant drawback of these materials is the relatively low power (or lower rate of charge–discharge) due to the slow diffusion of ions within the bulk of the electrode [24].

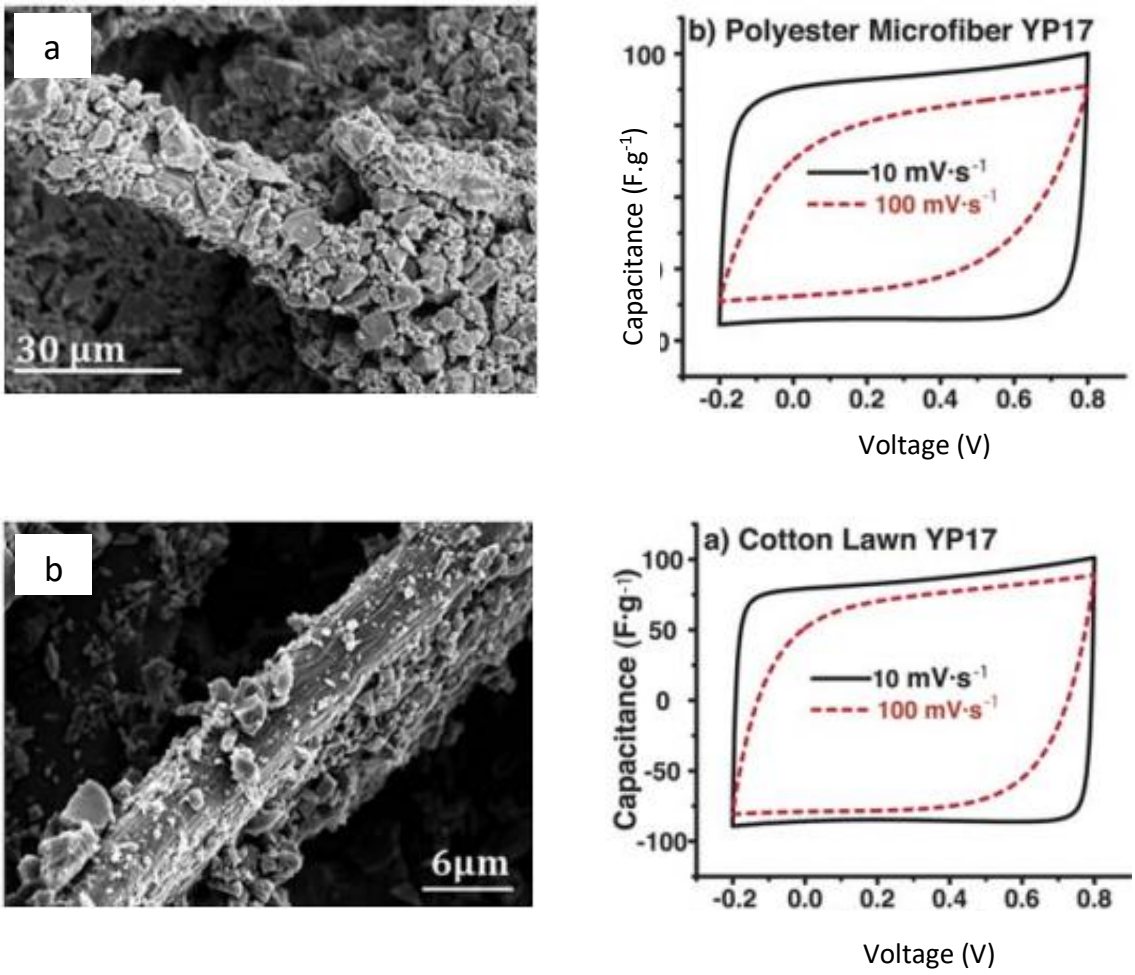

Figure 2.7. SEM images of carbon coated (a) polyester microfiber and (b) cotton lawn and their corresponding cyclic voltammetry tested in 1 M Na_2SO_4, at 10 and 100 mV.s^{-1}. Polyester microfiber tested in 1 M Na_2SO_4 shows more resistive behavior compared to cotton. [23]

Intrinsically conducting polymers (ICPs) are rendered conductive through a conjugated bond system along the polymer backbone. They are typically formed either through chemical or electrochemical oxidation of the monomer. Two oxidation reactions occur simultaneously – the oxidation of the monomer and the oxidation of the polymer with the coincident insertion of a dopant/counterion. The dopant or doping level (in this p-type conducting polymer) is typically below 1 dopant per polymer unit: approximately 0.3–0.5, i.e., 2–3 monomer units per dopant [24]. This is limited by how closely the positive charges (so-called polarons) can be spaced along

the polymer chain. The typical dopant level for these polymers, as well as their typical specific capacitances and voltage ranges, are given in **Table 2.5**. The polymers that are most commonly studied for use in supercapacitor devices are (1) polypyrrole, (2) derivatives of polythiophene, and (3) polyaniline (**Figure 2.8**).

Table 2.5. Theoretical and experimental specific capacitances of conducting polymers.

Conducting polymer	MW (g mol^{-1})	Dopant level	Potential range (V)	Theoretical specific capacitance (Fg^{-1})	Measured specific capacitance (Fg^{-1})
PANI	93	0.5	0.7	750	240
PPy	67	0.33	0.8	620	530
PTh	8	0.33	0.8	485	-
PEDOT	142	0.33	1.2	210	92

Further, they can be positively or negatively charged with ion insertion in the polymer matrix to balance the injected charge, a process called "doping". The positively-charged polymers, introduced by oxidation on the repeating units of polymer chains, are termed as '*p*-doped', while negatively-charged polymers generated by reduction are termed as '*n*-doped'. The potentials of these doping processes are determined by the electronic state of π electrons. Electronic conductivity can thus be induced in such a kind of polymers by oxidation or reduction reactions, which generate delocalized '*n*' electrons on the polymer chains. Pseudo-capacitors made entirely from conducting polymer electrodes can have one of three possible configurations [19], [24]:

(1) Type I (symmetric). This type of ES is named as a *p*–*p* ES in which both electrodes use the same *p*-dopable polymer. When fully charged, one electrode is in the full *p*-doped (positive) state and the other in the uncharged state. The voltage window is 0.8–1 V;

(2) Type II (asymmetric). This type is a *p*–*p* ES. Two different *p*-dopable polymers with a different range of oxidation and reduction electroactivities are used, such as polypyrrole/polythiophene;

(3) Type III (symmetric). This is an *n*–*p* type ES. Electrodes are from the same polymer which can be both *p*- and *n*-doped in the same molecule, such as poly(3-fluorophenyl)thiophene. The voltage window is up to 3.1 V in nonaqueous solutions. Type III is considered a significant advance in conducting polymers-based ES in terms of materials design and the stored energy density.

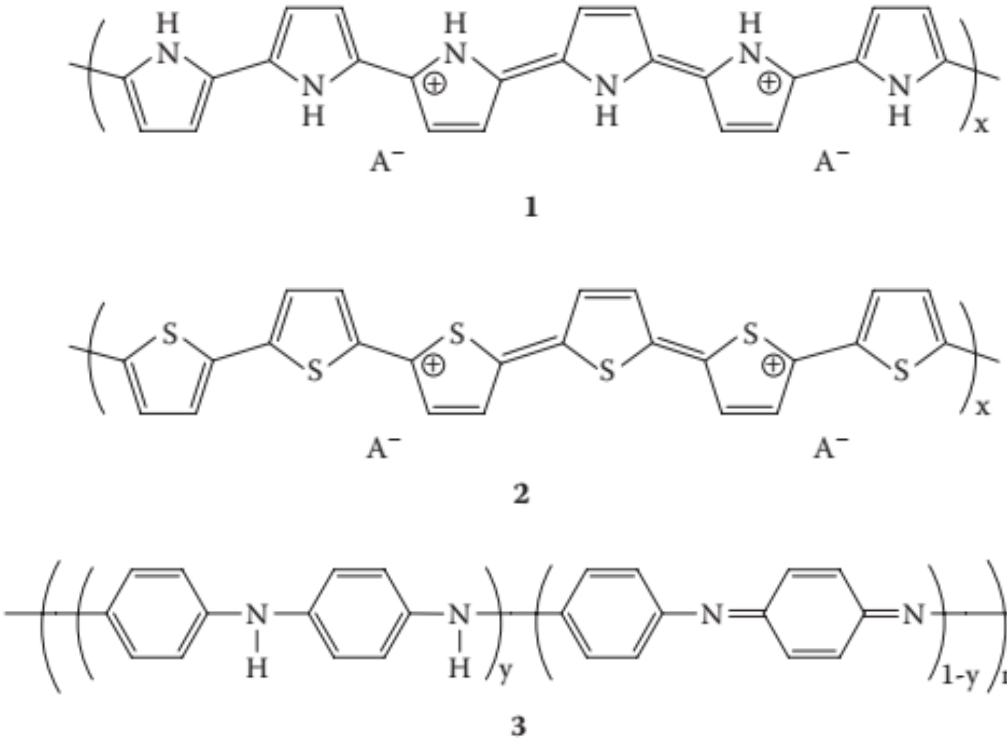

Figure 2.8. Three groups of intrinsically conducting polymers widely used in energy devices application: (1) polypyrrole, (2) polythiophene, and (3) polyaniline.

Table 2.6 highlights the main conducting polymers for ES applications and their composites with other materials showing their capacitances and voltage/potential windows. It should be noted that all conducting polymers have their own specific voltage window within which they can supply charge. Beyond this strict potential range, the polymer may be degraded at more positive potential, and as the potential is too negative, the polymer may be switched to an insulating state (un-

doped state) [19], [25]. Hence, the selection of a suitable potential range is crucial for the capacitor performance. From **Table 2.6** one can also see that the composite materials can give a wide distribution of capacitance values, which are also dependent on the parameters such as the constituents of composites, electrolytes used, scan rate, current load, and mass ratio of the components as well as cell configuration [19]. Additionally, the composite materials improve conductivity (particularly at the more negative/reducing potentials) and contribute for better cycleability, mechanical stability, and processability [24].

Table 2.6. Various conducting polymers composites and their electrochemical performances. [19]

CPs-based composite	Specific capacitance/F g^{-1}	Electrolyte	Voltage window/V	Current load or scan rate
Ppy-20wt%MWNTs/ PANI-20wt% MWNTs	320 (Type II)	1.0 M H_2SO_4	0–0.6	5 mV s^{-1}
PANI-20 wt% MWNTs	670 (3-Electrode)	1.0 M H_2SO_4	−0.8–0.4	2 mV s^{-1}
	344 (Type I)		0–0.6	
Ppy-20 wt% MWNTs	506 (3-Electrode)	1.0 M H_2SO_4	−0.6–0.2	5 mV s^{-1}
	192 (Type I)		0–0.5 (*vs.* Hg|Hg_2SO_4)	
PEDOT-Ppy (5 : 1)	230 (3-Electrode)	1.0 M $LiClO_4$	−0.4–0.6 (*vs.* SCE)	2 mV s^{-1}
	290 (3-Electrode)	1.0 M KCl	−0.4–0.6 (*vs.* SCE)	2 mV s^{-1}
	276 (Type I)	1.0 M KCl	0–1.0 (*vs.* SCE)	3 mA cm^{-2}
Ppy-CNTs//PmeT-CNTs	87 (Type II)	1.0 M $LiClO_4$ in AC	0–1.0	0.62 A g^{-1}
PPy-65 wt% carbon	433 (3-Electrode)	6.0 M KOH	−1.0–0(*vs.* Hg|HgO)	1 mV s^{-1}
Ppy-graphene	165 (Type I)	1.0 M NaCl	0–1.0	1 A g^{-1}
Ppy-MCNTs	427 (3-Electrode)	1.0 M Na_2SO_4	−0.4–0.6 (*vs.* Ag|AgCl)	5 mV s^{-1}
Ppy-29.22 wt% mica	197 (3-Electrode)	0.5 M Na_2SO_4	−0.2–0.8 (*vs.* SCE)	10 mA cm^{-2}
Ppy-67.36 wt% mica	103 (3-Electrode)			
Ppy-RuO_2	302 (3-Electrode)	1.0 M H_2SO_4	−0.2–0.7 (*vs.* Hg|HgO)	0.5 mA cm^{-2}
Ppy-MnO_2	602 (3-Electrode)	0.5 M Na_2SO_4	−0.5–0.5 (*vs.* Ag|AgCl)	50 mV s^{-1}
PANI-Ti	740 (3-Electrode)	0.5 M H_2SO_4	−0.2–0.8 (*vs.* Ag|Ag^+)	3 A g^{-1}
PANI-80wt% graphene	158 (3-Electrode)	2.0 M H_2SO_4	0–0.8 (*vs.* AgCl|Ag)	0.1 A g^{-1}
PANI-50wt% graphene	207 (3-Electrode)			
PANI-10wt% graphene	320 (3-Electrode)			
MPANI/CNTs	1030 (3-Electrode)	1.0 M H_2SO_4	−0.2–0.7 (*vs.* SCE)	5.9 A g^{-1}
PANI-Si	409 (3-Electrode)	0.5 M H_2SO_4	0–0.8 (*vs.* AgCl|Ag)	40 mA cm^{-2}
PEDOT-MCNTs (70 : 30)	120 (Type I)	1.0 M H_2SO_4		2 mV s^{-1}
	80	6.0 M KOH		
	60	1.0 M $TEABF_4$ in AN		
PEDOT-MCNTs (80 : 20)	160 (AC as the negative electrode)	1.0 M $TEABF_4$ in AN	0–1.5	0.2 A g^{-1}

Note: PPy: polypyrrole; PANI: polyaniline; Type I, II: defined by A. Rudge *et al.*;[139] PEDOT: poly(3,4-ethylenedioxythiophene); PTh: poly(thiophene); PMeT: poly(3-methylthiophene); PFPT: poly[3-(4-fluorophenyl)thiophene]; AN: acetonitrile; $TEABF_4$: tetraethylammonium terafluoroborate; PC: propylene carbonate; 3-electrode: standard 3-electrode cell; SCE: saturated calomel electrode; AC: activated carbon.

The third group of electrode materials, which is also faradaic/pseudo-capacitance materials, is metal oxides. In general, this group of materials can provide higher energy density for ES than conventional carbon materials and better electrochemical stability than polymer materials. They do not only store energy like electrostatic carbon materials but also exhibit electrochemical faradaic reactions between electrode materials and ions within appropriate potential windows. The

general requirements for metal oxides in ES applications are [19]: (1) the oxide should be electronically conductive, (2) the metal can exist in two or more oxidation states that coexist over a continuous range with no phase changes involving irreversible modifications of a 3-dimensional structure, and (3) the protons can freely intercalate into the oxide lattice on reduction (and out of the lattice on oxidation), allowing facile interconversion of $O_2 \leftrightarrow 2\ OH^{-1}$. To date, those investigated include ruthenium oxide, manganese oxide, cobalt oxide, nickel oxide, and vanadium oxide.

2.2.2.2 Electrolytes

As mentioned previously, the importance of electrolytes cannot be underestimated. Not only do they provide the ionic conductivity within the system, they also determine the supercapacitor performance which includes capacitance, energy/power density, thermal stability, cycle-ability, and equivalent series resistance (ESR), as well as their derived properties and qualities, as shown by **Figure 2.9**. Electrolytes are usually solutions with desired ionic conductivity. However, researchers are recently more and more focusing on the use of hydrogel electrolytes (quasi-solid-state) and solid-state electrolytes due to health and safety concerns over the use of liquid electrolytes for being toxic and flammable [26]. There are other considerations on the use of non-aqueous electrolytes such as high cost, low conductivity compared to aqueous electrolyte leading to power deterioration, low dielectric constant resulting in smaller capacitance, and complex purification procedure [22]. However, the real motivation for the switch from an aqueous electrolyte, which has a low operating voltage of 1 V (due to the thermodynamic decomposition of water), to a non-aqueous medium is due to the much higher voltage window possessed by the latter reaching up to about 2.5 V. As shown later by Equation (5), increasing the voltage is an effective strategy to increase energy density of ES because it is proportional to the square of voltage [26]. Additionally, the elimination of liquid may raise the cycle stability, avoid electrolyte leakage, and erase the necessity of separators [14].

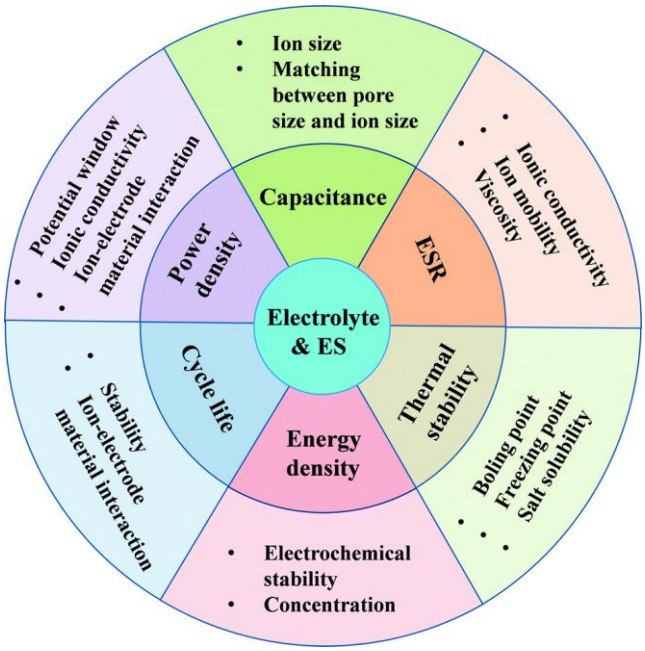

Figure 2.9. The effect of electrolyte on electrochemical capacitors performance (ES = electrochemical supercapacitors; ESR = equivalent series resistance [26].

Figure 2.10 shows the different types of electrolyte that are currently in use for electrochemical capacitors and their classification based on the material that comprises them. Electrolytes are mainly classified as liquid and solid/quasi-solid-state electrolytes. Liquid electrolytes can be further grouped into aqueous electrolytes, organic electrolytes and ionic liquids (ILs), while solid or quasi-solid state electrolytes can be broadly divided into organic electrolytes and inorganic electrolytes. The requirements for an ideal electrolyte include [26]: (1) a wide potential window; (2) a high ionic conductivity; (3) a high chemical and electrochemical stability; (4) high chemical and electrochemical inertness to ES components (e.g., electrodes, current collectors and packaging); (5) a wide operating temperature range; (6) well-matched with the electrode materials; (7) a low volatility and flammability; (8) environmentally friendly; and (9) a low cost. It must be noted, however, there has been no single electrolyte developed to date that meets all these requirements. Each has its own advantages and disadvantages as discussed in the following paragraphs [19], [26]. For example, while demonstrating both high conductivity and capacitance, ES using

aqueous electrolytes has limited working voltage due to the narrow decomposition voltage of aqueous electrolytes. Organic electrolytes and ILs can operate at higher voltages, but they normally suffer from much lower ionic conductivity, the same disadvantage shared by solid-state electrolytes despite the advantage they have in avoiding the potential leakage problem normally found with the liquid electrolytes. It is worth noting that our TESD is developed based on the use of PEDOT:PSS conductive polymer as an electrolyte while most studies used the polymer as active material and electrodes for the energy device system.

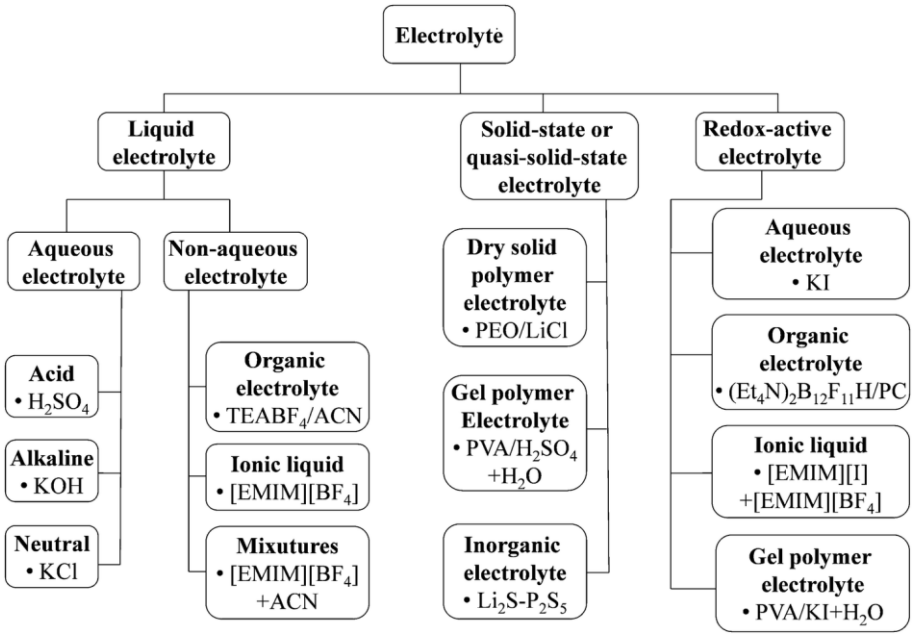

Figure 2.10. Different types of electrolytes for electrochemical capacitors and their classification [26].

2.2.3 Energy Storage Mechanisms in Electrochemical Supercapacitors

The fundamental difference between supercapacitors and batteries lies in the fact that energy is physically stored in a supercapacitor by means of ion adsorption at the electrode/electrolyte interface, hence the name electrical double-layer capacitors (EDLCs) [18]. Consequently, the EDLC has a specific capacitance that is proportional to the surface area of the electrode materials accessible to the electrolyte ions and

theoretically has an infinite lifetime. Electrode materials used for supercapacitors are thus required to have large specific surface area for ion adsorption, a suitable combination of micropores and mesopores for fast ion mobility, good electrical conductivity for electron transfer and surface wettability, and preferably favorable surface functionalities for pseudo-capacitance [11]. For those reasons, typical electrode materials for EDLCs are carbon and carbon derivatives, including activated carbon, porous carbon, ordered mesoporous carbon, carbon nanoparticle, carbon nanotube (CNT), carbon nanofiber, carbon microfiber, graphene, and reduced graphene oxide [16].

Pseudo-capacitors are another type of supercapacitors which are fundamentally different from EDLCs. Energy stored in a pseudo-capacitor is due to reversible surface or near-surface Faradaic reactions; thus, offering a higher specific capacitance, but a lower power density than the EDLCs. Transition-metal oxides such as MnO_2, $Ni(OH)_2$, TiN and electrically conducting polymers like polyaniline (PANI), polypyrrole (PPy), polythiophene (PTh), and poly(3,4-ethylenedioxythio-phene) (PEDOT) are typical electrode materials for pseudo-capacitors [16], [18]. However, these electrode materials suffer from problems such as high cost, low electric conductivity, and poor stability; this limits their applications as supercapacitor electrodes.

The mechanisms of energy storage for EDLCs and pseudo-capacitors are further described in the following paragraphs. The capacitance of the electrode/interface in an electrostatic or EDLCs is associated with an electrode-potential-dependent accumulation of electrostatic charge at the interface. The mechanism of surface electrode charge generation includes surface dissociation as well as ion adsorption from both the electrolyte and crystal lattice defects [19]. The electrical double-layer capacitance originates from electrode material particles, such as at the interface between the carbon particles and electrolyte, where an excess or a deficit of electric charges is accumulated on the electrode surfaces, and electrolyte ions

with counterbalancing charge are built up on the electrolyte side in order to meet electro-neutrality. During the process of charging, the electrons travel from the negative electrode to the positive electrode through an external load. Within the electrolyte, cations move towards the negative electrode while anions move towards the positive electrode. During discharge, the reverse processes take place. The charge-discharge mechanism of the double layer capacitor is described in **Figure 2.11**. In this type of ES, no charge transfers across the electrode/electrolyte interface, and no net ion exchanges occur between the electrode and the electrolyte. This implies that the electrolyte concentration remains constant during the charging and discharging processes. In this way, energy is stored in the double-layer interface.

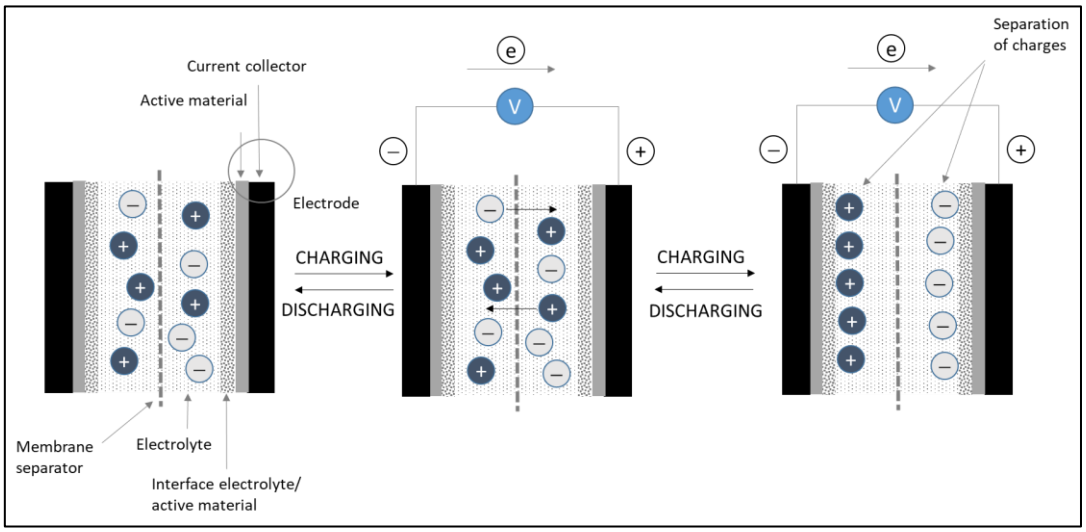

Figure 2.11. Charge-discharge mechanism of the double-layer capacitor

The processes that take place in a pseudo-capacitor is fundamentally different from those occurring in EDLCs. A fast and reversible redox reactions take place on the electrode materials when a potential is applied to a pseudocapacitor, followed by the passage of charge across the double layer, similar to the charging and discharging processes that occur in batteries, resulting in faradaic current passing through the supercapacitor cell [20]. Depending on the types of electrode materials, three types of faradaic processes occur at the electrodes: (1) reversible adsorption (for example, adsorption of hydrogen on the surface of platinum or gold), redox reactions of

transition metal oxides (e.g. RuO_2), and reversible electrochemical doping–dedoping in conductive polymer based electrodes [18]. As mentioned previously, since the electrochemical processes occur both on the surface and in the bulk near the surface of the solid electrode, a pseudo-capacitor in general exhibits far larger capacitance values and energy density than an EDLC.

At this point, it is worth noting that the two types of mechanisms may occur simultaneously with one being predominant over the other in the so-called hybrid supercapacitor where both types of electrode materials co-exist. In both mechanisms, large surface area, appropriate pore-size distribution, and high conductivity are essential properties of the electrode materials to achieve large capacitance.

2.2.4 Textile-Based Electrochemical Energy Storage Devices

Textile supercapacitors feature some attractive advantages including high power density, long cyclic life, decent energy density, wearability, and safety, making them promising candidates for next-generation wearable electronics [14] and it can come in at least two different shapes and configurations: one-dimensional fiber/yarn-shaped supercapacitors (FSS) and two-dimensional fabric- based supercapacitors (FBS). FSS are assembled primarily in four types of structures as shown in **Figure 2.12** and described below [16]:

a. Parallel type: Two fiber or yarn shaped electrodes (FSEs) are arranged side by side in parallel at a predetermined distance with a separator and electrolyte between them.
b. Twisting type: Two FSEs are twisted together with a separator and electrolyte between them.
c. Coaxial type: A core FSE is wrapped by another electrode with a separator and electrolyte between them.
d. Consecutive type: Two FSEs are assembled in series, i.e. in an end-to-end configuration to each other with a separator between them and covered by

electrolyte.

e-h. Fabric-shaped electrodes and different approached in the fabrication of fabric-shaped supercapacitor.

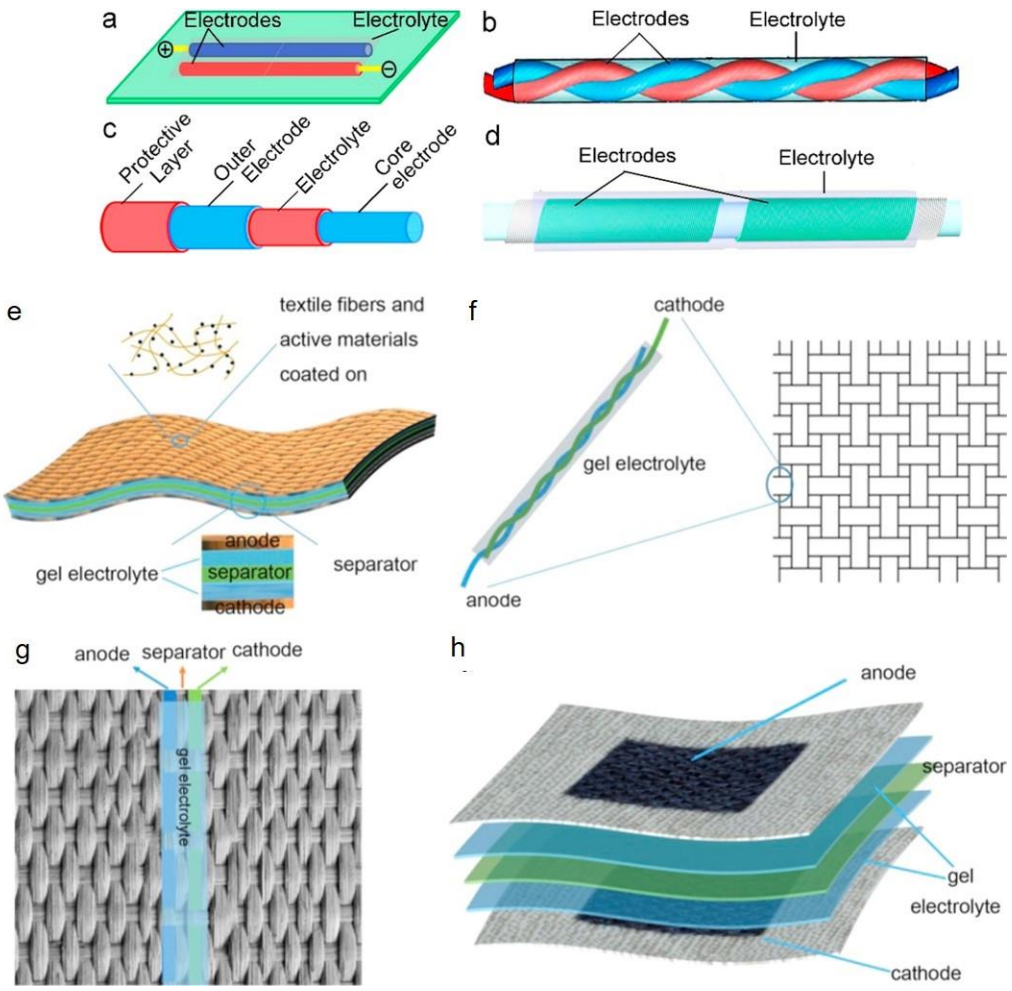

Figure 2.12. Schematic diagrams showing fiber/yarn-shaped in different structures and configuration: (a) parallel, (b) twisting, (c) coaxial, (d) consecutive and fabric-shaped electrodes and different approaches in the fabrication of fabric-shaped supercapacitors (e-h) [11], [16].

It is well known that the capacitance of a supercapacitor correlates to the accessible amount of active materials and the face-to-face area of the two adjacent electrodes within certain distance. This requires that active material must be accessible to electrolytes and thus must not be embedded in the electrodes unless it is accessible.

Regardless of the types of FSS, the two electrodes should be as close as possible to each other without any direct contact even when put under the flexible deformations normally occuring during the actual use. Based on these considerations, a brief comparison of the four types of FSS in **Figure 2.12** is given below [27].

Type (a) usually needs a flat substrate to support the two parallel electrodes (**Figure 2.12.a**). The distance between electrodes is easily controlled with minor risk of short circuit but the utilization efficiency of electrode materials is very limited due to the minimum confronting area of the two parallel FSEs, which may hinder storage capability. In one alternative configuration, the parallel FSEs are enclosed in a plastic tube filled with electrolyte and are separated by a helical spacer wire being wound on one of the FSEs [28]. In order to increase the confronting area of the two electrodes and improve the storage capability, the two parallel FSEs can be wound on a fiber scaffold [29] or they can also be arranged in parallel spiral forming a coiled fiber supercapacitors having an additional potential capacitance from non-adjacent opposite electrodes (**Figure 2.13**). The latter explains the superior electrochemical properties exhibited by the coiled fiber supercapacitor as shown by the cyclic voltammetry diagrams of straight and coiled configuration of electrodes (**Figure 2.13**).

Type (b) has two FSEs twisted together without using the auxiliary substrate (**Figure 2.12.b**). The practicality and specific performance will be improved, but the risk of short circuit is increased too. In type (c), with a core electrode and an outer shell electrode (**Figure 2.12.c**), the large surface area of electrodes facing to each other concentrically gives result to high utilization of electrode materials and thus a better capacitance performance. However, it must be noted that it has a high risk of short circuit. FSCs in type (d) may have a problem in full utilization of active materials due to the long distance from the opposite electrode (**Figure 2.12.d**).

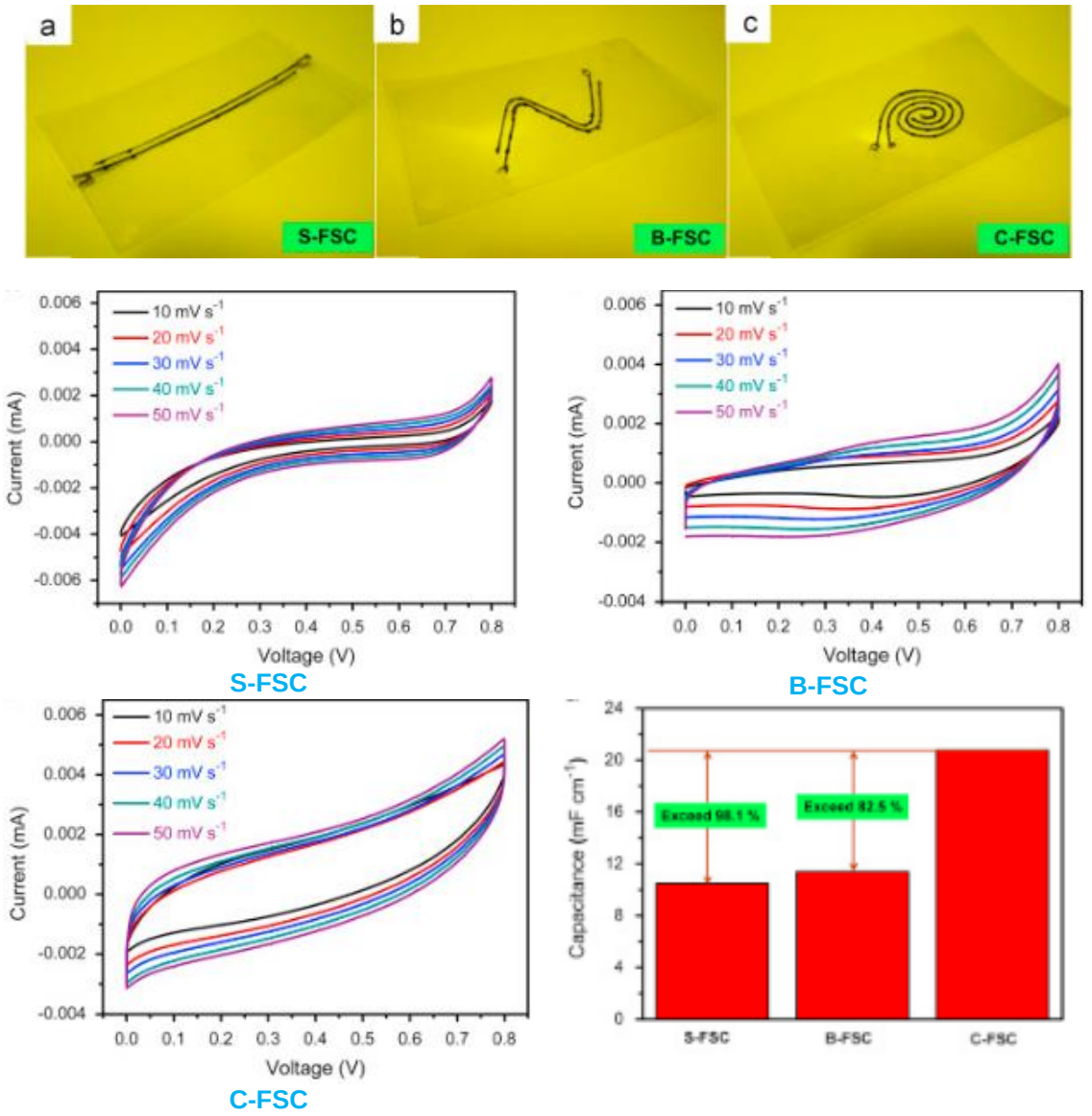

Figure 2.13. Electrochemical characterization of fiber-shaped supercapacitors in different configurations (straight, bent, and coiled) bicyclic voltammetry [27]

The first textile-shaped supercapacitor was developed by Cui's research group in 2010 [5], [6], [30]. In their work, pristine cotton fabrics were dip coated with single-walled carbon nanotubes (SWCNTs) to make the fabric electrodes, which were then assembled together with an addition of $LiPF_4$ as electrolyte to make a symmetrical fabric supercapacitor. The devices presented more than 10 times higher specific energy than the commercial supercapacitor, indicating the potential in practical

applications. The work was immediately followed by several other groups of researchers, e.g. Jost et al. in 2011 [23] and Bao and Li in 2012 [31] (**Figure 2.14**), with improvements in the design and configuration of the supercapacitors as well as their electrochemical performances. In the current research, two main approaches have been explored to fabricate and/or integrate supercapacitors into textiles. The pioneer work of Cui's group represents the most basic form of the first approach, the so-called top-down approach, to build 2D textile supercapacitors. As depicted in **Figure 2.12.e,** it starts with two pieces of existing textiles that serve as substrates for the deposition of energy storage electrode materials. The textiles are loaded with electrode materials, e.g. by dip coating or any other methods, and then sandwiched together with electrolytes and separators. The resulting supercapacitors can be further integrated with other fabrics. Depending on the methods of depositing the active materials, the assembled devices must ideally retain the flexibility that is sought for in textile. The second approach is a bottom-up strategy which starts with 1D yarn supercapacitors to construct energy storage textiles. The approach offers a possibility of seamless integration of device into textiles and textile products [6]. As shown in **Figure 2.12.f**, two yarn electrodes are first assembled by twisting them together with electrolyte/separator (**Figure 2.12.b**). Alternatively, one coaxial yarn with its core as one electrode and its outer surface as another electrode can also be used (**Figure 2.12.c**). The obtained 1D yarn supercapacitors are then weaved or knitted into flexible textiles.

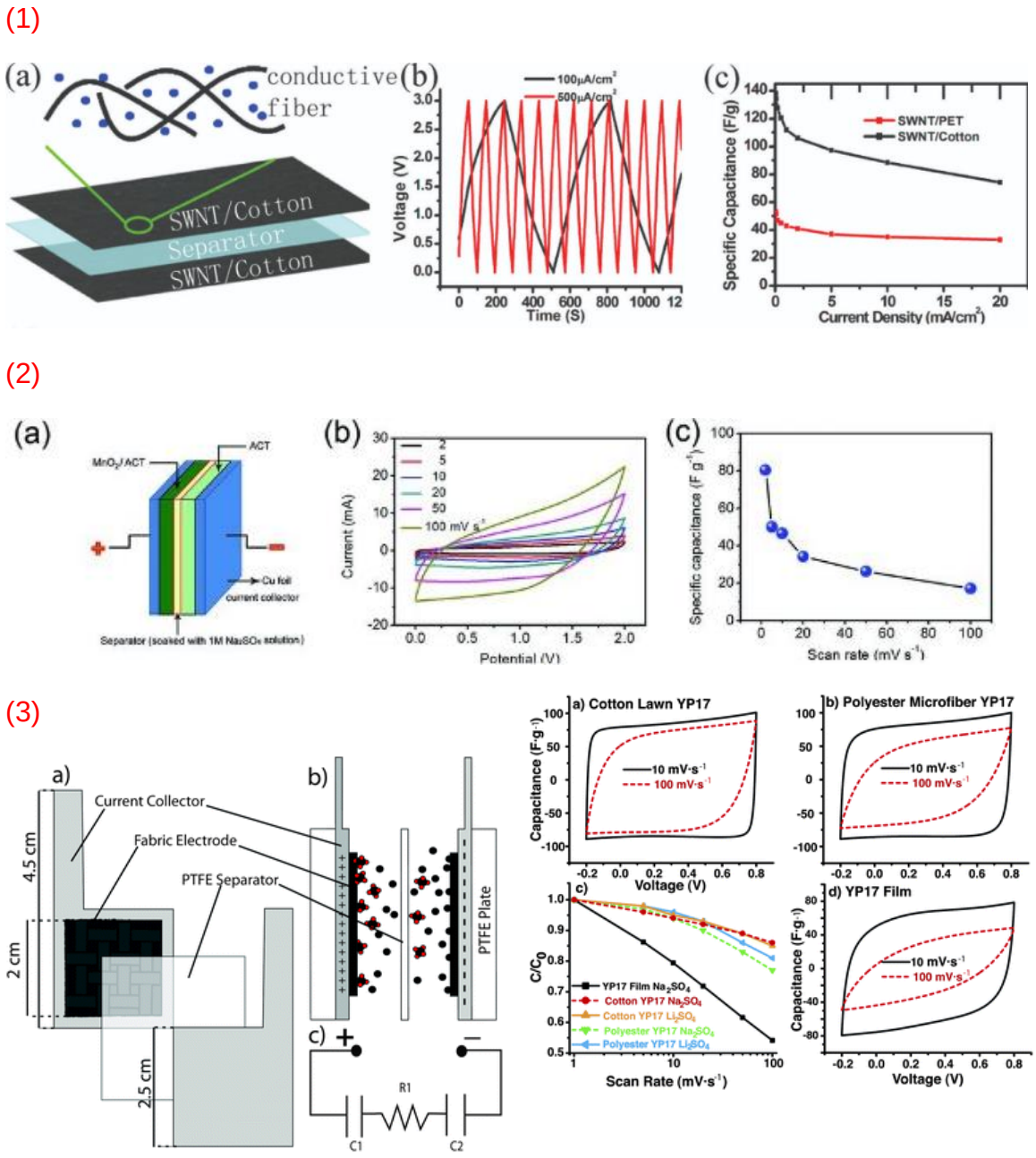

Figure 2.14. Early works on fabric-based supercapacitors by (1) Cui's group at Stanford [30], (2) Bao and Li at University of South Carolina [31], and (3) Jost et al. at Drexel University [23].

In addition to the above two approaches, there are a few studies that combine the top-down and bottom-up approaches [11]. In these studies, conductive yarns are first woven or knitted to form a small conductive area, which serves as current

collectors/substrates, in a larger non-conductive textile using the bottom up approach (see **Figure 2.12.g** and **h**). This is then subsequently followed by the deposition of energy storage electrode materials on the conductive portion. Using the top-down approach, two strips or two pieces of textiles loaded with electrode materials are then assembled in a sandwich structure. Early and obvious examples of this combined approach came from the works of Jost et al. in 2013 and 2015 [32], [33]. In their work with carbon fiber supercapacitor [32], carbon fiber yarns were knitted into an existing non-conductive knitted textile to form stripes of carbon that serve as both substrates and current collectors for the supercapacitor. Activated carbon that functions as the energy storage material was then screen printed on these carbon strips with a high mass loading up to 12 mg/cm^2. As illustrated in **Figure 2.15.a**, the 2D supercapacitor was assembled in sandwich structure with PTFE membrane serving as separator and $H_4SiW_{12}O_{40}$ (known as SiWA) gel as solid electrolyte. The flexible textile device yielded a specific area capacitance of 0.51 F/cm^2 at 10 mV/s. In a more recent work, Jost et al. [33] coated regular cotton yarns with activated carbon and twisted them together with stainless steels yarns, which was functioned as current collector, to obtain a yarn-shaped electrode (**Figure 2.15.b**). Next, two rows of electrodes were knitted in parallel within a textile with a non-conductive strip between them as separator and the SiWA gel electrolyte was coated onto the electrode area on the fabric (**Figure 2.15.c**). This approach does not add thickness to the fabric and thus provides better flexibility and wearing comfortability.

An approach with a similar structural design of the textile energy device had been studied intensively since 2013 by Lieva Van Langenhove's group of smart textiles at Ghent University, Belgium [34]–[40]. The basic design of the device is based on the work of Bhattacharya et al. in 2009 (**Figure 2.16.a**) [41]. They used silver coated polybenzoxazole (Ag-PBO) conductive yarns, which were stitched into the textile substrate as electrodes, and solid electrolyte made of PEDOT:PSS conductive polymer. In our textile energy storage device, a pair of pure stainless steel (SS) filament yarns, which gives better results than Ag-PBO yarns, was used as the electrodes and stitched

in parallel into a textile substrate at a distance of typically 1-2 mm from each other. Following the original design, a small amount of PEDOT:PSS conductive polymer was then drop coated into a small designated area called "cell area", typically 10 × 6 mm, to cover the conductive yarn electrodes forming an assembly for a supercapacitor.

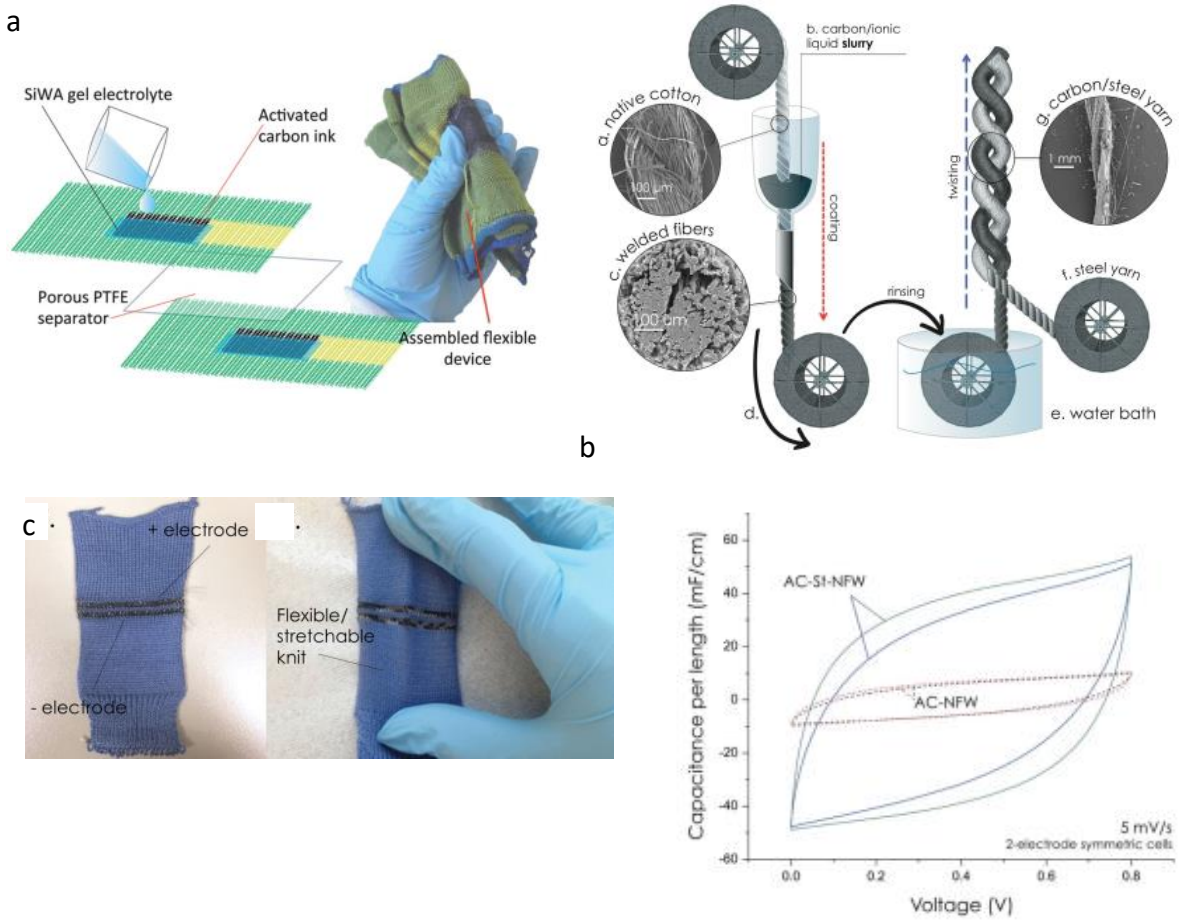

Figure 2.15. Combined top-down and bottom-up approach in the assembly of textile supercapacitors [32], [33].

As shown in **Figure 2.16.b**, our device has evolved from its original design to a more compact, robust and thinner device with only one layer of fabric potentially feasible for full and seamless integration into the textile structures. As previously mentioned, the use of solid electrolyte, which in this particular case is PEDOT:PSS conductive polymer, eliminates the need for a separator, which is usually needed to prevent short circuit. The most important contribution of our work and device is the simplicity of the design and yet it is fully functional with a potential for further

development into a fully and seamlessly integrated textile energy storage devices, which we will elaborate toward the end of this chapter. The transformation of the device from its original design to its present state is presented and discussed in the following Chapter 3.

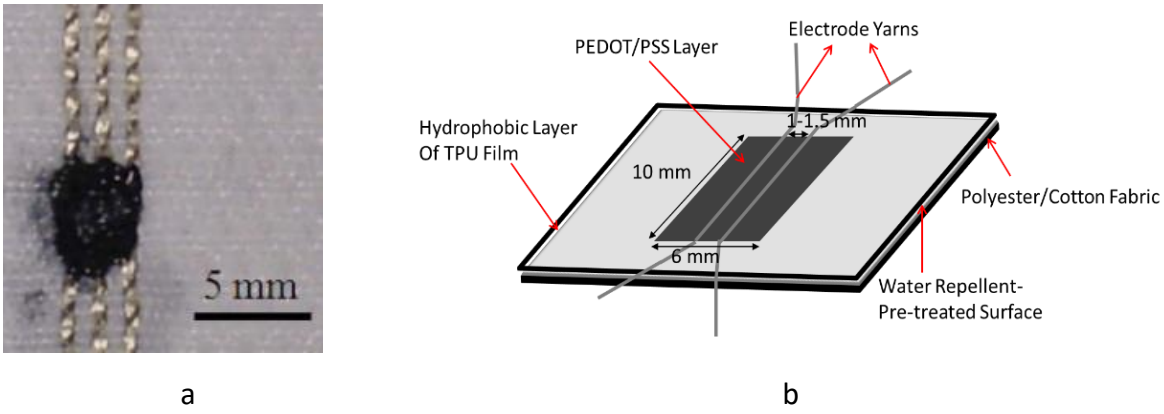

Figure 2.16. PEDOT:PSS textile energy storage device: (a) Bhattacharya's device [41], (b) our 3rd generation of TESD.

2.3 PEDOT:PSS : Its Properties and Roles in the Storage of Energy

Since the beginning of our endeavor to develop TESD for smart textile applications it is well understood that one of the major challenges is to improve the capacitive performance of the device. In the early stage of our study, with our first generation of TESD, it was estimated based on assumptions and observation that our PEDOT:PSS TESD had a capacitance of 180 μF [37]. It is rather difficult to make a direct comparison with the work of others who reported their results in specific capacitance, i.e. capacitances per gram (F g^{-1}) or per cm^2 of active material for one electrode. For example, Jost et al. [33] reported a specific capacitance of 120 F g^{-1} from their TESD shown in **Figure 2.15.c**. More can be found in **Table 2.1** and it can be immediately seen that most of the developed supercapacitors have specific capacitance in the millifarad to Farad region. The difficulty is related with the unusually simple but functional structural design that uses PEDOT:PSS as both an active material and electrolyte. Nevertheless, this device of ours had been successful

in powering LED and mini calculator showing their potential for an energy device even at its early stage [35], [37]. It only lasted for a very short time, 37 s, indicating that self-discharge is also an issue that needs to be addressed.

Energy density and power density have been the most important characteristics and measures of device performance. As mentioned previously, it is the capacity to perform work and expressed by Equation 2.1 below [22]:

$$E_{max} = \frac{1}{2} C_T V^2 \quad (2.1)$$

As shown by Equation (2.1), the energy density (E_{max}) of supercapacitors is proportional to the total capacitance in Farads (C_T) and the square of the voltage (V). Increasing either or both of the capacitance and the cell voltage is an effective way to increase the energy density. Increasing energy density has been one of the strategic approaches to improve the performance of energy device, which is particularly true for supercapacitors whose energy density is commonly low compared to batteries and fuel cells. For example, EDLCs commonly have an energy density of < 10 $Whkg^{-1}$; even for both pseudo-capacitors and hybrid-capacitors, their energy densities are generally less than 50 $Whkg^{-1}$ [26] and cannot fully meet the growing demand of the applications where high energy density is required. The routes to achieve this include [26]: (1) developing pseudo-capacitors based on pseudo-capacitive materials (e.g. some electroactive transition-metal oxides and conducting polymers) with high specific capacitance contributed from the pseudo-capacitance; (2) enlarging the cell voltage via the development of a new electrolyte; and (3) exploring supercapacitors with novel structures or new concepts, such as the hybrid (or asymmetric) capacitors.

From Equation (2.1), it can be clearly seen and understood that increasing the energy density (E_{max}) can be achieved more efficiently by enlarging the cell voltage than by increasing electrode capacitance. This is because the energy density is proportional to the square of the cell voltage, hence more dependent on the latter. Therefore, higher priority must be given in the development of new

electrolytes/solutions with wide potential windows than that of new electrode materials. However, it is worth noting that the three elements, i.e. electrode materials, electrolytes and structure or configuration of cell/device are closely interrelated to each other, so that their interaction must be considered to promote synergistic effect. A higher energy density can be achieved with the design of structure or configuration of the cell that warrants such an interaction. For example, in the design and preparation of porous carbon electrode materials one should consider the matching between the pore structure and the size of the electrolyte ions in order to make a high capacitive electrode [26]. Likewise, the development of some electrolytes should consider their possible interaction with the electrode materials such as in the case of hybrid capacitors. The idea that puts importance to the development of electrolyte as described above puts more value to the significance of understanding the mechanism(s) that brings to the storage of charge and control the charge transport in a cell that uses PEDOT:PSS conductive polymer as an electrolyte and probably an active material too.

While there have been many excellent reviews concerning electrode materials, reviews focusing on the electrolytes of supercapacitors are rather limited [26], [42]–[45] and it is even worse for PEDOT:PSS. The review and research papers reporting the use of PEDOT:PSS in energy device have been dominated by its function and role as an active material for electrodes. Except for the works reported by Bhattacharya et al. [41] and our group of smart textile [34-40], [46] none has reported its use and properties as electrolyte.

Better understanding of the mechanism(s) and the working principles behind this particular device is significant and strategic to any effort to improve its performance. In this part of the chapter, we will discuss the chemical and physical properties, electrical-electronical properties, morphology and transport properties of PEDOT:PSS in an endeavor to obtain an understanding of the mechanism(s) that leads to the storage of charge and control the charge transport in our TESD, with a particular

view of its function as an electrolyte for the system.

2.3.1 Chemical and Physical Properties

Poly(3,4-ethylenedioxythiophene):poly(styrene sulfonate) (PEDOT:PSS) belongs to one of the most widely used conducting polymers, i.e. derivatives of polythiophene (**Figure 2.8**), and is a polymer electrolyte consisting of positively charged conjugated PEDOT and negatively charged saturated PSS (**Figure 2.17**). The latter is a polymer surfactant, which helps disperse and stabilize PEDOT in water and other solvents and contributes significantly for the commercial success of the polymer. PEDOT:PSS is the most successful conducting polymer in terms of practical applications. Its aqueous dispersion was first commercialized under the trade name of Baytron® by Bayer AG, then by H.C. Starck, and currently by Heraeus under the trade name of Clevios™ [47]. Agfa also introduced PEDOT:PSS for the large-scale printing application under the trade name of Orgacon™ .

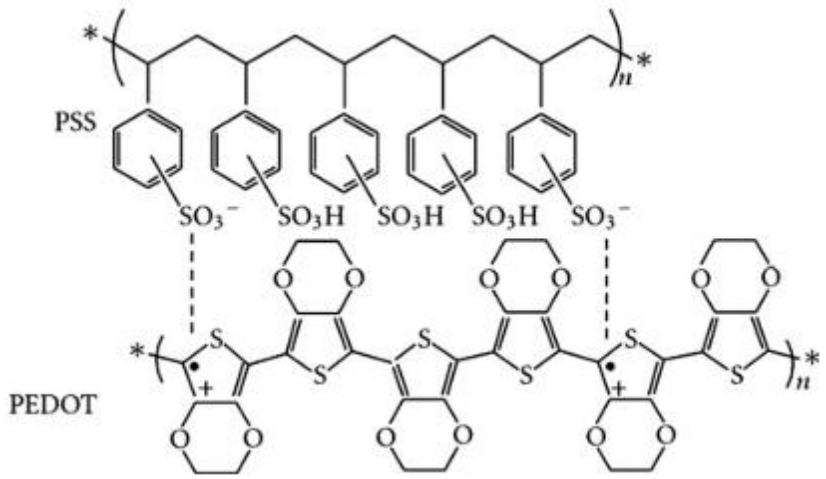

Figure 2.17. The chemical structure of PEDOT:PSS.

The commercially available PEDOT:PSS aqueous dispersion has a deep-blue opaque color. It readily forms a continuous thin film on either rigid or flexible substrates by various solution-processing techniques including spin and drop casting, doctor blade, slot die coating, spray deposition, inkjet printing, screen printing, slit

coating, and electrospinning [48-49]. Depending on the deposition technique, the PEDOT:PSS film is smooth and has a surface roughness generally less than 5 nm [49]. PEDOT:PSS exhibits a wide range of electrical conductivities from 10^{-2} to 10^{3} $S.cm^{-1}$, influenced by synthetic conditions, processing additives or post-treatment (*vide infra*). PEDOT:PSS films have a high work function of 5.0–5.2 eV. The superior conductivity and high work function can often induce spontaneous charge transfer with fast kinetics, thus providing PEDOT:PSS with catalytic properties. Commercially available PEDOT:PSS with different ratio of PEDOT and PSS and their corresponding physical as well as electronic properties is presented in **Table 2.7**.

Table 2.7. Commercial PEDOT:PSS dispersions in water and their physical and electronic properties. [48]

Trade Name	Solids Content in Water (w/w) (%)[a]	PEDOT:PSS Ratio (w/w)	Viscosity at 20°C (mPas)[a]	Particle Size d_{50} (nm)[a]	Conductivity (S/cm)[a]
Clevios P	1.3	1:2.5	80	80	<10
Clevios PH	1.3	1:2.5	20	30	<10
Clevios P VP AI 4083	1.5	1:6	10	40	10^{-3}
Clevios P VP CH 8000	2.8	1:20	15	25	10^{-5}
Clevios PH 500	1.1	1:2.5	25	30	500[b]
Clevios PH 750	1.1	1:2.5	25	30	750[b]
Clevios PH 1000	1.1	1:2.5	30	30	1000[b]

[a] Typical values for solids content, viscosity, particle size, and conductivity are given; no specification.
[b] Conductivities for Clevios PH 500, PH 750, and PH 1000 are measured for dispersions containing 5% dimethyl sulfoxide.

PSS as a counterion for PEDOT is always used in excess, that is, as host polyelectrolyte (HPE). The molar ratio of thiophene groups to sulfonic acid groups in standard PEDOT:PSS dispersions is in the range of 1:1.9 to 1:15.2, which corresponds to a weight ratio range of 1:2.5 up to 1:20 [48]. Since only one charge is found for every three to four thiophene rings [48], [50], the charge excess of PSS is between 6-fold and 46-fold. Due to the delocalization of positive charges in PEDOT, the resulting weak polar groups and the different spacing of charges in PEDOT compared to PSS, it is

reasonable to assume that the structure of PEDOT:PSS shows the form of a scrambled egg type because pairing of charges as required in the ladder type is not possible (**Figure 2.18**) [48]. **Figure 2.19** shows the synthesis of PEDOT:PSS and its primary, secondary and tertiary structure [51].

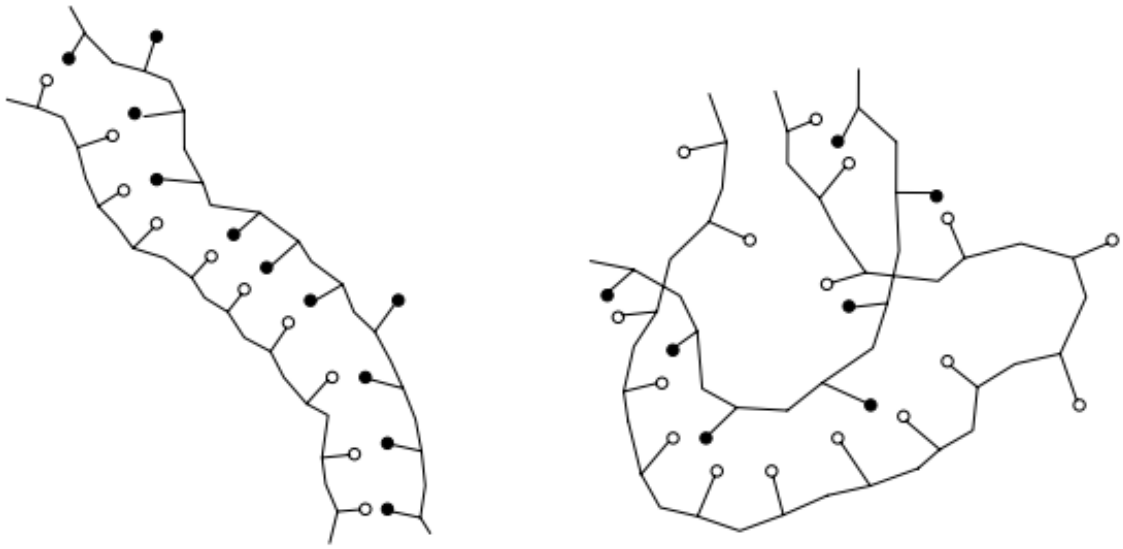

Figure 2.18. The conformation of polyelectrolyte complex (e.g. PEDOT:PSS) in ladder type (left) and scrambled egg type (right). [48]

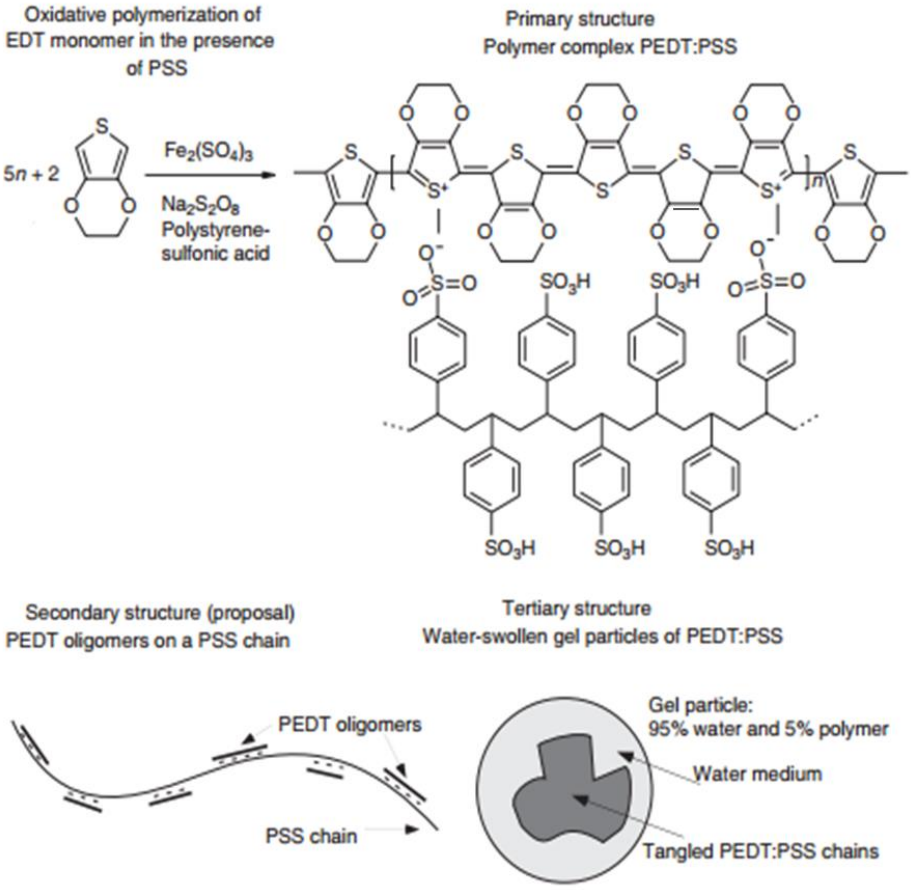

Figure 2.19. The synthesis, primary, secondary, and tertiary structure of PEDOT:PSS [51]

The conductions by electrons in conducting polymers is basically due to the presence of conjugated single and double bonds along the polymer skeleton. However, the conjugated system alone does not produce high conductivity. Only when an electron is removed from the valence band by oxidation (*p*-doping) or added to the conducting band by reduction (*n*-doping) does the polymer become highly conductive (**Figure 2.20**). The presence of dopant removes an electron from a delocalized bonding arrangement creating a hole. Then, an electron at a neighboring position jumps and fills that hole, generating a new hole and allowing charge to flow through the polymer chain. The π-bond between the first and second carbon atoms is transferred to the position between the second and third carbon atoms. In turn, the π-bond between the third and fourth carbon travels to the next carbon, and so forth. As

a result, the electrons in the double bonds move along the carbon chain [52].

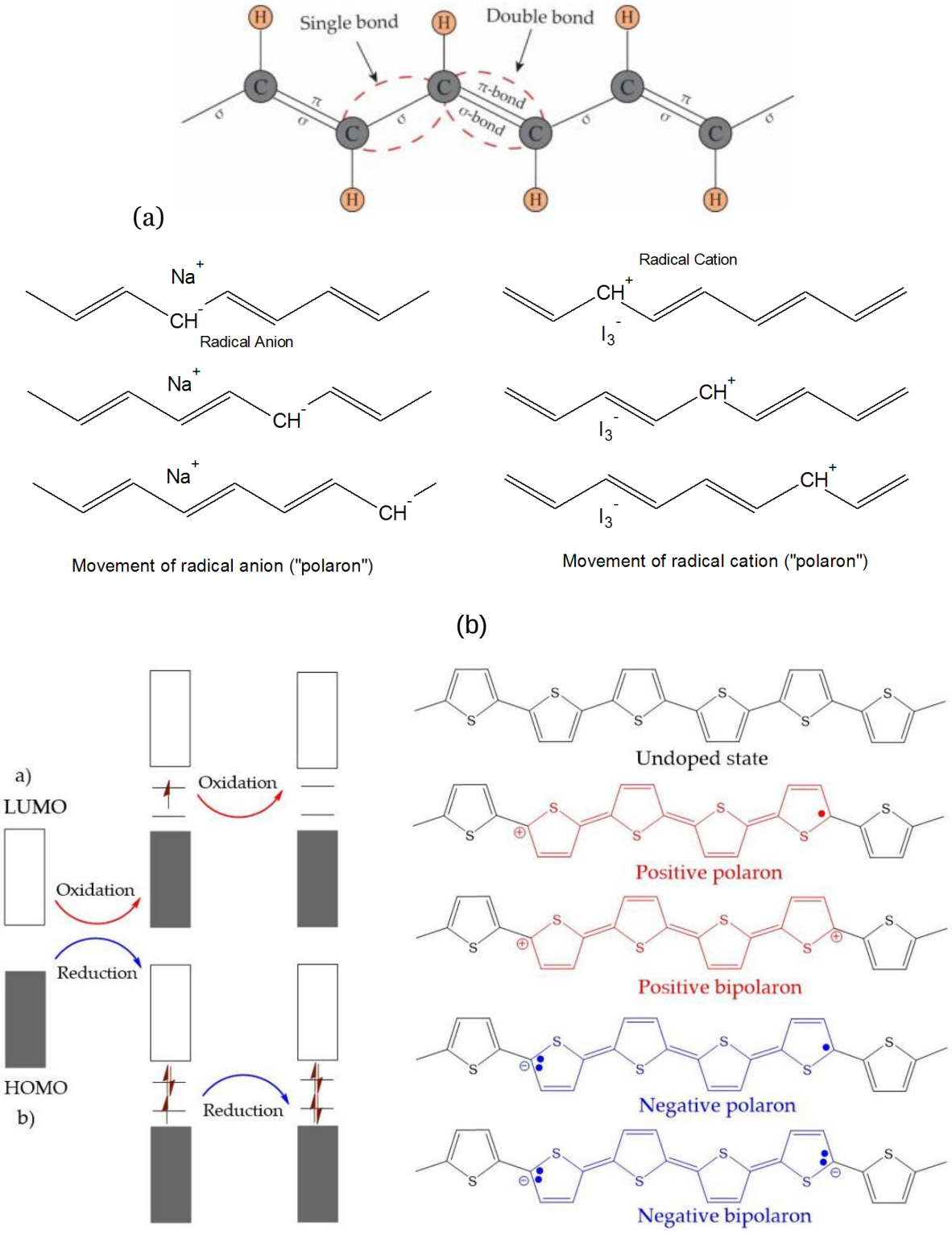

Figure 2.20. (a) The movement of radical cation and anion in polyaniline. (b) The electronic band and chemical structures of (a) *p*-type and (b) *n*-type doping in polythiophene. [52]

Commercial PEDOT:PSS is available in the form of polymer dispersion with a concentration normally below 5%. The concentration must be kept low because of the strong dependence of viscosity on the concentration. The average size of PEDOT:PSS particles in the dispersion is in the range of 10 nm to 1 μm. As shown in **Table 2.7**, the conductivity of the polymer coating decreases with smaller size of particles, which is dues to the increase in internal resistance.

2.3.2 Morphology

Despite large differences in interpretation and experimental data, it is generally believed that charge transport in PEDOT:PSS occurs by a hopping mechanism [53], which involve intra- and inter-chain transport between electronic active sites created by a series of redox processes within the polymer film [27]. Hopping also takes place between grains of PEDOT:PSS from one PEDOT-rich conductive region to the next, bridging an area of less conductivity, which consists of PSS or defects [48], [54]. In this model, the ordering of the PEDOT segments in the film is crucial for the transport of charges and conductivity of the film. These views support the significance of film formation in relation to the conformation of chains and morphology of PEDOT:PSS film. The appropriate combination of surface morphology and conductivity is required for various applications of PEDOT:PSS. For example, antistatic coating applications require high conductivity for the PEDOT:PSS layer, whereas organic light-emitting diode (OLED) requires low conductivity for efficient hole-injection layer in the active seminconductor and the polymer must be smooth in order to prevent micro-shorts leading to dark spots [55]. Furthermore, the surface roughness of highly conducting PEDOT:PSS was recently shown to be responsible for the reduced performance in polymer solar cells [56], putting more emphasize on the significance of morphology on the performance of energy device. Based on their observation on the effect of sorbitol to the arrangement of polymers, Timpanaro et al. [57] concluded that morphology is a crucial issue for both controlling and understanding the charge carrier transport in the PEDOT:PSS system. Further, they

also asserted that the observed morphologies are correlated to the macroscopic conductivity of the films, and found that the morphology in the top layer of the films was found to differ substantially from the bulk morphology.

Different models exist to describe the morphology of PEDOT:PSS films. A lamellae model was proposed by Ionescu-Zanetti et al. [58] based on their work with phase-shift atomic force microscopy (AFM). Paracrystalline terraced structures were detected and were interpreted as molecular lamellae of PEDOT and PSS. The PEDOT lamellae were found to be conductive, whereas the PSS lamellae are electrically isolating. The interlamellae distance was estimated to be 3 nm.

A different morphological model for the bulk properties of PEDOT:PSS films was proposed by Nardes et al. [59] who suggest a film morphology resembling stacked pancakes (**Figure 2.21.a**). This model is derived from the morphology of PEDOT:PSS in solution where gel particles with a PSS-rich outer shell are formed [60]. When these sphere-shaped gels dry to form a film, their original structure is maintained, but due to a shrinkage predominantly in the vertical direction, they form disc-like shapes, which exhibit PSS-rich regions in the contact areas (**Figure 2.21.b**). This model will explain why the anisotropic conductivity of spin-cast Clevios P AI 4083 films, which was determined to be 1 × 10–3 S/cm in the horizontal direction (parallel to the substrates surface at room temperature) and about 500 times lower in the vertical (perpendicular) direction. According to this model, free charge carriers passing a film composed of disc-like structures will travel easier along the long axis than along the short axis of the discs. The regions of PSS enrichment are believed to be poor electrical conductors due to a lack of PEDOT charge transport sites and hence form energetic charge barriers. Indeed, the density of PSS-enriched grain boundaries between the discs was found to be higher parallel to the substrate's surface than in the vertical direction.

Employing high angle annular dark field (HAADF) scanning transmission electron microscopy (STEM), Lang et al. [60] have evidenced the model of a granular

structure of PEDOT:PSS gel particles maintained during film formation. The lateral size of the dried grains in the films was found to be in the order of 50 nm similar to the grain size of swollen particles in dispersion (**Figure 2.22.a**). These grains forming larger aggregates and exhibiting brighter contrast were detected on the film's surface.

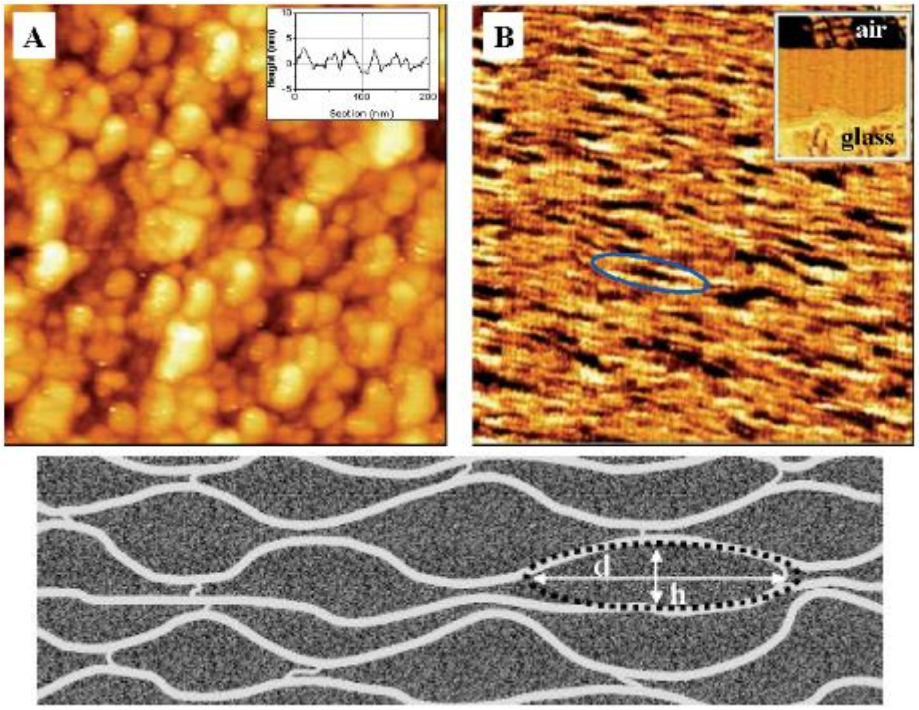

Figure 2.21. (a) 200 nm × 200 nm topographic scanning tunnel microscope (STM) image of PEDOT:PSS on ITO at 2.3 V, tunneling current 10 pA, and vertical scale 15 nm, the inset shows a line section. (b) 200 nm × 200 nm cross-sectional atomic force microscope phase image (X-AFM) of cleaved PEDOT:PSS on glass, vertical scale is 8°. The glass substrate is on the bottom side of the image, as shown by the inset of 530 nm × 580 nm and a vertical scale 70°. A pancake-like particle is highlighted by the ellipse. (c) Cross-sectional view of the schematic morphological model for PEDOT:PSS thin films derived from combined STM and X-AFM measurements. PSS-rich lamella is composed by several pancake-like particles as shown by the dotted lines. The typical diameter (d) of the particles is about 20 to 25 nm and a height (h) of 5 to 6 nm. [59]

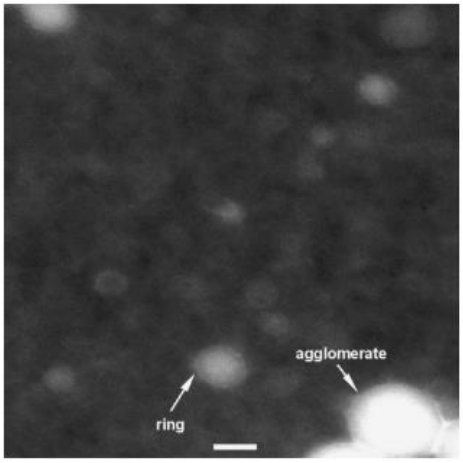

(a)

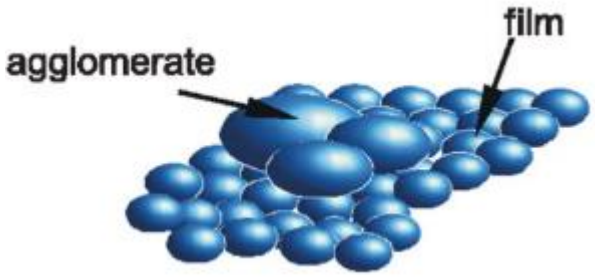

(b)

Figure 2.22. (a) HAADF–STEM image of a 25-nm-thick PEDOT:PSS film; (b) Schematic showing how agglomerates lie on top of film.

2.3.3 Electrical and Transport Properties

As discussed previously, PEDOT:PSS is an intrinsically conducting polymer with metal-like properties and charge transport stemming from free charge carriers. The thiophene rings form a conjugated π system being heavily *p*-doped. One net free positive charge is created per three to four thiophene rings which is due to the oxidative polymerization reaction triggered by radicals. The poly(styrenesulfonic acid) does not contribute to charge transport directly, but acts as a template to keep PEDOT in the dispersed state and provides film-forming properties.

Following the concept of charge transport in amorphous inorganic semiconductors, the conduction mechanism of conjugated polymers is commonly discussed in terms of charge hopping between adjacent sites. Segments of conjugated polymers are preferentially forming electronically active sites due to their ability of being easily oxidized and reduced. The charge is transported from one PEDOT-rich conductive region to the next, bridging an area of less conductivity, which consists of PSS or defects. The PEDOT particles have a much higher intrinsic conductivity than

the PEDOT depleted boundary, which is essentially insulating. Consequently, the main obstacle is to transport electric current between the PEDOT-rich particles [62]. The ordering of the PEDOT segments in the film results in pathways of very high conductivity, which are only created if the highly boiling solvent is present long enough to allow the thermodynamically driven order to occur. The insulating PSS chains are removed between the PEDOT-rich areas and a higher degree of organization between the PEDOT-rich particles is obtained resulting in a macroscopic increase of conductivity. Ouyang et al. [63] have interpreted the changes observed in the Raman spectra (**Figure 2.23**) as a change from a benzoid structure toward a quinoid structure of the PEDOT molecules due to a move from a coil structure toward an extended coil or linear structure of PEDOT chains.

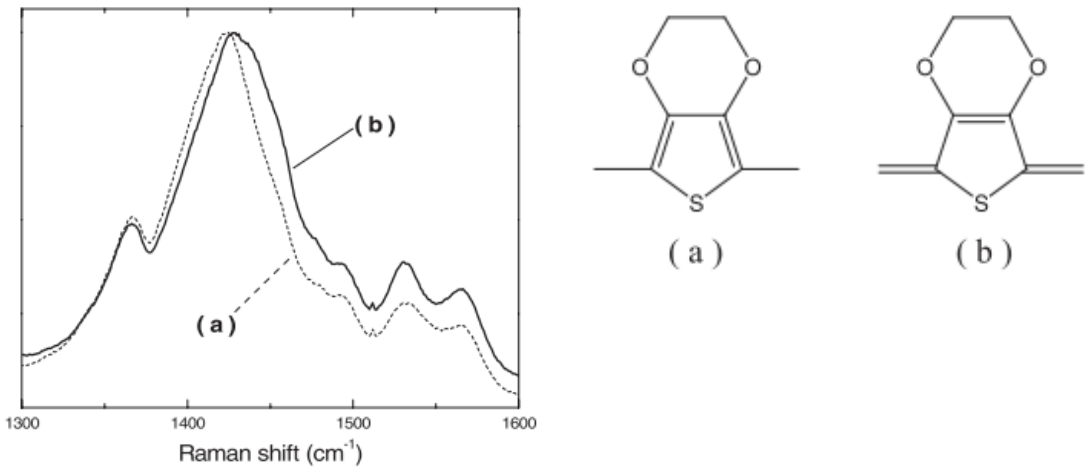

Figure 2.23. Raman spectra of a) a high-conductivity E-PEDOT:PSS film and b) an untreated PEDOT:PSS film excited by an HeNe laser at 632.8 nm. [63]

Bibliography

[1] T. Chittenden, "Skin in the game: the use of sensing smart fabrics in tennis costume as a means of analyzing performance," *Fash. Text.*, vol. 4, no. 1, p. 22, Dec. 2017.

[2] E. Pitt, "World-first 'Bionic Bra' inches closer to reality," *Media Releases*, 2014. [Online]. Available: https://media.uow.edu.au/releases/UOW184372.html. [Accessed: 19-Mar-2019].

[3] X. Tao, *Smart fibres, fabrics and clothing*, 1st ed. Manchester: CRC Press, 2001.

[4] M. Stoppa and A. Chiolerio, "Wearable Electronics and Smart Textiles: A Critical Review," *Sensors 2014, Vol. 14, Pages 11957-11992*, vol. 14, no. 7, pp. 11957–11992, 2014.

[5] Q. Huang, D. Wang, and Z. Zheng, "Textile-Based Electrochemical Energy Storage Devices," *Adv. Energy Mater.*, vol. 6, no. 22, p. 1600783, Nov. 2016.

[6] K. Jost, G. Dion, and Y. Gogotsi, "Textile energy storage in perspective," *J. Mater. Chem. A*, vol. 2, no. 28, p. 10776, 2014.

[7] V. Kaushik *et al.*, "Textile-Based Electronic Components for Energy Applications: Principles, Problems, and Perspective," *Nanomaterials*, vol. 5, no. 3, pp. 1493–1531, Sep. 2015.

[8] S. Kwon, H. Kim, S. Choi, E.G. Jeong, D. Kim, S. Lee, H.S. Lee, Y.C. Seo, and K.C. Choi, "Weavable and Highly Efficient Organic Light-Emitting Fibers for Wearable Electronics: A Scalable, Low-Temperature Process", *Nano Lett.*, vol. 18, pp. 347-356, 2018.

[9] S. Seymour, *Functional aesthetics : visions in fashionable technology*. Springer, 2010

[10] S. Seymour, *Fashionable Technology*. Vienna: Springer Vienna, 2008.

[11] S. Zhai *et al.*, "Textile energy storage: Structural design concepts, material selection and future perspectives," *Energy Storage Mater.*, vol. 3, pp. 123–139, Apr. 2016.

[12] W. Zuo, R. Li, C. Zhou, Y. Li, J. Xia, and J. Liu, "Battery-Supercapacitor Hybrid Devices: Recent Progress and Future Prospects," *Adv. Sci.*, vol. 4, no. 7, p.

1600539, Jul. 2017.

[13] W. Zeng, L. Shu, Q. Li, S. Chen, F. Wang, and X.-M. Tao, "Fiber-Based Wearable Electronics: A Review of Materials, Fabrication, Devices, and Applications," *Adv. Mater.*, vol. 26, no. 31, pp. 5310–5336, Aug. 2014.

[14] Z. Liu *et al.*, "Advances in Flexible and Wearable Energy-Storage Textiles," *Small Methods*, vol. 2, no. 11, p. 1800124, Nov. 2018.

[15] X. Wang, K. Jiang, and G. Shen, "Flexible fiber energy storage and integrated devices: recent progress and perspectives," *Mater. Today*, vol. 18, no. 5, pp. 265–272, Jan. 2015.

[16] F. Meng, Q. Li, and L. Zheng, "Flexible fiber-shaped supercapacitors: Design, fabrication, and multi-functionalities," *Energy Storage Mater.*, vol. 8, pp. 85–109, Jul. 2017.

[17] B. E. Conway, *Electrochemical Supercapacitors : Scientific Fundamentals and Technological Applications*. Springer US, 1999.

[18] J. Zhang and X. Zhao, "On the configuration of supercapacitors for maximizing electrochemical performance," *ChemSusChem*, vol. 5, no. 5, pp. 818–841, 2012.

[19] G. Wang, L. Zhang, and J. Zhang, "A review of electrode materials for electrochemical supercapacitors," *Chem. Soc. Rev.*, vol. 41, no. 2, pp. 797–828, Jan. 2012.

[20] Y. Zhang *et al.*, "Progress of electrochemical capacitor electrode materials: A review," *Int. J. Hydrogen Energy*, vol. 34, no. 11, pp. 4889–4899, Jun. 2009.

[21] B. Xu, F. Wu, S. Chen, C. Zhang, G. Cao, and Y. Yang, "Activated carbon fiber cloths as electrodes for high performance electric double layer capacitors," *Electrochim. Acta*, vol. 52, no. 13, pp. 4595–4598, Mar. 2007.

[22] L. L. Zhang and X. S. Zhao, "Carbon-based materials as supercapacitor electrodes," *Chem. Soc. Rev.*, vol. 38, no. 9, pp. 2520–2531, 2009.

[23] K. Jost *et al.*, "Carbon coated textiles for flexible energy storage," *Energy Environ. Sci.*, vol. 4, no. 12, p. 5060, 2011.

[24] G. A. Snook, P. Kao, and A. S. Best, "Conducting-polymer-based supercapacitor devices and electrodes," *J. Power Sources*, vol. 196, no. 1, pp. 1–12, Jan. 2011.

[25] A. Yu, V. Chabot, and J. Zhang, *Electrochemical Supercapacitors for Energy Storage and Delivery: Fundamentals and Applications.* CRC Press, 2017.

[26] C. Zhong, Y. Deng, W. Hu, J. Qiao, L. Zhang, and J. Zhang, "A review of electrolyte materials and compositions for electrochemical supercapacitors," *Chem. Soc. Rev.*, vol. 44, no. 21, pp. 7484–7539, Oct. 2015.

[27] B. Liu, B. Liu, X. Wang, D. Chen, Z. Fan, and G. Shen, "Constructing optimized wire electrodes for fiber supercapacitors," *Nano Energy*, vol. 10, pp. 99–107, Nov. 2014.

[28] Y. Fu *et al.*, "Fiber Supercapacitors Utilizing Pen Ink for Flexible/Wearable Energy Storage," *Adv. Mater.*, vol. 24, no. 42, pp. 5713–5718, Nov. 2012.

[29] Y. Ai *et al.*, "Meters-Long Flexible $CoNiO_2$ -Nanowires@Carbon-Fibers Based Wire-Supercapacitors for Wearable Electronics," *Adv. Mater. Technol.*, vol. 1, no. 8, p. 1600142, Nov. 2016.

[30] L. Hu *et al.*, "Stretchable, Porous, and Conductive Energy Textiles," *Nano Lett.*, vol. 10, no. 2, pp. 708–714, Feb. 2010.

[31] L. Bao and X. Li, "Towards Textile Energy Storage from Cotton T-Shirts," *Adv. Mater.*, vol. 24, no. 24, pp. 3246–3252, Jun. 2012.

[32] K. Jost *et al.*, "Knitted and screen printed carbon-fiber supercapacitors for applications in wearable electronics," *Energy Environ. Sci.*, vol. 6, no. 9, p. 2698, Aug. 2013.

[33] K. Jost *et al.*, "Natural Fiber Welded Electrode Yarns for Knittable Textile Supercapacitors," *Adv. Energy Mater.*, vol. 5, no. 4, p. 1401286, Feb. 2015.

[34] S. A. Odhiambo, C. Hertleer, L. Van Langenhove, G. De Mey, W. De Ferme, and J. Stryckers, "Comparison of commercial brands of PEDOT: PSS in Electric 'Capattery' integrated in textile structure," in *Mixed Design of Integrated Circuits and Systems. MIXDES*, 2013, pp. 389–391.

[35] S. A. Odhiambo, G. De Mey, C. Hertleer, A. Schwarz, and L. Van Langenhove, "Discharge characteristics of poly(3,4-ethylene dioxythiophene): poly(styrenesulfonate) (PEDOT:PSS) textile batteries; comparison of silver coated yarn electrode devices and pure stainless steel filament yarn electrode devices," *Text. Res. J.*, vol. 84, no. 4, pp. 347–354, Mar. 2014.

[36] S. Odhiambo, G. De Mey, and C. Hertleer, "Reliability testing of PEDOT: PSS capacitors integrated into textile fabrics," *Eksploat. i Niezawodn.*, vol. 16, no. 3, pp. 447–451, 2014.

[37] S. A. Odhiambo, "PEDOT:PSS Charge Storage Devices Integrated into Textiles for Smart Textile Application," 2015, p. 163.

[38] I. Nuramdhani, S. Odhiambo, C. Hertleer, and G. De Mey, "Electric Field Effect on Charge-Discharge Characteristics of Textile-Based Energy Storage Devices: In Search of the Underlying Mechanism.," *Tekstilec*, vol. 59, no. 2, 2016.

[39] I. Nuramdhani, M. Widodo, V. G. V. Putra, and M. Siahaan, "Fabrication and Characterization of PEDOT:PSS Textile Supercapacitor For Smart Textiles," in *Proceedings of the 2nd Indonesian Textile Conference*, 2017.

[40] I. Nuramdhani, G. De Mey, M. Widodo, C. Hertleer, and L. Van Langenhove, "Ionic shot noise in an electrochemical capacitor system made of poly(3,4-ethylenedioxythiophene)-poly(styrenesulfonate) film and silver-coated polybenzoxazole-stainless steel electrodes on textile fabrics," *Text. Res. J.*, p. 004051751876715, Apr. 2018.

[41] R. Bhattacharya, M. M. de Kok, and J. Zhou, "Rechargeable electronic textile battery," *Appl. Phys. Lett.*, vol. 95, no. 22, p. 314, 2009.

[42] H. Gao and K. Lian, "Proton-conducting polymer electrolytes and their applications in solid supercapacitors: a review," *RSC Adv.*, vol. 4, no. 62, pp. 33091–33113, Jul. 2014.

[43] Y. Wang and W.-H. Zhong, "Development of Electrolytes towards Achieving Safe and High-Performance Energy-Storage Devices: A Review," *ChemElectroChem*, vol. 2, no. 1, pp. 22–36, Jan. 2015.

[44] A. Hassibi, R. Navid, R. W. Dutton, and T. H. Lee, "Comprehensive study of noise processes in electrode electrolyte interfaces," *J. Appl. Phys.*, vol. 96, no. 2, pp. 1074–1082, 2004.

[45] N. A. Choudhury, A. K. Shukla, S. Sampath, and S. Pitchumani, "Cross-Linked Polymer Hydrogel Electrolytes for Electrochemical Capacitors," *J. Electrochem. Soc.*, vol. 153, no. 3, p. A614, Mar. 2006.

[46] I. Nuramdhani, A. Gokceoren, S. Odhiambo, G. De Mey, C. Hertleer, and L. Van

Langenhove, "Electrochemical Impedance Analysis of a PEDOT:PSS-Based Textile Energy Storage Device," *Materials (Basel).*, vol. 11, no. 1, p. 48, Dec. 2017.

[47] Y. Xia, K. Sun, and J. Ouyang, "Solution-Processed Metallic Conducting Polymer Films as Transparent Electrode of Optoelectronic Devices," *Adv. Mater.*, vol. 24, no. 18, pp. 2436–2440, May 2012.

[48] A. Elschner, S. Kirchmeyer, W. Lovenich, U. Merker, and K. Reuter, *PEDOT: Principles and Applications of an Intrinsically Conductive Polymer*. Boca Raton: CRC Press, 2011.

[49] K. Sun *et al.*, "Review on application of PEDOTs and PEDOT:PSS in energy conversion and storage devices," *Journal of Materials Science: Materials in Electronics*, vol. 26, no. 7. 2015.

[50] H.-S. Park, S.-J. Ko, J.-S. Park, J. Y. Kim, and H.-K. Song, "Redox-active charge carriers of conducting polymers as a tuner of conductivity and its potential window," *Sci. Rep.*, vol. 3, no. 1, p. 2454, Dec. 2013.

[51] S. Kirchmeyer and K. Reuter, "Scientific importance, properties and growing applications of poly(3,4-ethylenedioxythiophene)," *J. Mater. Chem.*, vol. 15, no. 21, p. 2077, May 2005.

[52] T.-H. Le, Y. Kim, and H. Yoon, "Electrical and Electrochemical Properties of Conducting Polymers," *Polymers (Basel).*, vol. 9, no. 4, p. 150, Apr. 2017.

[53] J. Ouyang, Q. Xu, C.-W. Chu, Y. Yang, G. Li, and J. Shinar, "On the mechanism of conductivity enhancement in poly(3,4-ethylenedioxythiophene):poly(styrene sulfonate) film through solvent treatment," *Polymer (Guildf).*, vol. 45, no. 25, pp. 8443–8450, Nov. 2004.

[54] A. Nardes, M. Kemerink, and R. Janssen, "Anisotropic hopping conduction in spin-coated PEDOT: PSS thin films," *Phys. Rev. B*, vol. 76, no. 8, p. 85208, 2007.

[55] C. S. Suchand Sangeeth, M. Jaiswal, and R. Menon, "Correlation of morphology and charge transport in poly(3,4-ethylenedioxythiophene)–polystyrenesulfonic acid (PEDOT–PSS) films," *J. Phys. Condens. Matter*, vol. 21, no. 7, p. 072101, Feb. 2009.

[56] Y. Zhou *et al.*, "Investigation on polymer anode design for flexible polymer solar cells," *Appl. Phys. Lett.*, vol. 92, no. 23, p. 233308, Jun. 2008.

[57] S. Timpanaro, M. Kemerink, F. J. Touwslager, M. M. De Kok, and S. Schrader, "Morphology and conductivity of PEDOT/PSS films studied by scanning-tunneling microscopy," *Chem. Phys. Lett.*, vol. 394, no. 4–6, pp. 339–343, 2004.

[58] C. Ionescu-Zanetti, A. Mechler, S. A. Carter, and R. Lal, "Semiconductive Polymer Blends: Correlating Structure with Transport Properties at the Nanoscale," *Adv. Mater.*, vol. 16, no. 5, pp. 385–389, Mar. 2004.

[59] A. M. Nardes *et al.*, "Microscopic Understanding of the Anisotropic Conductivity of PEDOT:PSS Thin Films," *Adv. Mater.*, vol. 19, no. 9, pp. 1196–1200, May 2007.

[60] X. Crispin *et al.*, "Conductivity, morphology, interfacial chemistry, and stability of poly (3, 4-ethylene dioxythiophene)–poly (styrene sulfonate): A photoelectron spectroscopy study," *J. Polym. Sci. Part B Polym. Phys.*, vol. 41, no. 21, pp. 2561–2583, Jul. 2003.

[61] U. Lang, E. Müller, N. Naujoks, and J. Dual, "Microscopical investigations of PEDOT: PSS thin films," *Adv. Funct. Mater.*, vol. 19, no. 8, pp. 1215–1220, Apr. 2009.

[62] A. M. Nardes, R. A. J. Janssen, and M. Kemerink, "A Morphological Model for the Solvent-Enhanced Conductivity of PEDOT:PSS Thin Films," *Adv. Funct. Mater.*, vol. 18, no. 6, pp. 865–871, Mar. 2008.

[63] J. Ouyang, C.-W. Chu, F.-C. Chen, Q. Xu, and Y. Yang, "High-Conductivity Poly(3,4-ethylenedioxythiophene):Poly(styrene sulfonate) Film and Its Application in Polymer Optoelectronic Devices," *Adv. Funct. Mater.*, vol. 15, no. 2, pp. 203–208, Feb. 2005.

3

Improvement of Fabrication Techniques

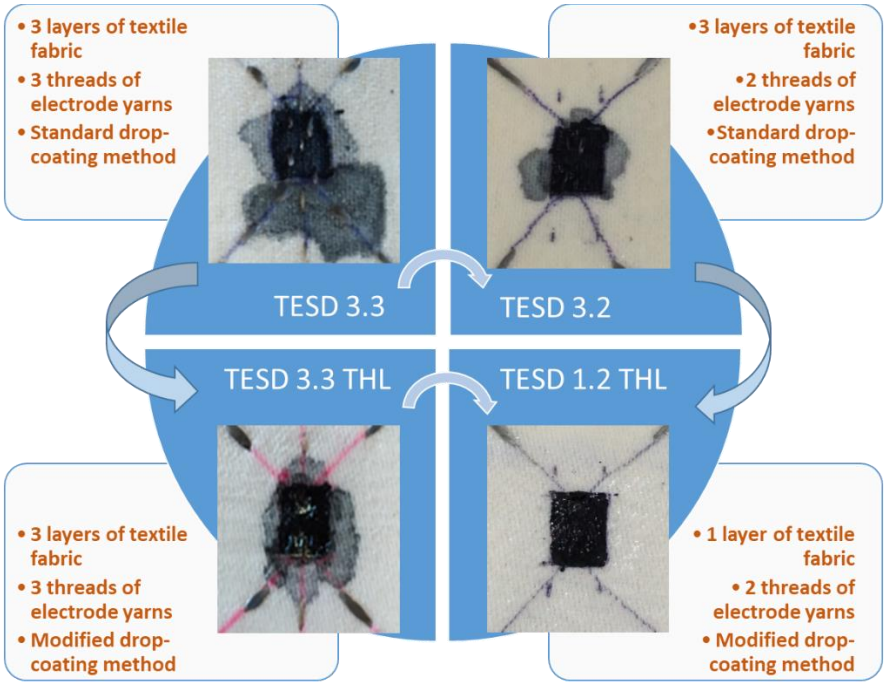

Main contents of this chapter were mainly redrafted from:

Nuramdhani I, De Mey G, Widodo M, *et al*. Ionic shot noise in an electrochemical capacitor system made of poly(3,4-ethylenedioxythiophene)-poly(styrenesulfonate) film and silver-coated polybenzoxazole-stainless steel electrodes on textile fabrics. Textile Research Journal **2018**, vol. 89, 7: pp. 1276-1285, https://doi.org/10.1177/0040517518767155.

Nuramdhani I, Odhiambo S, Hertleer C, *et al*. Electric Field Effect on Charge-Discharge Characteristics of Textile-Based Energy Storage Devices: In Search of the Underlying Mechanism. *Tekstilec* **2016**; 59(2), 162-7, DOI: 10.14502/Tekstilec2016.59.162-167.

3.1. Introduction

This chapter presents a series of gradual improvements of the textile energy storage devices under study in this research work. As described earlier, the development of a textile-based energy storage device is exceptionally beneficial to design so-called smart clothing [1]. Our device in its last design is made on a piece of fabric, which provides flexibility and lightness so that it does not become an obstruction to the clothing it is attached to. It can be attached to clothing by any existing techniques of joining such as stitching, using fusible adhesive interlining or Velcro tape. However, our ultimate goal is to fabricate the cell directly on the garment making it an integral part. In this regard, the device in its present design and form serves as a model with the textile substrate representing clothing fabric. The systematic and gradual improvements reported in this chapter were made based on that goal and understanding. A prototype of textile energy storage device with three identical stainless steel electrodes and conducting polymer PEDOT:PSS had been previously developed and successfully tested in our laboratory [2]. However, it was still far from an ideal energy storage device for smart textile applications [3]–[6], especially in terms of both its performance and its design. Some attempts to improve the performance and design of the device have been done through two different approaches, i.e. by improving the fabrication method to obtain better design and performance and by investigating the working principles and mechanisms of the device. This chapter is focused on the discussion of the first approach, i.e. by improving the fabrication method, while the latter is discussed subsequently in Chapter 4.

In summary, the device developed during the recent study has transformed from its earliest form into its latest form through four different and improved fabrication methods. For identification purpose, each device resulted from every fabrication method is given a code, as shown in a diagram in **Figure 3.1**. For

example, as can be seen from the diagram, the device TESD 3.3 has 3 layers of fabric and 3 threads of electrode yarn, whereas TESD 3.2 has 3 layers of fabric and 2 threads of electrode yarn. The first digit of the code refers to the number of fabric layers in the device, whereas the second digit denotes the number of electrode yarns. In order to understand the role of middle electrode, comparison was made between TESD 3.3 and TESD 3.2 hoping that performance would be improved in TESD 3.2. The next logical step was to see how coating might affect the storage of charge and improve the performance. So, TESD 3.3 THL with modified drop-coating method (THL stands for "thick layer") was fabricated and tested. This modification was mainly motivated by the inadvertent observation of the noise phenomenon in some of the experiments. The results and data that were collected and analyzed from TESD 3.3, TESD 3.3 THL, and TESD 3.2, led to the fabrication of TESD 1.2 THL and improvement of cell design and performance. It is the best form of our textile energy storage device up to this point. It is made of only one layer of fabric, which means that it is much thinner compared to the original design and thus more flexible as well as feasible for clothing. It consists of only two threads of electrode which gave a better charge storage capability. It also has a more defined PEDOT:PSS polymer in the cell area of the device because of two factors: (1) the application of water repellent agent which was very helpful to avoid diffusion of the dilute PEDOT:PSS dispersion during the drop-coating process; (2) modification of the drop-coating process as applied in the making process of the TESD 3.3 THL.

This chapter discusses the origins and development of ideas in the fabrication method of each device. The device TESD 3.3, which in this thesis is also called the standard device, adopted similar procedure from the previous PhD works of Odhiambo [2]. As mentioned in Chapter 1, the basic design of the device had followed the work of Bhattacharya *et al.* [7], who previously used three strands of silver coated polyamide yarn for the electrodes. Working with identical design except for type of electrode yarns, Odhiambo found different levels of charge

storage capability depending on type of electrode yarns. Only stainless steel and Ag/PBO yarns showed appreciable results, which is in contrast to copper. It was also shown that the output voltages from devices with Ag-PBO were about 50% lower than that with pure stainless-steel yarn electrodes. Based on those results, we, in this study, mainly used the less expensive pure stainless steel as our default electrode filament yarn, but Ag-PBO was also still used for some comparative studies. Apart from the mentioned reasons, the stainless-steel filament yarns are also flexible, and can be comfortably incorporated to textile fabrics. They show good electrical and thermal conductivity with high melting point that give further advantages of using this electro-conductive yarn as electrode in our fabricated textile based energy storage device [8].

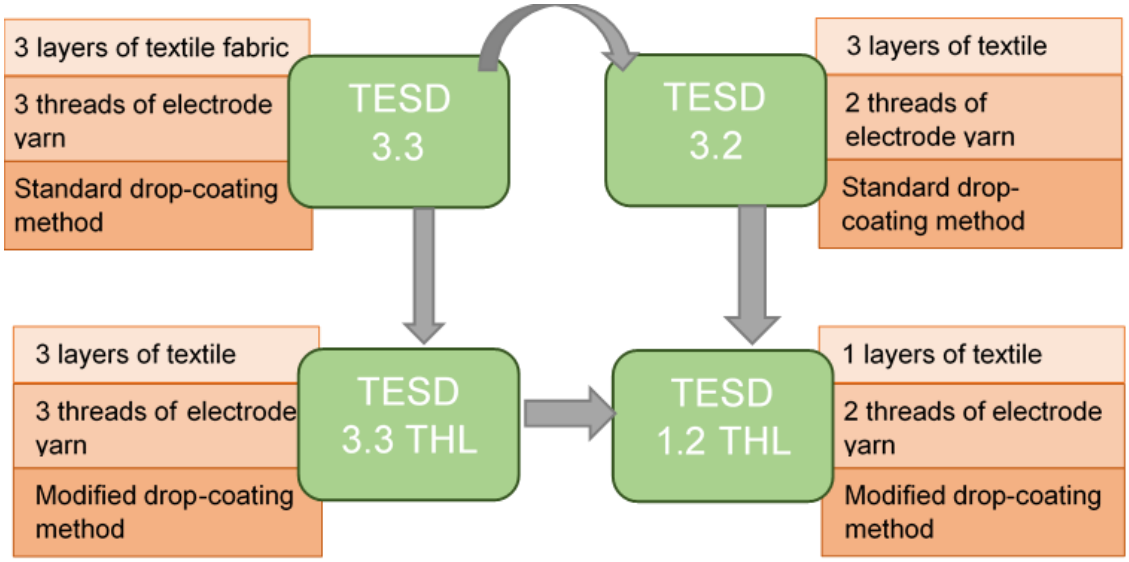

Figure 3.1. Transformation of the specification and name of devices based on the improvement of fabrication methods developed in this research

The purpose of this chapter is therefore to comprehensively describe and discuss the transformation that has taken place in the fabrication methods of our textile energy storage device including each detail procedure of fabrication, to produce its best form up to this stage of study. Prior to the discussion on the fabrication methods, a description about charge-discharge tests and measurements

method and few discussions on finding the optimum measurement condition such as charging voltage and time is presented in this chapter. The structure of the chapter was, thus, generally divided into two parts: (1) charge-discharge tests and measurements method; and (2) transformation of the device. The second part elaborates more in depth the motivations and some results which led to the improvement or modification of the device.

It should be noted here that the charge-discharge test or measurement was determined as the main method used to test the performance or storage capability of the device. Some supporting analyses such as microscopic-based characterizations or any other methods were also carried out when necessary to complete the information about the device behavior.

3.2 Charge-Discharge Measurement

3.2.1 Equipment

In general, charge-discharge tests and measurements for devices reported in this chapter used two different equipment. In the early stage of study, a National Instrument NI PXI 1033 (National Instruments, Austin, Texas, USA) was used. This equipment consists of a voltage generator, a digital voltage meter and a computer interface. The computer was equipped with a developed program that allowed the equipment to charge the device at specified voltages (V) and time (s) and also captured the voltage decay data automatically.

The main drawbacks of this equipment and its programming is that the charging profile cannot be observed. The test results present only the curve of discharge voltage. For that reason, different equipment was then developed and utilized to enable us to observe the charge-discharge profile of any devices under the test. The tool in question is a microcontroller "Arduino Uno" which was set up specifically for this particular purpose. Using this equipment, the progress of

charging and discharging voltages can be observed during the measurement. Although the information obtained from the National Instrument was not as complete as those obtained with Arduino Uno, the main results discussed in this chapter was still obtained from the National Instrument. **Figure 3.2** presents the visual appearance of both mentioned equipment used as well as circuitry diagram of each instrument and typical charge-discharge voltage obtained from each measurement.

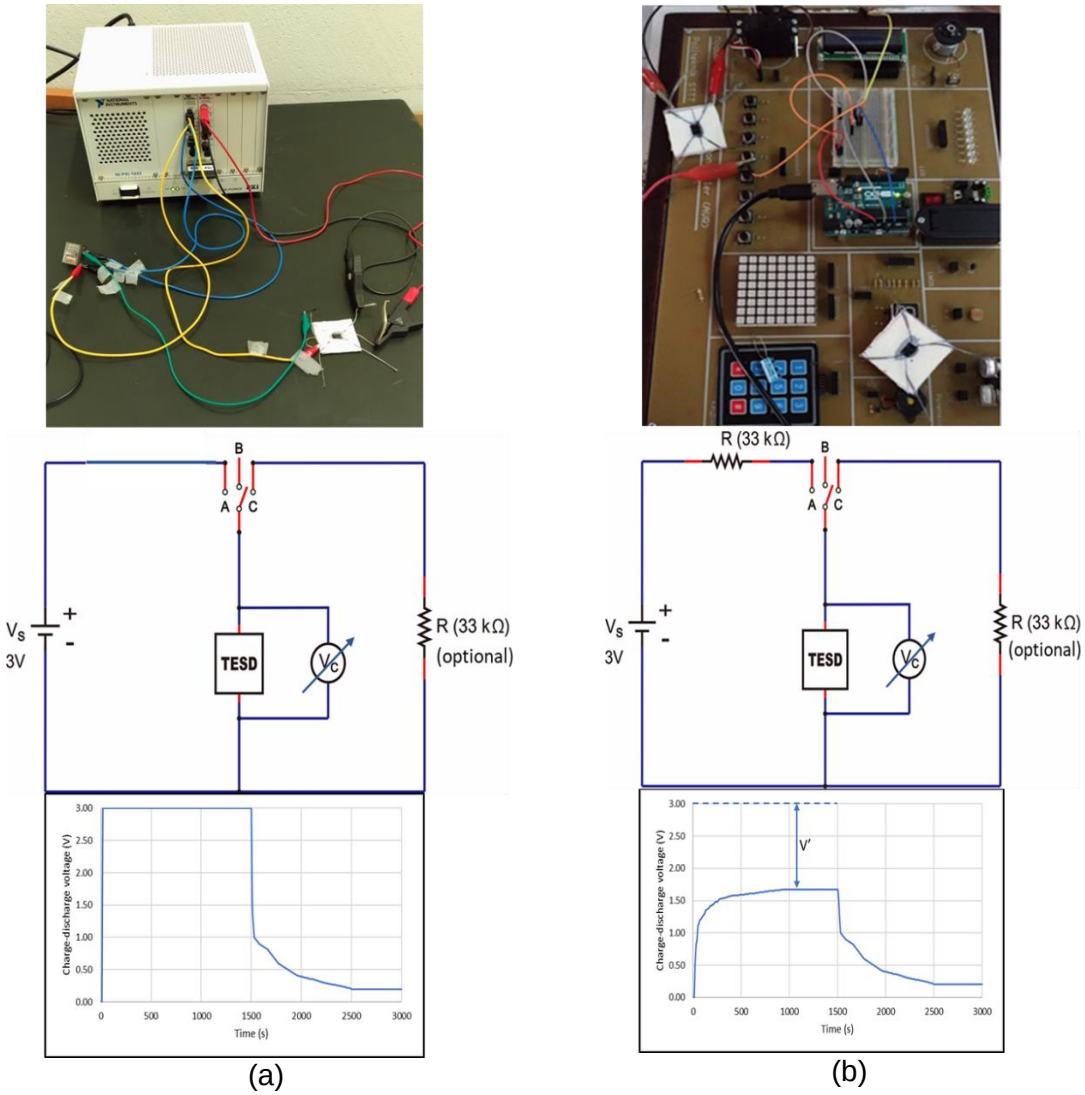

Figure 3.2. Visual appearance of the equipment used: (a) National Instrument NI PXI 1033; (b) Microcontroller Arduino Uno. Both are connected to the computer system to record and read the data. The circuitry diagrams and their typical charge-discharge profiles from the measurements are shown below each of the corresponding instruments.

Apart from the mentioned benefit of using the Arduino Uno, it is also worth mentioning that measurement using the National Instrument and the Arduino Uno microcontroller give some different results, especially for each observed discharge profile. The measurement results of the same device using both equipments showed about 20-30% difference in the discharge profile of the device, where measurement with the NI instrument gave higher discharge profile. As can be seen in **Figure 3.2**, the charge process in the National Instrument did not include resistance of 33 kΩ. So, from the manual recording, the value of its charging voltages was just exactly the same as the voltage value applied from the voltage source. In the National Instrument, the voltage stabilizer was also included, so the charge voltage levels were always controlled to reach its maximum value as applied. This kind of stabilizer was not added in the Arduino Uno, so the charge voltages observed were always around 50% lower that the applied voltage, beside the fact that 33 kΩ was also included during the charge process using this instrument. The resistance of 33 kΩ was applied during the charge process based on a series of preliminary trials to find the best value that gives a moderate time constant. Also, the voltage source of Arduino was not as strong as the one utilized in the National Instrument. The gap between applied and observed voltages is illustrated by the value of v' as shown in **Figure 3.2 (b)**.

3.2.2 Investigation of the Optimum Charging Voltage and Time

To obtain the optimum charging voltage, measurements with various charging voltages, i.e. 1.5 V, 3.0 V, 4.5 V, and 6.0 V were performed using the National Instrument NI PXI 1033 with two different charging times: short (300 seconds) and long (7,200 seconds). The devices used for this measurement had three strands of electrode yarns, but the measurements were performed on two pairs of electrodes placed at the distance of 1 mm. Every measurement used a different device but with similar characteristics, which all were the reproduction of TESD

3.3. During the course of the experiments, the devices were charged and discharged and their responses or voltage decays were recorded.

Figure 3.3 shows the profile of voltage decay of the devices with different charging voltages, which were charged in a long charging time (7,200 seconds). Identical charge decay behavior was also shown by the device given different charging voltage at the short charging time (300 second). From the data of long charging time as presented in **Figure 3.3**, it was found that the higher the charging voltage applied, the more the amount of accumulated charges in the device at its discharge phase. However, the increase in the stored energy was not proportional to the increase in the charging voltage given.

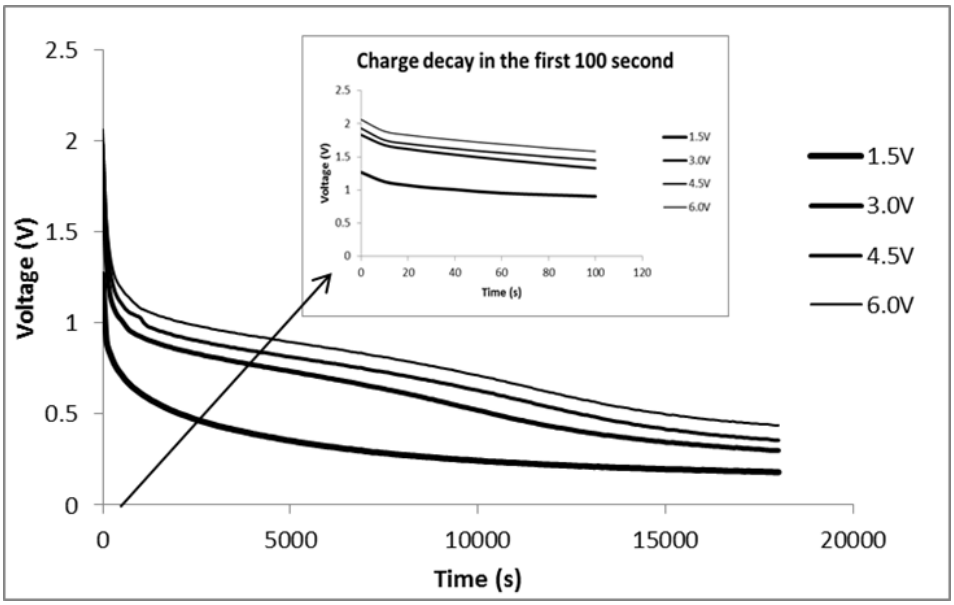

Figure 3.3. Voltage decay profile of the standard device with different charging voltages

It was observed that just after the power supply stopped, the charge level decayed drastically for each charging level. Graphs in **Figure 3.4**, which were taken from measurements using Arduino Uno, confirmed this observation. It can be seen from the graphs that although the higher charging voltage caused the higher charges that could be reached during the charging phase (comparing the curve

from device charged at 3 V and 5V), but the drastic decreases were observed from both devices. As discussed earlier, it confirmed that the increase in the charging voltage was not proportional to the decrease in the charge decays.

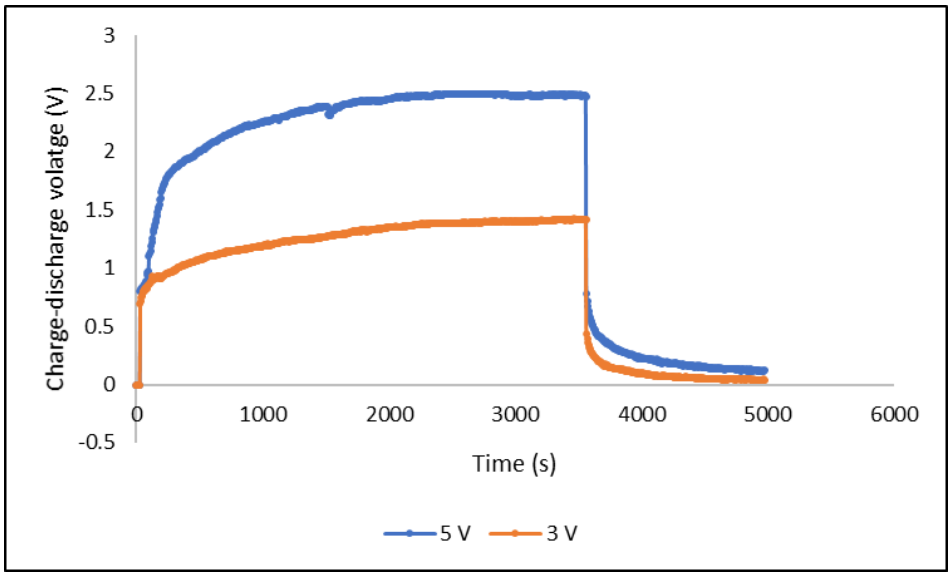

Figure 3.4. Charge-discharge profile of TESD charged at 3 V and 5 V using Arduino Uno

Furthermore, the data presented in **Table 3.1** show the percentage of voltage decay observed at the starting point (zero minute) of discharging phase for each of the different conditions. It would be noted here that the term "zero minute" (time = 0) is related to the time of initial measurement taken. It would be understood that during the charging process, the output voltage remained constant (input voltage = output voltage), until the time before the power supply was disconnected. Although the readings were done automatically using the software to minimize errors, there was still a gap between charge-discharge process (just before zero minute taken) where the voltage could not be recorded. Again, this is the drawback of the instrument that the charging voltage could not be observed progressively during the measurement.

Table 3.1. Voltage decay at the initial measurement (time = 0)

Charging voltage (V)	With short charging voltage (300 seconds)		With long charging voltage (7,200 seconds)	
	Detected voltage (V)	Percent decay (%)	Detected voltage (V)	Percent decay (%)
1.5	0.63	58	1.267	15
3.0	0.96	68	1.832	39
4.5	1.16	74	1.981	56
6.0	1.34	78	2.063	65

It can be seen that with a short charging time (300 seconds) the stored charges decayed more from 58% upwards at each charging voltage. With long charging time (7,200 seconds), the charge decay was less than 40% for devices constantly charged at 1.5 V and 3.0 V, while in higher charging voltage, the decay exceeded 56%. The data confirmed the typical performance as obtained from the previous result treated with various charging time.

The previous findings [2] have shown that increasing the charging time from 300 s (5 min) to 7200 s (120 min) significantly increased the discharge voltages accumulated up to 2-fold higher. However, prolonging the charging time up to 14,400 s (240 min) did not increase the accumulated charges in the device. This indicates that at certain extent the amount of residual charges stored in the device would not increase significantly. There is an upper limit of the charge density being able to be accumulated in the device. This assumption was confirmed by the charging profile of the same device measured with Arduino Uno, where the progress of charging voltage can be observed, as presented in **Figure 3.5**.

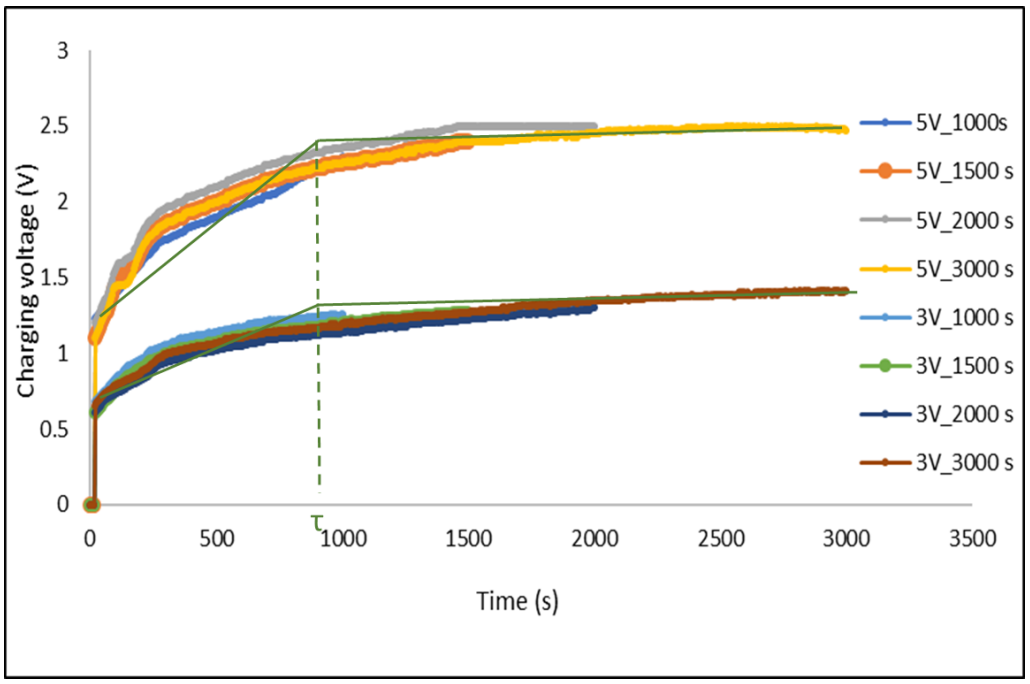

Figure 3.5. Charging profiles in various charging time

Figure 3.5 shows the charging profiles of devices in various charging times (1,000 s, 1,500 s, 2,000 s, and 3,000 s) which were charged at two different charging voltage (3 V and 5 V). The graphs indicate that the charging voltage increased slowly with time, and reached a constant value at a particular time. In general, it can be seen from all graphs that the steady states were reached some times before 1500 s. The more stable constant values were reached after 2000 seconds charging. These results led to the determination of 1500 s – 2000 s as our optimum charging time in the next experiments. As can be seen in **Figure 3.5**, the time constant (τ) of each charge curves are approximately 1000 s. Time constant can be calculated by multiplying resistance to capacitance ($\tau = RC$).

The charge decay profiles over 33 kΩ (**Figure 3.4**) also confirmed the previous finding [2] that the stored charges would drastically decrease up to a certain level where the decay was slower and the voltage profile became more constant. After a very long time, the voltage would reach the zero value. From our

experiment, it was found that the device could preserve the stored energy with a very slow decrease for 7 days when the voltage reached nearly the zero value. From the data concerning the very slow decay, the graph in **Figure 3.6** shows the relation between charging voltage and detected voltage observed at a given time (1,000 s, 6,000 s and 10,000 s respectively). In logarithmic scale, the increase of detected voltages at each observed time showed linear relations with consistent slopes number of around 0.1. From this relation, an empirical model: $V_2 = 0.1\ ln\ V_1 + C$, was obtained. A constant value of 0.1 was taken from the average slope values of each data series.

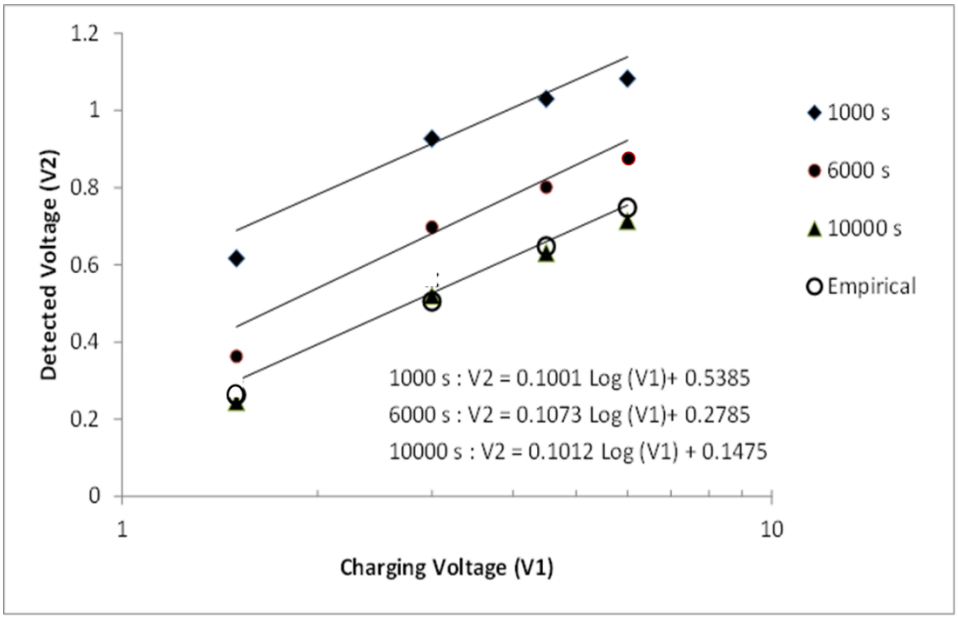

Figure 3.6. Log scale relations between charging voltage and detected voltage

Linear fit was done with $R^2 = 0.9976$, and it can be seen that the data points and the model built based on the empirical data are close enough. Although no physical interpretation can be assumed from this model, the relation between data from each point provided consistent slope and showed a linearity, that were good signs for a consistent data series observed. At the same time, it was also shown that the charging voltage (input) was not related proportionally to the detected voltage

(output) at several particular times. The doubling of the charging voltage did not result in a doubled detected voltage. That indicated that the device did not act as a pure capacitor because in capacitor, the increase in input voltage is proportional to the increase in the output voltage. The device did not act as a pure battery either because a constant output voltage is expected in a battery, regardless the input voltage level given to the device. Therefore, based on the discussions about measurement results with various charging voltage and time as shown above, it was then determined that the optimum charging voltage for the next measurements are at 3 V for 1500 s, although when required, we still tested the device in a longer charging time.

3.3. Transformation of the Devices

3.3.1 Fabrication Procedure of the Standard Device (TESD 3.3)

The standard device was a reproduction of the device that had been developed previously in the study of Odhiambo's [2], which consists of three strands of electrode yarns with symmetrical distance between the yarns. This type of device is named TESD 3.3. Each device was fabricated on three pieces of 5×5 cm^2 porous textile fabric. The textile substrate used was a twill woven polyester-cotton (PET/cotton) fabric with a warp density of 42 yarns/cm and a weft density of 29 yarns/cm. The electrode used was pure stainless steel filament yarns from Bekaert Bekinox VN 12-4X275-100S (Bekintex NV, Wetteren, Belgium), whereas the electro-active polymer dispersion M121 PEDOT:PSS AI 4083 (Ossila Ltd., Sheffield, UK) was utilized as solid electrolyte. In addition, thermoplastic polyurethane (TPU) layer from Epurex Films GmbH&Co (Bomlitz, Germany) with rectangle-shaped hole (6×10 mm^2) in the middle was employed to mask the surface and create the cell area. A standard commercial hot melt adhesive was used to join the fabrics together.

As for the procedure, first, the electrode yarns were stitched to the upper layer of the textile substrate (**Figure 3.7 (a)**). The electrodes were spaced equally at a distance of 1 mm. In every fabrication process, initial test should be performed to ensure the electrodes were well separated and there was no short circuit. Next, the three layers of fabric were joined together by applying fusible interlining between each layer, which was subsequently followed by a heat-press to melt the interlining and join the fabrics together a shown in **Figure 3.7 (b)**. The three layers of fabric were fused together to give body and a certain degree of stiffness that allow easier handling of the cell prototype during the fabrication, especially to prevent the dilute polymer (1.5-1.7 % dispersion in water) to diffuse through the fabric during the drop-coating process.

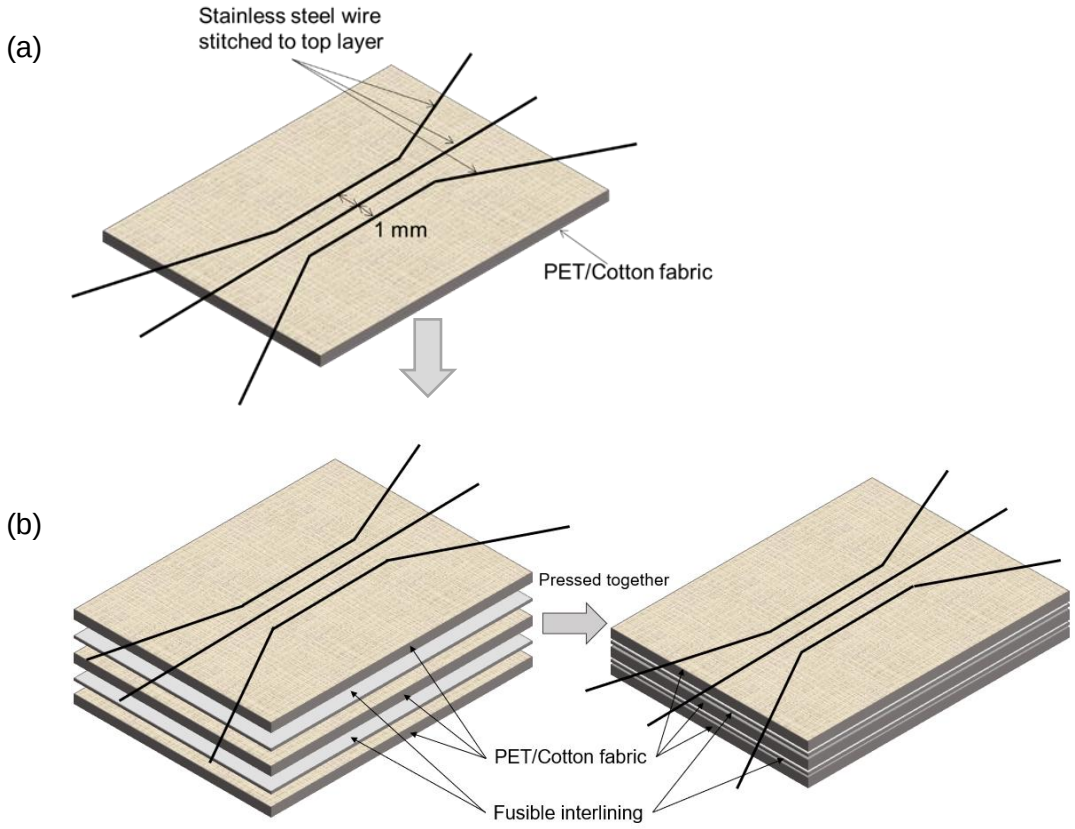

Figure 3.7. Illustration of assembling the electrodes on three-layered textile fabrics: (a) Stitching the electrode yarns; (b) Laminating the three-layered of textile fabrics.

The surface of the device was then masked with thermoplastic polyurethane (TPU) to give a hydrophobic layer on the fabric surface, except for the area where the solid electrolyte would be applied. The 6×10 mm^2 area in the middle of the upper layer where the electrodes were stitched was determined as cell area. As the content of the electrolyte polymer in the dispersion was low, the coating of cell area was done layer by layer by seven successive cycles of dropping and drying of PEDOT:PSS. Drying was done in an oven at 90-100 ^oC for 15 minutes before applying the next layers. **Figure 3.8** shows the pictorial steps of the surface masking and drop-coating processes.

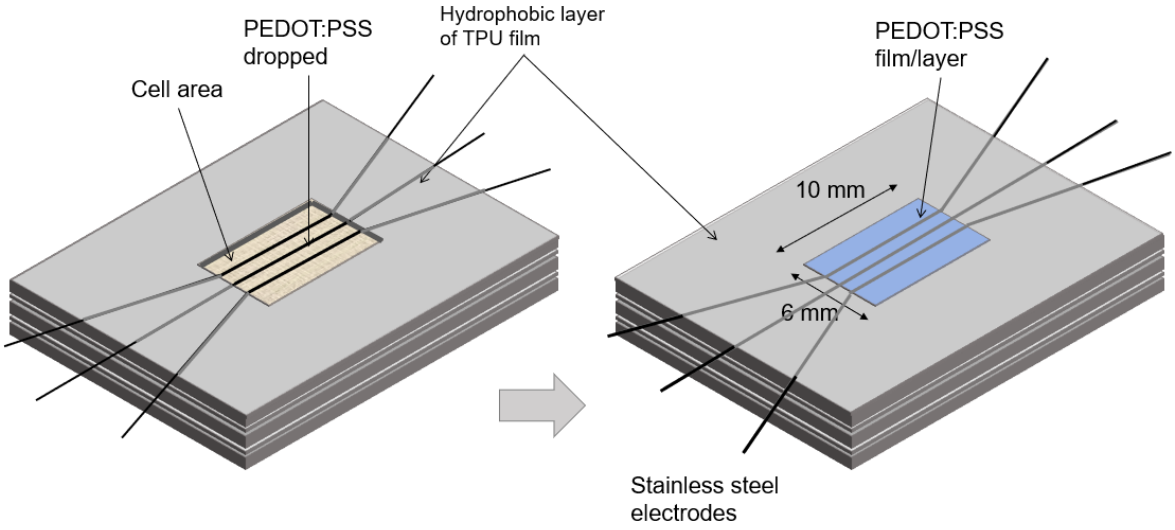

Figure 3.8. Illustration of covering the surface and drop-coating

Based on the stages illustrated above, it can be summarized that the construction procedure of the standard devices consists of four main steps:

1. Stitching of the electrode yarns into the textile fabric.
2. Laminating the three-layered of textile fabric using the interlining adhesive between each layer of the fabric.
3. Covering the surface by the hydrophobic polyurethane film.
4. Drop-coating and drying the PEDOT:PSS

3.3.2 From 3 to 2 Threads of Electrode

3.3.2.1 Background Study: Effect of the Middle Conductive Yarn

As mentioned before, the standard device, or so-called TESD 3.3 was a reproduction of the device made in the previous PhD work of Odhiambo, which had three threads of electrode yarn. There was no explanation before about the reason of inserting one middle yarn in between. To try to understand the role of the middle yarn, tests to some devices of TESD 3.3 using the National Instrument were carried out. Each device was charged at 3 V for 1500 s using the National Instrument, and the discharging voltages were observed. The results are presented in **Figure 3.9**.

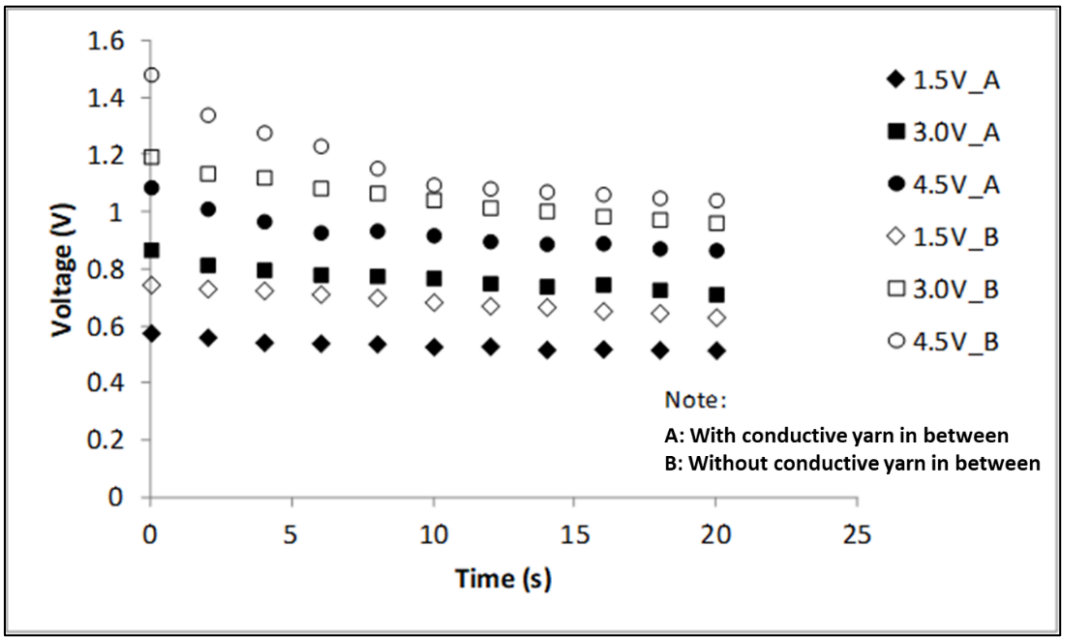

Figure 3.9. Discharge profiles of devices with and without middle conductive yarn, charged at 1.5 V, 3.0 V, and 4.5 V.

The graphs in **Figure 3.9** show the discharge profiles of devices A and B, all charged at various voltages: 1.5 V, 3.0 V, and 4.5 V, with the same distance between electrodes, i.e. 2 mm. All devices A had middle conductive yarn between the two electrodes (anode and cathode), which was not used as electrode, while devices B

did not. In general, it was observed that the presence of more conductive yarn between the measured electrodes had an effect on the performance of the device in its ability to store accumulated charge. The higher amount of accumulated charge was obtained from the devices that did not include a middle conductive yarn between the measured electrodes. This occurred for all measurements with different charging voltages (1.5 V, 3.0 V, and 4.5 V).

As mentioned above, the capacitive ability of the electro-active polymer PEDOT:PSS is associated with transport of charge carriers to the interface between the polymer and the yarn electrodes. Some characterization studies using SEM-EDX imaging and FTIR spectroscopy found the evidence of ion transport and redox reversibility in PEDOT:PSS [9], [10]. This was further confirmed by our analysis with EIS which is presented in Chapter 4. The ability to transport charges itself is caused by the presence of overlapping C=C bonds that give π orbitals along the polymer materials. They become electrically conductive due to mobile carriers (holes) created in the oxidized state [11]. From the previous work [12], it was suggested that dielectric polarization of PEDOT:PSS stimulated by the electric field applied through the charging process is the reason for charge storage capability of our developed device. As the stainless steel electrode yarn was not chemically inert and covered by a very thin layer of chrome oxide (Cr_2O_3) that can prevent further oxidation of the steel, it became capable of creating an insulating layer interface between the metal and the polymer [13], [14]. It has been reported that PEDOT:PSS film has no crystalline structure, it presents a strong effect on the charge transport, and therefore, the conductivity of the polymer was assumed to be due to its disordered conjugated system [11]. When the charging process is applied, an electric double layer was observed in both electrodes. Charge recombination then occurred just after the charging process stopped, when the separated ions from the polymer got back to their initial random arrangement [8], [12]. The graph shown in **Figure 3.9** confirmed this assumption. It can be seen from the graph that the

presence of the middle conductive yarn affected the amount of charges accumulated in the device. This could be because the PSS^- ions transport towards or from the end electrodes (anode or cathode) in the cell was restricted by the presence of the electrode between the measured electrodes. As it can be seen in the cross-section visualization of the cell presented in **Figure 3.10**, unlike electrons that can undergo a chemical reaction with metal, ions cannot. Therefore, the moving ions cannot penetrate and even their transport was restricted by the intermediate (middle) metal electrode. As the charge transport occurred on the surface of the device, the transport pathway also became longer as the ions would pass the surface of the middle metal electrode. These results proved further that the ionic transport principle occurred in the charge-discharge process of the device.

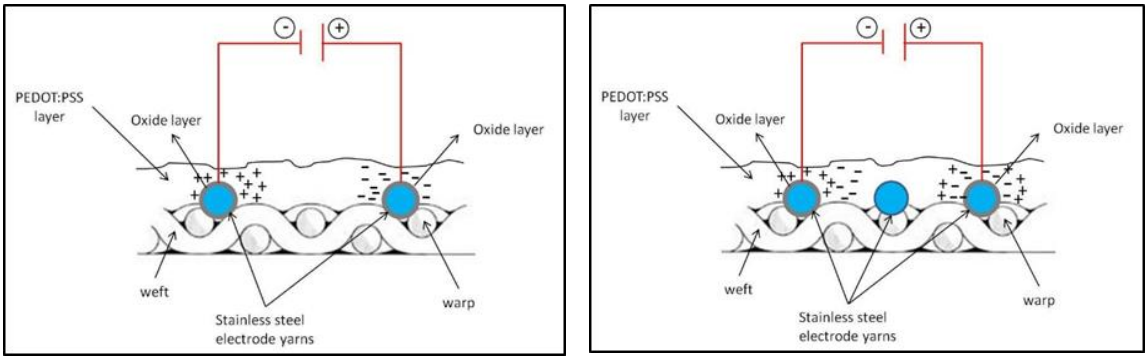

(a) (b)

Figure 3.10. Cross-section visualization of the device cell: (a) no middle electrode, (b) with middle electrode

3.3.2.2 Fabrication Procedure of the TESD 3.2

Based on discussions in the previous section, it can be said that the presence of the middle electrode in the device with three threads of electrode yarns does not effectively increase and improve the performance. Otherwise, it decreased the ability of the device to accumulate the stored charge. Thus, the device design was

transformed into two electrodes only, but still fabricated on the three-layered textile fabric (TESD 3.2).

The fabrication method of TESD 3.2 was similar to the one employed to the TESD 3.3 (section 3.2.1). The only difference was that only two threads of the electrode yarns stitched on the fabric. This type of device was also used for EIS (electrochemical impedance spectroscopy) analysis which is discussed in Chapter 4. The design of this type of device is also presented later in **Figure 4.1**.

3.3.3 Symmetrical versus Asymmetrical Electrodes

This part presents discussion about the ionic shot noise phenomenon inadvertently observed from some of the experiment results. The experiments were especially carried out to study the effect of asymmetrical electrodes. As reported in the previous study [8], only stainless steel (SS) and silver coated PBO (Ag-PBO) showed considerable results with charge storage capability in the discharge phase after having charged at particular charging voltage and time, although the performance was still far from ideal as an energy storage device. Making an asymmetrical device, where a thread of Ag-PBO yarn was inserted between the two parallel stainless steel, was one of the strategies to improve the device performance. The idea was that as stainless steel and Ag-PBO contain metal with different characteristics, i.e. size and polarity, mixing both as electrodes would allow the device to hold the charge longer. However, the hypothesis was not proven. Otherwise, unusual noise discharge profiles were observed from devices with asymmetrical electrodes. During a series of charge-discharge experiments for the characterization of its electrical properties we obtained noisy data showing fluctuation of voltages over time that resemble shot noise frequently found in electronic devices. From our comprehensive observation, it was believed that the PEDOT:PSS coverage on the cell surface played important role. In the following section, the study and discussion about this phenomenon is presented.

3.3.3.1 Background Study: The Phenomenon of Ionic Shot Noise

The phenomenon of noise in electronic devices and electrochemical noise has been known for a long time [15]–[17]. In an electrical conductor, it is a consequence of the quantization of charge. It can be used to obtain information on a system which otherwise is not available. In particular, shot noise experiments can determine the charge and statistics of the quasiparticles relevant for transport [18]. In an electrochemical system, noise can be observed as random fluctuations of current or potential under potentiostatic (galvanostatic) control which results from electrochemical reactions and diffusion [16]. The noise, according to Gabrielli [16], may originate from the microscopic processes at the electrode/electrolyte interfaces.

It was suggested that the noise observed during our discharge experiments with asymmetric device (Ag/PBO and stainless steel) might be related to ion transport within the bulk of PEDOT:PSS polymer and across the interface of polymer/electrodes. Thus, it might as well provide information on the mechanism and transport properties of charge within the device. It is generally believed that charge transport in PEDOT:PSS occurs by a hopping mechanism [9], [19]–[24], involving intra- and inter-chain transport between electronic active sites created by a series of redox processes within the polymer film [25]. Hopping also takes place between grains of PEDOT:PSS from one PEDOT-rich conductive region to the next, bridging an area of less conductivity, which consists of PSS or defects [11], [22]. In this model, the ordering of the PEDOT segments in the film is crucial for the transport of charges and conductivity of the film. These views support the significance of film formation in relation to the conformation of chains and morphology of PEDOT:PSS film. In this regards, it is interesting to note that the noise phenomenon in our experiments seemed to be related to film thickness.

The purpose of this work was therefore to obtain an understanding of the noise phenomenon observed during the discharge measurements of our asymmetrical device that consisted of stainless steel-Ag/PBO yarns and its relation with PEDOT:PSS film formation. The information obtained is then used to construct an idea of how charges are transported within the bulk of PEDOT:PSS film in our model device and improve the performance of the cell.

I. Experimental Details

Device used for this experiment was basically similar to the TESD 3.3, except that the middle electrode was replaced by Ag-PBO conductive yarn of Amberstrand (Syscom Advanced Materials Inc., Columbus, Ohio, USA). The fabrication method also followed that explained in Section 3.2.1. However, for this experiment, two different thicknesses of the PEDOT:PSS film were prepared. A thin film was obtained by following the standard drop-coating method as described in Section 3.2.1, whereas to make a thick film, the drop coating method was modified as described later in the Section 3.2.3.2. To ensure reproducibility, three identical devices having each type of layer were prepared and measured. Design of the device with asymmetrical electrodes as well as the visual appearance of each device can be seen in **Figure 3.11** and **Figure 3.12** respectively.

Charge-discharge tests and measurements were performed by using the National Instruments NI PXI 1033. In this experiment, each device was charged at 3.0 V for 3600 s by connecting the cell to the voltage source. One stainless steel electrode was first set as a positive potential and the Ag/PBO electrode at the negative potential, and then vice versa for the next experiment. Both stainless steel electrodes at both sides were measured the same way alternately. When the charging was completed, the instrument was automatically set to disconnect the cell from the voltage source, and the discharge curve was measured using a voltage meter with an input resistance of 10 MΩ. Measurement of each device was repeated

once in the following week to ensure that all remaining charges had been discharged before the next measurement.

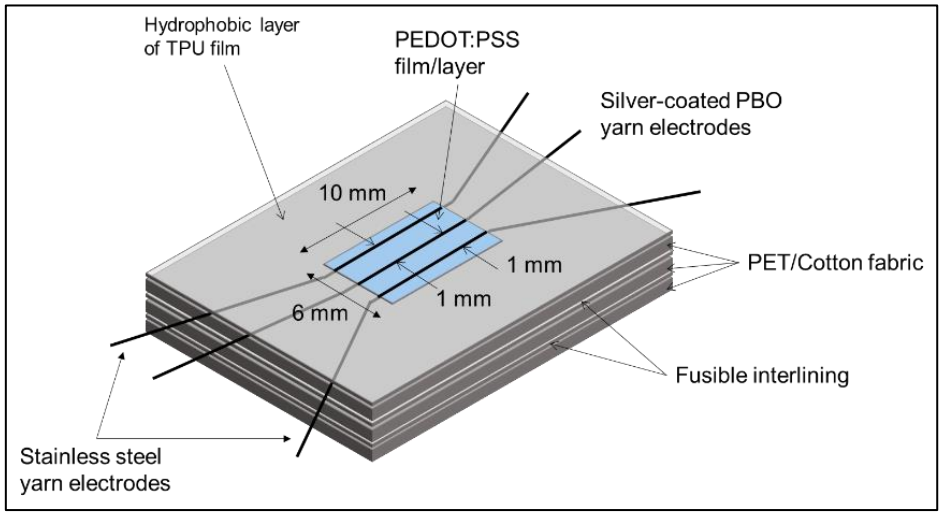

Figure 3.11. Design of the device with asymmetrical electrodes consisting of stainless steel and Ag/PBO yarns.

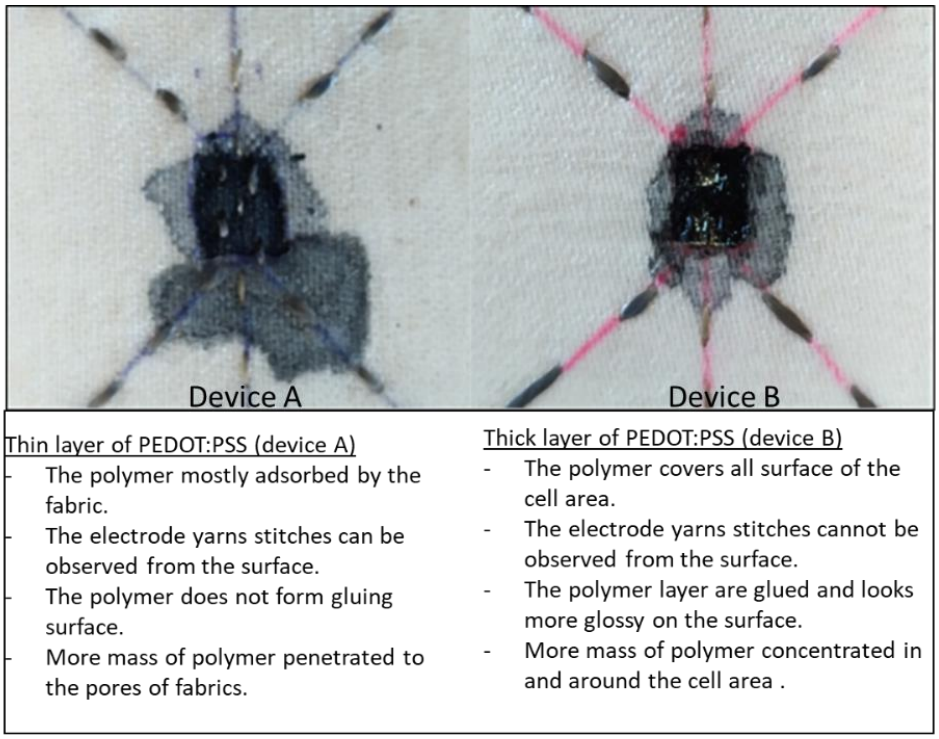

Figure 3.12. Visual appearance of devices having thin (A) and thick (B) PEDOT:PSS layers.

Observation of morphology. Surface morphology of the cells was detected by a stereo microscope Olympus SZX10 (Edmund Optics GmbH, Mainz, Germany) which was connected to the TOUPCAM CCD camera type L3CMOS14000KPA (USB2.0) (Hangzhou Touptec Photonics Co. Ltd., Zhejiang, China). The surface image of the devices was taken at 12.5 times magnification. Furthermore, the cross-section morphology of the cell was characterized by an integrated JEOL JSM 6510bSEM-EDS (Scanning Electron Microscopy-Electron Dispersive Spectroscopy) (JEOL USA Inc., Peabody, Massachusetts, USA). The image was taken from the middle part of the cell area, which was obtained by slicing the sample device with an 18 mm stainless steel rotary blade right at the middle. The prepared sample was subsequently placed in the sample holder of SEM for characterization and further analysis.

II. Discharge Profiles and Morphology

Figure 3.13 and **3.14** present the discharge profiles of devices with thin and thick PEDOT:PSS polymer layer, denoted as device A and B respectively. The term of thin and thick films here is further defined by the approximate measured thickness of the layer as described in the next section. Both devices had asymmetrical electrodes, i.e. Ag/PBO and stainless steel conductive yarns. The graphs in the two figures were obtained from different charging procedure where stainless steel and Ag/PBO electrodes were alternately set at positive and negative potential during charging of the device as denoted in each of the figures. It can be seen from **Figure 3.13**, the data from device with thin layer of PEDOT:PSS is very fluctuated and noisy. In a strong contrast, **Figure 3.14**, which was obtained from a device with a thick PEDOT:PSS film, shows two smooth curves of voltage decay typically found in our previous charge-discharge tests. Apparently, the formation and thickness of PEDOT:PSS film had an effect to the charge-discharge

measurements and may signify the transport of charges and ions within the bulk of polymer.

Despite the noise, however, the approximate lines obtained by smoothing of the noisy data in **Figure 3.13** look quite similar to the voltage decays in **Figure 3.14**, indicating that the two devices basically exhibited similar behavior. Consequently, the curves of **Figure 3.13** can be interpreted as the algebraic sum of a normal discharge curve and a strong noisy component. Furthermore, it can also be observed from the noisy graphs in **Figure 3.13** that the value of discharge voltages accumulated after charging was about two-fold lower compared to those with symmetrical stainless steel electrodes reported in the previous work [8]. As shown by the graphs in **Figure 3.13** and **3.14**, the starting point of discharge voltage is higher for device B, i.e. around 1-1.2 V, than device A, which is around 0.4 V. At the end of discharging, t = 3500 s, both devices had the same level of charges at around 0.1 V, which is also an indication that device B (with thicker layer of PEDOT:PSS film) decayed faster in the initial stage of discharging than device A. This observation confirms further that film formation and thickness might have an effect to charge storage capability of the device.

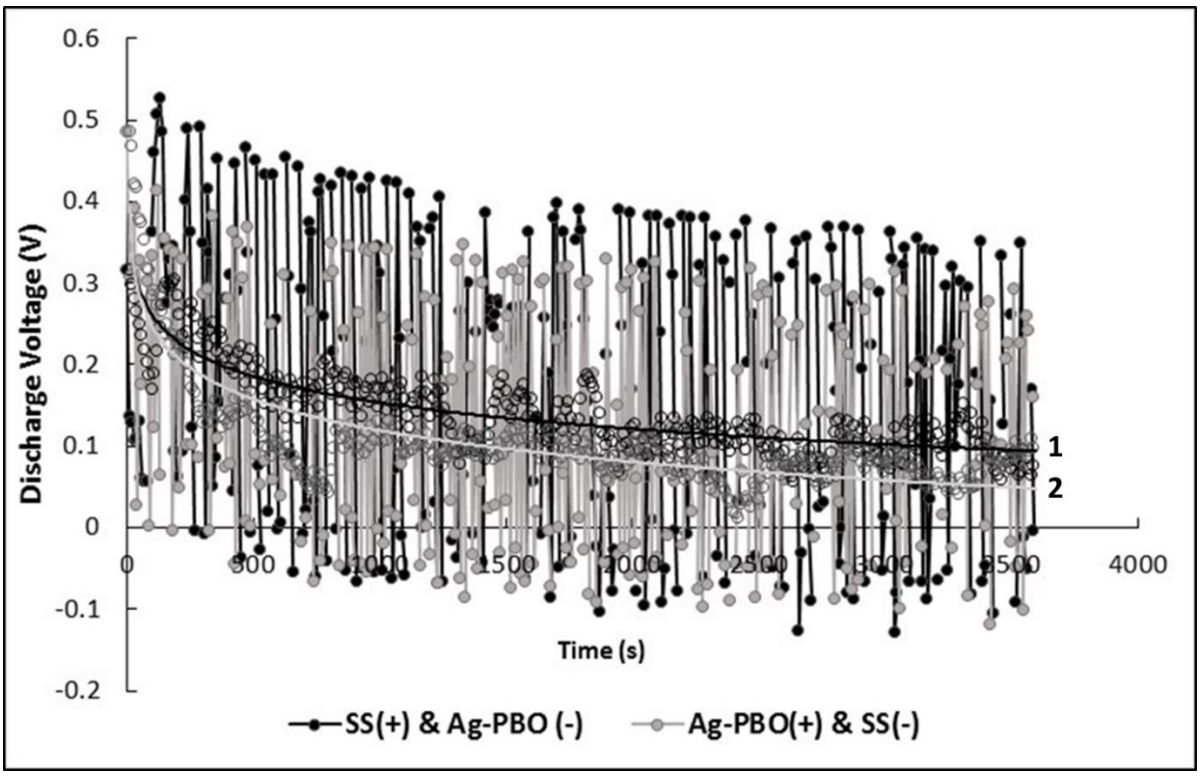

Figure 3.13. Noisy discharge profiles of a device with a thin layer of PEDOT:PSS. The lines with labels 1 and 2 are smooth fittings.

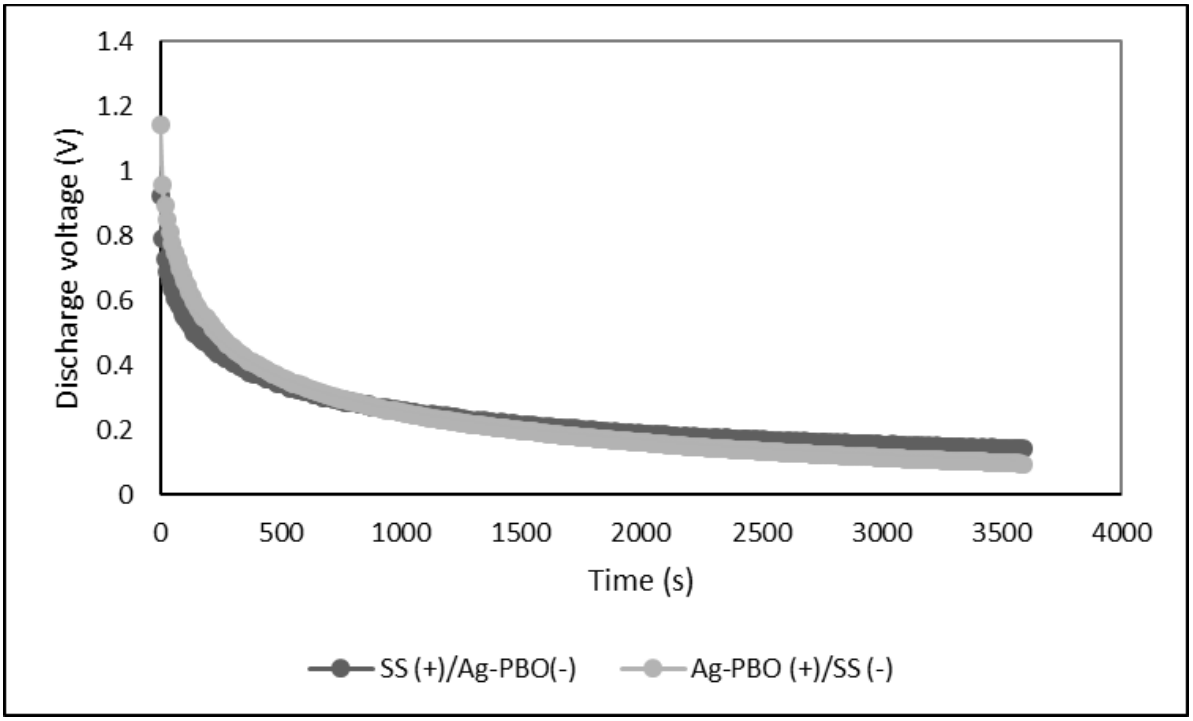

Figure 3.14. Discharge profiles of a device with a thick layer of PEDOT:PSS.

Different discharge behavior exhibited by the two devices has led to an assumption that coverage of polymer film on the surface of the cell played an important role. Surface morphology of the film on each of the devices as shown by **Figure 3.15** explains this phenomenon. As can be seen from the enlarged images (12.5 times magnification) of the cell area surface of device A and B presented in **Figure 3.15**, different characteristics of the cell surface are observable. In device A, the electrode yarns in the cell area are visible on the surface, whereas in device B, the electrode yarns are almost completely covered by the film of PEDOT:PSS polymer and thus are not discernible, which suggests better contact between PEDOT:PSS polymer and electrodes.

By using SEM-EDS (scanning electron microcope equipped with electron dispersive spectroscopy), Bhattacharya *et al*. [7] reported the migration of Ag^{+} from one electrode to another in their developed device, which clearly demonstrated that electrons or ions can move and travel through the solid PEDOT:PSS layers under the influence of an electric field. Assuming that our device followed the same mechanism, the silver ions originated from Ag/PBO yarn electrode, which resulted from the charging of the device, can migrate easier than the metal ions in the stainless steel such as nickel and/or chromium ions due to its smaller size and lower oxidation number. However, the migration was then held by the intermittent interactions between Ag+ ions and the conductive PEDOT:PSS polymer. In that situation the silver ions were trapped at some points until they found a negatively charged site from the polymer to excite. The delay of this type of ion movement could possibly cause the noise in the discharge curve.

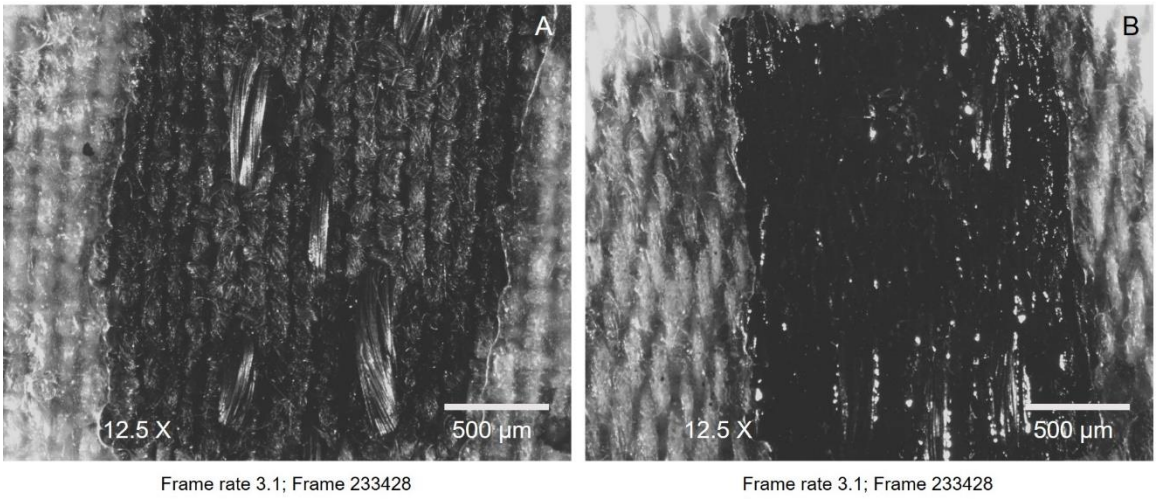

Figure 3.15. Magnified images of cell surface of devices having thin (A) and thick (B) PEDOT:PSS layers.

In device B, the case of delayed migration did not occur because continuous interactions between the silver and the polymer ions could be maintained. As shown by the image of device B in **Figure 3.15**, the drop-coating procedure applied to the device resulted in formation of PEDOT:PSS film with better coverage, hence better physical contact between the polymer and electrode yarns in the cell area. Formation of thicker film also means stronger interaction between the molecular chains in the polymer providing better conduction path for charge transport within the bulk of PEDOT:PSS film. Another aspect in the drop coating procedure of device B is that it took into account the main characteristics of the electrode, which is a porous cylindrical material composed of an assembly of filaments as opposed to a solid cylinder. In this regard, it must be noted though that the electrode yarn has a massive internal surface area. In order to achieve a thorough and close contact between these surfaces and PEDOT:PSS polymer electrolyte, it is necessary that the polymer dispersion penetrates the void spaces and interstices between the filaments in the yarn structure, which is the reason why the coating was not

initiated with pre-heated and more concentrated polymer. With a gradual heating of the polymer during the cycles of drop and dry, a controlled formation of PEDOT:PSS film was obtained in terms of penetration, film thickness and mass loading. The importance of film formation and chains interaction in the bulk polymer for charge transport and subsequently to conductivity has been confirmed and is supported by evidence in the literature [23], [24], [26]. For the sake of completeness, it must also be mentioned here that textile fabric is far from being a flat substrate as those used in the field of microelectronics. Moreover, the electroconductive yarns in the cell are not perfect cylinders either making it impossible to have a perfect electric contact along the entire surface of the yarns. Depositing a thin layer of PEDOT:PSS can give rise to a non-homogeneous conducting film. Such a structure can generate shot noise mechanism as well.

SEM-EDS image of cross-sectional view of the cell area in device B (**Figure 3.16**) shows the successive formation of polymer layers that made up the thick film. Based on the SEM analysis, the thickness of the film formed was identified to be approximately 940.38 μm (**Figure 3.16**). Looking at the cell surface appearance of Devices A and B shown in **Figure 3.15**, we assumed that the thickness of the thin film would be around three times less than the thick film because the electrode yarns being stitched onto the fabric were still visible quite apparently by naked eyes. From **Figure 3.16**, it can be seen how the polymer filled the spaces between the three conductive yarns. Elemental analysis by EDS in the cross section area of Ag/PBO yarn clearly shows that PEDOT:PSS was able to penetrate into the interstices of the yarn by the presence of sulfur (S) in the depicted area. Additionally, the analysis by EDS confirmed the presence of silver and the other main metals possibly contained in the stainless steel such as iron and nickel. They are distributed in the different orbital shells (K, L, M). The presence of silver metals or ions at different energy level shown by the chart also proved the distribution and excitation of silver electrons in the cell.

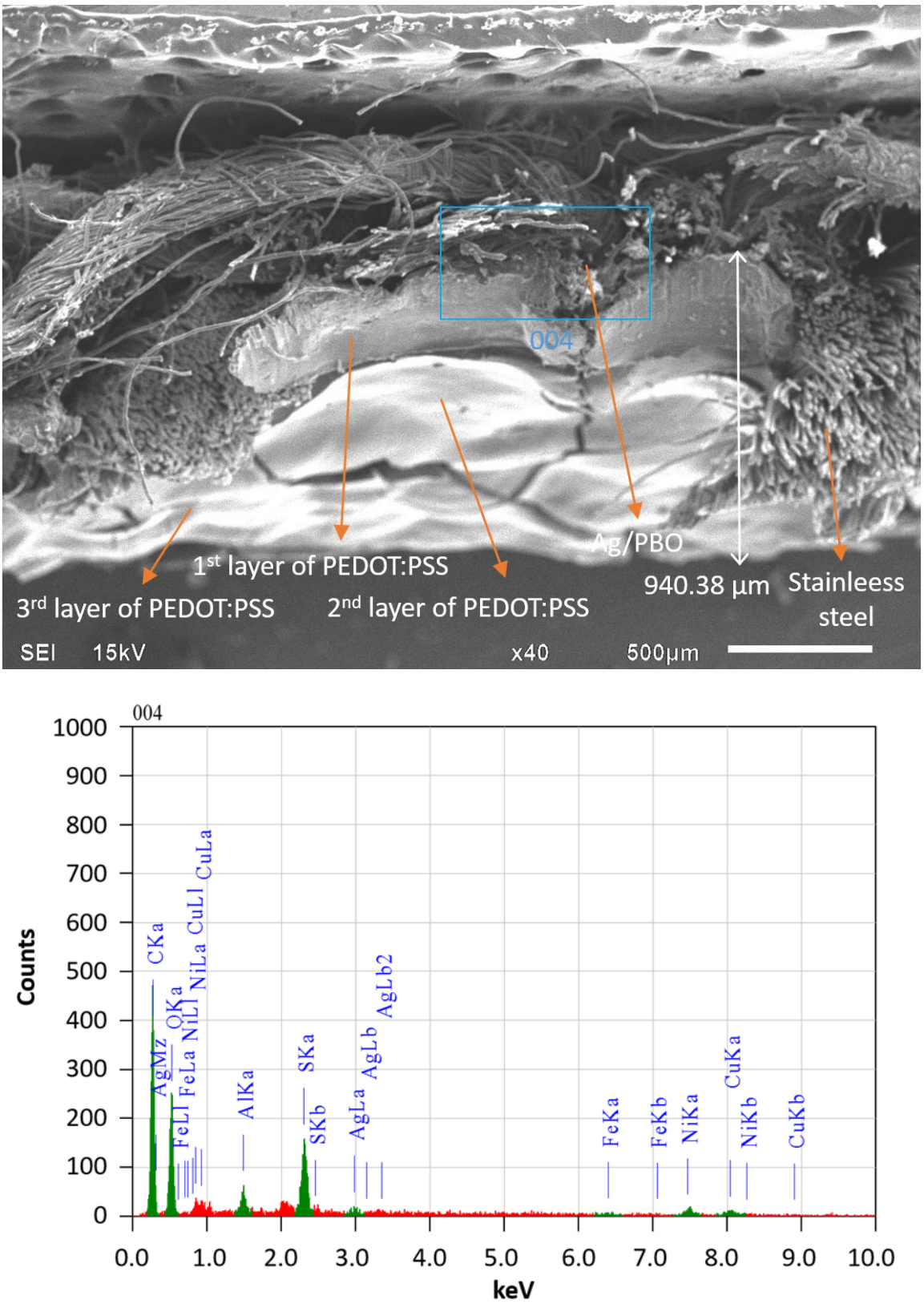

Figure 3.16. Cross-section image and elemental analysis of the device by SEM-EDS.

III. Physical Interpretation of the Noisy Discharge Profile

In order to explain the noisy component of the discharge curves (**Figure 3.13**), the autocorrelation function should be evaluated. The Fourier transform of the autocorrelation functions gives the spectrum of the noise. If we denote the discharge curve by the signal *v(t)*, the autocorrelation function $R(\tau)$ is defined by [27]:

$$R(\tau) = \lim_{T\to+\infty} \frac{1}{2T} \int_{-T}^{+T} v(t)v(t+\tau)dt \qquad (1)$$

The measurement time was limited to 1 hour (3600 s). Samples were taken with time intervals of Δt = 10 s or 360 samples in total. In order to convert the measured signal into a permanent signal (i.e. from $-\infty$ to $+\infty$), the experimental recorded signal was repeated periodically every 3600 *s*. The integral (1) can then be evaluated using the following numerical approximation:

$$R(\tau) = R(j\Delta t) = \frac{1}{360\Delta t} \sum_{i=1}^{360} v(i\Delta t)v((i+j)\Delta t) \qquad (2)$$

where $\tau = j\Delta t$ has been used. **Figure 3.17** shows a plot of the autocorrelation function calculated according to (2). For $\tau = 0$ the value of *R* is much larger than for $\tau > 0$. This suggests that the autocorrelation function can be an approximation of a dirac impulse function $\delta(\tau)$. The spectral density of which is a constant function also known as white noise. This kind of noise spectrum is typical for shot noise.

The PEDOT:PSS material is a mixture of PEDOT and PSS molecules. A small fraction of them being ionized to $PEDOT^+$ and PSS^-. PEDOT and PSS are both polymers and hence large molecules, in the range of 10 nm to 100 nm. As a consequence, the ions have a low mobility which explain the huge time constants observed in a discharge curve (**Figure 3.14**). The Ag^+ ions on the other hand are much smaller, more mobile and may give rise to faster transient phenomena, provided there is enough free space in between the large polymer molecules. It may

happen that a Ag^+ ion becomes blocked or trapped. Due to the slow movement of the $PEDOT^+$ and PSS^- ions, some free space can be made available so that the trapped Ag ions can jump to the next trap. The electric current observed from such a phenomenon is recognized as shot noise. The only difference is that we are dealing with mobile ions whereas in the literature shot noise is usually attributed to electrons, which can be trapped in the bulk of a material.

With this qualitative model, we can explain that the characteristic of **Figure 3.13** is the superposition of a normal discharge curve and a noisy component. The first one is due to the mobility of the $PEDOT^+$ and PSS^- ions. The noisy component is due to the movement of Ag^+ ions hopping from one trap to the next trap.

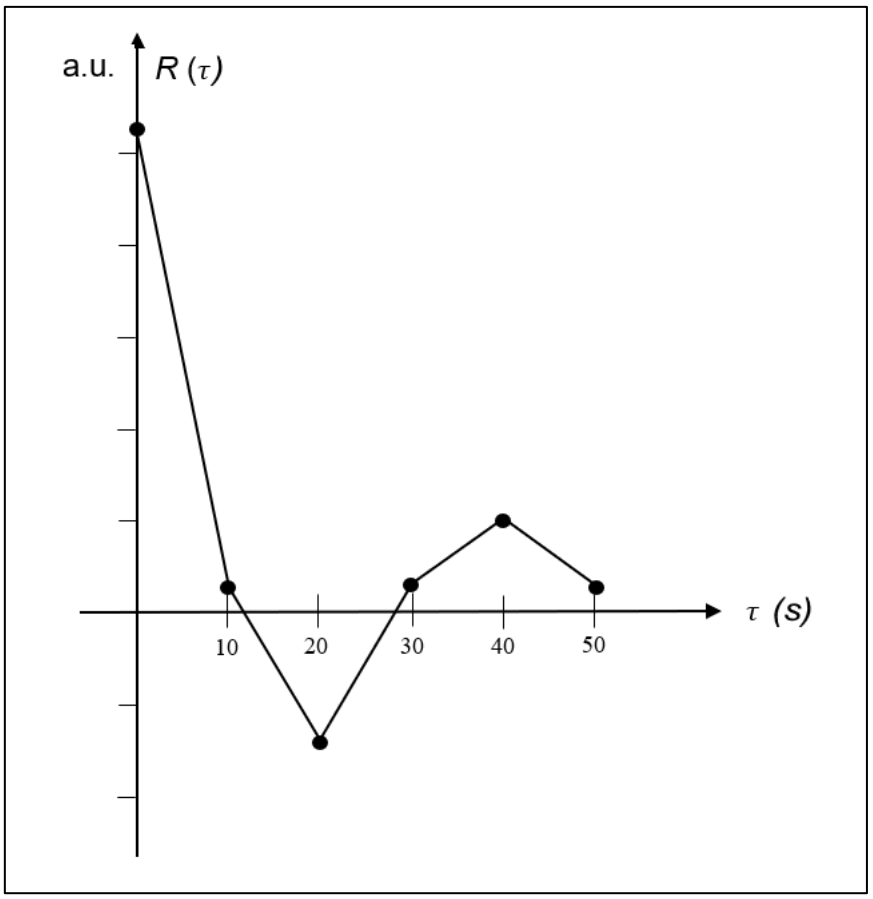

Figure 3.17. Numerically evaluated autocorrelation function of shot noise

One will remark that the noise is not observed for the discharge curve of cell containing Ag-PBO yarns in both electrodes as reported by Odhiambo et al [2], which looks contradicting with our findings about this shot noise phenomenon. In this case, apart from the importance of the continuous interaction between the Ag^+ with the PSS^- ions as described earlier, the Ag^+ ions can also always be deionized when they arrive at the negative Ag electrodes. In our experiment, only one electrode was made from Ag-PBO, while the Ag^+ ions could not be discharged at the stainless-steel electrode. More systematic studies are needed to prove this different phenomenon.

3.3.3.2 Modified Procedure of the Drop-Coating Method

It has been demonstrated that the noise is strongly related with the formation of PEDOT:PSS film and thickness. Device B (with thick layer of PEDOT:PSS film) was better than device A (with thin layer of PEDOT:PSS film) due to the better coverage of the electrode yarns by the PEDOT:PSS polymer, giving results to better connectivity and conduction path for charges and ions to travel through the polymer, as indicated by the less noisy discharge profile. These results have led to recommendation about the strategy of applying the PEDOT:PSS polymer on the cell via drop-coating method. It is therefore suggested to gradually heat the polymer dispersion during the drop-coating process to get a stepwise formation of polymer aggregate which allows more interactions between the polymer molecules and result in a good polymer coverage on the cell surface. This way, the possibility of getting a noisy device that cannot function as an effective energy storage device can be prevented.

With the standard drop-coating procedure, the coating of cell area was done layer by layer by seven successive cycles of dropping and drying of PEDOT:PSS. Drying was done in an oven at 90-100 ^oC for 15 minutes before applying the next layers. Thin layer of PEDOT:PSS film was obtained by dropping the unheated

PEDOT:PSS polymer dispersion. On the other hand, in order to obtain a thicker layer of PEDOT:PSS film, the polymer dispersion was kept in the oven and was allowed to slowly evaporate during the cycles of dropping and drying, making each drop more concentrated over time and resulting in a thicker film. Basically, with the latter procedure, the cell has larger mass loading than that with thin film. Also, with this modified procedure, the drop coating could be done only a maximum of 5 cycles, because mostly after the third drop, the polymer dispersion was expected to start gluing. Applying this more concentrated form of the polymer two times with drying for 10-15 minutes between each drop was enough to create a good coverage of the thick film within the cell area of the device.

3.3.4 The Importance of a Well-Controlled PEDOT:PSS in the Cell Area: From 3 to 1 Layers of Textile Fabric

As discussed earlier, the porous structure of the textile fabric and the electrode yarns have caused the intensive diffusion of the PEDOT:PSS dispersion during the drop-coating process, and thus the layer of the polymer spreads out of the cell area. This brought us to the idea to have the superhydrophobic surface of textile fabric, so that the polymer could be distributed only in the cell area. To realize this idea, the fabric used as textile substrate for devices in this research was pre-treated with a fluorocarbon-based water repellent agent to impart a hydrophobic effect on the fabric surface, and therefore prevent absorption of PEDOT:PSS into the fabric structure giving a confined PEDOT:PSS distribution within the cell area of the device. It can be seen later in the next section that in doing so, we found that there was no necessity anymore for the device to have three layers of textile fabric. One layer was enough, and this provided more advantages for the design of the textile energy storage device, i.e. thinner, lighter, and more flexible.

3.3.4.1 Application of Water Repellent Agent

As aforementioned, the idea with water repellent pretreatment was to prevent the drop of PEDOT:PSS dispersion from penetrating through and migrating across the fabric structure so that it was collected in a controlled amount and distributed within the cell area during the drop-coating process. For practical reason, the procedure was our attempt to control the mass loading of PEDOT:PSS during the process of coating so that it is reproducible for quantitative comparison when evaluating device performance.

NK-Guard NDN - 7 ENQ (Indonesia Nikka Chemicals Co. Ltd, Karawang, Indonesia) was utilized as the fluorocarbon-based water repellent (WR) agent. 2% of the solution was first impregnated onto the fabric by the padder set at 80% WPU (wet pickup), and then dried with stenter at 120 ^{o}C for 2 minutes. The drop test with water and PEDOT:PSS performed on the fabric showed an effective hydrophobicity as shown by **Figure 3.18**. It can be seen later in **Figure 3.20** that, as a result of water repellent pretreatment, PEDOT:PSS coating concentrated itself within the cell area whereas in the previous devices the polymer migrated out of the cell area (as can be seen in **Figure 3.12** for example). It demonstrated that the technique can be used to control the loading and distribution of PEDOT:PSS polymer dispersion during the coating process.

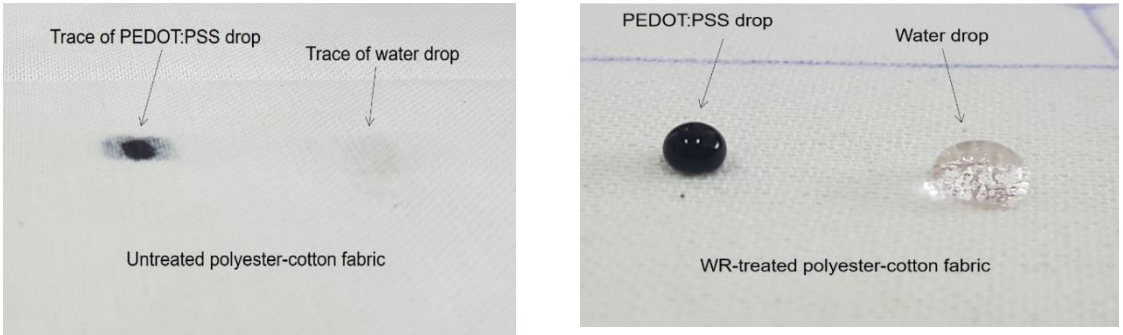

Figure 3.18. Drops of water and PEDOT:PSS polymer dispersion on (a) untreated fabric and (b) water repellent (WR)-treated fabric.

By pre-treating the textile fabric with the water repellent agent, we were also interested in different approaches and strategies to control and tune the performance of our device. We believe the ability to confine the formation of film within a predetermined cell area during the drop coating process can be critical to device performance and facilitate the more quantitative analysis on molecular interactions between the electrode yarns and the PEDOT:PSS. The contact area between PEDOT:PSS and the electrode yarn may have changed as well. This is not the focus of the study reported in this thesis, so we do not present any data or analysis regarding the distribution and molecular or electronic interaction of PEDOT:PSS in the cell area. However, a preliminary charge-discharge measurement to compare the performance of devices using WR pre-treated and non WR-pre-treated fabric was carried out beforehand to obtain the general result that, basically, the devices exhibited more or less identical charge-discharge behavior.

The devices measured here were made of PEDOT:PSS Ossila AI 4083 and a pair of stainless steel electrode yarns. As can be seen in **Figure 3.19**, during the charging process (5 volt for 1000 seconds), in general, the voltage of both devices increased gradually, and dropped sharply just after the charging stopped. The stored charges then dropped slowly and remained stable for some times during the discharge time. However, the charge-discharge voltage levels are slightly different, where the device with pre-treated fabric showed approximately 20% higher level of discharge voltage. It is possibly that the more confined PEDOT:PSS in the cell area of the WR-pretreated device has caused the lower internal resistance compared to non-WR-pretreated device, which therefore, causing the lower charging voltage. The more hydrophobic surface could also decrease the water uptake of the cell. This phenomenon is in line with our assumption about the possibility of the increase in the internal resistance due to the increase in the water uptake of the cell as presented later in **Figure 4.12** in Chapter 4.

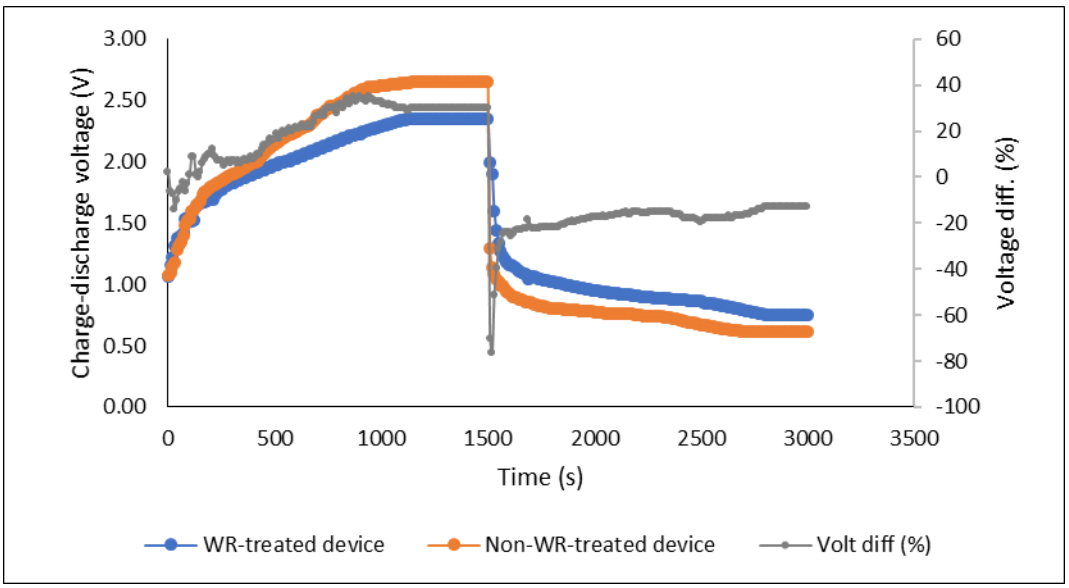

Figure 3.19. Charge-discharge profile of the water repellent versus non-water repellent pre-treated devices ("Volt diff" shows the difference of charge-discharge voltage of the two compared devices recorded along the measurement times)

3.3.4.2 Fabrication Procedure of the TESD 1.2 THL

This device was prepared on 5×5 cm^2-sized of the previously water repellent (WR) treated fabric. The cell area, which comprised of a pair of electroconductive yarns and drop-coated PEDOT:PSS film, was created by masking a layer of TPU film (thickness of 25 µm) to the fabric by a heat press at 100 °C for 2 minutes. The TPU film had at its center a rectangular hole of 6 mm to 10 mm to create an unmasked region and a confined area for the subsequent drop coating of PEDOT:PSS polymer dispersion. Before masking the surface and the drop-coating procedure, a pair of electrode yarns was stitched at a distance of 1-1.5 mm apart in the middle of the cell area (See **Figure 3.20 (b)**). An initial test with a multimeter was performed to each device to make sure that there was no short circuit due to contact between the stitched yarn electrodes. The drop coating of PEDOT:PSS, basically followed the procedure described in the section 3.2.3.2. However, a slight technical modification was done for the PEDOT:PSS coating method in this

research due to the hydrophobic surface properties of the fabric leading to having less amount of PEDOT:PSS polymer used for each device. With the perfect hydrophobicity on the fabric surface, there was no diffusion of the dilute polymer into the pores of the fabric as visually observed in the previous devices, and therefore, all polymer dispersion dropped into the cell surface can be completely distributed on the surface of the cell area. This way, instead of having seven drops as done in the previous works, five drops were sufficient to cover the cell area. As performed previously, drying of film was attained in the oven at 100 °C for 10-15 minutes layer by layer between each drop. During the coating procedure, the polymer dispersion was kept in the oven in order to make it more concentrated over time. After the fourth drop, the polymer dispersion had formed a paste, and thus, for the last coating, the paste was simply swept by a mini squeegee to improve the distribution. An example of the actual device can be seen in **Figure 3.20**.

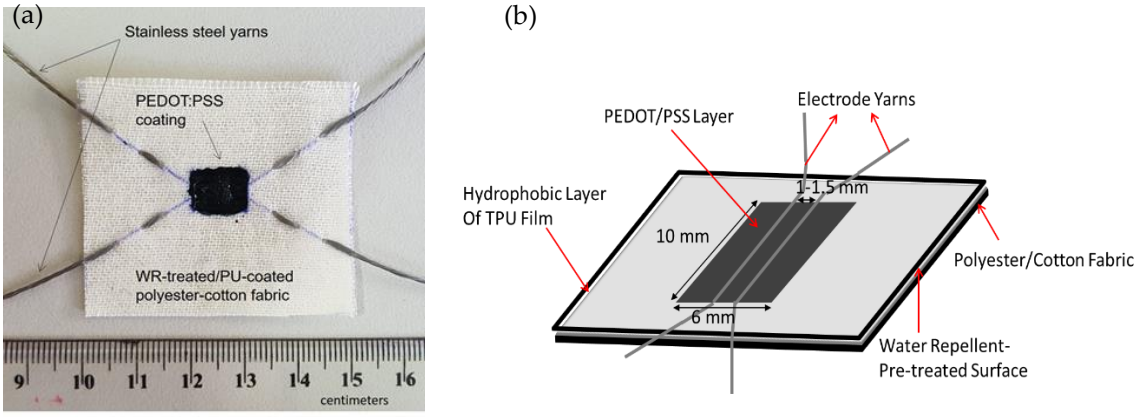

Figure 3.20. Example of the actual (a) and schematic design (b) of TESD 1.2 THL

3.4 Summary

The fabrication techniques of our textile energy storage device transformed from its basic design to its latest form. More efforts are still required to significantly improve the performance of the device, by either continuing further with the present approach or taking new direction but still related approaches.

Improvement in design, configuration, and performance has been achieved by the transformation from a device with basic design called TESD 3.3 up to the latest one so-called TESD 1.2 THL. The most important changes in the fabrication technique was that we have fabricated the device on a single layer textile fabric, while we previously made use of three-layered fabrics. This gave a lighter, thinner, and more flexible device. The distribution of PEDOT:PSS within the cell area was also more controlled because of the pre-treatment with the water repellent agent applied to the textile fabric which resulted in higher discharge voltages. It is important to note that some findings related to the mechanism, criteria, and method were obtained while changing the fabrication techniques. The change from 3 to 2 threads of electrodes was taken when we learned about the effect of the presence of middle electrode and its relation to the mechanism of ion movement in the device. The ionic shot noise phenomenon was another finding that was observed from the discharge profile of our energy storage device having asymmetrical electrodes of stainless steel and silver-coated PBO yarns with thin layer of PEDOT:PSS polymer. The assumption of ionic shot noise was confirmed by a qualitative model of autocorrelation function. The noise was suggested to be due to a series of interrupted movement or hopping of Ag+ ions across the bulk of polymer film from Ag/PBO yarn to stainless steel yarn electrode. It has been demonstrated that the noise is strongly related to the formation of PEDOT:PSS film and thickness. A better coverage of the electrode yarns by the PEDOT:PSS polymer gave results to a better connectivity and conduction path for charges and ions to travel through the polymer, as indicated by the less noisy discharge profile. These results had led to recommendation about the strategy of applying the PEDOT:PSS polymer on the cell via drop-coating method, which what we called the modified drop-coating method and resulting in devices so-called TESD 3.3 THL and TESD 1.2 THL. With this modified method, it was suggested to gradually heat the polymer dispersion during the drop-coating process to get a stepwise formation of polymer aggregate

which allows more interactions between the polymer molecules and results in a good polymer coverage on the cell surface. In this way, the possibility of obtaining a noisy device that cannot function as an effective energy storage device can be prevented.

Bibliography

[1] L. Van Langenhove and C. Hertleer, "Smart clothing: a new life," *Int. J. Cloth. Sci. Technol.*, vol. 16, no. 1/2, pp. 63–72, 2004.

[2] S. Odhiambo, "PEDOT:PSS Charge Storage Devices Integrated into Textiles for Smart Textile Application," Ghent University, Belgium, 2015.

[3] L. Bao and X. Li, "Towards Textile Energy Storage from Cotton T- Shirts," *Adv. Mater.*, vol. 24, no. 24, pp. 3246–3252, 2012.

[4] K. Jost, G. Dion, and Y. Gogotsi, "Textile energy storage in perspective," *J Mater Chem A*, vol. 2, no. 28, p. 10776, 2014.

[5] K. Jost, C. Perez, and J. K. McDonough, "Carbon coated textiles for flexible energy storage," *Energy Environ. Sci.*, vol. 4, p. 5060, 2011.

[6] X. Wang, K. Jiang, and G. Shen, "Flexible fiber energy storage and integrated devices: recent progress and perspectives," *Mater Today*, vol. 18, pp. 265–272, 2005.

[7] R. Bhattacharya, M. M. de Kok, and J. Zhou, "Rechargeable electronic textile batteries," *Appl. Phys. Lett.*, vol. 95, pp. 223305-1–3, 2009.

[8] S. Odhiambo, G. De Mey, C. Hertleer, A. Schwarz, and L. Van Langenhove, "Discharge characteristics of poly(3,4-ethylene dioxythiophehe):poly(styrenesulfonate) (PEDOT:PSS) textile batteries; comparison of silver coated yarn electrode devices and pure stainless steel filament yarn electrode devices," *Text. Res. J.*, vol. 84, no. 4, pp. 347–354, 2014.

[9] J. Ouyang, X. Qianfei, C. Chi-Wei, Y. Yang, L. Gang, and J. Shinar, "On the mechanism of conductivity enhancement in poly(3,4-ethylenedioxythiophene):poly(styrene sulfonate) film through solvent treatment," *Polym. Guildf*, vol. 45, no. 25, pp. 8443–8450, 2004.

[10] J. E. Collazos-Castro, J. L. Polo, G. R. Hernandez-Labrado, V. Padial-Canete, and C. Garcia-Rama, "Bioelectrochemical control of neural cell development on conducting polymers," *Biomaterials*, vol. 31, no. 35, pp. 9244–9255, 2010.

[11] A. Elschner, S. Kirchmeyer, W. Lovenich, U. Merker, and K. Reuter, *PEDOT: Principles and Application of an Intrinsically Conductive Polymer*. USA: CRC Press, 2011.

[12] S. Odhiambo, G. De Mey, C. Hertleer, and L. Van Langenhove, "Reliability Testing of PEDOT:PSS Capacitors Integrated Into Textile Fabrics," *Eksploat. Niezawodn. - Maint. Reliab.*, vol. 16, no. 3, pp. 447–451, 2014.

[13] F. Sundfors, H. Gustafsson, A. Ivaska, and C. Kvarnstrom, "Characterisation of the aluminium-electropolymerised poly(3,4-ethylenedioxythiopene) system," *J. Solid State Electrochem.*, vol. 14, no. 7, pp. 1185–1195, 2010.

[14] O. Inganas and I. Lundstrom, "Electronic properties of metal/polypyrrole junctions," *Synth. Met.*, vol. 10, no. 1, pp. 5–12, 1984.

[15] K. E. Nagaev, "On th eshot noise in dirty metal contacts," *Phys Lett A*, vol. 169, pp. 103–107, 1992.

[16] C. Gabrielli, F. Huet, and M. Keddam, "Fluctuations in electrochemical systems. I. General theory on diffusion limited electrochemical reactions," *J Chem Phys*, vol. 99, pp. 7232–7239, 1998.

[17] C. Gabrielli, F. Huet, and M. Keddam, "Fluctuations in electrochemical systems. II. Application to a diffusion limited redox process," *J Chem Phys*, vol. 99, pp. 7240–7252, 1998.

[18] Y. Blanter and M. Buttiker, "Shot noise in mesoscopic conductors," *Phys Rep*, vol. 336, pp. 1–166, 2000.

[19] K. S. Dongmin and S. G. Jeffrey, "Charge-transport model for conducting polymers," *Nat Mater*, vol. 16, pp. 252–257, 2017.

[20] T.-H. Le, Y. Kim, and H. Yoon, "Electrical and electrochemical properties of conducting polymers," *Polym. Basel*, vol. 9, p. 150, 2017.

[21] J. Y. Kim, J. H. Jung, D. E. Lee, and J. Joo, "Enhancement of electrical conductivity of poly(3,4-ethylenedioxythiophene)/poly(4-styrenesulfonate) by a change of solvents," *Synth. Met.*, vol. 126, pp. 311–316, 2002.

[22] A. M. Nardes, M. Kemerink, and R. A. J. Janssen, "Anisotropic hopping conduction in spin-coated PEDOT:PSS thin films," *Phys. Rev. B*, vol. 76, no. 8, p. 085208–1/7.

[23] X. Crispin *et al.*, "Conductivity, Morphology, Interfacial Chemistry, and Stability of Poly(3,4-ethylene dioxythiophene)–Poly(styrene sulfonate): A Photoelectron Spectroscopy Study," *J Polym Sci Part B Polym Phys*, vol. 41, pp. 2561–2583, 2003.

[24] H. Lee, J. Lee, and S. Park, "Electrochemistry of conductive polymers. 45. Nanoscale conductivity of PEDOT and PEDOT:PSS composite films studied by current-sensing AFM.," *J Phys. Chem. B*, vol. 114, pp. 2660–2666, 2010.

[25] J. F. Rubinson and Y. P. Kayinamura, "Charge transport in conducting polymers: insights from impedance spectroscopy," *Chem. Soc. Rev.*, vol. 38, pp. 3339–3347, Jul. 2009.

[26] A. Volkov, K. Wijeratne, and E. Mitraka, "Understanding the capacitance of PEDOT:PSS," *Adv Funct Mater*, vol. 27, p. 1700329.

[27] M. Woolfson and M. Woolfson, *Mathematics for physics*. New York, USA: Oxford University Press, 2010.

4

In Search of the Mechanism

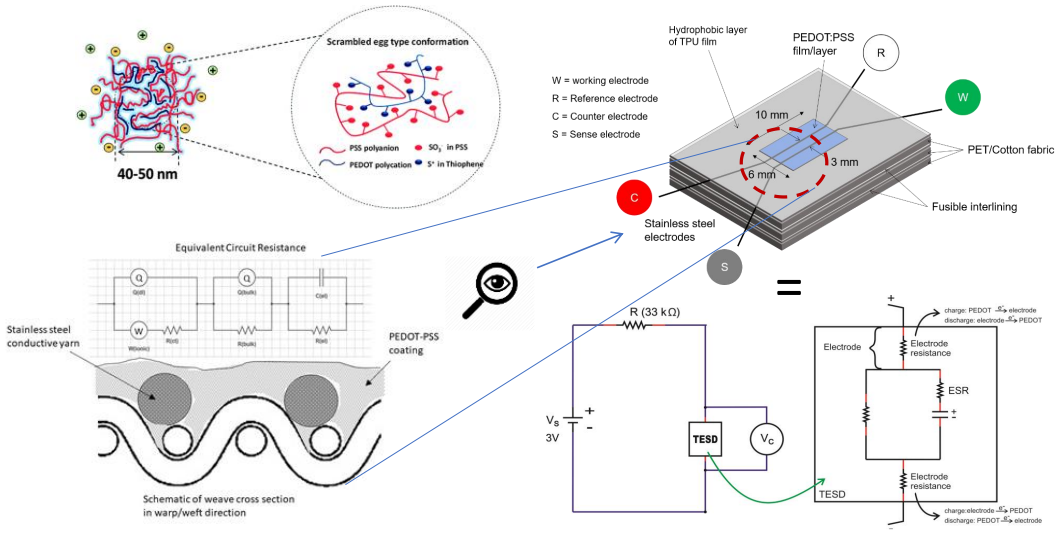

The main content of this chapter is mainly redrafted from:

Nuramdhani I, Gokceoren A, Odhiambo S, et al. Electrochemical Impedance Analysis of a PEDOT:PSS-Based Textile Energy Storage Device. *Materials (Basel)* **2017**; 11: 48; doi:10.3390/ma11010048.

Nuramdhani I, Jose M, Samyn P., et al. Charge-Discharge Characteristics of Textile Energy Storage Devices Having Different PEDOT:PSS Ratios and Conductive Yarns Configuration. *Polymers* 2019; 11(2), 345; https://doi.org/10.3390/polym11020345.

4.1. Introduction

One of the main issues that has attracted a considerable interest and attention in the development of textile energy storage devices is the underlying mechanisms of the device. The study on the mechanism is of a significant importance because the obtained knowledge can become a basis for improvements. A better understanding of the mechanisms will lead to a better strategy in which improvements can be made more systematically in a structured manner. However, for our textile energy storage device system, it is difficult to exactly determine the real single mechanism because a number of processes and conditions are involved. In this regard, it is worth emphasizing that the energy storage devices studied in this research were made of a piece of textile fabric coated in a defined area with an electroactive polymer of PEDOT:PSS as a solid organic polyelectrolyte complex, and electroconductive yarn electrodes. So that, at least three factors affected the way the devices worked: the characteristics of the textile fabric, the solid electrolyte PEDOT: PSS, and the electrode yarns used as well as their interactions.

In principle, there is a general and fundamental difference between the operational mechanisms of electrochemical capacitors and battery cells [1]. Ideally, with the double-layer type of capacitor (EDLCs), there is no electron transfer across the electrode interface and the storage of electric charge and energy is electrostatic. Charge accumulation is achieved electrostatically by positive and negative charges residing on two interfaces separated by a vacuum or dielectric. In battery-type processes, electron transfer takes place across the double layers. The charge storage is achieved by an electron transfer that produces chemical or oxidation state changes in the electroactive materials according to Faraday's laws related to electrode potential. Compared to batteries, supercapacitors or electrochemical capacitors demonstrate higher performance than batteries especially in terms of their power density, life cycle, and charge–discharge rate [2], although some

shortcoming issues such as high current leakage and low voltage window are still of concern in the field of research [3].

According to Bhattacharya et al. [4], the device they have developed worked based on the principles of a battery where a chemical interaction occurred at the Ag/PEDOT:PSS interface. SEM (*Scanning electron microscopy*) imaging and energy dispersive X-ray (EDX) analysis on the device have shown the movement of silver ions through the PEDOT:PSS from the anode to cathode under the bias of a high electric field. However, the previous PhD works of Odhiambo [5] that used stainless-steel electrode yarns indicated that possible other mechanism may also have come into play suggesting intermediate situations or hybrid mechanisms between battery and capacitors [6], [7]. A possible mechanism of charge storage could be that of charge separation within the structure of PEDOT:PSS. Different studies [8]–[14] have shown that PEDOT:PSS undergoes conformation changes from coil to more linear conformation under the effect of electric field followed by charge separation between the positively charged PEDOT and negatively charged PSS − each attracted towards negative and positive electrode respectively. Thus, it is plausible that both double layer capacitance and surface redox reaction exist in the operation of the device, hence the possibility of having a pseudo-capacitor.

This chapter presents some results from the study on the mechanism that have been carried out through several approaches in the current research. Electrochemical impedance spectroscopy (EIS) was selected as one of the methods as it is known as a sensitive technique for determining the mechanistic pathway of an electrochemical reaction [15]. It has been one of the routine analytical tools for the characterization and diagnosis of capacitors including textile energy storage devices. It allows estimation of frequency behavior, quantification of resistance, and the ability to model equivalent circuits of capacitor systems. EIS has been used to study the mechanisms of charge storage of different materials in different

electrochemical capacitors [15]–[23]. Cyclic voltammetry and constant current charge discharge methods were used in conjunction with EIS to discern different storage mechanisms which are knowingly unique for each of the materials [16]. In this study, cyclic voltammetry and EIS were used to investigate the ionic and electronic activity within the bulk of PEDOT:PSS and at its interfaces with stainless-steel yarn electrodes in our textile energy storage device. Equivalent circuit models were adopted as an approach to elucidate the contribution of different charge transfer or transport processes to the overall impedance of electrodes in the device.

The other approach for investigating the mechanism presented in this chapter is by looking at the effect of the PEDOT:PSS ratio to the charge-discharge performance of the textile energy storage device. As described in the previous chapter, PEDOT:PSS has attracted a great interest and has been the subject of many intensive studies because it is considered as one of the most technologically important electronic materials thanks to its excellent simultaneous properties, such as high electrical conductivity, processability, high stability, flexibility and good transparency [24]. Those exceptional properties land this polymeric system to a large variety of applications such as polymeric anodes for organic photovoltaic [25], [26], light-emitting diode [27]–[30], flexible electrodes [31], [32], supercapacitors [18], [22], [33], [34], electrochromic devices [35], [36], field-effect transistors [37], [38] and antistatic coatings [39]. Quite different from the majority of applications which mostly focused on its electrical conductivity due to its use as electrode in electronic devices [40]–[45], PEDOT:PSS has been used in our textile-based energy devices as a solid electrolyte layer that covered two parallel electrode yarns made of stainless steel and/or silver coated polybenzoxazole (Ag/PBO). In regard with different ratios of PEDOT and PSS in the complex polymer of PEDOT:PSS, we, in this study, were particularly interested in how the resulting different conductivities affect the working and performance of the textile-based energy storage devices. It was quite

plausible that the performance of the device be affected by the conductivity of PEDOT:PSS film to give different storage capability for each of the devices.

In this chapter, fabrication methods of the devices used in each approach to study the mechanism are not described in detail because all the fabrication methods have been presented and discussed specifically in Chapter 3. The experimental procedures for test and analysis are included in detail in each relevant sub-section.

4.2. Study on Mechanism from Cyclic Voltammetry and Electrochemical Impedance Analysis

For this study, cyclic voltammetry (CV) and electrochemical impedance spectroscopy (EIS) were performed in the Advanced Electrochemical System Parstat 2273 of "Princeton Applied Research" which was available in the Laboratory of Smart Textiles, Department of Materials, Textiles, and Chemical Engineering, Ghent University. The instrument was equipped with a built-in software (PowerSuite, Ametek Scientific Instrument, Elancourt, France) for data processing and analysis. The impedance spectra were measured at charged and uncharged devices in the frequency range between 100kHz – 100 μHz. A two-point probe system was devised using a Princeton Applied Research Parstat 2273 Potentiostat in conjunction with Powersuite software. Two electrode experiments measure the whole cell, that is, the sense leads measure the complete voltage dropped by the current across the whole electrochemical cell: working electrode, electrolyte, and counter electrode. The design of the device and its physical setup for measurement is shown schematically in **Figure 4.1**: two leads, working and reference electrodes, were connected to one side of the sample, with two more leads, the counter and sense electrodes, at the other side of the sample. An equivalent circuit was used to fit the experimental data, with the help of the standalone ZSimpWin v3.20 software. The charged conditions were achieved via

chronoamperometry, where the device was charged at 2 V for 1 hour before the EIS reading.

The devices used for this analysis were similar to those described as TESD 3.2 in Chapter 3. Details of the device fabrication, as mentioned before, can be found in Chapter 3 section 3.3.2.2, but with the modified drop-coating method as illustrated in section 3.3.3.2. It should be noted here that the distance between electrodes in the devices was varied: 3 mm and 6 mm.

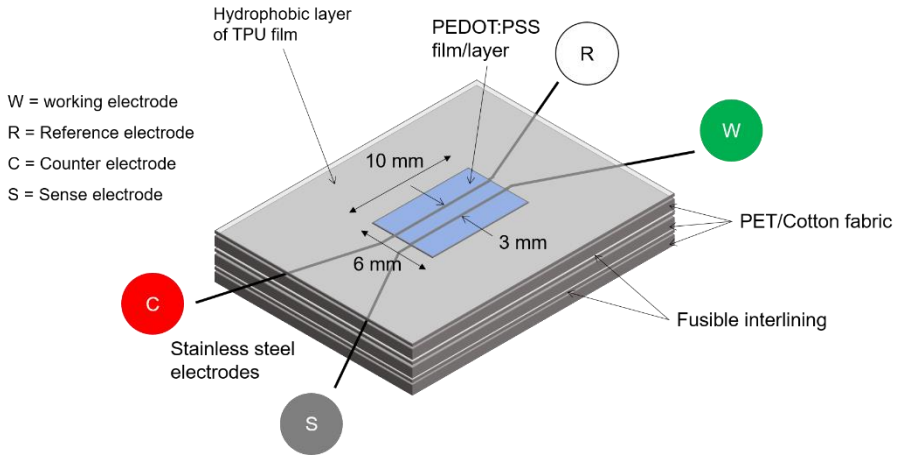

Figure 4.1. The design of energy storage device used for CV and EIS experiments and its set-up of electrodes for the measurements.

Electrode yarns used in the textile energy storage devices measured in these experiments were similar to those used in the so-called standard device, i.e. pure stainless steel (SS) Bekaert Bekinox (Bekintex NV, Wetteren, Belgium). An inert platinum (Pt) wire, however, was also used in some devices. The Pt wire (Goodfellow Cambridge Limited, Huntingdon, England) had purity of 99.99% with diameter of 0.40 mm. So, for solid state materials, there were two types of devices: both stainless steels (SS/SS) and both platinum wires (Pt/Pt). Additionally, a device with a combination of SS/Pt electrodes was also prepared to check the movement of ions. For measurement of cyclic voltammetry in a liquid solution

system, the inert Pt and stainless-steel yarn were also used and compared as a working electrode, while Ag/AgCl was employed as a reference electrode.

Likewise, similar conductive polymer M121 PEDOT:PSS AI 4083 (Ossila Ltd., Sheffiled, UK) was used as the solid electrolyte for this analysis. From the technical data, the electroconductive polymer was known to have conductivity of 0.002−0.0002 S/cm. For measurement of cyclic voltammetry in the solution system, the liquid PEDOT:PSS was measured at its dispersion concentration given by the company without any dilution, i.e. 1.3−1.7 wt.% (in water). 0.1 M of NaCl as supporting electrolyte was also included in the dispersion.

4.2.1. Evidence of Redox Reactions in PEDOT:PSS by Cyclic Voltammetry

For the analysis of electroactive species, cyclic voltammetry is one of resourceful methods which consists of cycling the potential of an electrode, and measuring the resulting current. The results are represented in a cyclic voltammogram which contains the current at the working electrode during the potential scan. It presents the current versus potential which are usually varied linearly with time [46]. **Figures 4.2–4.4** show the cyclic voltammograms of PEDOT:PSS in aqueous dispersion and in the form of thin films on glass surface and on fabric with stainless-steel (SS) yarn electrodes at different distances, i.e., 3 mm and 6 mm.

The electrochemical activity of liquid PEDOT:PSS is given in **Figure 4.2**. It should be noted that measurement with an inert Pt electrode showed no ionic behavior from the electrode that was differently showed by the stainless-steel electrode. From the measurement using stainless-steel yarn as the working electrode, it can be seen from the diagram in **Figure 4.2** that two consecutive weak oxidation peaks appeared at 1.05 V and at 1.4 V, while a single and strong reduction peak is observed at 0.8 V. The reduction peak increases with the root mean square

of the scan rate, obeying the Randles-Sevcik equation [46], confirming a diffusion-controlled process on a thin film. The results confirmed one of the properties of PEDOT:PSS, which acted as a polyelectrolyte for this electrochemical system. In this redox reaction, diffusion of reactants, which occurred most probably due to the charge transport originated from free charge carriers of the PEDOT in oxidized state, went slower than the formation of the reaction product from its activated complex. Based on the literature, the PSS does not contribute to charge transport directly, but it acts as a template to keep PEDOT in the dispersed state and provide film-forming properties [47].

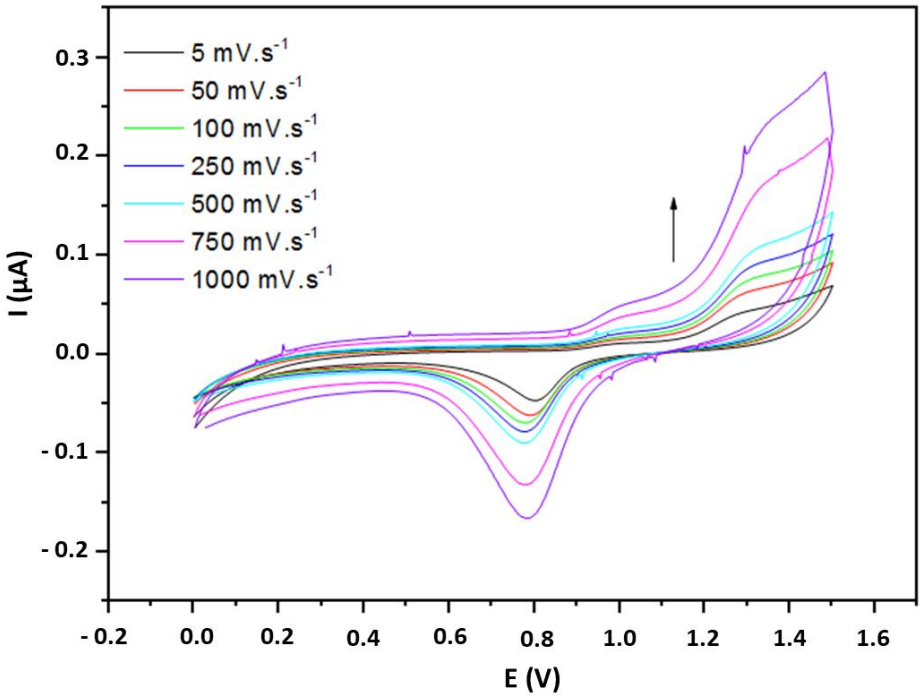

Figure 4.2. Cyclic voltammogram at various scan rates for PEDOT:PSS solution.

The measurements of PEDOT:PSS coating on the glass surface with SS (stainless-steel) yarn electrodes spaced at two different distances (3 mm and 6 mm) are given in **Figure 4.3**. As shown by the cyclic voltammograms (**Figures 4.3.a** and **4.3.b**), the distance of the electrodes (*d*) had a major influence on the conductivity and capacitive behavior of the samples. The square-like or hysteresis structure

observed between 0–1.8 V regions from the sample with a 3-mm electrode distance provides a visual confirmation of the capacitive behavior (**Figure 4.3.a**) of the cell, while the higher current intensities define its better conductivity. On the other hand, the sample with a 6-mm electrode distance (**Figure 4.3.b**) has lower conductivity and weaker capacitive behavior.

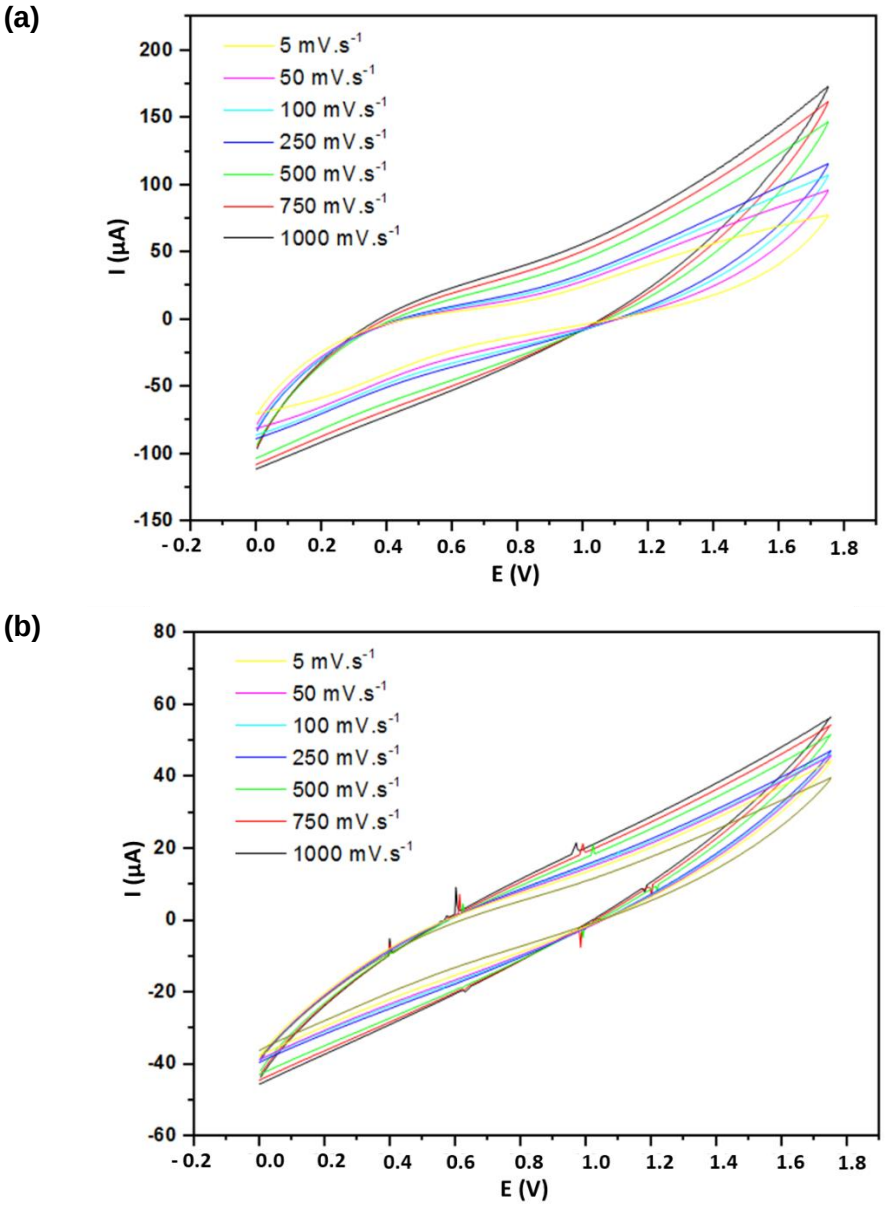

Figure 4.3. Cyclic voltammogram at various scan rate for PEDOT:PSS film on glass surface with electrode distance *d* of (**a**) 3 mm and (**b**) 6 mm.

Similarly, the sample on the fabric surface showed the same behavior as the sample on the glass surface (**Figure 4.4**). The capacitance of each device can be determined by calculating the surface area integrated between the two curves in the voltammogram. Based on the calculation, the sample on the glass surface has a capacitance of 127 µF and 45 µF for electrode distances of 3 mm and 6 mm respectively, while the sample on the fabric surface showed a capacitance of 66 µF and 36 µF for the 3-mm and 6-mm electrode distance. In both cases, increasing the electrode distance lowered the capacitance. However, it was found that capacitance is higher on the glass surface than on the fabric surface due to the higher dielectric constant of glass which is around 5-10 at 20 °C. This was most likely due to the diffusion of ions into the yarn and inner structure of the fabric, which has a strong character of resistance, giving a more discernible result to the lowering of entire capacitive behavior of the device. Additionally, it must be pointed out that the spreading of PEDOT:PSS polymer might have caused an increase in the length of conduction path within the polymer, which eventually reduced the capacitance of the system.

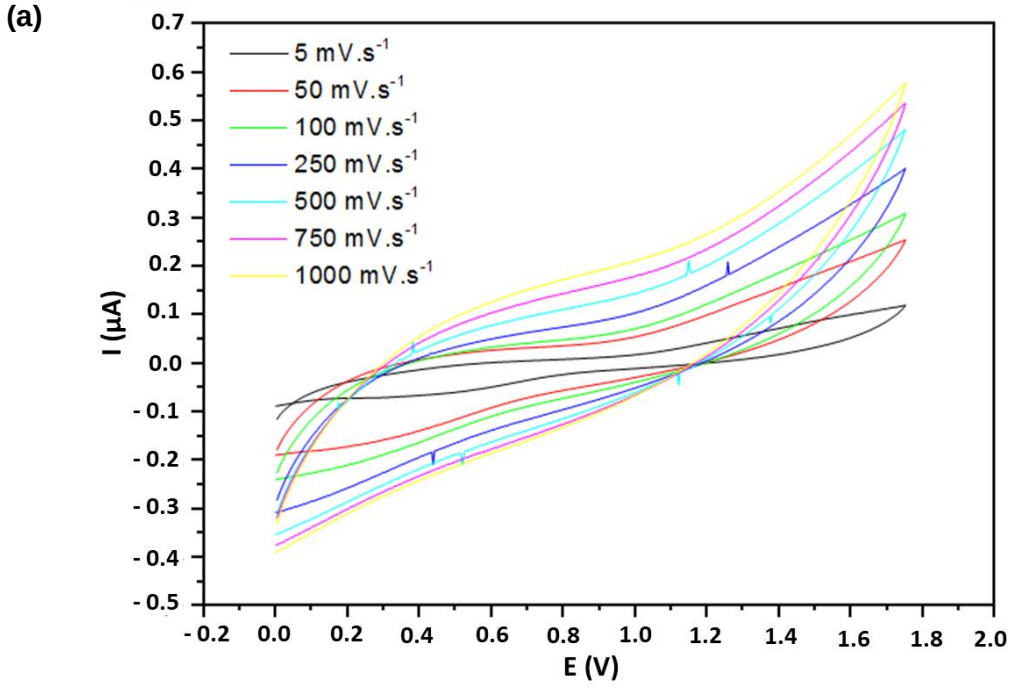

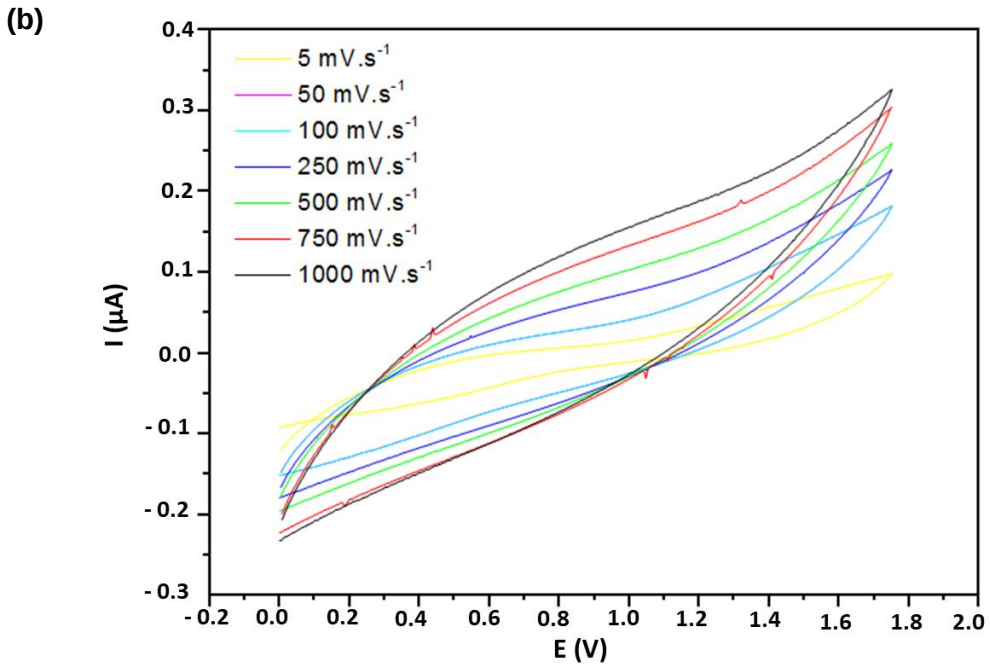

Figure 4.4. Cyclic voltammogram at various scan rate for PEDOT:PSS coating on fabric with (**a**) 3-mm and (**b**) 6-mm electrode spacings.

4.2.2. Evidence of Conductive and Capacitive Behavior from Nyquist and Bode Plots

The usual concept of modeling an impedance spectrum is by fitting an electrical circuit that has a frequency response equivalent to that of the measured cell. The circuit models consist of various parameters such as resistors (*R*), capacitors (*C*), constant phase elements (*CPE* or *Q*) and Warburg (*W*) elements. Just as resistance *R* is the ratio of voltage to current in a DC (direct current) circuit, the impedance Z is the ratio of voltage to current in an AC (alternate current) circuit. While the resistance is an extent of the opposite to DC flow, the impedance is a measure of the opposition to AC flow and describes both the resistance and the phase shift of the resulting signal as a complex number. Whereas the real part corresponds to the resistance, the imaginary part refers to the phase difference. **Figure 4.5** presents the general model for such a plot.

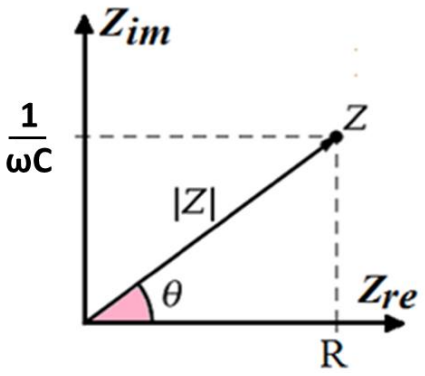

Figure 4.5. General model of plot of real and imaginary part

From the **Figure 4.5**, it can be expressed that:

$$R = Z_{re} = |Z| \cos\theta, \qquad (1)$$
$$\frac{1}{\omega C} = Z_{im} = |Z| \sin\theta, \qquad (2)$$

where the modulus and the phase angle are given by:

$$|Z| = \sqrt{[\![Z_{re}]\!]^2 + [\![Z_{im}]\!]^2}, \qquad (3)$$
$$\theta = \arctan\left(\frac{Z_{im}}{Z_{re}}\right). \qquad (4)$$

In the case of resistive character, the impedance (Z) is identical to the resistance R, i.e. the phase shift θ equals zero and Z is a purely real quantity. The ratio between the voltage and the current is thus described by Ohm's law:

$$Z_{re} = \frac{\mathrm{v(t)}}{\mathrm{i(t)}} = \frac{V \sin(\omega t)}{I \sin(\omega t)}. \qquad (5)$$

For purely capacitive behavior, the response to the voltage $v(t)$ is described by:

$$C = \frac{\mathrm{q}}{\mathrm{v(t)}}, \qquad (6)$$

where C is the capacitance and q is the electric charge. Then the resulting current is:

$$i(t) = \frac{dq}{dt} = C\frac{dv(t)}{dt}. \qquad (7)$$

The constant-phase element (CPE, Q) is a distributed equivalent circuit element which can be viewed as the non-ideality of the capacitors. The finite distribution of the sample in space makes it a non-ideal element, but other imperfections such as the roughness of the electrodes may also contribute here [48].

$$Q = \frac{1}{Y(i\omega)^n} \ , \qquad (8)$$

Y is the CPE parameter, ω the angular frequency, and n the CPE exponent ($0 < n < 1$). Y and n are constants and independent of frequency. An ideal capacitance has n equal to 1 while n for porous films, rough surface and non-uniform current distribution deviates from 1 [48]. Warburg element is a distributed equivalent circuit element which models semi-infinite diffusion. When charge passes in a cell for a prolonged time, diffusion of the active ions to the surface of the electrodes interface must take place to maintain the concentration of these ions. A process that is limited by the diffusion rate will appear as an additional time-dependent contribution to the impedance spectrum. This contribution can be modeled by the Warburg element, which has a constant phase of 45° with n = 0.5.

The Nyquist plots of the textile energy storage devices made on glass and fabric surfaces each with two different distances between electrodes, i.e., 3 mm and 6 mm can be seen in **Figures 4.6** and **4.7** respectively**.** Each sample was charged at 2 V for a period of 120 min. The plots (insets) exhibit two consecutive semicircles, each of which is followed by a tail formation at the low frequency region, for both glass (**Figure 4.6**) and fabric surfaces (**Figure 4.7**). The first semicircle with a smaller diameter is related to the bulk PEDOT:PSS polymer, while the second semicircle represents the interface region between PEDOT:PSS and the surface of SS yarn electrodes and the interaction therein. The third section of the plot as defined by a tail-like formation with a phase angle reaching ~45° can be described by the

Warburg impedance (Bode phase plot) at samples with 1 mHz-100 kHz frequency region (**Figure 4.8**).

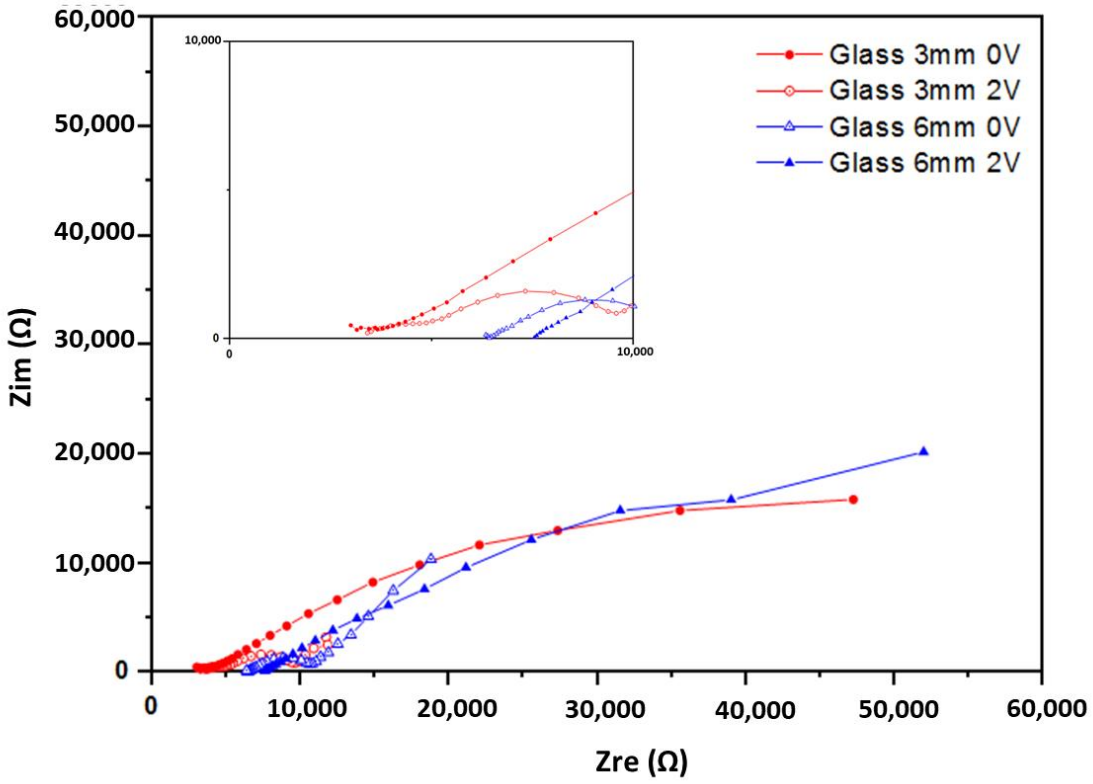

Figure 4.6. Nyquist plot of PEDOT:PSS film on glass surface with different distances of electrodes (3 mm and 6 mm). Inset: high frequency region.

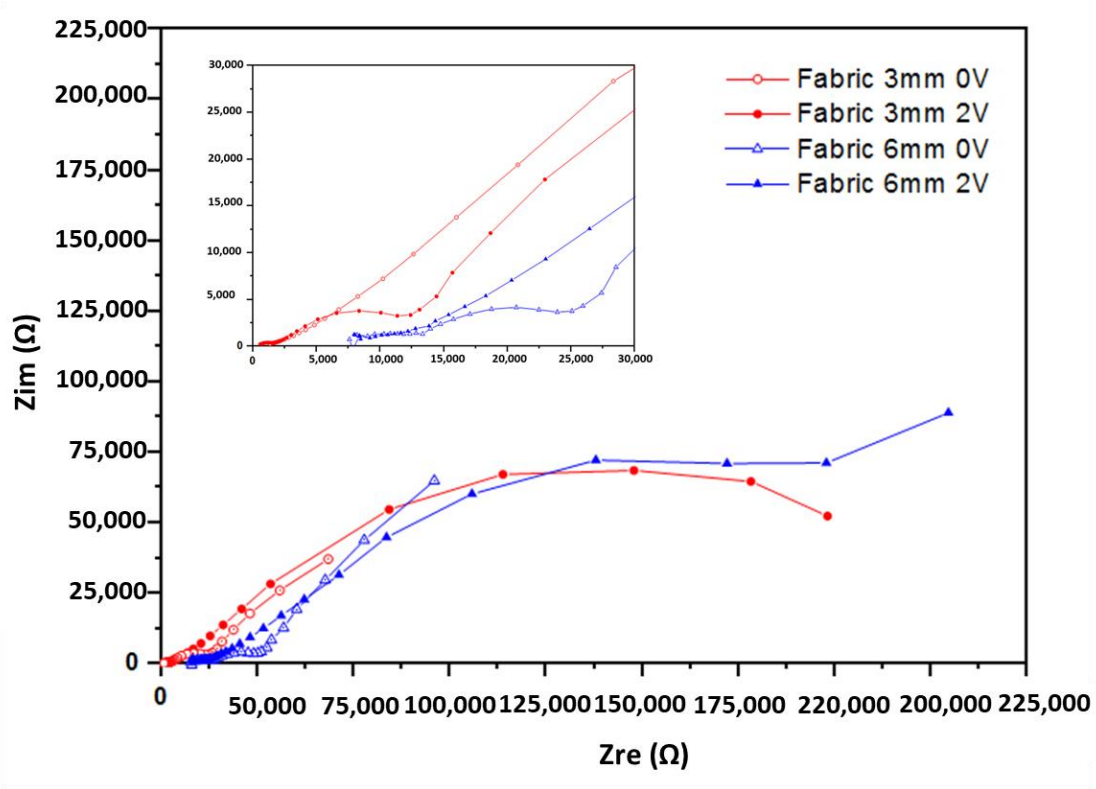

Figure 4.7. Nyquist plot of PEDOT:PSS film on fabric surface with different distances of electrodes (3 mm and 6 mm). inset: high frequency region.

The electrochemical impedance analysis (EIS) is a well-known method to determine the conductivity and capacitive behavior of a sample by a single analysis, although it is more common in solution than in solid state. The bulk of solid state materials usually show a single resistive and capacitive value. However, our PEDOT:PSS-based devices exhibited both electronic and ionic characters. From the analysis, the interaction between PEDOT:PSS and the SS electrode surface at the interfacial region was affected by the distance between electrodes, type of electrode and thickness of the PEDOT:PSS layer on the surface of the cell. The obtained impedance spectrums are fitted by an electrical circuit modeling with a frequency response equivalent to that of the measured sample. The effect of the current

applied at different frequencies is analyzed under voltage. Whereas the real part corresponds to the resistance, the imaginary part refers for the phase shift [48].

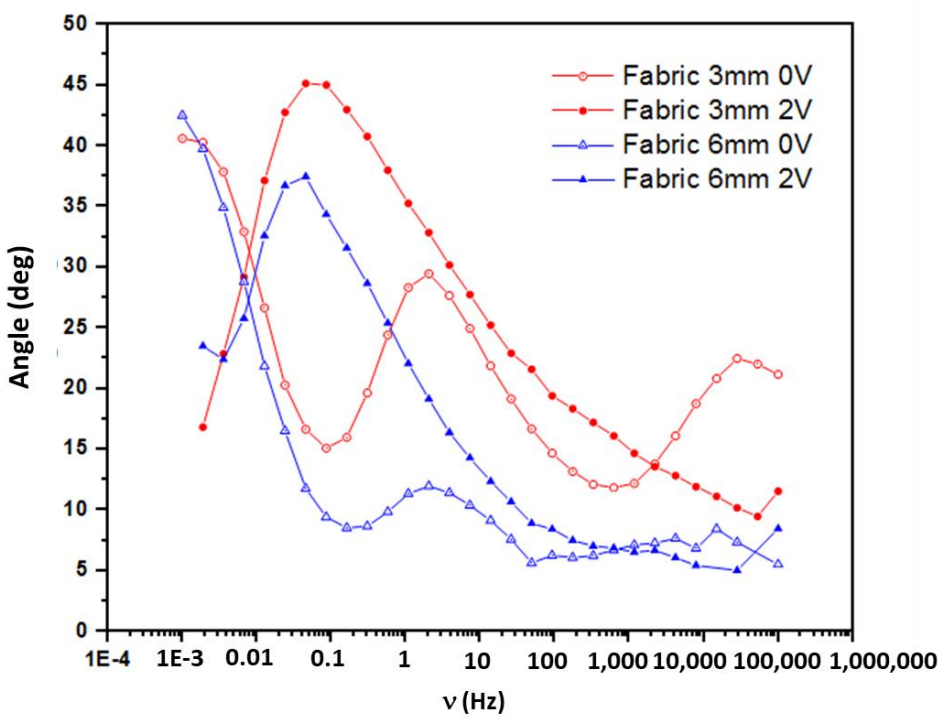

Figure 4.8. Bode phase plot for samples coated on fabric surface at different distance.

As shown by Nyquist and Bode, in the phase plots in **Figures 4.6–4.8**, the first semicircles that represent the bulk polymer properties—either on glass and fabric surfaces—show no apparent changes of its ionic conductivity. PEDOT:PSS is a p-doped conducting polymer that can be solution-processed to form transparent and conducting thin films. PSS is used to p-dope PEDOT and also improve its water solubility [47]. The PEDOT:PSS complex consisting of PSS chains to which the PEDOT oligomer firmly attaches itself forms a stacked arrangement with the counter-ions [44]. The EIS results indicate the presence of ionization and migration of the electrolyte PSS units, leaving the PEDOT units—which are known to be the conductive counterpart—naked and thus increasing its solid-state conductivity.

The presence of Warburg element (**Figure 4.8**) also confirms this process related to the electrode and electrolyte interface. As a result, the resistance decreases, while conductivity increases on every charged sample.

4.2.3. Simulation of Circuit Model

The simulated equivalent circuit models with ZSimpWin (version 3.20, Ann Arbor, MI, USA) software compared with experimental results obtained from the Nyquist (**Figures 4.6** and **4.7)** and Bode magnitude plots (R_{ct}, C_{dl} and R_{el}) are shown in **Table 4.1**.

Table 4.1. Equivalent circuit element for uncharged and charged samples on glass and fabric surfaces.

Sample	Q_{el}* ($\mu S\ s^{-n}$)	n	R_{el} (kΩ)	Q_{bulk} (μF)	n	R_{bulk} (kΩ)	Q_{dl} ($\mu S\ s^{-n}$)	n	R_{ct} (kΩ)	W_{ionic} ($\mu S\ s^{-1/2}$)	X
On glass											
3 mm	1.11	0.6479	1.3	5.10	0.7856	2.46	64.6	0.4736	375.48	-	1.25×10^{-4}
3 mm_ch*)	124.7	0.2144	4.9	4.00	0.9999	1.7	40.23	0.6564	55.43	92.9	1.11×10^{-3}
6 mm	38.68	0.9052	2.19	0.23	0.4888	17.3	49.43	0.3281	185.1	-	9.90×10^{-5}
6 mm_ch*)	87.6	0.717	95.7	6.98	0.6834	2.2	22.53	0.002	23.73	9.26	8.02×10^{-5}
On fabric											
3 mm	8.06	0.3754	2.35	902.9	0.7812	128	34.62	0.6781	10.93	-	6.71×10^{-4}
3 mm_ch*)	293.75	0.0869	1.93	86.5	0.8384	124	56.02	0.3951	171.05	316.6	1.19×10^{-4}
6 mm	18.0	0.7861	5.41	456.67	0.7329	39.69	38.41	0.7398	18.2	-	4.01×10^{-4}
6 mm_ch*)	192.8	0.09875	59.9	17.35	0.1392	21.64	32.94	0.4822	215.3	73.7	6.28×10^{-4}

*) ch = charged.

Triangles and circles in the curves shown in **Figures 4.6–4.8** represent the points of data from experiments, while the lines show the simulated data taken from the circuit modeling. It can be seen from the graphs that at lower frequencies, the shifted points are more visible, while at higher frequencies, the regions are mostly similar. The results showed two distinct equivalent circuit models of

(QR)(QR)(QR) for the uncharged and of (QR)(QR)(Q(RW)) for the charged samples (**Figure 4.9**), with $\chi 2$ defined as the sum of the squares of the residuals minimized to 10^{-4} error. As can be seen in the **Table 4.1**, Qel corresponds to the constant phase element of the electrode, R_{ct} corresponds to the ionic charge transfer resistance, Q_{dl} and R_{el} correspond to the double-layer phase element and electronic resistance at the electrode surface and the solution interface, while Q_{bulk}, R_{bulk} and W_{ionic} each correspond to the bulk constant phase element (or capacitance), resistance and Warburg element respectively.

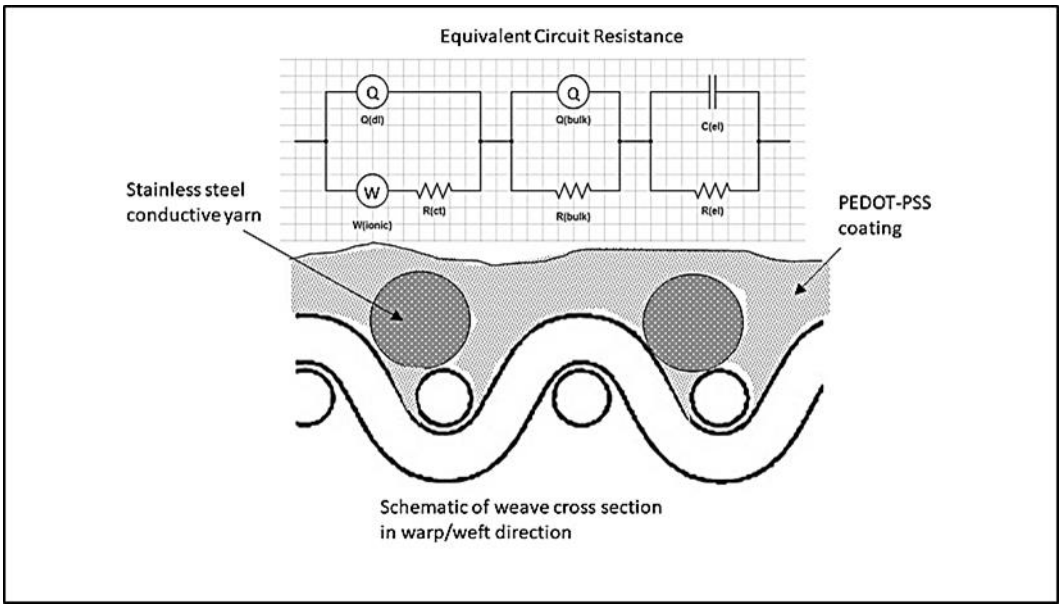

Figure 4.9. Equivalent circuit models of charged and uncharged device on fabric surface.

It can be seen from **Table 4.1** that the Q_{el} constant phase element and the $R_{el,}$ electronic resistances mostly increased for the charged samples except for the device on fabric with a 3-mm distance, and differs significantly with the electrode distance or the coating on fabric or glass material. The resistance given by extrapolating the end point of the circle related to the electronic conductivity decreased when charged. The second semicircle related to the grain boundaries

(R_{bulk}) defined by the Brick Layer Model dropped drastically on charged samples, while they altered with the electrode distance. Since the conductivity of a material is an extensive quantity and depends on its dimensions and its electrical resistance, the coating thickness also affects the conductivity. During the course of measurements, we found that samples prepared with thinner PEDOT:PSS coating showed no apparent peak on CV (Cyclic Voltammetry) measurements neither any accurate EIS results, and therefore, cannot be presented in this report. This is due to the absorption and migration of the PEDOT:PSS solution into the fabric structure of the device samples and out of the cell area into which it must be confined. It is common knowledge that polyester from which the fabric was made is an insulating material and therefore does not allow transport of charges through it, which in other words is of high resistance. For this reason, absorption of polymer is not desirable and must be avoided. From the data in **Table 4.1**, it can also be seen that the double-layer capacitance (Q_{dl}) and the charge transfer resistance (R_{ct}) values decreased for the charged samples on glass surface, while increased for samples prepared on fabric. The presence of the Warburg element for the charged samples proved that the diffusion of ions to the SS yarn electrode surface also affected the value of R_{ct}. Therefore, the migration of the PSS counterpart on the fabric surface was more challenging and then decreased the ionic charge transfer.

4.3. Study on Mechanism from Characteristics of the Devices Charge-Discharge Performance

Devices measured in the experiments of this section were those annotated as TESD 1.2 THL in Chapter 3, i.e. textile energy storage device fabricated on one layer of textile fabric, with PEDOT:PSS layer being more confined within the cell area. The fabrication method is described in the Section 3.3.4.2 in Chapter 3. The focus of this section is characterization the PEDOT:PSS ratio of three different commercial brands of PEDOT:PSS, compare the results with the properties given by the technical data, and then test the charge-discharge performance of each device. The

three different brands of PEDOT:PSS used for this analysis are: (1) M121 PEDOT:PSS AI 4083 (Ossila Ltd., Sheffield, UK); (2) Clevios P-VP-AI-4083 (Heraeus, Hanau, Germany), and (3) Orgacon ICP 1050 (Sigma Aldrich, Darmstadt, Germany). The resistivity of each PEDOT:PSS layer on glass at 2.5 × 2.5 cm^2 was measured by two points measurement method. To complete the data, sulphur content and thermogravimetric analysis were also carried out to each PEDOT:PSS being investigated. Charge-discharge characteristics of the devices prepared using the various types of commercial PEDOT:PSS polymer were measured by the microcontroller Arduino/Uno. Two types of electrode yarns were used for various configuration of electrode pair of the device for this study, i.e. pure stainless steel Bekaert Bekinox (Bekintex NV, Wetteren, Belgium) and silver-coated polybenzoxazole (Ag-PBO) of Amberstrand (Syscom Advanced Materials Inc., Columbus, Ohio, USA).

4.3.1 PEDOT:PSS Ratio and Sulphur Content

Determination of the composition of PEDOT and PSS in the PEDOT:PSS polymer dispersion was performed by ^1H NMR (Nuclear Magnetic Resonance) analysis. The elemental analysis to determine the concentration of the sulphur (S) content in each the PEDOT:PSS samples sulphur content was analyzed by ICP-OES (inductively coupled plasma-optical emission spectroscopy). All experiments using ^{1}NMR and ICP-OES as well as measurement of resistivity were conducted in the Laboratory of Applied and Analytical Chemistry, Institute of Materials Research, Hasselt University, Belgium.

The proton (^1H) NMR spectra were recorded on a 400 MHz (9.4 Tesla) Inova spectrometer (Agilent Technologies Inc., United State) using a 5 mm four-nucleus PFG (pulsed-field-gradient) probe. The PEDOT:PSS dispersion was here diluted with deuterium oxide (D_2O). The chemical shift scale (δ) in ppm was calibrated relatively to TSP-d4 (3-(trimethylsilyl)-2,2,3,3-tetradeuteropropionic acid sodium

salt) as a chemical shift reference at 0 ppm. Free induction decays were collected with a 90° pulse of 6.0 μs, a spectral width of 6 kHz, an acquisition time of 4 s, and a preparation delay of 12 s. Each free induction decay was zero-filled to 65 K points and multiplied by a 0.5 Hz exponential line-broadening function prior to Fourier transformation.

The ICP-OES machine system used to analyze the concentration of Sulphur content consisted of an Optima 8300 (Perkin Elmer, USA) and a S10 autosampler equipped with the Syngistix software version 2.0.0.2236. Emission lines of the Sulphur were monitored at the wavelengths of λ= 181.975 nm, 180.669 nm, and 182.863 nm and averaged. Materials prepared for the measurement were 1000 mg/l S (sulphur) standard solution purchased from Merck KGaA (Darmstadt, Germany), 69.0-70 % nitric acid (HNO_3) purchased from J.T. Baker (Deventer, The Netherlands), and MilliQ water (arium 611UV, Sartorius, Gottingen, Germany). Each sample of PEDOT:PSS was diluted in 100-fold with 0.5% HNO_3 and mixed thoroughly prior to the ICP-OES analysis. Sulphur calibration standards were prepared by serially diluting the standard S working solution with 0.5% HNO_3, resulting in a concentration of 1, 5, 10, 50 and 100 mg/L S. Each sample was prepared in 3 replicates.

The proton (^1H) NMR spectra presented in **Figure 4.10** showed the peaks in the spectral area between 3-4 ppm (PEDOT) and 0-2 ppm (PSS), which are the characteristics of PEDOT:PSS. During the analysis we found that Clevios and Ossila exhibited identical spectra, which gave an indication that they might be of similar composition. This is further confirmed by their respective technical information as shown in **Table 4.2**. On the other hand, slight but significantly different peaks were observed for Orgacon, particularly in the spectral area of 3-4 ppm, leading to different results of calculation on the ratio of PEDOT and PSS. Calculation of the area under each of the above mentioned peaks gave quantitative information

regarding weight and molar ratios of the three commercial brands of PEDOT:PSS used and being investigated in this research.

From **Table 4.2**, the molar and weight ratio of PEDOT and PSS in the polymer dispersion of Clevios and Ossila is 1.00 : 5.26 and 1.00 : 6.92 respectively, whereas Orgacon is 1.00 : 4.65 and 1.00 : 6.11. From this analysis, except for slight difference in sulphur content, it can be concluded that Clevios P-VP-AI-4083 and Ossila AI 4083 are identical. Orgacon ICP 1050, on the other hand, is different and has a smaller average number of PSS units electrostatically attached per PEDOT polymer chain, which is also evident from the lower sulphur content measured by ICP-OES. At this point, it can also be seen that the differences in PEDOT:PSS ratio between the three commercial samples are in agreement with their resistivity and hence conductivity, although ratio is not the only factor. The other factors like additional solvent and secondary dopants can also affect the conductivity as well as polymer length. However, the fact that we observed different performance of devices using each type of PEDOT:PSS under study tells us that other factors like different batch and storage time might play important role as well. From the measurement, both Clevios and Ossila have the same resistivity ρ of 1000 Ω.cm, which is obviously much larger than that of Orgacon's, 0.25 – 1 Ω.cm. Our measurements are in reasonably good agreement with the technical data provided by each of the manufacturer companies. As shown by the data, what appears to be only slight difference in PSS content turns out to be highly important and has a tremendous effect on the electronic properties of PEDOT:PSS, which in this particular case is their resistivity.

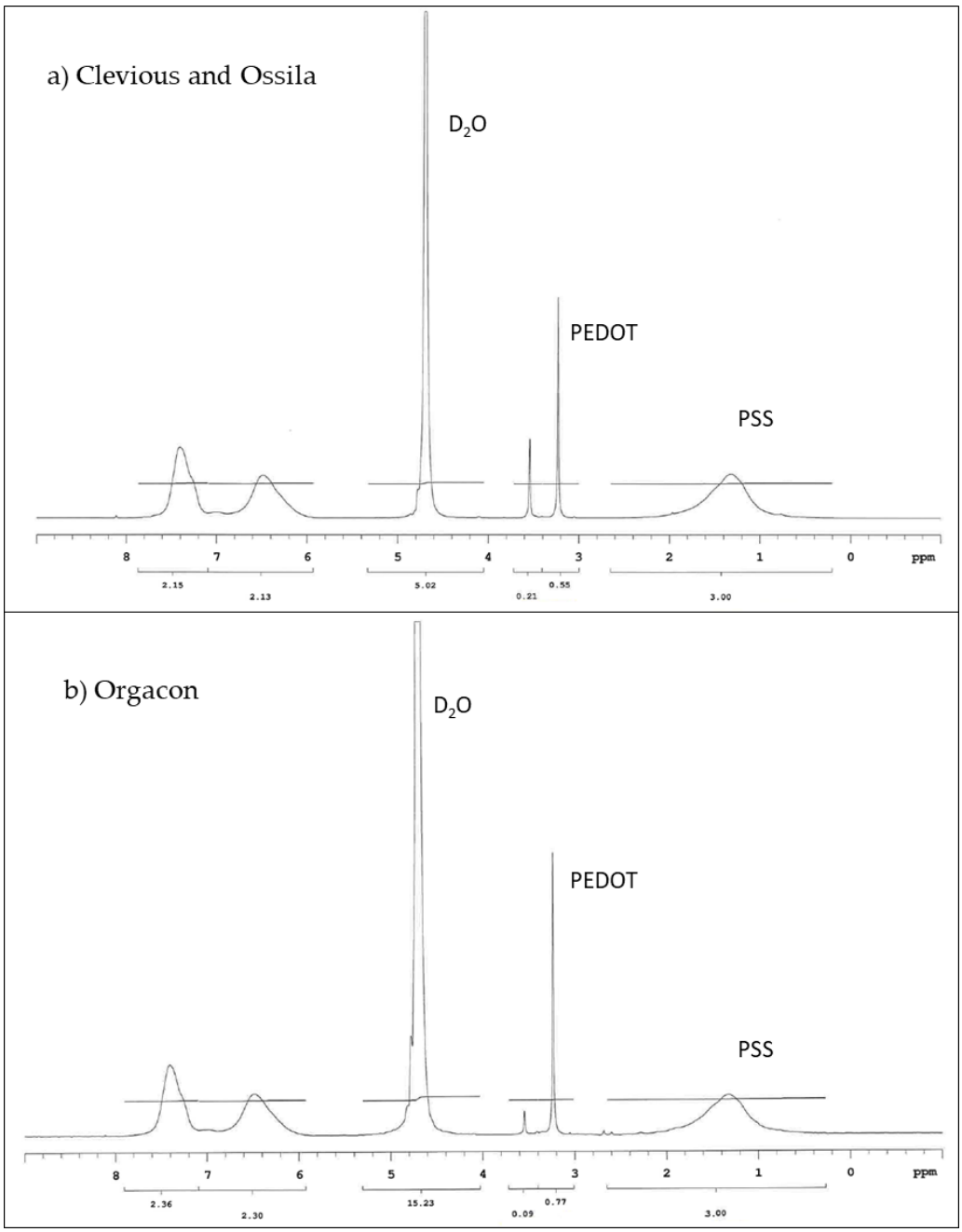

Figure 4.10. ^{1}H NMR spectra of PEDOT:PSS (a) Clevios and Ossila (b) Orgacon

It is important to note here that PEDOT:PSS ratio is not the only factor that has an effect to its conductivity, hence resistivity. Although some other factors as mentioned before can also affect the conductivity of the PEDOT:PSS, discussion in

this study is restricted and focused on the observation that different ratios of PEDOT:PSS's under study here resulted in different resistivity and charge-discharge performance of the textile energy storage device, even for those that used Clevios and Ossila which are assumed as similar product.

Table 4.2. PEDOT:PSS physical and chemical characteristics based on measurement (^{1}H NMR and ICP-OES) and technical information.

Characteristics	Clevios P-VP-AI-4083	Ossila A1 4083	Orgacon ICP 1050
	Measurement results)**		
PEDOT:PSS molar ratio	1.00 : 5.26	1.00 : 5.26	1.00 : 4.65
PEDOT:PSS weight ratio	1.00 : 6.92	1.00 : 6.92	1.00 : 6.11
Concentration of sulphur (mg/l)	2799 ± 10	2845 ± 10	2120 ± 10
Resistivity, ρ (Ω.cm)	1000	1000	0.25 - 1
	Technical information*)**		
Solid content (% in water)	1.3-1.7	1.3-1.7	1.1
PEDOT:PSS weight ratio	1:6	1:6	N/A
Resistivity, ρ (Ω.cm)	500-5000	500-5000	N/A
Resistance (Ω/sq) *)	N/A	N/A	<100
Work function (eV)	5.2	5.0-5.2	N/A

*) The unit was presented differently as Ω/sq (sheet resistance (R_{sq})), where $\rho = R_{sq} \cdot d$ (resistivity equals to sheet resistance times the layer thickness – when the thickness d is 1, the resistivity equals to resistance). The PEDOT:PSS Orgacon ICP 1050 itself was classified as highly conductive grade.

**) All the data presented in the upper block was taken experimentally from our measurements.

***) All the data presented in the lower block was taken from the technical information provided by each company [49-51].

As understood from the literature [47], the conductivity of PEDOT:PSS has a direct relation with the ratio of PEDOT to PSS because of the way the intrinsic conductivity of this polymer formed. With the same amount of PEDOT molecules, the larger proportion of PSS in the polyelectrolyte system leads to lower conductivity. This can be explained by the fact that with more polyanionic PSS in the polymer, the density of charge transporting PEDOT sites are lower. The PSS itself is known to not directly support the charge transport [47]. With its highly acidic and polar sulfonic group, it functions more as a counter ion to form a stable dispersion in the system of polyelectrolyte complex paired with PEDOT. However, the excess amount of PSS leads to the formation of an intramolecular interaction between the PEDOT and PSS molecules in addition to the coulomb interaction between anionic ions from PSS with the free cationic ions in the PEDOT, creating a scramble egg-like arrangement of the molecule mixture [47], [52]. As a consequence, the mobility of the conjugated charge carrier decreased accordingly leading to much higher resistivity, i.e. 1000 Ω.cm (compared with only 0.25-1 Ω.cm for Orgacon) and lower conductivity for both Clevios and Ossila. As will be seen later, this differences in resistivity and conductivity have significant consequences to the behavior and performance of the devices made of each of the Clevios and Ossila on one hand and Orgacon on the other. A similar phenomenon has been observed in semiconductor compounds like GaAs, InP, CdS, CdSe, etc. For GaAs, for example, the intrinsic material has a very low electric conductivity [53]. A small excess of Ga converts the GaAs into a n-type semiconductor, with an increased electric conductivity. An excess of As gives rise to a p-type semiconductor with an increased conductivity as well [53]. Our discussion will center and focus on explaining why and how the two groups of PEDOT:PSS differ in their behavior and performance.

4.3.2 Thermogravimetric Analysis

Thermogravimetric analysis was conducted to obtain particular information on water uptake of PEDOT:PSS, i.e. the amount of bound water molecules in the film. The experiment was conducted in the laboratory of instrumental analysis in Politeknik ATK Yogyakarta, the partner university of Politeknik STTT in Indonesia. Similar three types of the commercial PEDOT:PSS were used for this analysis.

For the measurement, 50 ml of each PEDOT:PSS dispersion was freeze dried for 24 hours by an Eyela FD-5N freeze dryer (Tokyo Rikakikai Co. Ltd., Japan), and then stored in the desiccator to make sure that it did not take up any extra water or moisture and remained dry while in store before the thermogravimetric analysis (TGA). TGA was performed on a Diamond TG/DTA instrument by Perkin Elmer (USA) operating from 30 to 600 °C at a heating rate of 5 °C/min under the flux of nitrogen at 20 ml/min. For the TGA measurements, 0.897, 1.751, and 2.177 mg PEDOT:PSS sample from Orgacon, Ossila, and Heraeus respectively was taken and placed in aluminium pan for the analysis.

The TGA analysis is of importance in relation to the discussion about the conductivity of the polymer. By this method, we can determine not only the amount of absorbed water but also the adsorbed or bound water molecule in the internal structure of PEDOT:PSS film, which has been known to be highly hygroscopic polymer due to the presence of sulphonic acid groups. It was suspected that the presence of bound water molecules may have an effect in increasing the conductivity of the polymer. **Figure 4.11** presents the TGA curves of the Ossila, Orgacon, and Clevios PEDOT:PSS used in this research.

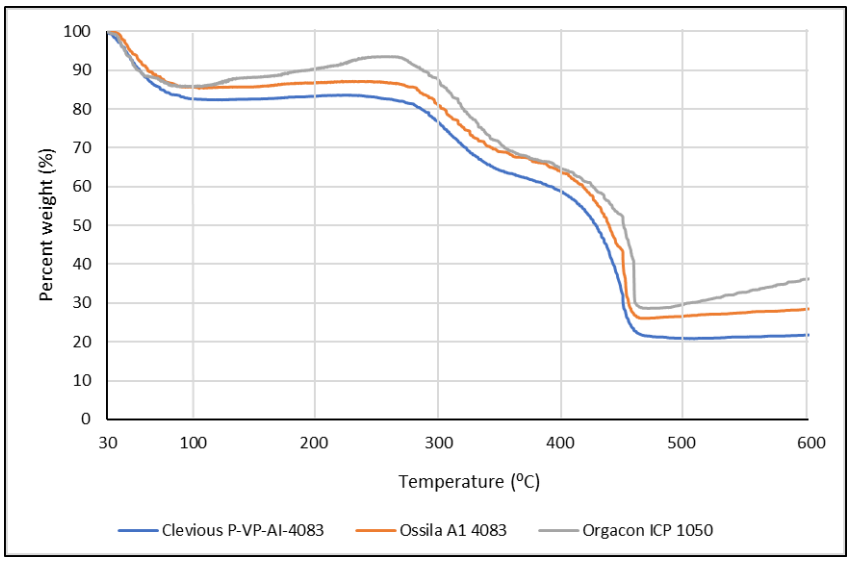

Figure 4.11. TGA curves of Clevios, Ossila, and Orgacon PEDOT:PSS.

It can be seen from the curves that significant weight loss occurred during the first stage of heating from 30 to 100 °C, which originated from the evaporation of absorbed water. Based on the amount of weight loss at 100 °C, the water content of the three polymers after being freeze dried was found to be approximately 14.14%, 14.37%, and 17.42% for Orgacon, Ossila, and Clevios respectively. On further heating to 250 °C, there was no further weight loss indicating the absence of adsorbed and bound water molecule in the internal structure of PEDOT:PSS films under investigation.

PEDOT:PSS has been known to have a very good thermal stability [47], [54]. It can withstand heat treatment of up to 250 °C without considerable decomposition. However, gradual decrease of weight appears on further heating to 350 °C, which can be considered as an indication for the breaking up of the PSS sulfonate groups leading to a weight loss of approximately 30%. Elschner et al. [47] explained a similar phenomenon in their TGA results of PEDOT:PSS at between 100-250 °C as the fragmentation of the sulfonate group which was indicated by the increase in the ion currents because of the presence of the resulting SO_2 ions [47].

As the PSS proportion in Orgacon is less than those in Clevios and Ossila, the loss of weight due to the destruction of PSS sulfonic group is lower as shown by the curve in **Figure 4.11**. Furthermore, significant decreases occurred at temperatures between 350-450 °C. Weight loss of up to approximately 70%, 74% and 78% were exhibited by Orgacon, Ossila, and Clevios respectively. This indicated the oxidation of sulphur or carbon atoms in the thiophene rings which possibly led to the formation of a nonconducting sulphoxide and sulphone structures or hydroxyl group followed by rearrangement into its oxide form [47]. From the TGA curves, it can be concluded that the three PEDOT:PSS's have a good thermal stability up to 200 °C. In this respect and in relation to the heat treatment of PEDOT:PSS in the fabrication of our devices, the only heating applied was the repeated drying at temperatures between 90 – 110 °C during the drop-coating of PEDOT:PSS dispersion into the cell area. Looking at the TGA data, the heat treatment should not disturb the integrity of the PEDOT:PSS polymeric structure neither to its conductivity, even though the heating was carried out repeatedly.

The presence of sulphonic acid groups in PEDOT:PSS leads to strongly hygroscopic characteristic which allows the formed film to easily take up moisture in the ambient condition [47]. Based on visual observation, the PEDOT:PSS film on our device do not seem to undergo visible swelling under ambient condition during the 3 months storage. However, there was a consistent change in the charge-discharge performance: the voltage level of charging increased while the discharging voltage level decreased with storage time (**Figure 4.12**). Graphs in **Figure 4.12** show the results from a series of a consecutive measurements of a device made of PEDOT:PSS Ossila AI 4083 and stainless steel electrode yarns. The device was first measured just after it was made, week 0, and then it was stored in room conditions for the next measurements after every two weeks until the week 12. The charge-discharge voltage was measured with the Arduino Uno (charging at 3 volt for 1500 seconds and discharging for another 1500 seconds).

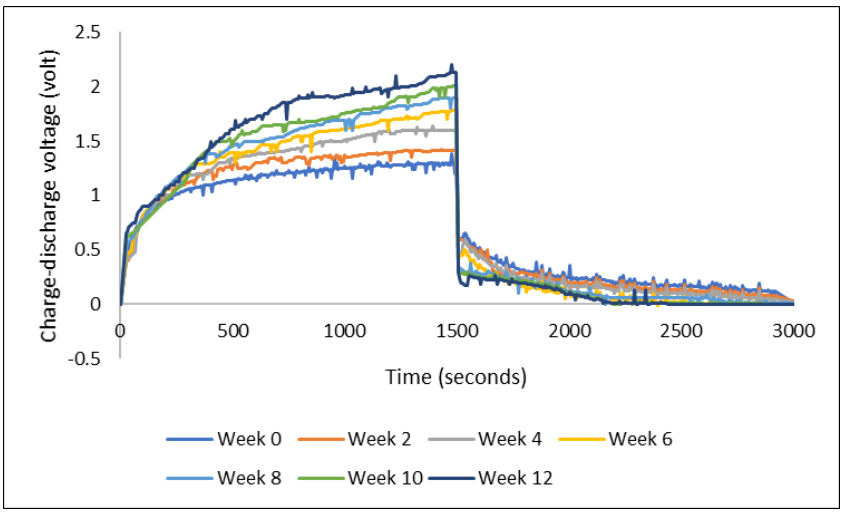

Figure 4.12. Charge-discharge profiles of a device along the storage in ambient condition

The increase and decrease of charging and discharging voltage described above, while the load of the external resistance remained the same (i.e. 33 kΩ throughout the experiments), can be taken as an indication of increasing internal resistance of the device over time. The larger internal resistance had caused the charging voltage to increase. The same phenomena were also shown by devices with and without water repellent-pretreatment as shown in Figure 3.19. However, when discharging, assuming that the textile energy storage device (TESD) had the same voltage after being charged, the device needed to overcome the internal resistance which then led to the observation of lower discharging voltage. It is still questionable, though, as to what has caused this increase in the internal resistance of the device. The fact that PEDOT:PSS is highly hygroscopic could be one of the reasons. Water uptake during the storage could have caused some changes in the internal structure leading to decrease in the mobility of charge carriers which then appeared as increase in internal resistance. Further investigations are certainly needed to corroborate the above suggested explanations.

4.3.3 Charge-Discharge Characteristics

Charge-discharge characteristics of all devices were measured by using a microcontroller "Arduino/Genuino-Uno" which was set up specifically for this particular purpose with the circuitry shown in **Figure 4.13**. The charging of the device was done by switching to position A which supplied the device with a DC voltage (V_s) of 3 V with an external resistance of 33 kΩ (R). The charging process was stopped by switching to position C after 1500 seconds when the voltage reading (V_c) reached maximum and remained stable at that level. Discharging took place with the same external resistance of 33 kΩ (R). During the process of charging and discharging, the output voltage (V_c) was recorded automatically by the program. The position of the device in the circuitry is represented by the name TESD, which stands for textile energy storage device. The hypothetical schematic circuit in the TESD cell is presented in the next part of this section.

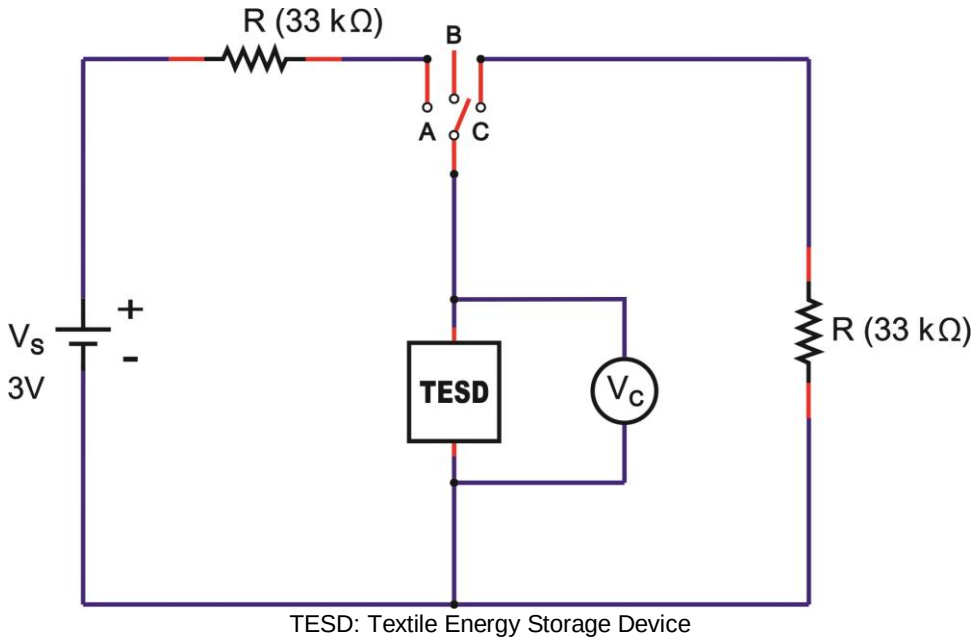

Figure 4.13. Schematic diagram of charge-discharge measurements set up

With this study we expected to obtain more information for further elucidation of the storage mechanisms of the device. In order to support the latter, the investigation was also conducted with different design configuration involving the use of symmetrical and asymmetrical electrode yarns from inert and non-inert materials. Nine devices with different combinations of types of electrodes and electrolyte plus three so-called blank devices by the method of fabrication as presented in Chapter 3 (TESD 1.2 THL) is presented in **Table 4.3.**

Table 4.3. Variation set up of the devices

Name of device	*Electrodes pair*	*Electrolyte*
A1	SS/SS	Ossila AI 4083
A2	Ag-PBO/Ag-PBO	Ossila AI 4083
A3	SS/Ag-PBO	Ossila AI 4083
B1	SS/SS	Clevios P-VP-AI-4083
B2	Ag-PBO/Ag-PBO	Clevios P-VP-AI-4083
B3	SS/Ag-PBO	Clevios P-VP-AI-4083
C1	SS/SS	Orgacon ICP 1050
C2	Ag-PBO/Ag-PBO	Orgacon ICP 1050
C3	SS /Ag-PBO	Orgacon ICP 1050
Blank 1	SS/SS	-
Blank 2	Ag-PBO/Ag-PBO	-
Blank 3	SS/Ag-PBO	-

Note: SS and Ag-PBO are abbreviations for the pure stainless-steel and silver-coated polybezoxazole electrode yarns.

Charge-discharge characteristics of each device using combination of electrodes with different type of PEDOT:PSS as listed in **Table 4.3** were measured and then compared, particularly to see the effect of the ratio of the PSS to PEDOT as well as the influence of the electrode material in the same devices towards the charge-discharge performance of each device. The graphs in **Figure 4.14** present the charge-discharge characteristics of devices A1, B1, C1 (**Figure 4.14 (a)**) and A2, B2, C2 (**Figure 4.14 (b)**), where the symmetrical SS/SS and Ag-PBO/Ag-PBO electrode

yarns were used respectively. On the other hand, asymmetrical SS/Ag-PBO electrode yarns were employed to devices A3, B3, and C3; their charge-discharge measurement results can be seen in **Figure 4.15**. Different electrical potential was applied during the measurements of these devices. The positive potential was applied to the SS electrodes first, and therefore the Ag-PBO electrodes had negative potential (**Figure 4.15 (a)**). Given one week to empty the charge in the devices, the opposite measurements, where the positive potential was given to the Ag-PBO electrodes, were then carried out (**Figure 4.15 (b)**). Each device was charged at 3 volt for 1500 seconds, then subsequently followed by discharging right after the charge was stopped. The decay of charges initially stored in the device was then observed for another 1500 seconds. As can be seen, the charge-discharge profiles presented in **Figures 4.14** and **4.15** are mostly noisy. The noise was found in all measurements using Arduino/Uno. As the curves still show typical charge-discharge profile of our device, the noise is neglectable in this discussion. In addition, it is important to note that according to the previous publication [55] as well as the discussion in Chapter 3, the noisy curves were observed from the devices with a thin layer of PEDOT:PSS film in the cell surface. The mobile ions inside the PEDOT:PSS gave inevitable rise to noise. The ions being polymer and hence quite large, create the typical shot noise. By evaluating the autocorrelation function of the noise, it was proven that we were dealing with the shot noise. The PEDOT:PSS layer was made to be thick and covered the cell surface to avoid the noise, but it is still shown. So, we believe that the noise should mostly come from the shift of measurements.

It can be seen from the graphs in **Figures 4.14** and **4.15** that different PEDOT:PSS polymer showed different charge-discharge profile, especially for those using Orgacon compared to Ossila and Clevios. In all charge-discharge measurements, regardless of the electrode yarns used and their set of combinations, devices using Orgacon as solid electrolyte showed zero level of charge and

discharge voltage at all time of observation. The discharge profiles from these results are similar to those found in the previous works of Sheila et al. [5-6]. As discussed earlier, based on our characterization and analysis using NMR and ICP-OES, the Orgacon ICP 1050 was found to be of low resistance and thus high conductive type of PEDOT:PSS which for the most part stems from the lower proportion of PSS in the mixture as compared to Clevios and Ossila.

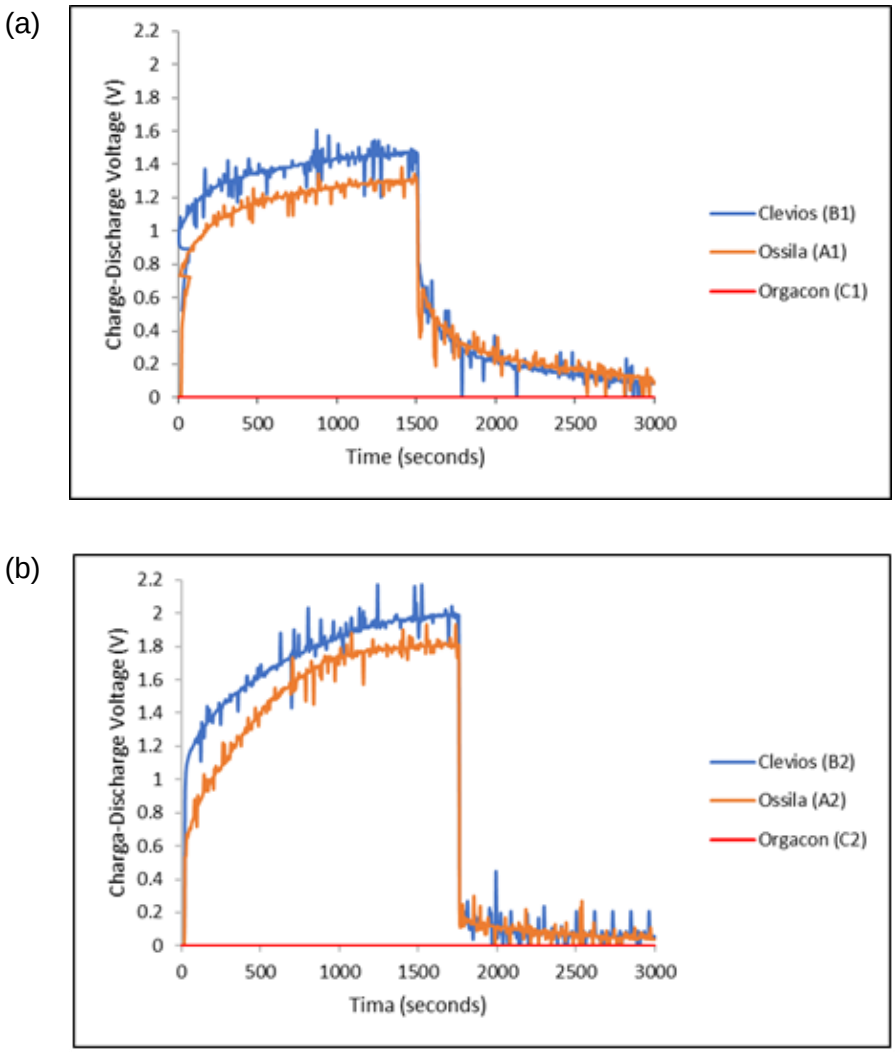

Figure 4.14. Charge-discharge characteristics of devices of different type of PEDOT:PSS with (a) SS/SS electrodes and (b) Ag-PBO/Ag-PBO electrodes, each charged at 3 volt.

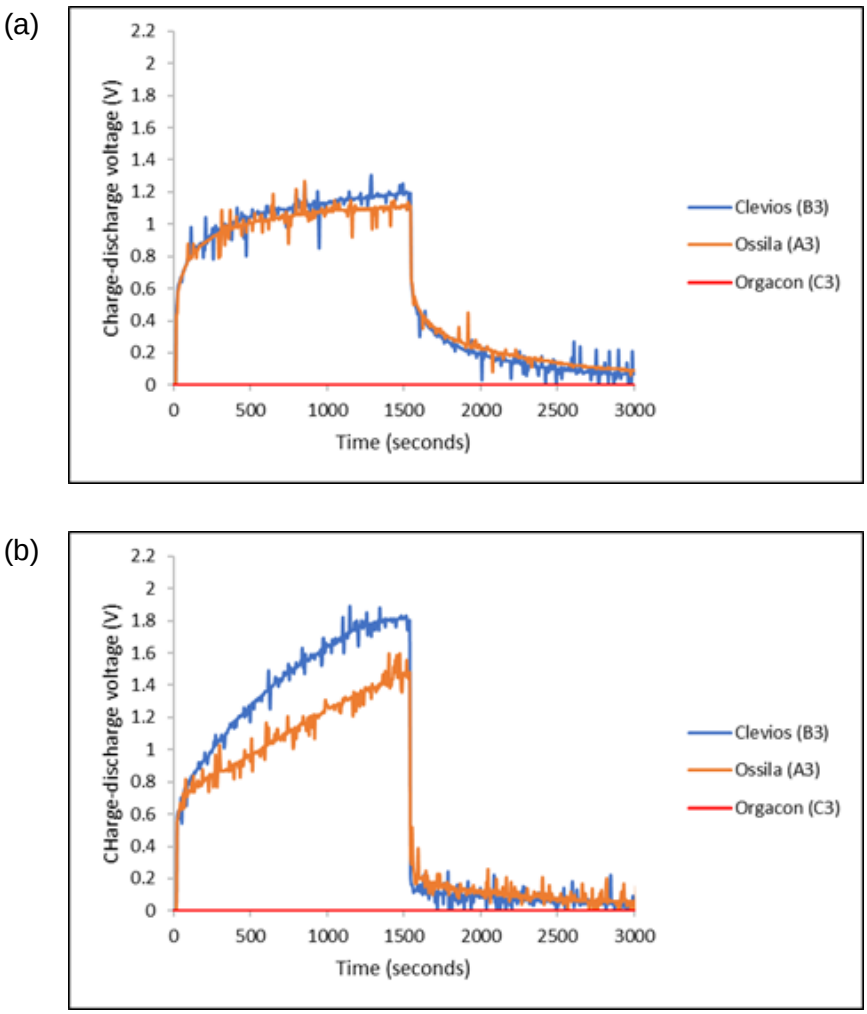

Figure 4.15. Charge-discharge characteristics of devices of different type of PEDOT:PSS using SS/Ag-PBO electrodes with different polarity of the applied voltage: (a) SS(+3V)/Ag-PBO(0V) and (b) SS(0V)/Ag-PBO(+3V).

The zero charge-discharge profile of devices having Orgacon PEDOT:PSS as observed in **Figure 4.14** and **4.15** suggested the absence of capacitive behavior in the system which caused no charging and discharging voltage observed. The polymer of Orgacon ICP 1050, which is a very good conductor, acted as a resistor with very low resistivity, even almost a short circuit, while the electrodes themselves were still perfect. With this assumption, a schematic circuit depicting the measurement of Orgacon device showing no capacitive behavior is presented

in **Figure 4.16**. It should be noted that the circuit is only a simplification of the system, where the device behaved as a wire instead of a TESD. In the simplified circuit, R is the external resistance of the system, V_s and V_r is the source and device output voltages respectively. Here, the device is represented only by its internal resistance r. By following the Kirchhoff's Law, as the total potential difference in the system is zero, $\sum V = 0$, the mathematical relationship between all the elements then can be derived as follows:

$$I(R + r) - V_s = 0 \quad (1)$$

$$I = \frac{V_s}{R+r} \quad (2)$$

$$V_r = I.r \quad (3)$$

$$V_r = \frac{r}{R + r} V_s \quad (4)$$

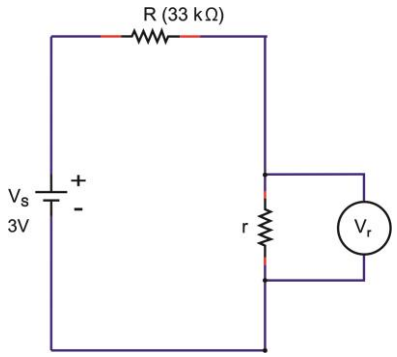

Figure 4.16. The hypothetical schematic circuit of the Orgacon ICP 1050-containing device with no capacitive behavior.
Note: the TESD here is only represented by the presence of r *and* V_r which is practically zero value.

From (4), when $r << R$ the device voltage V_r will be close to zero regardless of how much voltage supplied to the system by the power source V_s. This explains our observation on flat and practically zero charging of these particular devices made up from Orgacon ICP 1050. The complete opposite charge-discharge profiles

should be obtained on blank devices, as then no current can flow between the electrodes (infinite resistance). This is presented in the **Figure 4.17**, which shows that the absence of PEDOT:PSS solid electrolyte in the devices caused no current flows with an immediate voltage over the electrodes as applied by the source.

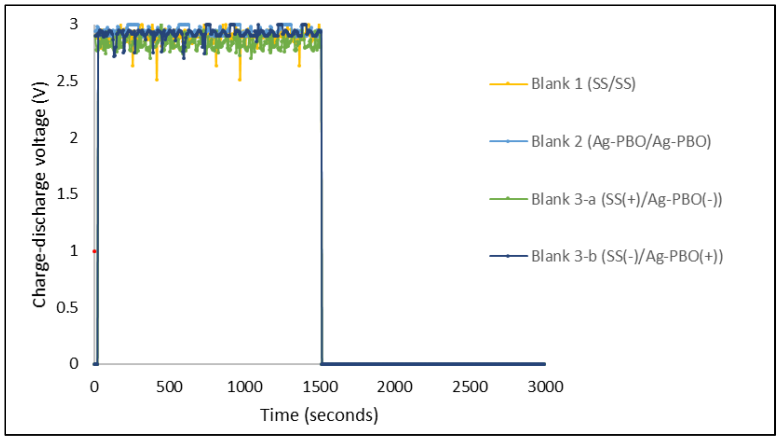

Figure 4.17. Charge-discharge characteristics of blank devices (without PEDOT:PSS) using various electrodes (SS/SS, Ag-PBO/Ag-PBO, SS(+)/Ag-PBO (-), and SS(-)/Ag-PBO(+)), each charged at 3 volt.

On the other hand, devices with PEDOT:PSS having Clevios VP-AI-4083 and Ossila AI 4083 both showed pseudo-capacitive behavior, represented by the charge-discharge profiles as shown in **Figure 4.14** and **4.15.** In general, all devices showed almost identical charge-discharge profiles, except that different combinations of electrode yarns with the same type of PEDOT:PSS, Clevios or Ossila, resulted in different charge-discharge levels. This indicates that we need to consider the electrode−PEDOT resistances in the forward (current moving to PEDOT) and backward (current moving out of PEDOT) configuration. For the same polymer coating, the charging capacity should be equal, which can be represented by an internal capacitance and equivalent series resistance (ESR) of the device, as well as an internal discharge. **Figure 4.18** presents the possible configuration of the TESD cell having Clevios and Ossila PEDOT:PSS which consistently showed capacitive behavior.

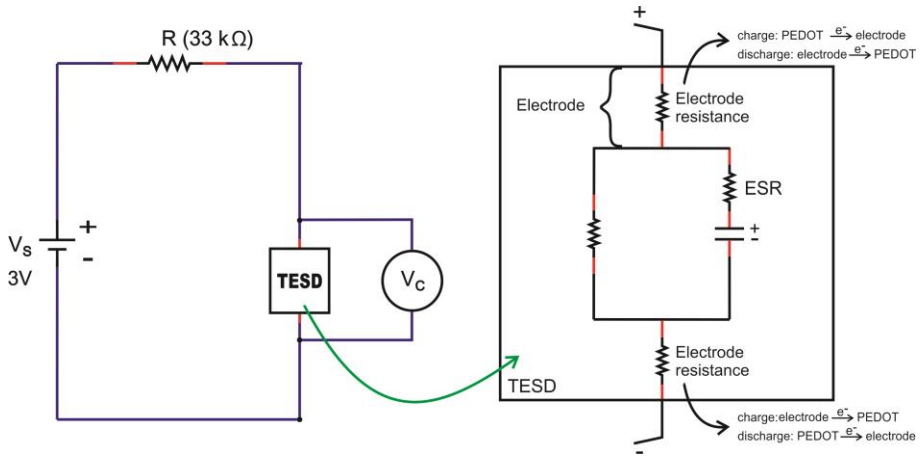

Figure 4.18. Possible configuration of the electronic system in the TESD cell with capacitive behavior

As can be seen in **Figure 4.14 (a)** and **(b)**, devices using a pair of Ag/PBO electrode yarns exhibited higher charging voltages at 1500 seconds than those using SS electrode yarns, but lower discharging voltage. Following our previous argument, this means that the internal resistance of our TESD is higher when using Ag/PBO yarns as the electrode material. As the only difference is the electrode, this indicates that Ag/PBO has a higher resistance than SS yarns. It can be observed that **Figure 4.15(a)** shows a similar discharge behavior as in **Figure 4.14(a)**, whereas Figure **4.15(b)** is similar to **Figure 4.14(b).** Comparing the two sets of figures provides an explanation to the different behavior caused by the use of different electrode materials as well as the role of their internal resistance to the performance of device. In the devices having an asymmetrical configuration of electrodes SS/Ag-PBO, the electrode resistance of current flowed from PEDOT to Ag was apparently high. As current flows from positive to negative, and electrons in the opposite direction, so when SS was set to positive (+) and Ag-PBO negative (−) (**Figure 4.15(a)**), electrons needed to move from Ag into PEDOT (+) sites. This also explains the high charging voltage in **Figure 4.15(b)**: as SS was set as the negative electrode, so electrons needed to move also at the Ag electrode, electrons then need to move into PEDOT (+) sites. The inverse, current flowing from Ag to PEDOT (so

electrons from PEDOT to Ag to form a PEDOT+ site) is not problematic, as the observed discharge and charge is then comparable to the SS electrodes.

In general, charge-discharge profile of devices with Clevios and Ossila is identical, although from all measurements, Clevios always showed slightly higher charging voltage than Ossila, and a bit lower discharging voltage, indicating a somewhat higher internal resistance. The weight and molar ratios of both are exactly similar, hence, their conductivities. Based on our characterizations and analysis, the only different characteristic between the two polymers is that Clevios has less sulphur content than Ossila. This might have relations with the higher internal resistance as explained earlier, although more investigations are needed to draw a conclusion.

It is also important to mention again here that our PEDOT:PSS-based device is a non-linear component, i.e. the stored charge is not linearly proportional to the applied voltage, so the capacitance value is strictly speaking not defined. However, it is possible to define an "equivalent" capacitance by the following equation (5) and (6), assuming for the device charged at 3V, as detailed in our previous report [56].

$$\frac{1}{2} C_{eq} V_0^2 = E_{el} = 0.8101\, mJ = 0.22\, \mu Wh \qquad (5)$$

The value of E_{el} was known to be 0.8101 mJ = 0.22 μWh by the calculation described in the paper [40], an therefore, the value of the equivalent capacitance can be calculated as follow:

$$C_{eq} = \frac{2E_{el}}{V_0^2} = 180\ \mu F \qquad (6)$$

4.4. Summary

Electrochemical impedance spectroscopy has been employed as one of techniques selected to study the mechanism of our developed textile energy storage device. By presenting the cyclic voltammograms of PEDOT:PSS in the form of electrochemical solution and in its solid state on the glass and the fabric surfaces, ionic behavior of the electroactive polymer PEDOT:PSS has been confirmed through the redox reaction. In general, the distance between electrodes played an important role to the conductivity and capacitive behavior of the PEDOT:PSS. The distribution of PEDOT:PSS polymer film in the solid state also affected its capacitive behavior. The device on a glass surface always exhibited higher capacitive behavior than the device on a fabric surface, which presents a unique challenge that needs to be addressed in later research. From the Nyquist and bode-phase plots of the device, both the ionic and electronic activities of the PEDOT:PSS film in the cell were found, mostly due to the complicated interaction in the interfacial region between the PEDOT:PSS polymer and the stainless-steel electrode. Two different equivalent circuit models were found by simulating the model with the experimental results: (QR)(QR)(QR) for the uncharged samples and (QR)(QR)(Q(RW)) for the charged samples. The results provide a better understanding about the underlying mechanism of the device.

With the other approach on the study of the mechanism, energy storage devices using three different commercial brands of PEDOT:PSS, Clevios P-VP-AI-4083, Ossila AI 4083, and Orgacon ICP 1050, as the solid electrolyte, were assembled especially to study the effect of ratio of PEDOT to PSS towards their charge-discharge performances. As electrodes, we used stainless steel (SS) and silver-coated polybenzoxazole (Ag-PBO) yarns, with various combinations: symmetrical SS/SS and Ag-PBO/Ag-PBO as well as asymmetrical SS/Ag-PBO. From the NMR analysis, we found that the Clevios and Ossila are almost identical, as evidenced by

the similar NMR spectra as well as their molar and weight ratio, i.e. 1.00:5.26 and 1.00:6.92 respectively. Utilization of these two types of PEDOT:PSS gave good charge-discharge profiles of the devices. Otherwise, devices with the Orgacon showed no charge-discharge profiles. Its PEDOT:PSS molar and weight ratios are 1.00:4.65 and 1.00:6.11 respectively. The lower proportion of PSS leads to a higher conductivity of the polymer. From the results, it can be concluded that for our specific developed energy storage devices, PEDOT:PSS with lower conductivity is more suitable, and the ratio significantly affects the conductivity. It should be investigated if further increasing of the ratio would lead to further benefits. It can be also concluded that the resistance of electrode – PEDOT must be low, which is not the case for Ag used as the positive electrode. In addition, the lower sulphur in PEDOT:PSS content seems to improve the results as shown by Ossila A1 4080 that has the best discharge properties. Further works are needed to elaborate more the effect of the PEDOT:PSS ratio by modifying from the doping process or with secondary doping. This finding gives directions into the improvement of devices performance with higher capacitive behavior.

Bibliography

[1] C. BE, Electrochemical Supercapacitors: Scientific Fundamentals and Technological Application. USA: Springer, 1999.

[2] Z. Su et al., "Co-electro-deposition of the MnO2-PEDOT:PSS nanostructured composite for high-areal mass, flexible asymmetric supercapacitor devices," J Mater Chem A, vol. 1, pp. 12432–12440, 2013.

[3] R. Genc et al., "High-Capacitance Hybrid Supercapacitor Based on Multi-Colored Fluorescent Carbon-Dots," Sci Rep, vol. 7, pp. 11222-1–13, 2017.

[4] R. Bhattacharya, M. M. de Kok, and J. Zhou, "Rechargeable electronic textile batteries," Appl. Phys. Lett., vol. 95, pp. 223305-1–3, 2009.

[5] S. A. Odhiambo, "PEDOT:PSS Charge Storage Devices Integrated into Textiles for Smart Textile Application," 2015, p. 163.

[6] S. A. Odhiambo, G. De Mey, C. Hertleer, A. Schwarz, and L. Van Langenhove, "Discharge characteristics of poly(3,4-ethylene dioxythiophene): poly(styrenesulfonate) (PEDOT:PSS) textile batteries; comparison of silver coated yarn electrode devices and pure stainless steel filament yarn electrode devices," Text. Res. J., vol. 84, no. 4, pp. 347–354, Mar. 2014.

[7] I. Nuramdhani, S. Odhiambo, C. Hertleer, and G. De Mey, "Electric Field Effect on Charge-Discharge Characteristics of Textile-Based Energy Storage Devices: In Search of the Underlying Mechanism.," Tekstilec, vol. 59, no. 2, 2016.

[8] M. . S. Mahajan, D. M. Marathe, S. S. Ghosh, V. Ganesan, and J. V. Sali, "Changes in in-plane electrical conductivity of PEDOT:PSS thin films due to electric field induced dipolar reorientation," RSC Adv, vol. 5, no. 105, pp. 86393–86401, 2015.

[9] J. Ouyang, Q. Xu, C.-W. Chu, Y. Yang, G. Li, and J. Shinar, "On the mechanism of conductivity enhancement in poly(3,4-ethylenedioxythiophene):poly(styrene sulfonate) film through solvent treatment," Polymer, vol. 45, no. 25, pp. 8443–8450, Nov. 2004.

[10] J. Ouyang, C.-W. Chu, F.-C. Chen, Q. Xu, and Y. Yang, "High Conductivity Poly(3,4-ethylenedioxythiophene):Poly(styrene sulfonate) Film and Its Application in Polymer Optoelectronic Devices," Adv Funct Mater, vol. 15, no. 2, pp. 203–208.

[11] S. Timpanaro, M. Kemerink, F. J. Touwslager, M. M. De Kok, and S. Schrader, "Morphology and conductivity of PEDOT/PSS films studied by scanning-tunneling microscopy," Chem. Phys. Lett., vol. 394, no. 4–6, pp. 339–343, 2004.

[12] A. M. Nardes et al., "Microscopic Understanding of the Anisotropic Conductivity of PEDOT:PSS Thin Films," Adv. Mater., vol. 19, no. 9, pp. 1196–1200, May 2007.

[13] L. Ouyang, C. Musumeci, M. J. Jafari, T. Ederth, and Inganäs,O., "Imaging the Phase Separation between PEDOT and Polyelectrolytes during Processing of Highly Conductive PEDOT:PSS Films," ACS Appl Mater Interfaces, vol. 7, no. (35), pp. 19764–19773, 2015.

[14] N. Chaturvedi, F. Alam, S. K. Swami, and V. Dutta, "Effect of electric field on the spray deposited poly(3,4-ethylenedioxythiophene):poly(styrene sulfonate) layer and its use in organic solar cell.," J Appl Phys, vol. 114, no. (18), p. 845101, 2013.

[15] J. Maddala, K. Sambath, V. Kumar, and S. Ramanathan, "Identification of reaction mechanism for anodic dissolution of metals using Electrochemical Impedance Spectroscopy.," J Electroanal Chem, vol. 638, no. (2), pp. 183–188, 2010.

[16] A. Yu, V. Chabot, and J. Zhang, Electrochemical Supercapacitors for Energy Storage and Delivery: Fundamentals and Applications. CRC Press: USA, 2017.

[17] K. Jost, G. Dion, and Y. Gogotsi, "Textile energy storage in perspective," J Mater Chem A, vol. 2, no. 28, p. 10776, 2014.

[18] F. Su and M. Miao, "Flexible, high performance two-ply yarn supercapacitors based on irradiated carbon nanotube yarn and PEDOT/PSS," Electrochimica Acta, vol. 127, no. 4, pp. 2553–2560, 2014.

[19] N. Yang and C. G. Zoski, "Polymer Films on Electrodes: Investigation of Ion Transport at Poly(3,4-ethylenedioxythiophene) Films by Scanning Electrochemical Microscopy," Langmuir, vol. 22, no. 25, pp. 10338–10347, 2006.

[20] L. Bao and X. Li, "Towards Textile Energy Storage from Cotton T- Shirts," Adv. Mater., vol. 24, no. 24, pp. 3246–3252, 2012.

[21] J. Bae, M. K. Song, Y. J. Park, J. M. Kim, M. Liu, and Z. L. Wang, "Fiber Supercapacitors Made of Nanowire-Fiber Hybrid Structures for Wearable/Flexible Energy Storage," Angew Chem Int, vol. 50, no. 7, pp. 1683–1687, 2011.

[22] G. A. Snook, P. Kao, and A. S. Best, "Conducting polymer-based supercapacitor devices and electrodes," J Power Sources, vol. 196, no. 1, pp. 1–12, 2011.

[23] Y. Fu et al., "Integrated power fiber for energy conversion and storage," Energy Env. Sci, vol. 6, no. 3, pp. 805–812, 2013.

[24] T. Takano, H. Masunaga, and A. Fujiwara, "PEDOT Nanocrystal in Highly Conductive PEDOT:PSS Polymer Films.," Macromolecules, vol. 45, pp. 3859–3865, 2012.

[25] F. Zhang, M. Johansson, and M. R. Andersson, "Polymer Photovoltaic Cells with Conducting Polymer Anodes," Adv Mater, vol. 14, pp. 662–665, 2002.

[26] H. J. Snaith, H. Kenrick, M. Chiesa, and R. H. Friend, "Morphological and electronic consequences of modifications to the polymer anode 'PEDOT:PSS," Polym. Guildf, vol. 46, pp. 2573–2578, 2005.

[27] X. Crispin et al., "Conductivity, Morphology, Interfacial Chemistry, and Stability of Poly(3,4-ethylene dioxythiophene)–Poly(styrene sulfonate): A Photoelectron Spectroscopy Study," J Polym Sci Part B Polym Phys, vol. 41, pp. 2561–2583, 2003.

[28] Y. Cao, G. Yu, C. Zhang, R. Menon, and A. J. Heeger, "Polymer light-emitting diodes with polyethylene dioxythiophene± polystyrene sulfonate as the transparent anode," Synth. Met., vol. 87, pp. 171–174, 1997.

[29] T. M. Brown, J. S. Kim, R. H. Friend, F. Cacialli, R. Daik, and W. J. Feast, "Built-in field electroabsorption spectroscopy of polymer light-emitting diodes incorporating a doped poly(3,4-ethylene dioxythiophene) hole injection layer," Appl. Phys. Lett., vol. 75, no. 12, p. 1679, Sep. 1999.

[30] P. K. H. Ho et al., "Molecular-scale interface engineering for polymer light-emitting diodes," Nature, vol. 404, pp. 481–484, Mar. 2000.

[31] T. Cheng et al., "Inkjet-printed flexible, transparent and aesthetic energy storage devices based on PEDOT:PSS/Ag grid electrodes," J. Mater. Chem. A, vol. 4, no. 36, pp. 13663–14034, Sep. 2016.

[32] T. Aernouts et al., "Printable anodes for flexible organic solar cell modules," Thin Solid Films, vol. 451–452, pp. 22–25, 2004.

[33] K. Sun et al., "Review on application of PEDOTs and PEDOT:PSS in energy conversion and storage devices," J Mater Sci Mater Electron, vol. 26, pp. 4438–4462, 2015.

[34] V. Kaushik, J. Lee, and J. Hong, "Textile-Based Electronic Components for Energy Applications: Principles, Probles, and Perspective," Nanomaterials, vol. 5, pp. 1493–1531, 2015.

[35] A. A. Argun, A. Cirpan, and J. R. Reynolds, "The first truly all polymer electrochromic device," Adv. Mater., vol. 15, no. 15, 2003.

[36] S. Kirchmeyer and K. Reuter, "Scientific importance, properties and growing applications of poly(3,4-ethylenedioxythiophene)," J Mater Chem, vol. 15, pp. 2077–2088, 2005.

[37] B. Sun et al., "Recent advances in flexible and stretchable electronic devices via electrospinning," J Mater Chem, vol. 2, pp. 1209–1219, 2014.

[38] H. Shi, C. Liu, Q. Jiang, and J. Xu, "Effective Approaches to Improve the Electrical Conductivity of PEDOT:PSS: A Review," Adv. Electron. Mater., vol. 1, pp. 1500017-1–16, 2015.

[39] F. Jonas and J. T. Morrison, "3,4-polyethylenedioxythiophene (PEDT): conductive coatings technical applications and properties," Synth. Met., vol. 85, pp. 1397–1398, 1997.

[40] J. Y. Kim, J. H. Jung, D. E. Lee, and J. Joo, "Enhancement of electrical conductivity of poly(3,4-ethylenedioxythiophene)/poly(4-styrenesulfonate) by a change of solvents," Synth. Met., vol. 126, pp. 311–316, 2002.

[41] X. Crispin et al., "The origin of the high conductivity of poly (3, 4-ethylenedioxythiophene)-poly (styrenesulfonate)(PEDOT-PSS) plastic electrodes," Chem. Mater., vol. 18, no. 18, pp. 4354–4360, 2006.

[42] B. Fan, X. Mei, and J. Ouyang, "Significant Conductivity Enhancement of Conductive Poly(3,4-ethylenedioxythiophene): Poly(styrenesulfonate) Films by Adding Anionic Surfactants into Polymer Solution," Macromolecules, vol. 41, pp. 5971–5973, 2008.

[43] M. Do¨bbelin et al., "Influence of Ionic Liquids on the Electrical Conductivity and Morphology of PEDOT:PSS Films," Chem Mater, vol. 19, pp. 2147–2149, 2007.

[44] T. Stocker, A. Kohler, and R. Moos, "Why Does the Electrical Conductivity in PEDOT:PSS Decrease with PSS Content? A Study Combinig Thermoelectric Measurements with Impedance Spectroscopy," J Polym Sci Part B Polym Phys, vol. 50, pp. 976–983, 2012.

[45] J. Ouyang, X. Qianfei, C. Chi-Wei, Y. Yang, L. Gang, and J. Shinar, "On the mechanism of conductivity enhancement in poly(3,4-ethylenedioxythiophene):poly(styrene sulfonate) film through solvent treatment," Polym. Guildf, vol. 45, no. 25, pp. 8443–8450, 2004.

[46] P. T. Kissinger and W. R. Heineman, "Cyclic Voltammetry," J. Chem. Educ., vol. 60, no. 9, 1963.

[47] A. Elschner, S. Kirchmeyer, W. Lovenich, U. Merker, and K. Reuter, PEDOT: Principles and Applications of an Intrinsically Conductive Polymer. Boca Raton: CRC Press, 2011.

[48] J. R. Macdonald and W. B. Johnson, Fundamentals of Impedance Spectroscopy. In Impedance Spectroscopy: Theory, Experiment and Applications, 2nd ed. New York, USA: Wiley Interscience, 2005.

[49] https://www.heraeus.com/media/group/doc_group/products_1/conductive_polymers_1/p/CLEVIOS_P_VP_AI_4083.pdf.

[50] https://www.ossila.com/products/pedot-pss.

[51] https://www.sigmaaldrich.com/catalog/product/aldrich/739332?lang=en&region=ID

[52] Ashok PR, Thomas MR, Varughese S. Multi-region to single region shear thinning transitions in drying PEDOT:PSS dispersions: Contributions from charge density fluctuations. *Soft Matter* 2015; 1-3.

[53] Levinshtein ME and Rumyantsev SL, Gallium Arsenide (GaAS), in: Ed. Levinshtein ME, Rumyantsev SL, Shur M, *Handbook Series on Semiconductor Parameters.* vol. 1, World Scientific Publishing Co. Pte. Ltd.: Singapore, 2000, pp. 77-102.

[54] Yan H, Arima S, Mori Y, et al. Poly(3,4-ethylenedioxythiophene)/poly(4-styrenesulfonate): Correlation between colloidal particles and thin films. *Thin Solid Films* 2009; 517: 3299-3303.

[55] Nuramdhani I, De Mey G, Widodo M, et al. Ionic shot noise in an electrochemical capacitor system made of poly(3,4-ethylenedioxythiophene)-poly(styrenesulfonate) film and silver-coated polybenzoxazole-stainless steel electrodes on textile fabrics. *Text Res J* 2018; 4051751876715.

[56] Odhiambo SA, Fiszer P, De Mey G, et al., The electric energy stored in PEDOT:PSS capacitors integrated on textile substrate: Limits and possibilities. *IJCST* 2018; 30(6): 808-816.

5

Washability of the textile energy storage device

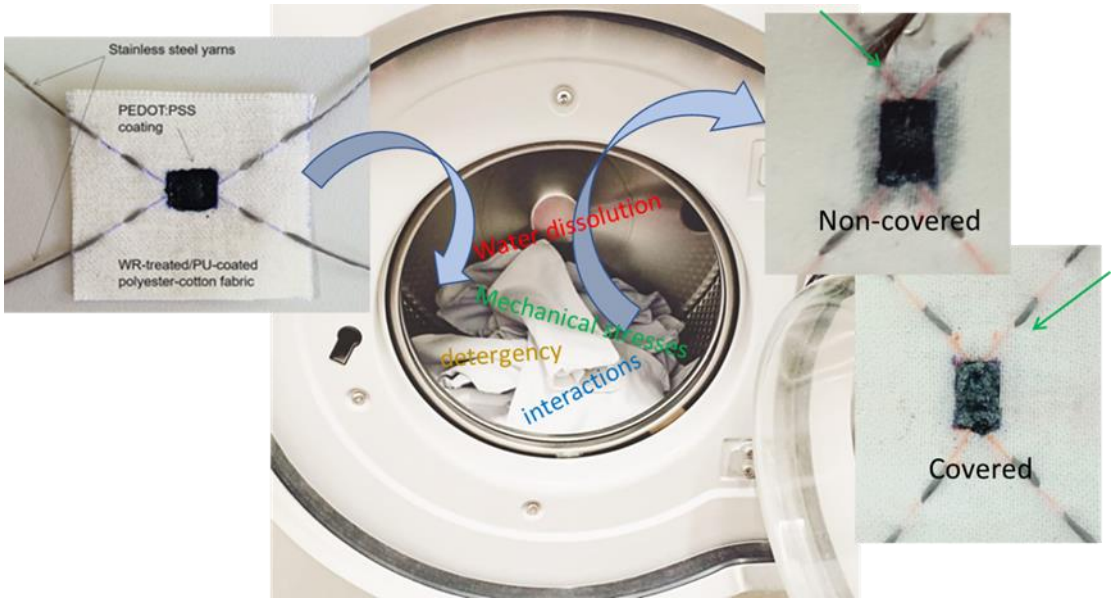

5.1. Introduction

As already understood, PEDOT:PSS is one of the most important classes of conjugated materials which is generally water-dispersible due to the presence of poly(styrenesulfonate) (PSS) in the polymer mixture [1]. The coating of PEDOT:PSS in the wide range of textile materials has been used for any textile electronic applications such as textile sensors [2]–[5], electrodes for dye sensitized solar cells [6], [7], electrode for flexible fabric keyboard [5], electrochemical transistors [8], [9], and many others including our textile energy storage devices [10]–[14]. Those examples have shown tremendous progress of research in the area of development of textile electronics, bringing it closer to the real applications. However, washability is still one of the most challenging problems faced by anyone who is developing products of smart textiles, particularly those that need regular washing.

Our latest developed energy storage device, so-called TESD 1.2 THL, has shown improvement in its form and characteristics. The cell was assembled on one layer of textile fabric, which means that it is much thinner, lighter, and more flexible than its previous design with three layers of fabric. The coating of conjugated PEDOT:PSS polymer which functioned as a solid electrolyte was also well concentrated within the cell area, without any diffusion into the structure of the textile fabric. This means that technically the distribution of the polymer coating in the device was more controlled and not only visually better but has led to better performance as well. Compared to the device with previous design, the voltage stored in the latest device during the discharge phase was about 20% higher (**Figure 3.19**), although more improvement is required to make it truly applicable as a textile energy storage device. Apart from the improvements, washability has become the next major concern, especially because in the present device, the coated PEDOT:PSS is still left naked on the surface of the textile fabric.

Washability has been one of the long-standing challenges for the

development of smart textiles, particularly wearables and smart clothing. The idea of having a shirt that can talk or provide vital information, for example, has been around for some time. The market is waiting and the number one question asked by the consumers is related to washability. How do you wash it? Can it withstand regular domestic washing? How often can you wash your smart textile garments? Washing is also psychological in a sense that it is related with one's perception on cleanliness, hygiene, and health. Unless there is a change or at least shift of paradigm about washing, one should not underestimate the significance of washability in the design of his/her product of smart textiles.

Fastness to washing is one of basic important quality requirements for wearable textiles and clothing. Concerning the daily used conditions, mechanical stresses provoked by the washing process is the other major aspect to consider. Few attempts have been made by other researchers to fabricate a washable textronic, for instance, by protecting the electronic devices with silicone-encapsulation [15] and permanently integrating the conducting polymer into the fiber *via* the dyeing process [16]. The PEDOT:PSS used in our device is known to have good water solubility, which will make it prone to being washed away in regular and repeated washing during the use of the product. Although basically known to be non-toxic, peeled off PEDOT:PSS film from the fabric or clothing to which it is attached to may rise some health concerns and create uncomfortable feelings to the consumers. Therefore, protecting the cell surface is one of possible ways to avoid dissolution of the PEDOT:PSS during the washing.

This chapter presents our initial study on washability of the devices. Two approaches aiming at creating a water-resistant surface are presented: (1) by covering the cell surface with a layer of thermoplastic polyurethane; and (2) by applying a fluorocarbon-based water-repellent chemical on the cell surface. The effect of both treatment to the charge-discharge profile was observed. The washing

tests were then carried out step by step from the very mild and soft condition up to the standardized real daily washing condition to see the effect of each washing method. Possible changes on the cell morphology were also characterized by using scanning electron microscopy (SEM).

5.2 Experimental Details

5.2.1 Fabrication of the Device

The devices used in the washability study described in this chapter were those that are labeled as TESD 1.2 THL. The device was fabricated by adopting the similar procedure as described in chapter 3 section 3.3.4.2, using similar materials as well. The visual appearance of the initial device used on this study has been shown in **Figure 3.20**.

To protect the cell surface, two different approaches were applied to the fabricated devices:

1. Masking the cell surface with thermoplastic polyurethane.
   To mask the cell surface, a layer of TPU film of 80 micron (μm) thickness was applied to the fabric by a heat press at 100 °C for 2 minutes.
2. Coating the cell surface with the fluorocarbon-based water repellent agent.
   Two different approaches to apply the water repellent agent into the cell surface were employed, i.e. by the impregnation using padder with 80% w.p.u. (2 times padding) and by exhaustion for 5 minutes, both were followed by 2 times drying with stenter at 120 °C for 2 minutes each.

5.2.2 Test of Washability

The test of washability was carried out in three gradual steps, called as washing 1, washing 2, and washing 3. The reason of having the three steps of washing was to see every effect of the washing process, from the mildest to the

heaviest interaction, using the standard washing condition. Washing 1 and 2 were initial washing process carried out for each device. After having the initial washings, the same device was treated by the standard washing process to get more standardized analysis. At least a week was determined as the gap time between each washing. The standard document used for this analysis was SNI-ISO 105-C06: 2010 [17]. The SNI-ISO 105-C06 is an identical adoption of ISO 105-C06: 1994 (E), Textiles – Test for Color Fastness, Part C06: Color fastness to domestic and commercial laundering, third edition, include technical corrigendum 1 ISO 015-C06: 1994/ Cor. 1:2002 (E) and technical corrigendum 2 ISO 015-C06: 1994/ Cor. 2:2002 (E), by the translation method. The reason of taking this standard was because the PEDOT:PSS is a colored material which is water soluble, and it is potentially detached from the fabric by the washing process. In addition, the standard condition applied to this process allowed us to include the mechanical stresses during the washing process as detailed in the later paragraph. All the washing tests were done in the standard testing laboratory of Politeknik STTT Bandung, Indonesia.

5.2.2.1 Initial Washings

For washing 1, each device was dipped in 200 ml water for 5 minutes with a constant stirring at 400 RPM at room temperature. Similarly, in washing 2, each device was placed in 200 ml water but 0.8 g (=4 g/l) commercial detergent was added and the washing was carried out for 5 minutes with a constant at 400 RPM at room temperature. After the washing 2, the device was rinsed once with the flowing water, and then dried using a dryer until the device was completely dry.

5.2.2.2 Standard Test for Fastness to Domestic and Commercial Washing (SNI-ISO C06: 2010)

Test principle. A specimen of the textile in contact with specified adjacent fabric or fabrics is laundered, rinsed, and dried. Specimens are laundered under

appropriate conditions of temperature, alkalinity, bleaching and abrasive action such that the results is obtained in a conveniently short time. The abrasive action is accomplished by the use of a low liquor ratio and an appropriate number of steel balls. The change in color of the specimen and the staining of the adjacent fabric are assessed by comparison with grey scales.

Apparatus, materials and reagents. The suitable mechanical device for this standard consists of a water bath containing a rotatable shaft which supports, radially, stainless steel containers (75 mm ± 5 mm diameter × 125 mm ± 10 mm high) of capacity 550 ml ± 50 ml, the bottom of the containers being 45 mm ± 10 mm from the center of the shaft. The shaft container assembly is rotated at a frequency of (40 ± 2) min^{-1}. The temperature of the water bath is thermostatically controlled to maintain the test solution at the prescribed temperature ± 2ºC. The machine used in this test was the Autowash II (Code 311B – C – D) from Mesdan Lab, Italy, as shown in **Figure 5.1**. Non-corrodible stainless steel approximately 6 mm in diameter was used to impart mechanical action to the tested material to resemble the actual washing situation. Adjacent fabrics used for the test were layers of cotton and polyester fabrics. Standard detergent without optical brightener was prepared with the following composition:

Linear alkylsulfonate, sodium salt (LAS)	(14.00 ± 0.02) %
Alcohol ethoxylate	(2.30 ± 0.02) %
Soap – high molecular mass	(2.50 ± 0.02) %
Sodium tripolyphosphate	(48.00 ± 0.02) %
Sodium silicate (SiO_2/Na_2O = 2/1)	(9.70 ± 0.02) %
Sodium sulfate	(15.40 ± 0.02) %
Carboxymethylcellulose (CMC)	(0.25 ± 0.02) %
Water	(7.85 ± 0.02) %

Test procedures. 150 ml wash liquor made by dissolving 4 g/l detergent in water was prepared. Based on the standard, for this test, the pH was not adjusted and 10 steel balls were added to every wash bath. The device was added into the

bath. The maximum washing temperature based on standard was 40 °C, and the washing time was 30 minutes. At the end of the washing process, the device was removed from the bath and then rinsed twice for 1 minute each in two separate 100 ml portions of water at maximum 40 °C. The device was then dried by hanging it in air at temperature not exceeding 60 °C. The test results were evaluated by visual examination and comparing the washed and unwashed samples. Portion of film being eroded or peeled of will be signs for low degree of washability.

Figure 5.1. Standard machine for the washing test (Autowash II - Mesdan Lab)

5.2.3 Charge-Discharge Test

Charge-discharge tests were carried out using Arduino Uno following the procedure shown by the circuitry diagram presented in **Figure 4.13**. The tests were performed to the same set of devices before and after masking, and after each washing. Each device was charged at 3 V for 1500 s, and then discharged for another 1500 s.

5.2.4 Analysis of the Cell Morphology

The possible change of cell morphology after washing was evaluated by visual examination and scanning electron microscopy (SEM). The examination by SEM targeted the top surface of the film and the cross-section areas of the masked device, after washing 3. The procedure of analysis with SEM was similar to what was described in the section 3.3.3.1. (part of "observation of morphology) in Chapter 3.

5.3 Results and Discussion

As described earlier, all tests of washability carried out in this study were performed to the device labelled TESD 1.2 THL. The original devices were then either covered by thermoplastic polyurethane or treated by the fluorocarbon-based water-repellent agent (WR-treated). It is worth to mention here that water repellent agent used for this purpose was different from those described in Chapter 3. By the time of research, it was realized that the previous chemical was based on the chemistry of perfluorooctanoic acid, which is broadly recognized as C8. It is considered as environmentally problem. So, for this part, another type of water-repellent agent called NK-GUARD S-22 (Indonesia Nicca Chemicals Ltd., Karawang, Indonesia), which mainly consists of perfluorohexanoic acid, or commonly called C6, apart from the other additives such as non-ionic surfactant, propylene glycol, monomethyl ether, glycol-based solvent and water, was employed to replace the previous one. It is developed as a more human and environmentally friendly product to counteract against the C8 [18], which has been broadly used in conventional fluorocarbon products. The polyurethane, in addition, is a block copolymer comprising of alternating sequences of hard and soft segments made from cyanate with long and short chain of diols, making it a thermoplastic and flexible [19].

In the experiment, WR treatment was applied by impregnation (padding) and exhaust methods. So, there were four samples tested in total: three samples were TPU-covered or WR-treated, plus one original sample where the cell was left naked. To ensure the reproducibility, each sample was duplicated once. Every stage of washing test (washing 1, 2, and 3) was performed to the same device. Therefore, one week was given to each device to wait until the next washing. The data presented for each charge-discharge curve in this chapter are the average value of the two replicated devices.

5.3.1 Effect of Washing to the Charge-Discharge Profile

Figure 5.2 presents charge-discharge profiles of all device samples before washing. It can be seen from the graphs that all devices exhibited typical charge-discharge curves at their original form, which means that protecting the cell surface retained conductivity and capacitive behavior of all devices. However, it was observed that after being treated with water repellent agent or covered with TPU, all charge voltages increased, with devices covered by TPU showed highest increase, i.e. about 2-folds. It is presumably because the TPU layer created more contacts or physical interactions with the PEDOT:PSS film, which in turn intensified the charge separation between $PEDOT^+$ and PSS^-, and then increased the accumulation of charge voltages. In some literatures [20]–[22], PEDOT:PSS was found to be able to interact with polyurethane, either combined in a mixture or coated, without significantly changing each component's properties, including the PEDOT:PSS conductivity. This implies that the differently drastic increase in the charge voltages of device covered with TPU was caused more by the physical contacts between PEDOT:PSS and TPU rather than the chemical interactions. Similar possible physical interaction also occurred in the device treated with the water-repellent agent, although the increase in the resulting charge voltages was not as high as the device covered with TPU.

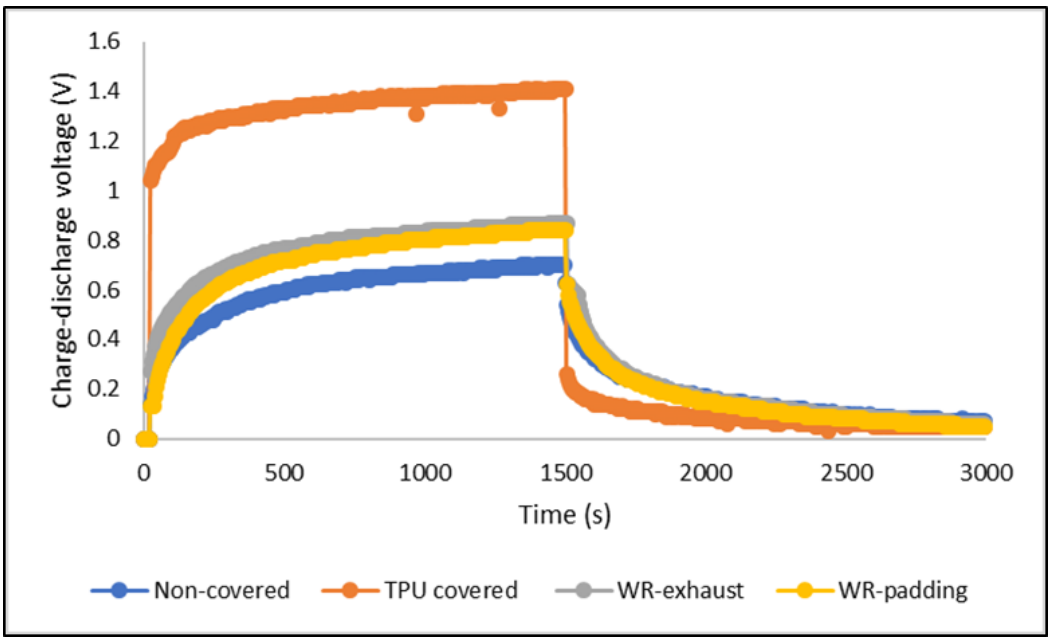

Figure 5.2. Charge-discharge profile of all types of device sample before washing

As shown in **Figure 5.3**, after washing 1, where the devices were dipped only on 200 ml of water with constant stirring, all devices showed stability at their charge-discharge profiles, retaining their typical charge-discharge characteristics, except that device with pad-cure WR-treatment showed an increase in its charge voltages. Here, we can see that stirring did not change the configuration of the cell too much, and the following drying process could perfectly return all the cell properties back. However, in contrast, washing with detergent destroyed the charge-discharge behavior of all devices, except one with TPU covered, as shown by the graphs in **Figure 5.4.** The TPU-covered device preserved its charge-discharge characteristics, although the charge voltages decreased and the discharge voltage increased. On the other hand, the rests behaved like blank devices (**Figure 4.17** in Chapter 4), where there was no current flow during the charge process, with an immediate voltage over the electrodes, but still lower than the voltage applied by the source. This indicated that the washing process caused a gradual detachment

of the PEDOT:PSS film. The diminishing coverage of PEDOT:PSS can be also confirmed by the visual appearance of each device as presented later in **Figure 5.7** of this chapter.

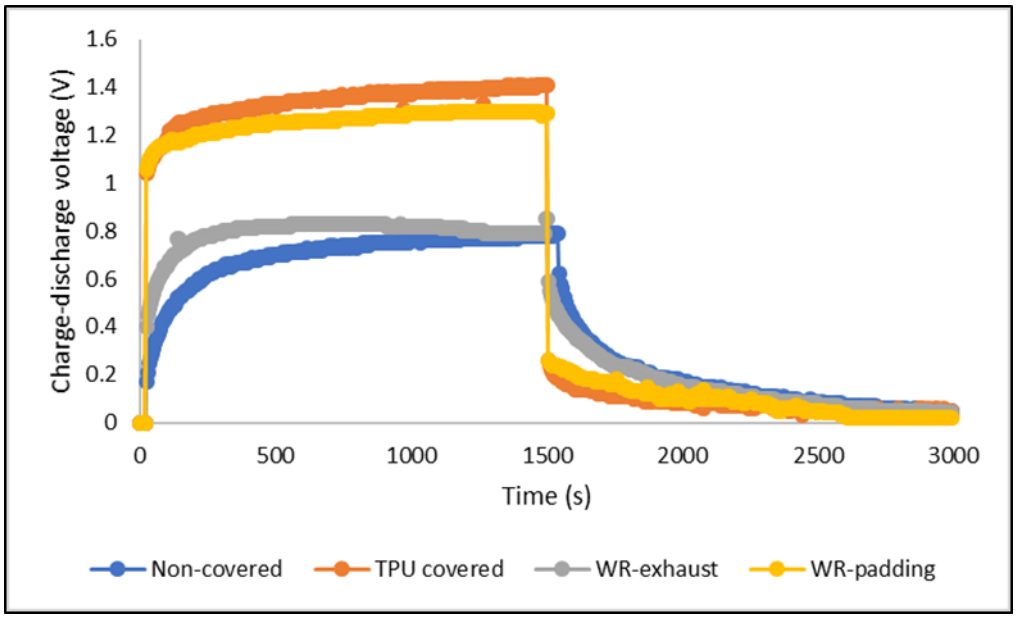

Figure 5.3. Charge-discharge profile of all types of device sample after washing 1

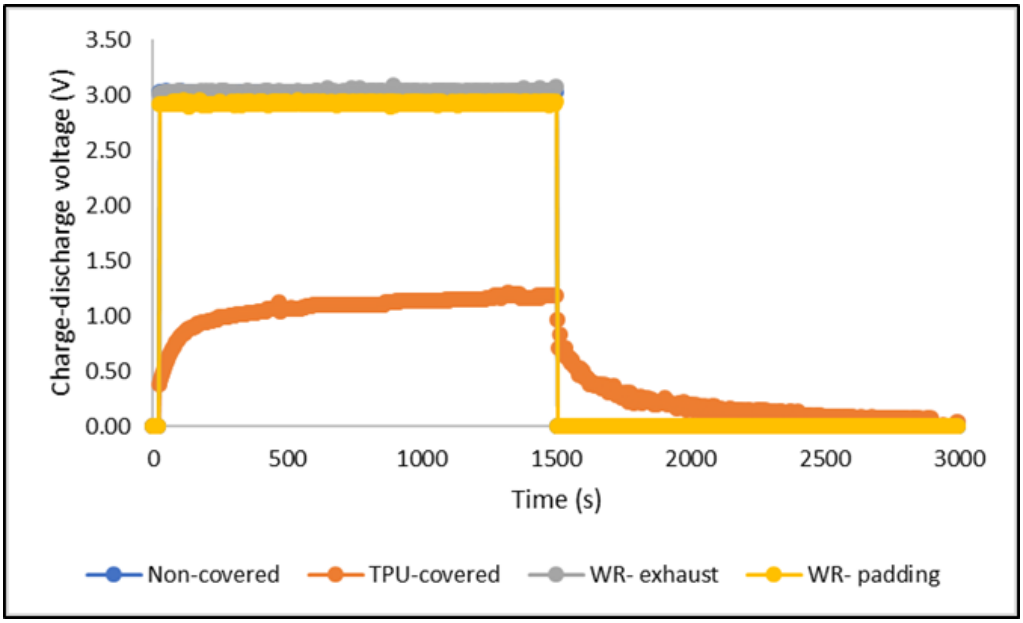

Figure 5.4. Charge-discharge profile of all types of device sample after washing 2

It is also interesting to briefly discuss here why the naked PEDOT:PSS film was not immediately dissolved or re-dispersed in the water during the washing 1. Based on our observation during the washing tests, gradual release of a small portion of PEDOT:PSS film from the device into the washing solution started to take place in washing 2, i.e. when detergent was added, but again, they were only distributed in the water, not dissolved. This can be explained by the changes of molecular arrangement of PEDOT:PSS as presented in **Figure 5.5**. It can be seen that molecular arrangement of PEDOT:PSS changes with the change of its physical state. Commercially, the PEDOT:PSS is available in the form of dispersion of a poly-ion complex as colloidal gel particles (tertiary structure) with a diameter of several tens of nm. So, here in water dispersion, the hydrophobic PEDOT molecules aggregate away from the surrounding water molecules and "hide" within the confinement of the longer hydrophilic PSS chains which then form crosslinks via hydrogen bonding with the adjacent globular colloidal gel particles. In the form of thin solid film as what we made in our devices, a hard and brittle film is formed because of the hydrogen bonding between sulfonic acid groups of the PSS as illustrated in the picture (quaternary structure). Even though soluble in water, the dissolution of PEDOT:PSS film in our device did not occur immediately upon contact with the liquid. It must have occurred gradually and slowly, so that the application of water-based water-repellent agent did not interfere with the integrity or cause any leaching of the film. This is confirmed by the results of the treatment, particularly those treated with exhaust method. The film softened (and hardened again after drying) but was still intact within the boundary of cell area. Similar observation regarding the integrity of the film was also found with water-repellent treatment using pad-dry method, except that the film deformed and spread out of the cell area due to high pressure exerted by the padding mangle during the process.

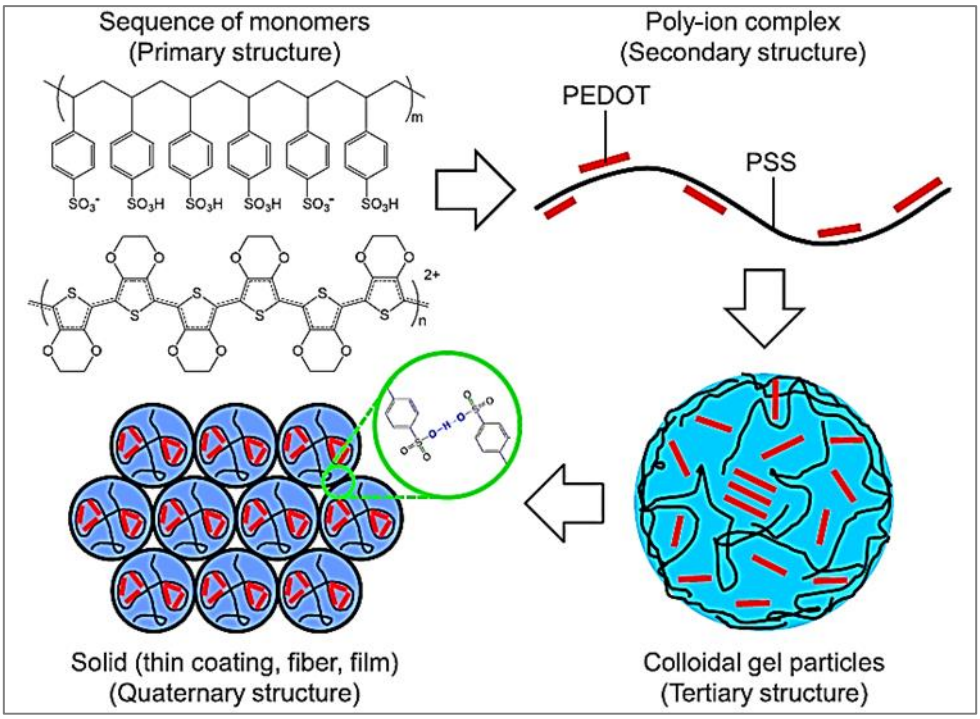

Figure 5.5. Changes of molecular arrangement of PEDOT:PSS [21]

To further confirm washability of the devices, especially the TPU-covered device for this case, washing 3 was performed. It was based on the ISO standardized method to test the fastness of colored materials to domestic and commercial washing. In this washing method, the factors of mechanical stresses and contacts were also taken into account especially by the addition of ten steel balls in the washing batch to create mechanical contacts with the sample. As expected, all devices except that covered by TPU cannot retain their capacitive behavior (**Figure 5.6**). By the way of washing tests performed, it is indicated that the original and WR-treated devices were prone to abrasion due to the possible bending and wear. Interestingly, the device covered with TPU still maintained its capacitive behavior after this washing test as shown by its charge-discharge curve in **Figure 5.6**. Second and third washings with this standardized method were also performed to check the durability, and charge-discharge characteristics were

retained. This indicated that covering with TPU is a promising method to promote the washability of this energy storage device. Different charge-discharge profiles of devices that have undergone different procedures of washing are presented in the appendix of this chapter (**Figure A.5.1-A.5.4**).

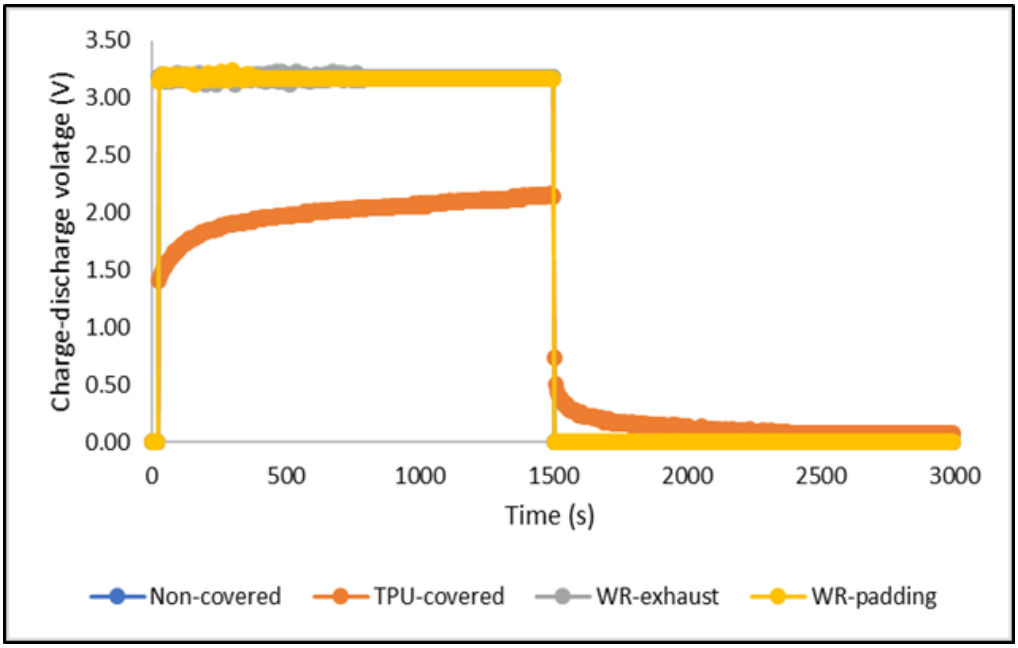

Figure 5.6. Charge-discharge profile of all types of device sample after washing 3

5.3.2 Effect of Washing to the Cell Morphology

Figure 5.7 presents the visual appearance of all devices under this study before and after each washing. In general, it is shown that protecting the cell surface with a layer of thermoplastic polyurethane can prevent the PEDOT:PSS film from dissolving out to the washing solution. On the other hand, the application of water-repellent agent on the cell surface does not seem to provide adequate protection against the mechanical action of washing. PEDOT:PSS film on the WR-treated devices gradually detached from the fabric with the progress of washing. Up to a certain extent, the detachment was still acceptable in a sense that the capacitive behavior of the device was still retained. However, further releases of the

PEDOT:PSS film cut the connection between the solid electrolyte and the two electrodes. This is indicated by the loss of capacitive behavior of the original device as well as devices covered with water repellent agent after washings 2 and 3. This further indicates that thicker film is preferable and is of significant importance for a better and more stable performance of our PEDOT:PSS energy storage device [14]. This, however, may put a challenge to the need for a non-obtrusive, thin and flexible coating that is required of an ideal fully integrated device. From the pictures presented in **Figure 5.7**, it can also be seen that there were no considerable changes of morphology of the cell caused by the washings. The electrode yarns conductivity was also still preserved, as indicated by the presence of charge curves during the charging process of all devices after washings. The only observed change was that of the swollen electrode yarns due to temporary water absorption, which quickly disappeared after drying.

Figures 5.8 and **5.9** are presented to specifically show the changes in morphology of the TPU-covered device before (**Figure 5.8**) and after (**Figure 5.9**) the three washings with a repetition of the washing 3. Using SEM, it can be observed that after two times of washing 3, the TPU layer has a potential to break due to the bending and mechanical stresses during the washing. However, it was demonstrated that all washings did not eliminate the capacitive behavior. Further tests are needed to assess the durability of the device to washing more thoroughly. From the cross-section images shown in **Figures 5.8** and **5.9**, it can be seen that there was only rearrangement of the electrode yarn because of the possible water absorbed into the cell as well as the mechanical contacts during the washing. This is indicated by the change of yarn diameter from 656.634 μm before washing to 740.594 μm after washing. The total yarn density must be still the same, and there were no broken threads observed in the cell either after the washing process.

Although TPU-covered devices have shown satisfactory fastness and durability to washing, it should be mentioned here that it is not final as more ways with potentially better results are available for further consideration and research. One of the possible routes to excellent durability is by dyeing the PEDOT:PSS into the conductive yarn electrodes. Optimizing the application of water-repellent agent can also become a potential research direction. In the future works, it is also important to test the washability by the standardized method which represents the durability up to 50 cycles or more.

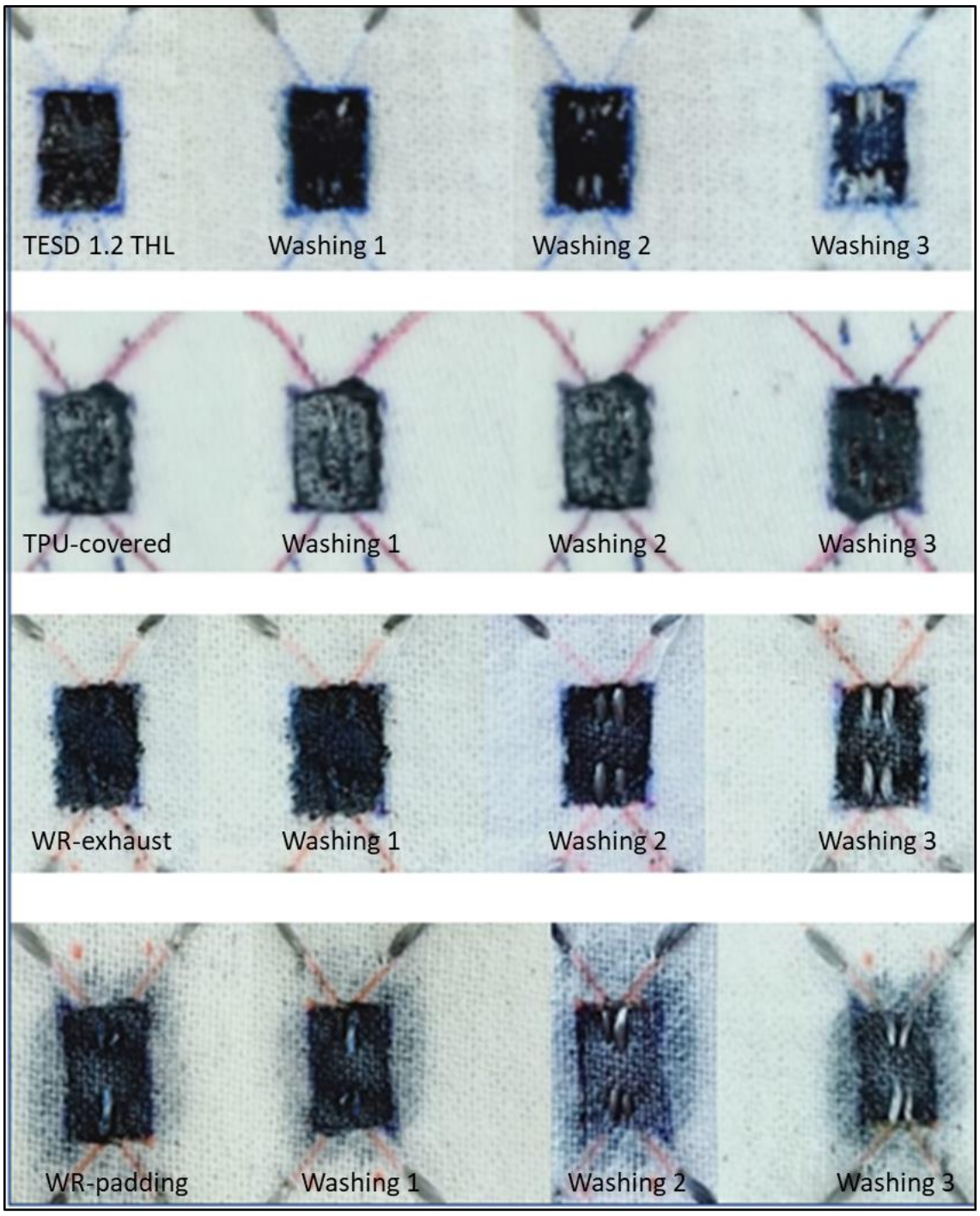

Figure 5.7 Visual appearance of devices before and after washing

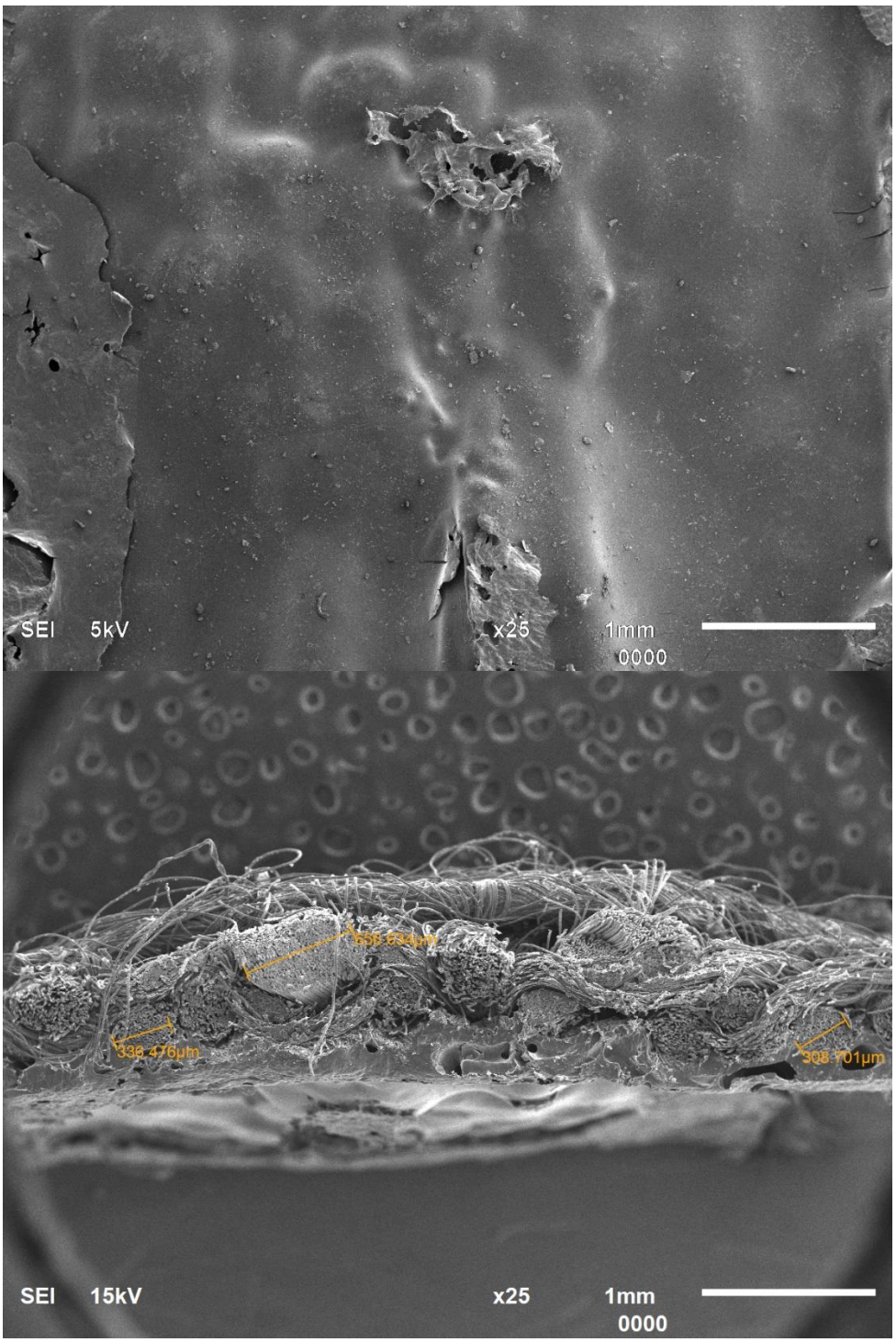

Figure 5.8. Surface (above) and cross-section (below) morphology of the device covered with TPU – Before washing

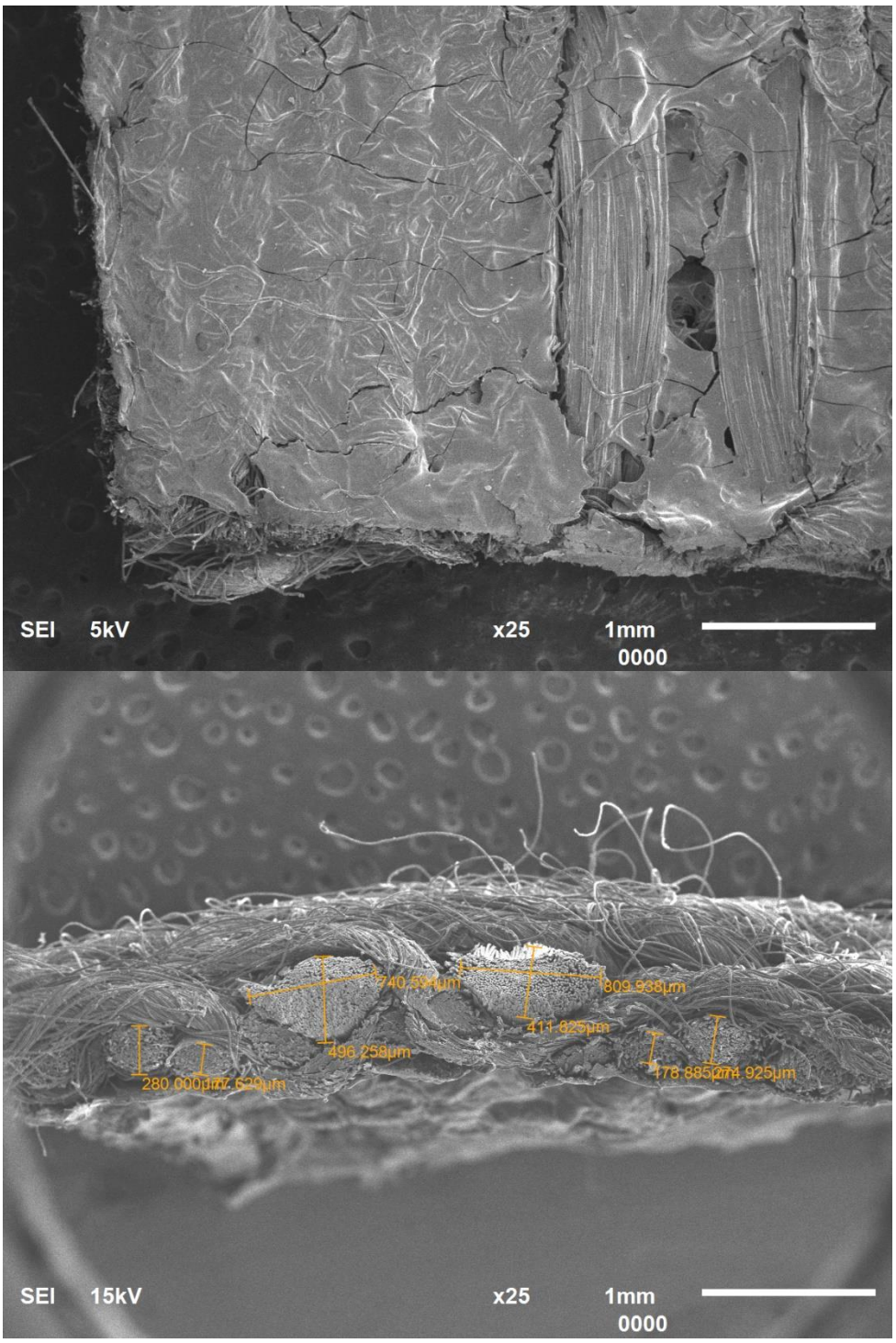

Figure 5.9. Surface (above) and cross-section (below) morphology of the device covered with TPU – after washing 3

5.4 Summary

Washability of our developed energy storage devices has been studied. The main idea was to protect the cell which contained a thick layer of PEDOT:PSS film. Two approaches have been employed to protect the cell: (1) by covering the cell surface with a fluorocarbon-based water-repellent agent which was applied by two different methods, i.e. impregnation by padding and exhaustion methods which was followed by two times drying at 120 °C; (2) by masking the cell surface with a layer of thermoplastic polyurethane (TPU). Three stages of washings were performed to each device. The results showed that TPU-covered device exhibited the best performance, where the capacitive behavior was still retained after two times of washing 3 (based on the SNI-ISO C06: 2010). Also, there were no significant changes in the morphology of the TPU-covered device after the sequence of washings. The results are promising for further study as well as for further development of a more applicable textile energy storage device.

Bibliography

[1] A. Elschner, S. Kirchmeyer, W. Lovenich, U. Merker, and K. Reuter, *PEDOT: Principles and Application of an Intrinsically Conductive Polymer*. USA: CRC Press, 2011.

[2] T. Vuorinen, J. Niittynen, T. Kankkunen, T. M. Kraft, and M. Mäntysalo, "Inkjet-Printed Graphene/ PEDOT:PSS Temperature Sensors on a Skin-Conformable Polyurethane Substrate," *Sci. Rep.*, vol. 6, no. 35289, 2016.

[3] G. U. Siddiqui, M. Sajid, J. Ali, S. W. Kim, Y. H. Doh, and K. H. Choi, "Wide range highly sensitive relative humidity sensor based on series combination of MoS2 and PEDOT:PSS sensors array," *Sens. Actuators B Chem.*, vol. 266, pp. 354–363, 2018.

[4] C. Cochrane, V. Koncar, M. Lewandowski, and C. Dufour, "Design and Development of a Flexible Strain Sensor for Textile Structures Based on a Conductive Polymer Composite," *Sensors*, vol. 7, pp. 473–492, 2007.

[5] S. Takamatsu, T. Imai, T. Yamashita, T. Kobayashi, K. Kobayashi, and T. Itoh, "Flexible fabric keyboard with conductive polymercoated fibers," *IEEE*, vol. 978-1-4244-9289–3/11, 2011.

[6] W. Hong, Y. Xu, G. Lu, C. Li, and G. Shi, "Transparent graphene/PEDOT–PSS composite films as counter electrodes of dye-sensitized solar cells," *Electrochem. Commun.*, vol. 10, pp. 1555–1558, 2008.

[7] Y. H. Kim, C. Sachse, M. L. Machala, C. May, L. Müller-Meskamp, and K. Leo, "Highly Conductive PEDOT:PSS Electrode with Optimized Solvent and Thermal Post-Treatment for ITO-Free Organic Solar Cells," *Adv Funct Mater*, vol. 21, pp. 1076–1081, 2011.

[8] P. Gkoupidenis, N. Schaefer, B. Garlan, and G. G. Malliaras, "Neuromorphic Functions in PEDOT:PSS Organic Electrochemical Transistors," *Adv Mater*, vol. 27, pp. 7176–7180, 2015.

[9] I. Gualandi, D. Tonelli, F. Mariani, E. Scavetta, M. Marzocchi, and B. Fraboni, "Selective detection of dopamine with an all PEDOT:PSS Organic Electrochemical Transistor," *Sci. Rep.*, vol. 6, no. 35419, 2016.

[10] S. Odhiambo, G. De Mey, C. Hertleer, A. Schwarz, and L. Van Langenhove, "Discharge characteristics of poly(3,4-ethylene dioxythiophehe):poly(styrenesulfonate) (PEDOT:PSS) textile batteries;

comparison of silver coated yarn electrode devices and pure stainless steel filament yarn electrode devices," *Text. Res. J.*, vol. 84, no. 4, pp. 347–354, 2014.

[11] S. Odhiambo, G. De Mey, C. Hertleer, and L. Van Langenhove, "Reliability Testing of PEDOT:PSS Capacitors Integrated Into Textile Fabrics," *Eksploat. Niezawodn. - Maint. Reliab.*, vol. 16, no. 3, pp. 447–451, 2014.

[12] I. Nuramdhani, S. Odhiambo, C. Hertleer, G. De Mey, and L. Van Langenhove, "Electric Field Effect on Charge-Discharge Characteristics of Textile-Based Energy Storage Devices: In Search of the Underlying Mechanism," *Tekstilec*, vol. 59, no. 2, pp. 162–167, Apr. 2016.

[13] I. Nuramdhani, A. T. Gokceoren, S. Odhiambo, G. De Mey, C. Hertleer, and L. Van Langenhove, "Electrochemical Impedance Analysis of a PEDOT:PSS-Based Textile Energy Storage Device," *Materials*, vol. 11, no. 48, pp. 1–11, 2018.

[14] I. Nuramdhani, G. De Mey, M. Widodo, C. Hertleer, and L. Van Langenhove, "Ionic shot noise in an electrochemical capacitor system ade of poly(3,4-ethylenedioxythiophene)-poly(styrenesulfonate) film and silver coated polybenzoxazole-stainless steel electrodes on textile fabrics," *Text. Res. J.*, vol. 0, no. 00, pp. 1–10, 2018.

[15] X. Tao, V. Koncar, T.-H. Huang, C.-L. Shen, Y.-C. Ko, and G.-T. Jou, "How to Make Reliable,Washable, and Wearable Textronic Devices," *Sensors*, vol. 17, p. 673, 2017.

[16] J. D. Ryan, D. A. Mengistie, R. Gabrielsson, A. Lund, and C. Müller, "Machine-Washable PEDOT:PSS Dyed Silk Yarns for Electronic Textiles," *ACS Appl Mater Interfaces*, vol. 9, p. 9045−9050, 2017.

[17] "SNI-ISO 105-C06: 2010 - Adoption of ISO 105-C06: 1994 (E), Textiles – Test for Color Fastness, Part C06: Color fastness to domestic and commercial laundering, third edition,include technical corrigendum 1 ISO 015-C06: 1994/ Cor. 1:2002 (E) and technical corrigendum 2 ISO 015-C06: 1994/ Cor. 2:2002 (E)." Badan Standarisasi Nasional, Indonesia, 2010.

[18] "MSDS NK_GUARD S-22." Indonesia Nicca Chemicals Ltd., 2018.

[19] C. Hepburn, *Polyurethane elastomers*, Second. England: Elsevier Applied Science, 1992.

[20] M. Z. Seyedin, J. M. Razal, P. C. Innis, and G. G. Wallace, "Strain-Responsive Polyurethane/PEDOT:PSS Elastomeric Composite Fibers with High Electrical Conductivity," *Adv. Funct. Mater.*, vol. 24, pp. 2957–2966, 2014.

[21] Y. Li, R. Tanigawa, and H. Okuzaki, "Soft and flexible PEDOT/PSS films for applications to soft actuators," *Smart Mater. Struct.*, vol. 23, pp. 074010-1–8, 2014.

[22] X. Wu, Y. Han, X. Zhang, and C. Lu, "Highly Sensitive, Stretchable, and Wash-Durable Strain Sensor Based on Ultrathin Conductive Layer@Polyurethane Yarn for Tiny Motion Monitoring," *Appl. Mater. Interfaces*, vol. 8, pp. 9936–9945, 2016.

Appendix 5.1. Charge-discharge profiles of all types of device before and after washings

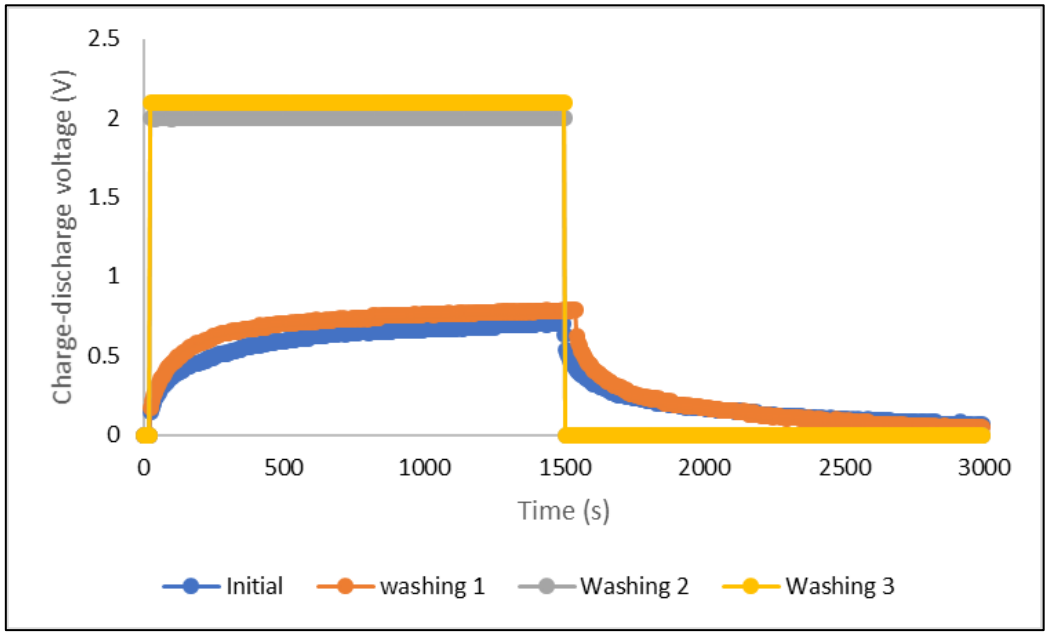

Figure A.5.1. Charge-discharge profile of the device TESD 1.2 THL (non-covered) - before and after washings

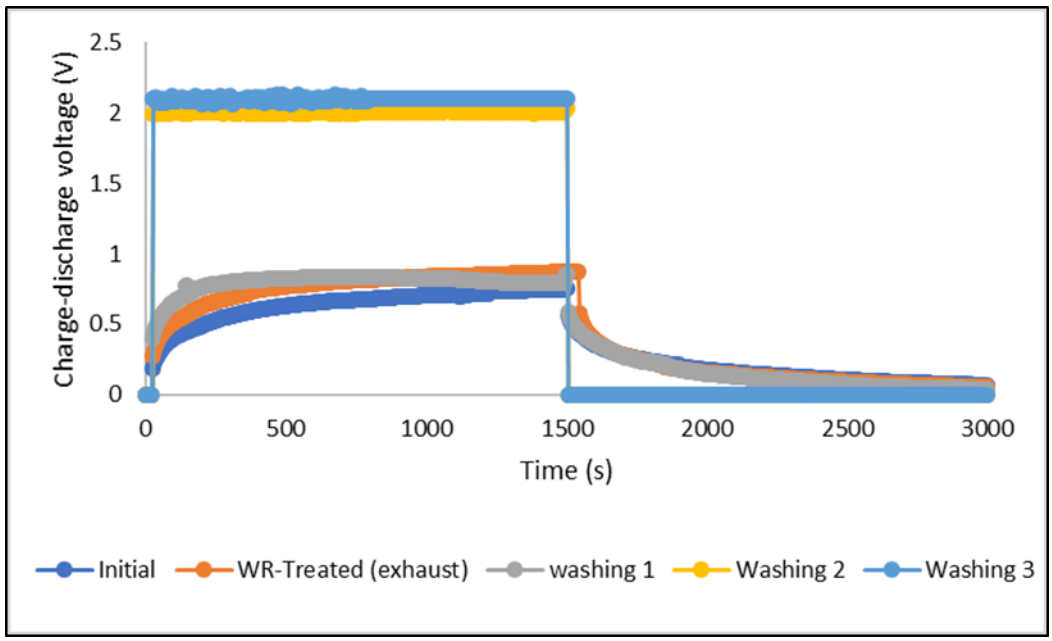

Figure A.5.2. Charge-discharge profile of the device TESD 1.2 THL treated with water-repellent agent (exhaust) - before and after washings

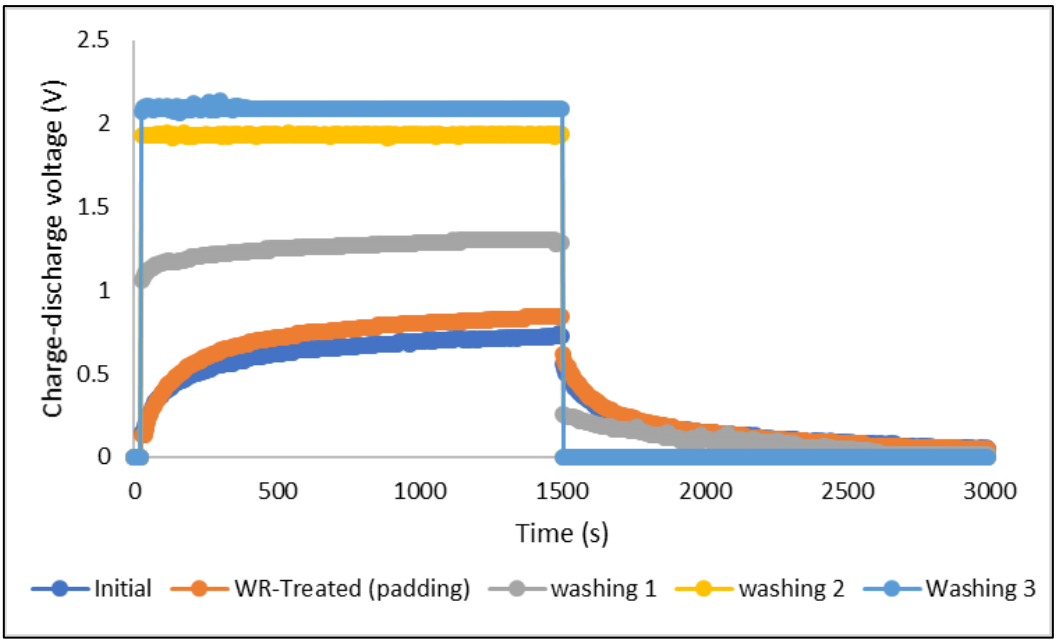

Figure A.5.3. Charge-discharge profile of the device TESD 1.2 THL treated with water-repellent agent (padding) - before and after washings

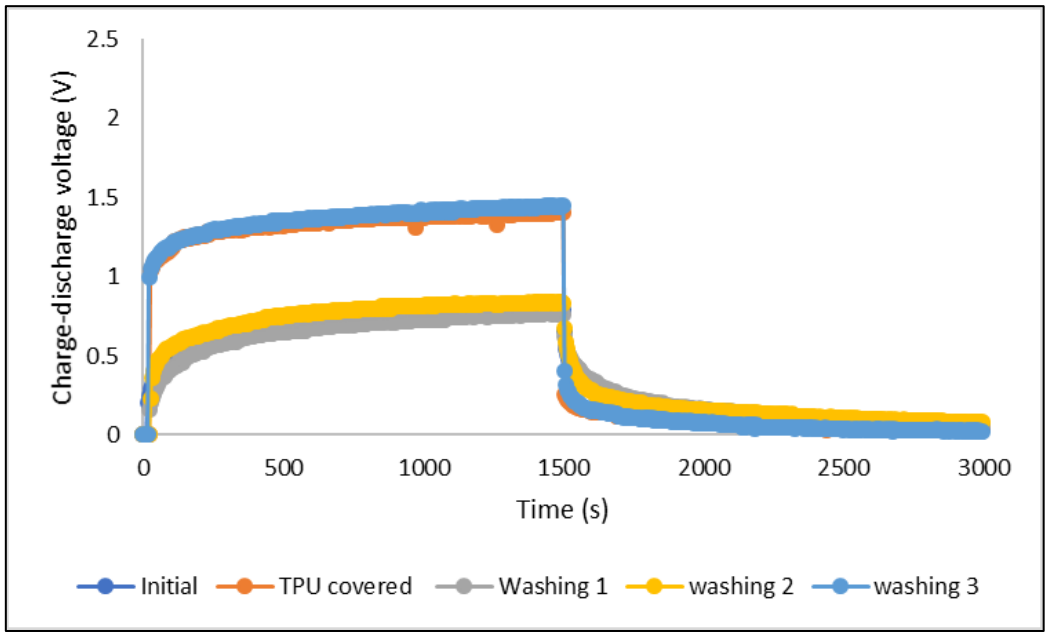

Figure A.5.4. Charge-discharge profile of the device TESD 1.2 THL covered by TPU (thermoplastic polyurethane) - before and after washings

6

Seamlessly-Integrated Device

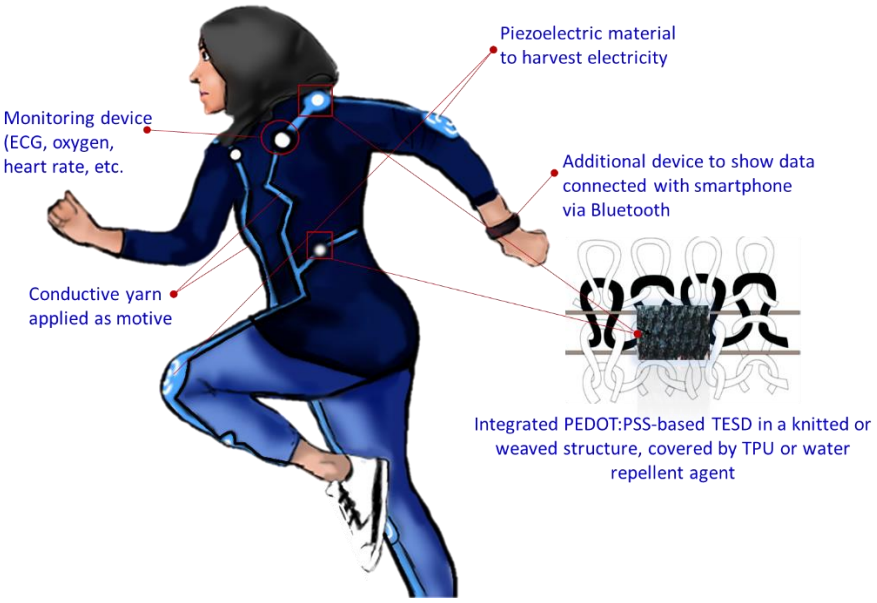

"Conceptual design of integrated textile energy storage device (TESD) and embedded other electronic devices in a sportswear/activewear. Image courtesy of Jagat Ranggatama, Textile Chemistry student at Politeknik STTT Bandung."

This chapter elaborates our conceptual design for the integration of our textile energy storage device (TESD) in clothing and reports the preliminary works that have been done toward its realisation. It also serves as point of departure for our planned further research in the development of electronic-based smart garment. In this chapter, approaches and procedure for the integration, which started with the simplest form of insertion technique in knitting and weaving, is explained and discussed with an intention to obtain an understanding about the challenges and prospects for improvement. This is still in an early stage but we have obtained promising results that confirms our approach and direction. The whole concept of the work, which is aimed for seamless integration of TESD for smart textiles applications, is illustrated by the image above.

6.1. Introduction

An extensive discussion has been provided in the previous chapters to show how the last design of our textile energy storage device is taking shape toward better compatibility with clothing, particularly being more flexible and lighter in weight. The PEDOT:PSS coating is now also distributed more uniformly in a confined cell area. Two of the main challenges in our endeavor to develop a facile and yet functionally powerful textile energy storage device for smart textiles applications are understanding the working principles and mechanisms of charge storage for future improvement of its capacitive behavior and secondly looking at strategies and approaches for seamless integration. As discussed in previous chapters, the design and configuration of our energy storage device, which is a uniquely horizontal sandwich of two threads of stainless-steel electrode yarns and PEDOT:PSS solid electrolyte in between has been proven to be functional and effective. With the present design, however, the device needs to be attached or embedded like a patch in the existing fabric or clothing. While it offers flexibility in the fabrication of smart textile products, a seamless and full integration of the device is believed to produce a more robust end product. Given some more systematic exploration and research we believe the device will integrate smoothly with clothing. This chapter presents preliminary results of an attempt to fully integrate the device in the fabric structure through knitting and weaving techniques.

Knitting and weaving are two of well-established techniques of textile fabric manufacturing by mechanically manipulating yarn into fabric through interlooping and interweaving respectively [1]. The techniques can be performed either by hand or machine operations. As shown in **Figure 6.1**, the basic structure of interweaving consists of interconnection of two straight threads in warp and weft (XY) directions, while in interlooping structure, a series of loops are

interconnected with each other in any XYZ directions [2]. By these two techniques, especially knitting, the textile wearable device can be made fully shape-adaptive, flexible, and stretchable to withstand any possible mechanical deformations like stretching, bending, and twisting. It is important to note that highly stretchable woven fabric is difficult to achieve through weaving process because of the straight horizontal and vertical interlacing yarns in the fabric structure which in turn limits its practical application. Some prototypes and products have been reported to use these two fabrication methods among others to construct flexible electronic textiles such as fiber supercapacitors, artificial muscles, sensors and actuators [2]–[9].

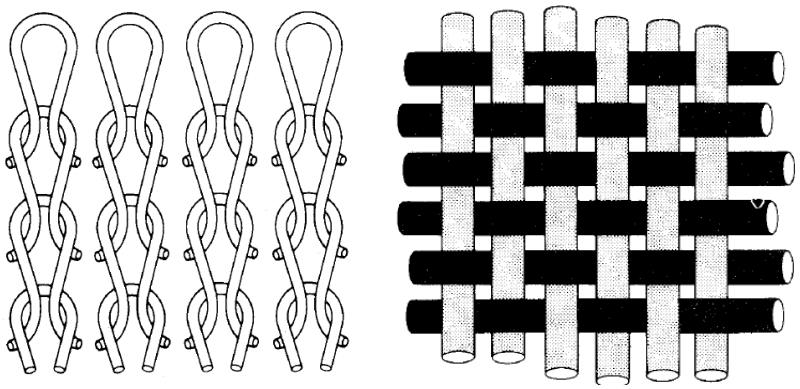

Figure 6.1. Basic structure of interlooping (left) and interweaving (right) [1]

For our textile energy storage device, it is the stainless-steel conductive yarns that can possibly be fully integrated in the knitted or woven textile fabric. The main purpose of this early stage is to prove that by inserting the conductive yarns, the interfacial interactions between PEDOT:PSS layer and the stainless-steel conductive yarns, which are required for the cell to have capacitive behavior, are still attainable and are still intact during the process of insertion. This chapter serves to provide early confirmation on seamless integration by knitting and weaving, and build the foundation for prospective continuations for this project.

6.2 Insertion *via* Knitting

With this approach, the stainless-steel conductive yarns were inserted to the knitted structure made of acrylic yarns Nm 32/2 using the computerized knitting machine Stoll 7.2 G (Stoll GmbH, Reutlingen, Germany), which was automatically connected to the software "Stoll M1 Plus", produced by the same company, to construct and set the design. One of benefits of assembling the textile energy storage device by knitting method was that with the appropriate set-up in the computerized knitting machine, less yarn was needed and fabric with various geometries as required could be constructed [7]. Technically, the insertion was carried out continuously from right side in, left side out, left side in, right side out, and so on. The knitting fabric constructed was the simplest 1×1 rib type, with interloop structure and insertion results as presented in **Figure 6.2**. The reason of selecting this rib type is that because the resulting knitted fabric has two faces, where the technical face of plain knitted fabric is appeared on both sides. When inserted into this type of structure, the conductive yarns stayed in the middle of the fabric. They are not appeared on the fabric surface, except when the fabric is stretched, as shown by the image in **Figure 6.2**.

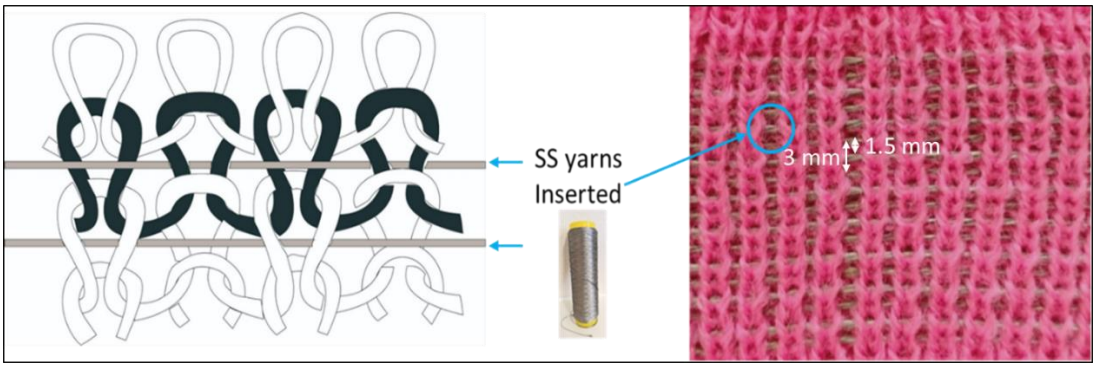

Figure 6.2. Inserted stainless steel electrode yarns in the structure of knitted fabric

One of the ideas in regard with the design and circuitry of the device in the garment is to have a number of individual devices being connected in series to

provide more capacity for charge storage and thus higher power. However, to avoid complications in the testing procedure in this early work, the device was prepared as a single device in this study. An example of the single device is shown in **Figure 6.3**. PEDOT:PSS solid electrolyte was applied to the fabric in particular area by the modified drop-coating method as described in Chapter 3. Seven drops were applied with drying at 90-100 ºC for 10 minutes between each drop. From visual observation during the process, almost all dropped PEDOT:PSS dispersion were neatly contained in the previously designated area by the bulky structure of the knitted fabric and the stainless-steel yarns.

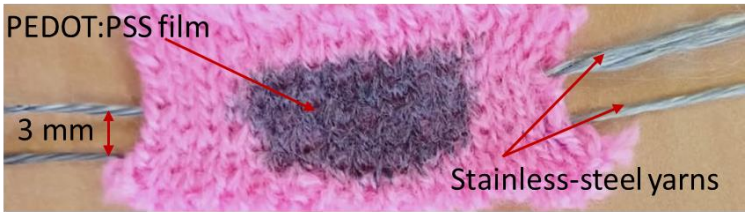

Figure 6.3. Example of the TESD in a knitted structure (longer distance = 3 mm)

Devices with different distance between the two electrodes were prepared. Here, each device was named as "closer" and "longer" electrode distances. Measured manually, it was found that device with closer and longer distances respectively had 1.5 mm and 3 mm spaces between electrodes. Technically, the former had one row of interloops between the two conductive yarns, while the latter had two rows of interloops in between. Each device was made in 2 duplicates and each was tested by Arduino Uno. The charge-discharge profiles of each type of device presented in **Figure 6.4** were taken from the average value of charge-discharge voltages of the two devices from each type.

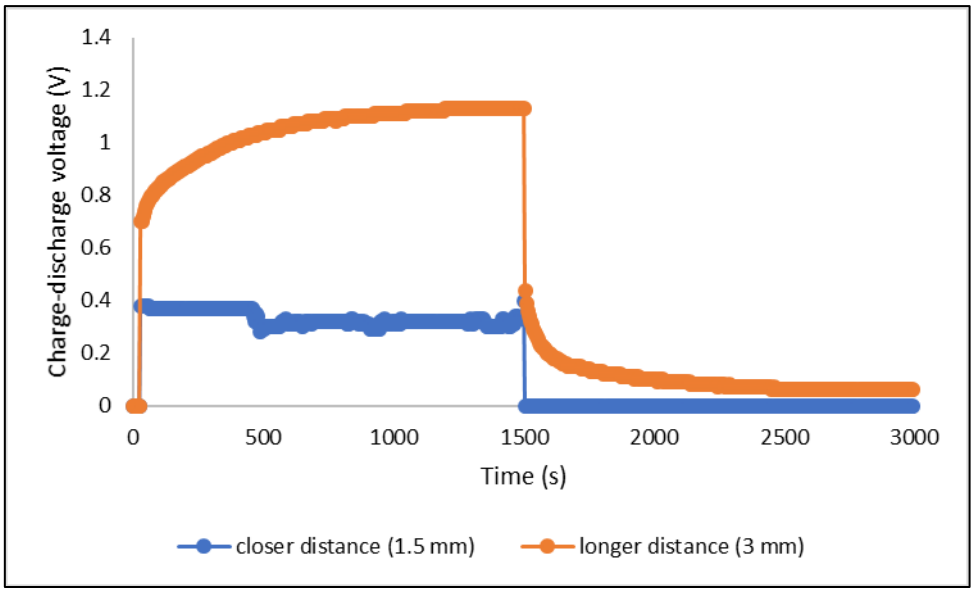

Figure 6.4. Charge-discharge profile of TESD in a knitted fabric

As can be seen in **Figure 6.4**, the devices with longer distance has a better charge-discharge profile than those with closer distance between electrodes, which do not show any capacitive behavior because the curve immediately dropped into zero once the discharge phase was started. The charge voltages of devices with smaller distance was also much lower. This is contrary to the previous findings from our original device on woven polyester fabric, which showed stronger capacitive behavior with smaller distance between pair of electrodes. As this is still in the very early stage of our investigation, it is premature to judge the results. It might be related to the porous structure of the knitted fabric or it could also be due to micro cracks in the PEDOT:PSS film. It is also plausible there might be interaction with the acrylic yarns that made up the knitted fabric. The work should be repeated with more various parameters and completed by other tests and analysis, including evaluation of the knitted fabric characteristics. Nevertheless, the results in general show that assembling our TESD with bottom-up approach into a knitted structure is doable even using the simplest technique of insertion. The results are promising and lead to more possibilities for further exploration and elaboration for fully and

seamlessly integration of the device into clothing in many different fields of applications including sports and medical and even for aesthetical purposes like in fashion. One of the most important observations is that the capacitive performance of our TESD in the knit structure did not show any significant changes after being stretched confirming its flexibility during actual use in clothing.

6.3 Insertion *via* Weaving

The weaving process was performed by using the laboratory scale weaving machine. Cotton and acrylic yarns were used as warp and weft yarns respectively, and the stainless-steel conductive yarn was inserted between the acrylic yarn in the weft direction. All were constructed in a plain weave structure as shown in **Figure 6.5**. It must be noted here that the distance between electrodes was determined by the number of yarns between the inserted pair of electrode yarns. For example, for the closer distance of electrodes, one thread of acrylic yarn was set between the two electrodes, while for device with longer distance, two threads of acrylic were applied in between, each giving result to 3 mm and 6 mm distance between the electrodes respectively.

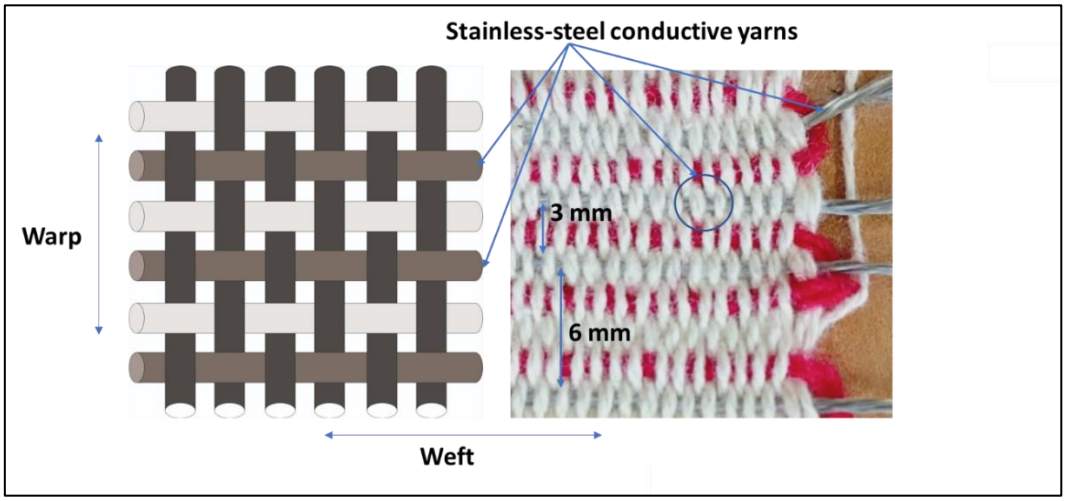

Figure 6.5. Inserted stainless steel electrode yarns in the structure of woven fabric

The formation of cell area followed the same procedure as described for knitted fabric. PEDOT:PSS was drop-coated into the fabric in a particular area by the modified drop-coating method as described in Chapter 3. Seven drops were applied while the PEDOT:PSS dispersion was kept in the oven during the drop-coating process (the solution gradually thickened with time). Drying at 90-100 °C for 10 minutes between each drop was also employed. Example of the TESD in a woven structure is presented in **Figure 6.6**. Here, two devices were also made and measured for each type.

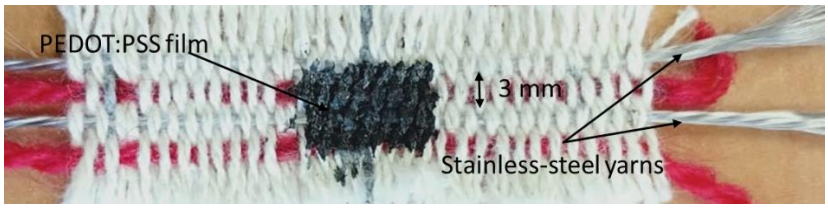

Figure 6.6. Example of the TESD in a woven structure (shorter distance = 3 mm)

As shown by the graphs in **Figure 6.7**, device with closer distance between electrodes (3 mm) has a better charge-discharge profile than the device with longer electrode distance (6 mm). Compared to the profile of device in the knitted fabric, the woven fabric showed less capacitive behavior, especially that the discharge voltages are around two times lower than the knitted fabric with the same distance (3 mm). Likewise, more works, tests and evaluations related to the woven fabric properties are also required to confirm these results.

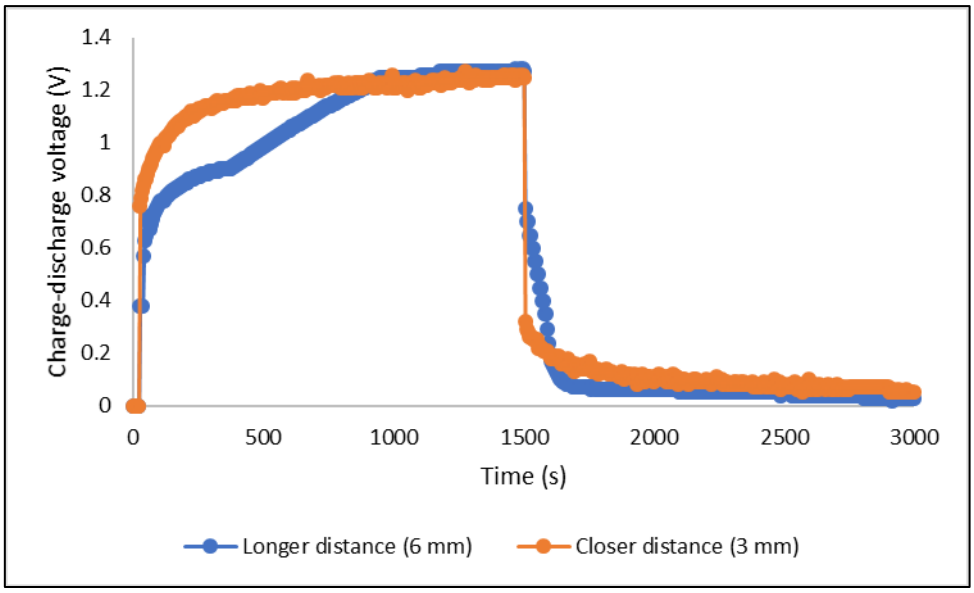

Figure 6.7. Charge-discharge profile of TESD in a woven fabric

6.4 Summary

Integration of PEDOT:PSS TESD into textile structure with bottom-up approach by insertion *via* knitting and weaving has been performed and was successful. Generally, except for device with shorter distance in the knitted fabric, the integrated devices performed well and did not show any significant changes that can be attributed to the process of integration. The strategy and direction for further work is confirmed. Although it is still preliminary, it is noteworthy that, at the same distance between electrodes, device in knitted structure showed higher discharge profiles than device in woven structure. More systematic tests and characterizations are still needed for any types of device configuration.

Bibliography

[1] D. J. Spencer, *Knitting Technology - A comprehensive handbook and practical guide*, 3rd ed. Cambridge, England: Woodhead Publishing, 2001.

[2] K. Jost *et al.*, "Knitted and screen printed carbon-fiber supercapacitors for applications in wearable electronics," *Energy Environ. Sci.*, 2013.

[3] S. Shi *et al.*, "Flexible supercapacitors," *Particuology*, vol. 11, pp. 371–377.

[4] L. Li and W. S. Man, "A Resistive Network Model for Conductive Knitting Stitches," *Text. Res. J.*, vol. 80, no. 10, pp. 935–947, 2010.

[5] K. Jost, G. Dion, and Y. Gogotsi, "Textile energy storage in perspective," *J Mater Chem A*, vol. 2, no. 28, p. 10776, 2014.

[6] C. A. Winterhalter *et al.*, "Development of Electronic Textiles to Support Networks, Communications, and Medical Applications in Future U.S> Military Protective Clothing Systems," *IEEE Trans. Inf. Technol. Med.*, vol. 9, no. 3, Sep. 2005.

[7] K. Jost *et al.*, "Natural Fiber Welded Electrode Yarns for Knitted Textile SUpercapacitors," *Adv. Energy Mater.*, vol. 5, no. 1401286, pp. 1–8, 2015.

[8] L. Li and W. S. Man, "A NOvel Design Method for an Intelligent Clothing Based on GArment Design and Knitting Technology," *Text. Res. J.*, vol. 79, no. 18, pp. 1670–1679, 2009.

[9] A. Maziz, A. Concas, A. Khaldi, J. Stalhand, N.-K. Persson, and E. W. H. Jager, "Knitting and weaving artificial muscles," *Sci. Adv.*, vol. 3, no. 1, e1600327, Jan. 2017.

7

Conclusion and outlook

"The science of today is the technology of tomorrow"

– Edward Teller -

This chapter wraps up the whole work presented in this thesis. Starting with a comprehensive review about the recent progress on development of textile-based energy storage device using PEDOT:PSS and other electroactive materials, the study was focused mainly on two objectives: (1) improvement of fabrication techniques of the device to obtain a better performance and visual appearance; and (2) better understanding of the mechanism to further improve the capacitive behavior of the developed device. Additionally, washability study of the device was also presented in this thesis. Finally, initial result of the attempt to seamlessly-integrate the device in textile fabric by insertion *via* knitting and weaving was also included in the last part of this thesis.

7.1. Conclusion

A systematic work on the development of PEDOT:PSS-based textile energy storage device (TESD) has been successfully done in this study. In principle, the device was fabricated directly on existing textile substrates, i.e. cotton/polyester fabrics, and it consisted of stainless-steel electroconductive yarn as electrode and PEDOT:PSS film which functioned as a solid polyelectrolyte complex. In its early stage of development, the device was made on a three-layered textile fabric with three threads of stainless-steel conductive yarns stitched on it. The device was named TESD 3.3. This device showed promising performance as it could store charges after particular time of charging process. However, the PEDOT:PSS dispersion diffused through the porous structure of textile fabrics so that the cell area was not well defined and there was concern that it might affect the performance of the device, beside the fact that it did not look visually good either.

Our very first attempt to improve the design and performance of the device began with the study on the effects of middle conductive yarn in the original design and configuration of our device. The results from this study showed that two threads of electrode yarn was a more ideal configuration for our TESD and gave us an important clue to the mechanism of ion movement that might contribute to the working of the device. From the measurements of devices having two and three conductive yarns carried out at three different voltages (1.5 V, 3.0 V, and 4.5 V), we found that the presence of the middle yarn had an effect to the discharge profile of the device: it consistently lowered the accumulated discharge voltages in all measurements. That led us the design and fabrication of TESD 3.2.

One of important findings during the study was the shot noise phenomenon observed from devices with asymmetrical electrodes (stainless-steel/Ag-PBO) and thin layer PEDOT:PSS film. Such phenomenon was not observed from the device with the same configuration but with a thicker PEDOT:PSS film. The assumption

of ionic shot noise was confirmed by a qualitative model of autocorrelation function. The noise was suggested to be due to a series of interrupted movements or hopping of Ag^+ ions across the bulk of polymer film from Ag/PBO yarn to stainless steel yarn electrode. This finding validated the modified drop-coating method to obtain a better coverage of the electrode yarns by the PEDOT:PSS polymer film. With this modified method, the polymer dispersion was put in constant heating at 60-70 ^oC during the drop-coating process to get a stepwise formation of polymer aggregate which allows more interactions between the polymer molecules and results in a good polymer coverage on the cell surface. In this way, the possibility of obtaining a noisy device that cannot function as an effective energy storage device can be prevented due to a better connectivity and conduction path for charges and ions to travel through the polymer. This strategy resulted in device called TESD 3.3 THL.

For technical reasons and aesthetical considerations, the distribution of PEDOT:PSS dispersion being coated in the cell area must be well-controlled so that it is well-confined in the designated area and does not penetrate through the porous structure of the fabric. More concentrated and well-defined distribution of coating was expected to give better performance due to higher mass loading per unit length of electrodes and better visual appearance. In order to realize it, the fabric was pretreated with water repellent chemical to prevent the diffusion/penetration of polymer dispersion through the fabric. The most important improvement we have from this new approach of fabrication technique was that we are able to fabricate the device on a single layer of fabric giving result to a lighter, thinner and more flexible device. More importantly, the new fabrication technique with more confined distribution of the PEDOT:PSS within the cell area also resulted in better performance of the device: up to 20% higher level of discharge voltage after it reached the constant voltage (between 1000-2000 seconds).

Understanding the working principle and mechanism of the device can lead to a better strategy in which improvements can be made more systematically in a structured manner. For this, electrochemical impedance analysis has been employed as one of techniques selected to study the mechanism of our developed textile energy storage device. The first important information from this analysis was obtained from the cyclic voltammogram of PEDOT:PSS in the form of electrochemical solution and in its solid state on the glass and fabric surfaces. Here, the occurrence of redox reactions was evidenced, which substantiated the characteristics of pseudocapacitance behavior by the cell. This also confirmed the role of PEDOT:PSS as a polyelectrolyte for this electrochemical system. The ionic behavior in the form of solution using standard electrodes showed stronger oxidation-reduction phenomenon.

For the case of an energy storage device, capacitive behavior is an important property. The Nyquist and bode plots of the devices proved their conductive and capacitive behavior. Our PEDOT-PSS-based devices also exhibited both electronic and ionic character which was mostly due to the complicated interaction in the interfacial region between the PEDOT:PSS polymer and the stainless-steel electrode. The EIS results indicated the presence of ionization and migration of the electrolyte PSS units, leaving the PEDOT units, which thus increase its solid-state conductivity. The Warburg element also confirmed the process related to the electrode-electrolyte interface which results in an increase in conductivity.

In general, it was also confirmed that the distance between electrodes affect the conductivity and capacitive behavior of the PEDOT:PSS. The distribution of PEDOT:PSS polymer film in the solid state also affected its capacitive behavior. The device on a glass surface always exhibited higher capacitive behavior than the device on a fabric surface, which presents a unique challenge that needs to be addressed in later research. Two different equivalent circuit models were found by

simulating the model with the experimental results: (QR)(QR)(QR) for the uncharged samples and (QR)(QR)(Q(RW)) for the charged samples. From the EIS analysis, we reconfirmed that coating thickness also affected the conductivity. During the course of measurements we found that samples prepared with thinner PEDOT:PSS coating showed no apparent peak on cyclic voltammetry measurements and neither any accurate EIS results.

Further study on the working principle and mechanism of the device was carried out by analyzing the characteristics of the device charge-discharge performance. For this purpose, energy storage devices using three different commercial brands of PEDOT:PSS, Clevios P-VP-AI-4083, Ossila AI 4083, and Orgacon ICP 1050, as the solid polyelectrolyte, were assembled especially to study the effect of ratio of PEDOT to PSS towards their charge-discharge performances. As electrodes, we used stainless steel (SS) and silver-coated polybenzoxazole (Ag-PBO) yarns, with various combinations: symmetrical SS/SS and Ag-PBO/Ag-PBO as well as asymmetrical SS/Ag-PBO. NMR spectra of each type of PEDOT:PSS showed that the Clevios and Ossila are almost identical, as also evidenced by their similar molar and weight ratio, i.e. 1.00:5.26 and 1.00:6.92 respectively. Utilization of these two types of PEDOT:PSS gave good charge-discharge profiles of the devices. Otherwise, devices with the Orgacon showed no charge-discharge profiles. Its PEDOT:PSS molar and weight ratios are 1.00:4.65 and 1.00:6.11 respectively. The lower proportion of PSS leads to the higher conductivity of the polymer. From the results, it can be concluded that for our specific developed energy storage devices, PEDOT:PSS with lower conductivity is more suitable. The ratio significantly affected the conductivity, apart from the other factors like the solvents and/or additives added, secondary doping, etc. Further investigation is needed to see if increasing the ratio any further would lead to more benefits. It can also be concluded that the resistance of electrode – PEDOT must be low, which is not the case in the case where Ag-PBO was used as the positive electrode. In addition, the

lower sulphur content seems to improve the results as shown by Ossila A1 4080 that has the best discharge properties. **Figure 7.1** below presents the illustrative summary of the possible mechanisms of the device with the function of PEDOT:PSS as electrolyte.

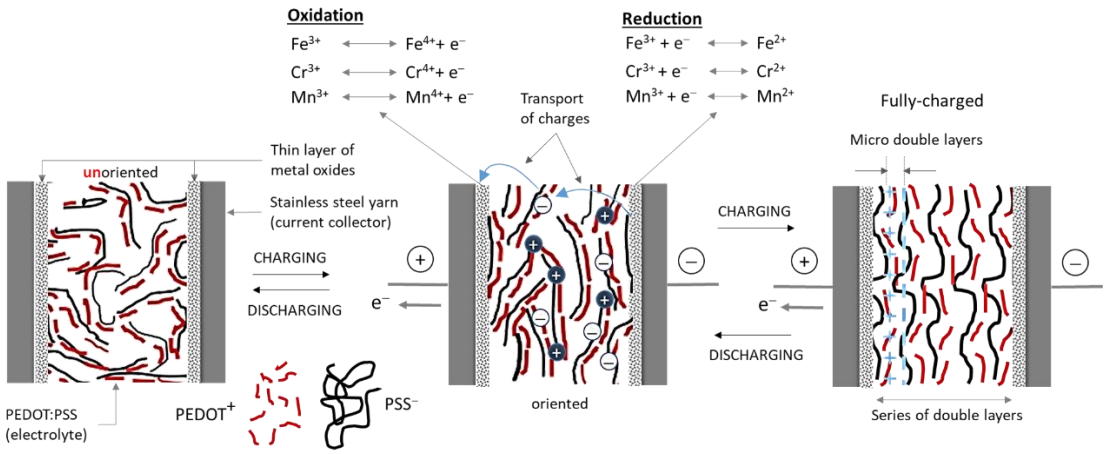

Figure 7.1. Illustrative summary of the possible mechanisms of the device (PEDOT:PSS as electrolyte)

As washability has been one of the long-standing challenges for the development of smart textiles, particularly wearables and smart clothing, we explored some studies on it. In this initial stage, the main idea was to protect the cell which contained a thick layer of PEDOT:PSS film by applying two approaches: (1) covering the cell surface with a fluorocarbon-based water-repellent agent which was applied by two different methods, i.e. impregnation by padding and exhaustion; (2) masking the cell surface with a layer of thermoplastic polyurethane (TPU). Three stages of washing were performed to each device. The results showed that TPU-covered devices exhibited better performance, where the capacitive behavior of the cell remained after two times of washing 3 (based on the SNI-ISO C06: 2010). Also, there were no significant changes observed in the morphology of the TPU-covered device after the sequence of washings. The results are promising for further study as well as for further development of a more applicable textile energy storage device.

Seamless integration of the TESD in the structure of textile fabric, which was meant to be the next stage for further research, has been started in this study. It was really still an initial part with few results, but quite promising. By insertion technique, stainless-steel conductive yarns could be fully-integrated in the knitted and woven fabric structure without changing its conductivity. The conductive yarns inserted functioned as electrode in this system. Likewise, PEDOT:PSS was drop-coated onto the fabric by the same method applied before. Capacitive behavior was shown by the integrated device prepared with both methods (knitting and weaving). At the same distance between electrodes, device in knitted structure showed higher discharge profiles than device in woven structure. More systematic tests and characterizations are still needed for any types of device configuration, together with further methods to increase its washability.

Overall, the present work has resulted in significant results and findings, particularly in the understanding of device electrical behavior and mechanisms. Additionally, improvements have also been made in the fabrication of device leading to a better design toward seamless integration with textiles. In regard to the latter, the textile-based energy storage device that came from this study is superior compared to the existing textile devices. Despite the accomplishments, it must be noted, however, that the capacitance of the device is two or three orders of magnitude lower than that of the other existing devices shown in **Table 2.2** in Chapter 2. Although formal assessment of Technology Readiness Level (TRL) has not been done for our device, it can be suggested that the present work has significant contribution in moving the device up from TRL 3 to TRL 4 with a potential of an accelerated progress toward TRL 7-8 when integration by weaving and knitting can be realized. Indeed, improvement of performance (capacitance)

and realization of seamless integration hence possibility to make a leaping into higher TRL will be the focus of our work.

7.2. Outlook

Apart from the promising results obtained in the present study, many more spaces to explore in further study are still available and emerged. More efforts are still required to significantly improve the performance of the device, by either continuing further with the present approach or taking a new direction but still related approaches. Before going into more detail about the recommended further studies, it is interesting to go back to the mind-map diagram presented in Chapter 1 which also mention some prospective future works (highlighted in green blocks) that are still missing from the present study:

(1) To improve the device performance, it is suggested to do some experiments on PEDOT:PSS modification such as making PEDOT:PSS in various different ratio, applying dopants which possess permittivity instead of PSS, and applying secondary doping on the available PEDOT:PSS;

(2) In the part of study on mechanism, it is interesting to investigate the possibility of self-discharge in the device by modeling and simulation; and

(3) To seamlessly integrate the conductive electrode yarns into fabric, it is worth to include embroidery technique in addition to the knitting and weaving. In order to create a more permanent coating of PEDOT:PSS and the stainless-steel electrode yarn, applying the PEDOT:PSS into the stainless steel electrode yarn *via* a dyeing method is another interesting option.

7.2.1 Further Improvement of the Device Performance

Improvement in design, configuration, and performance has been achieved

by the transformation from device with basic design called TESD 3.3 up to the latest called TESD 1.2 THL. **Figure 3.19** compares the charge-discharge profiles of TESD 1.2 THL *vs*. TESD 3.2 THL. It can be seen that making the well-confined PEDOT:PSS film within the cell area could increase the stored charges only 20% during the discharging stage. Additionally, from the study of PEDOT:PSS ratio, it is also known that PEDOT:PSS with lower conductivity, hence more PSS portion in the mixture, showed better performance. Therefore, it would be interesting to investigate further if increasing the ratio would lead to further benefits. It is possible to start with the other commercially available PEDOT:PSS with different conductivity or resistivity. However, making the PEDOT:PSS dispersion with customized ratio is more recommended, as this would allow to obtain the most optimum ratio at which the best performance can be achieved.

Furthermore, modifying the resistivity of PEDOT:PSS can also be achieved by replacing the dopant using other chemicals instead of PSS. Selection of the materials which will result in polymerization product of EDOT with the most appropriate conductivity will give a more comprehensive idea to improve the performance of the developed device. As reference, some possible counter-ions that can be used for electrochemical polymerization of EDOT are as follow: ClO_4^-, BF_4^-, PF_6^-, NO_3^-, SO_4^-, Tos^-, $N(SO_2CF_3)_2^-$, $N(SO_2C_2F_5)_2^-$, $N(SO_2C_3F_7)_2^-$, $N(SO_2C_4F_9)_2^-$, $CF_3SO_3^-$, $C_4F_9SO_3^-$, and $C_8F_{17}SO_3^-$ [1].

Additionally, as mentioned in the preceding chapters and sections, PEDOT:PSS was meant to be and used in this study as solid electrolyte while most of other similar studies in this area of research used this polymer as an electrode material. One of the most interesting features of our device is its simplicity and straightforward design in which the conductive polymer was functioned to serve as both an electrolyte as well as active material for the device. However, from the very beginning we have been aware that its capacitance is notably low compared

to existing similar devices from work of others (**Table 2.2**). Based on our new findings and understanding about the mechanisms of charge storage in our device we believe that addition of a layer of activated carbon, for example, as an active material on the stainless steel conductive yarn, as illustrated in **Figure 7.2**, would augment the redox reactions at the electrodes giving rise to an increased charge storage and transport in the system resulting in a larger capacitance. One of the most obvious challenges faced by our device is that it undergoes a very fast self discharge. It is hypothesized that the use of active material like activated carbon or CNT might slow the process of self discharge.

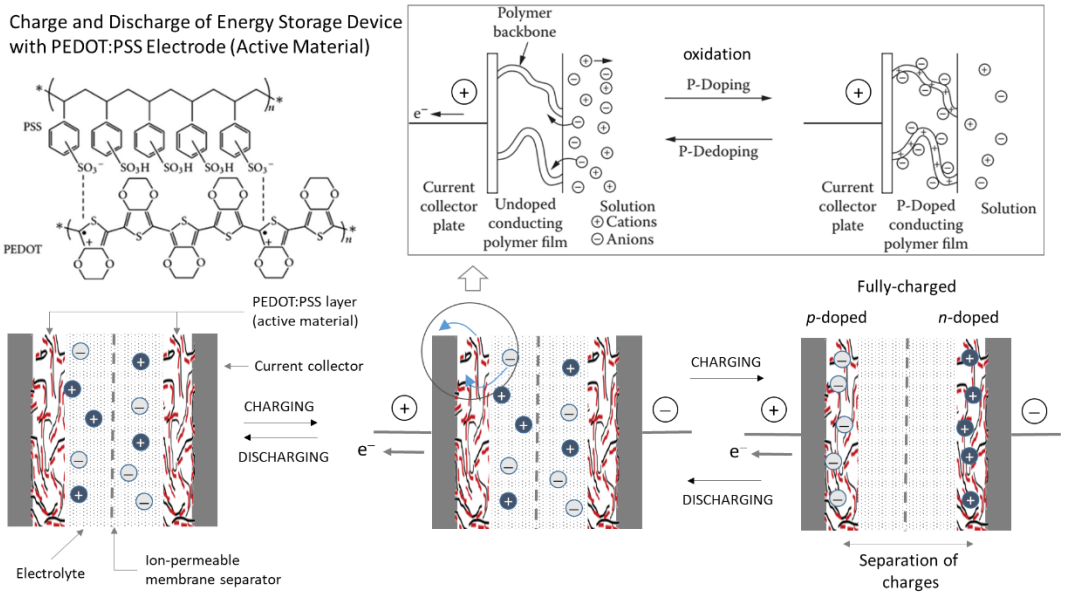

Figure 7.2. Illustration of possible mechanisms of PEDOT:PSS as electrode/active material

7.2.2 Further Study on Mechanism

To further study on the mechanism, it is interesting to continue to characterize TESD 1.2 THL with the electrochemical impedance analysis to prove that with the more confined distribution of PEDOT:PSS, the capacitive behavior of the device can be better. To study the device behavior of the device made of

PEDOT:PSS with customized ratio will be another important and interesting part in the future.

Further in depth study of mechanism, modeling and simulation of the developed device behavior will be one of the most interesting parts to explore in the future. The modeling can include the general mathematical model for charge-discharge characteristics of our device [2], [3]. Study on modeling of the possibility of "self-discharge" [4], [5] of the device is also appealing, although during our experiments in the present study, the self-discharge phenomenon has not been observed so far.

7.2.3 Further Study on the Washability and Seamlessly Integration

On the subject of the washability study, although it was found that covering the cell with TPU film showed better fastness to washing, it is still worth to explore the possibility of the use of water repellent agents or other kinds of hydrophobic-making substances to protect the PEDOT:PSS coating. This will be beneficial to be applied in the integrated system as we did by the insertion of stainless-steel yarns via knitting or weaving. With those techniques, the PEDOT:PSS was not only distributed on the one surface, but also spread in the three dimensional structure of the fabric. In addition to the showcased techniques, embroidering the stainless-steel conductive yarns is another interesting alternative to integrate them in the fabric. It should be noted here that tests of mechanical and electrical properties of the conductive yarn in the integrated system should be carried out.

It was mentioned earlier that interaction between the interfaces of stainless-steel electrode yarn and the PEDOT:PSS film played important role in creating the device capacitive behaviour. To make a more permanent coating of PEDOT:PSS on the stainless-steel electrode yarn, it is interesting to use the dyeing method which allow a stronger bonding between PEDOT:PSS and the stainless steel yarn. From literature [6], dyeing PEDOT:PSS into silk yarn resulted in a machine-washable

electroconductive silk yarn which can be used for any applications of electronic textiles. This showed that it is possible and doable to coat the PEDOT:PSS by the dyeing technique, although some modifications will be needed because stainless steel yarn has no similar characteristics to silk yarn, especially for its affinity to the PEDOT:PSS dispersion.

For the analysis of the washability, it is also important to support the results with cyclic voltammetry to obtain a better visibility of the results. Further, XPS (X-ray photoelectron spectroscopy) analysis is also suggested to obtain a better understanding about the change in chemical surface properties of the material after the washing. For the washing procedure, it is encouraged to do the standardized ISO 6330 tests of the domestic laundry and drying to get a closer applicability with a real daily washing process. It is also suggested to attach the device in the real clothing.

Bibliography

[1] A. Elschner, S. Kirchmeyer, W. Lovenich, U. Merker, and K. Reuter, *PEDOT: Principles and Application of an Intrinsically Conductive Polymer*. USA: CRC Press, 2011.

[2] S. Allu, B. V. Asoka, W. A. Shelton, B. Philip, and S. Pannala, "A generalized multi-dimensional mathematical model for charging and discharging processes in a supercapacitor," *J. Power Sources*, vol. 256, pp. 369–382, 2014.

[3] S. Odhiambo *et al.*, "The electric energy stored in PEDOT:PSS capacitors integrated on textile," *Int. J. Cloth. Sci. Technol.*, vol. 30, no. 6, pp. 808–816, 2018.

[4] H. A. Andreas, "Self-Discharge in Electrochemical Capacitors: A Perspective Article," *J. Electrochem. Soc.*, vol. 162, no. 5, pp. A5047–A5053, 2015.

[5] Y. Diab, P. Venet, H. Gualous, and G. Rojat, "Self-Discharge Characterization and Modeling of Electrochemical Capacitor Used for Power Electronics Applications," *IEEE Trans. POWER Electron.*, vol. 24, no. 2, Feb. 2009.

[6] J. D. Ryan, D. A. Mengistie, R. Gabrielsson, A. Lund, and C. Müller, "Machine-Washable PEDOT:PSS Dyed Silk Yarns for Electronic Textiles," *ACS Appl Mater Interfaces*, vol. 9, p. 9045−9050, 2017.

Appendix:
Statistical analysis

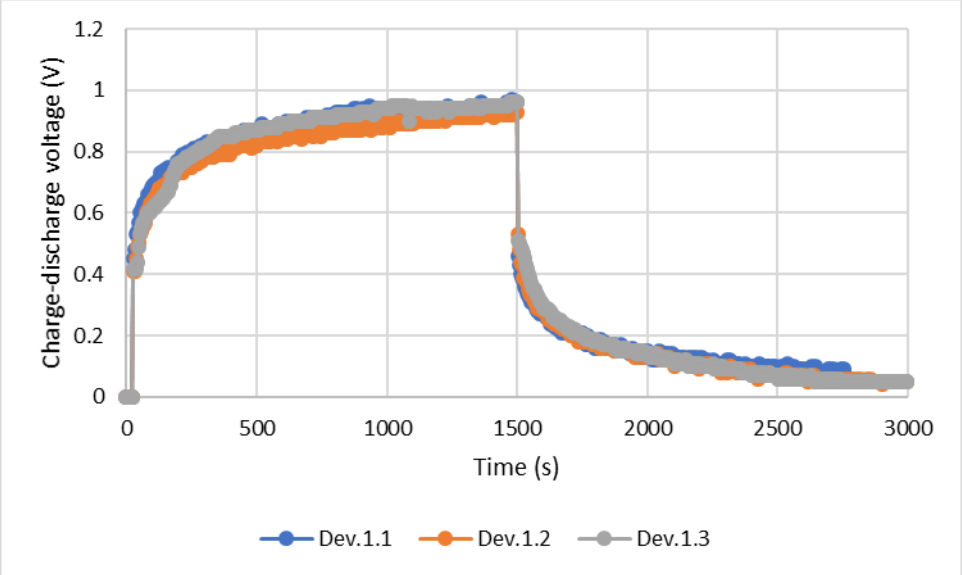

Repeatable measurements of one device

A statistical analysis has been carried out to test the validity and reliability of the data resulted from the measurement. For every measurement, at least two identical samples were prepared to ensure reproducibility of the device, and at least three measurements done with every device to ensure the consistency and repeatability of the measurement. Here, two identical samples of device TESD 1.2 THL were taken as representation of the measurements taken along this study. T-test was also performed to compare the two identical devices. All data were processed with SPSS V. 17.0. An example of identical and reproducible results of the measurement is presented in the graphs above.

A.1 Realibility Test

Realibity tests were carried out to two identical devices, referred to TESD 1.2 THL. Each device was measured three times, and the validity, reliability and consistence of the measurement results are analysed from the value of Cronbach's alpha. With all values of the Cronbach's alpha > 0.6, all the measurements are reliable, which means that the repetition of measurement was valid and consistent.

Case Processing Summary

		N	%
Cases	Valid	601	100.0
	Excluded[a]	0	.0
	Total	601	100.0

Reliability Statistics

Cronbach's Alpha	Cronbach's Alpha Based on Standardized Items	N of Items
.992	.998	6

Item Statistics

	Mean	Std. Deviation	N
D_1.1	0.4047	0.29811	601
D_1.2	0.4962	0.38128	601
D_1.3	0.4742	0.36710	601
D_2.1	0.3794	0.26425	601
D_2.2	0.3734	0.24600	601
D_2.3	0.3998	0.25845	601

Inter-Item Correlation Matrix

	D_1.1	D_1.2	D_1.3	D_2.1	D_2.2	D_2.3
D_1.1	1.000	.992	.995	.995	.993	.994
D_1.2	.992	1.000	.998	.981	.978	.980
D_1.3	.995	.998	1.000	.985	.981	.983
D_2.1	.995	.981	.985	1.000	.999	.999
D_2.2	.993	.978	.981	.999	1.000	1.000
D_2.3	.994	.980	.983	.999	1.000	1.000

Summary Item Statistics

	Mean	Minimum	Maximum	Range	Maximum / Minimum
Item Means	.421	.373	.496	.123	1.329
Item Variances	.094	.061	.145	.085	2.402
Inter-Item Covariances	.090	.064	.140	.076	2.198
Inter-Item Correlations	.990	.978	1.000	.022	1.022

Summary Item Statistics

	Variance	N of Items
Item Means	.003	6
Item Variances	.001	6
Inter-Item Covariances	.000	6
Inter-Item Correlations	.000	6

Item-Total Statistics

	Scale Mean if Item Deleted	Scale Variance if Item Deleted	Corrected Item-Total Correlation	Squared Multiple Correlation	Cronbach's Alpha if Item Deleted
D_1.1	2.1230	2.280	.999	.	.988
D_1.2	2.0315	2.043	.990	.	.993
D_1.3	2.0535	2.080	.994	.	.991
D_2.1	2.1483	2.385	.995	.	.990
D_2.2	2.1543	2.443	.993	.	.991
D_2.3	2.1279	2.404	.994	.	.990

Scale Statistics

Mean	Variance	Std. Deviation	N of Items
2.5277	3.267	1.80757	6

A.2 t-Test : To Compare Two Identical Devices

The t-test was carried out to compare two identical devices, to check their reproducibility. For this case, 3 devices were made, and named Dev. A, B, and C. Comparation was made between Dev. A vs. B and Dev A vs. C. With the "sig" value (p-value) > 0.05, both comparations showed that the three devices were identical, which means that the reproducibility is good.

t-Test for Dev. A *vs* B

Group Statistics

	Device	N	Mean	Std. Deviation	Std. Error Mean
Voltage	Dev_A	601	.3794	.26425	.01078
	Dev_B	601	.3794	.26425	.01078

Independent Samples Test

		Levene's Test for Equality of Variances		t-test for Equality of Means	
		F	Sig.	t	df
Voltage	Equal variances assumed	.000	1.000	.000	1200
	Equal variances not assumed			.000	1200.000

Independent Samples Test

		t-test for Equality of Means		
		Sig. (2-tailed)	Mean Difference	Std. Error Difference
Voltage	Equal variances assumed	1.000	.00000	.01524
	Equal variances not assumed	1.000	.00000	.01524

Independent Samples Test

		t-test for Equality of Means	
		95% Confidence Interval of the Difference	
		Lower	Upper
Voltage	Equal variances assumed	-.02991	.02991
	Equal variances not assumed	-.02991	.02991

t-Test of Device A *vs* C

Group Statistics

	Device	N	Mean	Std. Deviation	Std. Error Mean
Voltage	Dev_A	601	.3794	.26425	.01078
	Dev_C	601	.3998	.25845	.01054

Independent Samples Test

		Levene's Test for Equality of Variances		t-test for Equality of Means	
		F	Sig.	t	df
Voltage	Equal variances assumed	1.966	.161	-1.349	1200
	Equal variances not assumed			-1.349	1199.410

Independent Samples Test

		t-test for Equality of Means		
		Sig. (2-tailed)	Mean Difference	Std. Error Difference
Voltage	Equal variances assumed	.178	-.02033	.01508
	Equal variances not assumed	.178	-.02033	.01508

Independent Samples Test

		t-test for Equality of Means	
		95% Confidence Interval of the Difference	
		Lower	Upper
Voltage	Equal variances assumed	-.04991	.00925
	Equal variances not assumed	-.04991	.00925

List of Publications

A1

"Ionic shot noise in an electrochemical capacitor system made of poly(3,4-ethylenedioxythiophene)-poly(styrenesulfonate) film and silver-coated polybenzoxazole-stainless steel electrodes on textile fabrics"
Nuramdhani, I; De Mey, G; Widodo, M; Hertleer, C; Van Langenhove, L. TEXTILE RESEARCH JOURNAL Volume: 89 Issue: 7 Pages: 1276-1285 DOI: 10.1177/0040517518767155 Published: APR 2019.

"Charge-Discharge Characteristics of Textile Energy Storage Devices Having Different PEDOT:PSS Ratios and Conductive Yarns Configuration"
Nuramdhani, I; Jose, M; Samyn, P; Adriaensens, P; Malengier, B; Deferme, W; De Mey, G; Van Langenhove, L. POLYMERS Volume: 11 Issue: 2 Article Number: 345 DOI: 10.3390/polym11020345 Published: FEB 2019.

"The electric energy stored in PEDOT:PSS capacitors integrated on textile substrate: Limits and possibilities"
Odhiambo, SA; Fiszer, P; De Mey, G; Hertleer, C; **Nuramdhani, I**; Van Langenhove, L; Napieralski, A. INTERNATIONAL JOURNAL OF CLOTHING SCIENCE AND TECHNOLOGY Volume: 30 Issue: 6 Pages: 808-816 DOI: 10.1108/IJCST-12-2017-0190 Published: 2018.

"Electrochemical Impedance Analysis of a PEDOT: PSS-Based Textile Energy Storage Device"
Nuramdhani, I; Gokceoren, AT; Odhiambo, SA; De Mey, G; Hertleer, C; Van Langenhove, L. MATERIALS Volume: 11 Issue: 1 Article Number: 48 DOI: 10.3390/ma11010048 Published: JAN 2018.

A2

"Electric Field Effect on Charge-Discharge Characteristics of Textile-Based Energy Storage Devices: In Search of the Underlying Mechanism"
Nuramdhani, I; Odhiambo, S; Hertleer, C; De Mey, C; Van Langenhove, L. TEKSTILEC Volume: 59 Issue: 2 Pages: 162-167 DOI: 10.14502/Tekstilec2016.59.162-167 Published: 2016.

C1

"Study on capacitive behavior of PEDOT:PSS-based Energy storage device by modeling the charge-discharge profile" – Conference Paper (oral presentation)
Nuramdhani, I; Vidia Putra, VG; Widodo, M; Hertleer, C; De Mey, G; Van Langenhove, L. Conference of **Intelligent Textiles and Mass Customization (ITMC 2017)**, Gent, Belgium, 2017.

"Fabrication and characterization of PEDOT:PSS textile supercapacitor for smart textiles" – Poster Presentation.
Nuramdhani, I; Vidia Putra, VG; Siahaan M; Widodo, M. **The 2nd Indonesian Textile Conference**, Bandung, Indonesia, 2017.

"Electric Field Effect on Charge-Discharge Characteristics of Textile-Based Energy Storage Devices: In Search of the Underlying Mechanism" – Oral Presentation.
Nuramdhani, I; Odhiambo, S; Hertleer, C; De Mey, C; Van Langenhove, L. **16th World Textile Autex Conference**, Ljubljana, Slovenia, 2016.